Numerical Modelling of Geothermal Borehole Heat Exchanger Systems

Miaomiao He

This thesis is submitted in partial fulfilment
of the requirements of De Montfort University
for the award of Doctor of Philosophy

Institute of Energy and Sustainable Development
De Montfort University, Leicester, UK
February 2012

Abstract

The large proportion of energy used in the built environment has made improving energy efficiency in buildings, in particular their heating, ventilation, and air conditioning (HVAC) systems, a policy objective for reducing energy consumption and CO_2 emissions nationally and internationally. Ground source heat pump (GSHP) systems, due to their high coefficient of performance (COP) and low CO_2 emissions are consequently, receiving increasing attention.

This work is concerned with the modelling of borehole heat exchangers (BHEs), the commonest form of ground heat exchangers found in GSHP systems. Their careful design is critical to both the short timescale and long timescale performance of geothermal heat pump systems. Unlike conventional components of HVAC systems, BHEs cannot be designed on the basis of peak load data but require application of dynamic thermal models that are able to take account of the heat transfer inside the borehole as well as the surrounding ground.

The finite volume method has been applied to develop a dynamic three-dimensional (3D) model for a single BHE and BHE arrays. The multi-block boundary fitted structured mesh used in this model allows the complex geometries around the pipes in BHEs and the surrounding ground around the borehole to be represented exactly. The transport of the fluid circulating along the pipe loop has been simulated explicitly in this model. The ground underneath the borehole has also been represented in this model. Validation of the 3D model has been carried out by reference to analytical models of borehole thermal resistance and fluid transport in pipes, as well as experimental data.

In this work, the 3D numerical model has been applied to investigate the three-dimensional characteristics of heat transfer in and around a BHE at both short and long timescales. By implementing a two-dimensional (2D) model using the same numerical method and comparing the simulation results from the 3D and 2D models, the most significant three-dimensional effects have been identified and quantified. The findings have highlighted some of the limitations of 2D models, and based on the findings, methods to improve the accuracy of a 2D model have been suggested and validated.

Furthermore, the 3D and 2D finite volume models have been applied to simulate an integrated GSHP system and their effects on overall system performance predictions have been investigated. The 3D numerical model has also been applied to examine thermal interactions

within BHE arrays and to evaluate the assumptions of the line source model and their implications in the analysis of thermal response test data.

Acknowledgements

I would like to express my deepest gratitude to my first supervisor, Dr. Simon Rees, for his inspiring guidance and encouragement through my work and for the invaluable influence he has made in my academic life. I am also deeply grateful to my second supervisor, Prof. Li Shao, for giving me this opportunity and for his help and support in my work.

I am thankful to many colleagues in IESD, who have made IESD a great place to work, who have helped and encouraged me through my studies, who have inspired me, and with whom I have established friendship that I cherish in my life. Special thanks go to Graeme Stuart, Kate Irvine, Rob Liddiard, Carl Holland, Sherif Ezzeldin, Ivan Korolija, Stephen Porritt, Divine Novieto, Andrew Wallace, Yingchun Ji, Tong Yang, and Yi Zhang.

I am hugely grateful to my parents, for their endless love, support and complete understanding all the way through.

My loving thanks also to my husband, Denis, for always being there to help and support me, to care and encourage me, and for always being patient with me. And to our daughter, who is on her way to the whole new world.

Without the financial support from De Montfort University, this work and thesis would never have been realised.

Contents

List of Tables

List of Figures

Nomenclature

α	thermal diffusivity (m^2/s)
β	equation fit coefficient (dimensionless)
μ	viscosity (kg/m.s)
τ	time (dimensionless)
θ	phase (radians)
ρ	density (kg/m^3)
A	amplitude
C	volume thermal capacity ($J/(m^3.K)$
c_p	specific heat capacity (J/kg.K)
COP	coefficient of performance (dimensionless)
D	diameter (m)
F	diffusion heat flux (W/m^2)
f	frequency (Hz)
g	g-function
H	depth (m)
h	convective heat transfer coefficient ($W/m^2.K$)
J_0	Bessel function of first kind of zeroth order
J_1	Bessel function of first kind of first order
k	thermal conductivity (W/m.K)

L	distance (m)
LA	tank volume (m^3)
m	mass flow rate (kg/s)
Nu	Nusselt number (dimensionless)
P	period (radians)
Q	heat transfer rate (W/m)
Pr	Prandtl number (Dimensionless)
q	Heat flux (W/m^2)
R	thermal resistance (m.K/W)
Re	Reynolds number (dimensionless)
r	radius (m)
S	surface area (m^2)
T	temperature (°C)
t	time (s)
v, V	fluid velocity (m/s)
$\dot{v}$	volume flow rate (m^3/s)
Y_0	Bessel function of second kind of zeroth order
Y_1	Bessel function of second kind of first order

Chapter 1 Introduction

1.1 Research Background

The Climate Change Act 2008 has set a target that the UK should reduce emissions of carbon dioxide and the other greenhouse gases at least 80% by 2050 relative to the 1990 baseline. Buildings account for nearly 40% of total energy consumption in the UK, and in turn are responsible for almost half of the UK's carbon emissions (Perez-Lombard et al., 2008). For domestic buildings, heating and hot water account for over 80% of the total energy consumption; and for non-domestic buildings, heating, ventilation and air conditioning (HVAC) systems are the main end use, which account for more than 50% of the energy consumption (Perez-Lombard et al., 2008). Therefore, improving heating and cooling system efficiency can make a huge impact on carbon emission reduction in buildings and reaching these targets.

Ground Source Heat Pump (GSHP) systems, due to their higher Coefficients of Performance (COP) and lower CO_2 emissions, have been proposed as sustainable systems to provide heating and cooling for buildings in the UK. GSHP systems use the ground as a heat source or a heat sink to extract or dissipate heat, depending on the operation of the systems, by circulating fluid inside ground heat exchangers. A diagram of GSHP heat exchanger types is shown in Figure 1.1.

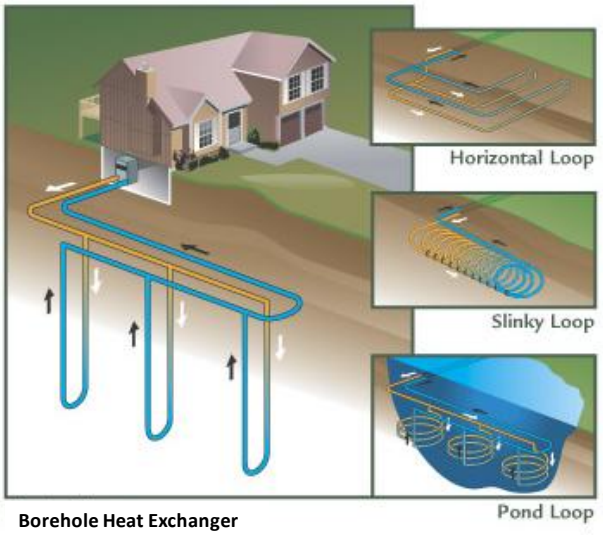

Figure 1.1 A diagram of GSHP heat exchanger types. (Source: http://www.daviddarling.info/encyclopedia/G/AE_geothermal_heat_pump.html)

The main advantage of using the ground is that its temperature is much more stable than the ambient air temperatures. It is higher in the winter and lower in the summer, which can make the COP higher than other systems, such as, air source heat pump systems. A recent study shows that a suitably sized GSHP system could achieve almost 40% CO_2 savings when compared to a conventional gas boiler (Jenkins et al., 2009). Even though GSHP systems have well established in North America and many parts of Europe, there are still relatively a few systems installed in the UK. However, because of their potential to reduce energy consumption and CO_2 emissions, GSHP systems are receiving increasing interest.

Pipes formed in a 'U' loop and grouted into vertical boreholes are probably the commonest form of ground heat exchangers found in GSHP systems and are known as Borehole Heat Exchangers (BHEs) (Figure 1.1). Their careful design is critical to the short-term and long-term performance of geothermal heat pump systems. BHEs of this type are not only used in conventional building heating and cooling systems but also in large thermal storage schemes. BHEs can not be designed on the basis of peak load data but required application of dynamic thermal models that are able to take account of the heat transfer inside the borehole as well as the surrounding soil/rock formation.

1.2 Problem Definition

A review of existing models for BHEs shows that models of BHEs have been developed for three principal applications: 1) Analysis of in-situ ground thermal conductivity test data; 2) Design of BHEs; 3) Integration with building system simulation. The heat transfer processes in and around BHEs are complex and occur over a wide range of spatial and timescales. Assumptions are usually made in order to simplify the process so that models can be developed to simulate such systems without excessive computational effort. These assumptions, as a result, limit the applicability of the models.

Analytical models such as the line source solution and cylinder source solution can be applied to simulate the BHEs by ignoring the geometry of the borehole and considering the borehole as an infinitely long heat source. This type of model can be applied to both the design of BHEs and analysis of in situ test data, but are not suitable for applications such as integration with building system simulation, where the transient heat transfer within the borehole at short timescales is the dominant heat transfer process.

A number of approaches that have combined analytical and numerical methods have been developed that are more suitable for design tasks. Although the heat transfer within the borehole was not represented explicitly, a thermal resistance was used to define the relationship between the fluid and borehole wall temperatures. Neglecting the thermal mass of the fluid, pipes and grout in the borehole makes these models only suitable for simulation timescale of over one month.

Applications of models for system simulation tasks – unlike design tasks – require the ability to operate at much shorter timescales than one month. Numerical methods have been applied to simulate the heat transfer within a borehole in one or two dimensions, taking into account the thermal mass of the pipes and grout. Models of this type have been implemented in annual building energy simulation software.

Three-dimensional numerical models offer a general and accurate representation of heat transfer in and around BHEs. Variation in fluid temperature with depth can be simulated explicitly. Thus, assumptions that need to be made for two-dimensional models can be avoided. However, due to the constraint of computational power, all the three-dimensional models that are available in literature adopted a 'de-coupling and coupling' approach. While the heat transfer of the ground surrounding boreholes was simulated in a true three dimensional manner, the heat transfer within the borehole was simplified so that a one or two dimensional model can be applied.

1.3 Aims and Objectives

The aim of this work has been to develop a dynamic three-dimensional numerical model for borehole heat exchangers (BHEs) in order to investigate the transient heat transfer in and around BHEs in three dimensions in various applications. The heat transfer within a borehole is simulated explicitly, taking into account the dynamics of fluid transport in the pipes.

The following objectives were identified:

1. Review BHE model developments;
2. Develop a fully discretised 3D numerical model for BHEs and validate this model;
3. Investigate the three-dimensional characteristics of heat transfer in and around a BHE;
4. Develop insight into the limitations of two-dimensional models and suggest ways in which they can be improved;

5. Study the effects of simulating a BHE using a dynamic 3D numerical model on the predictions of system performance;
6. Examine the thermal interactions within borehole fields using a dynamic 3D numerical model;
7. Evaluate the accuracy of applying the line source model in the analysis of thermal response tests.

1.4 Thesis Structure

This thesis is structured according to the objectives of this study and presented in nine chapters. This chapter introduces the background and the problem defined of this study, as well as the aims and objectives.

Chapter 2 provides a review of BHE model developments. This chapter also outlines the research questions of this thesis.

Chapter 3 presents the methodology applied to the model development. This includes the numerical method used to develop the 3D model and the implementation of a 2D model. This chapter also presents the validations of the models through comparisons with analytical models and experimental data.

Chapter 4 describes the characteristics of heat transfer in and around a single BHE in three dimensions. The differences in terms of model predictions purely caused by the 3D effects are highlighted through comparisons of simulation results of step response tests by the 3D and 2D models.

Chapter 5 demonstrates methods to improve the accuracy of 2D models based on the findings from Chapter 4.

Chapter 6 presents a study of a ground source heat pump system for a domestic building. The aim of this chapter is to investigate the effects of simulating the BHE using the 3D and 2D models on the predictions of system performances.

Chapter 7 presents the investigation of the thermal interactions within borehole fields.

Chapter 8 presents an evaluation of the limitations of the line source model in the analysis of thermal response test data.

Chapter 9 presents a summary of key findings from this work and a discussion of the contribution to knowledge. The achievement of aims and objectives is highlighted. Potential areas for future research are suggested.

Chapter 2 Borehole Heat Exchanger Models

This chapter presents a literature review of borehole heat exchanger model developments. Literature review regarding model validations and applications is discussed in relevant Chapters/Sections later in this thesis.

Borehole Heat Exchangers (BHEs) are probably the commonest form of ground heat exchanger found in Ground Source Heat Pump (GSHP) systems and thermal storage systems. Several types of BHEs are commonly used: single U-tube; double U-tube; and, concentric tubes. Figure 2.1 shows a diagram of these three types. The tubes are typically made of high-density polyethylene pipes with heat fused joints, which is not only highly durable but also efficient for heat transfer. Fluid, usually anti-freeze solution, circulates inside the tubes as the heat transfer medium to extract/reject heat from/into the ground. The gap between the tubes and the borehole is normally backfilled with grout to improve the heat transfer with the surrounding ground and protect the groundwater from contamination, although in some countries BHEs are not grouted (e.g. Sweden).

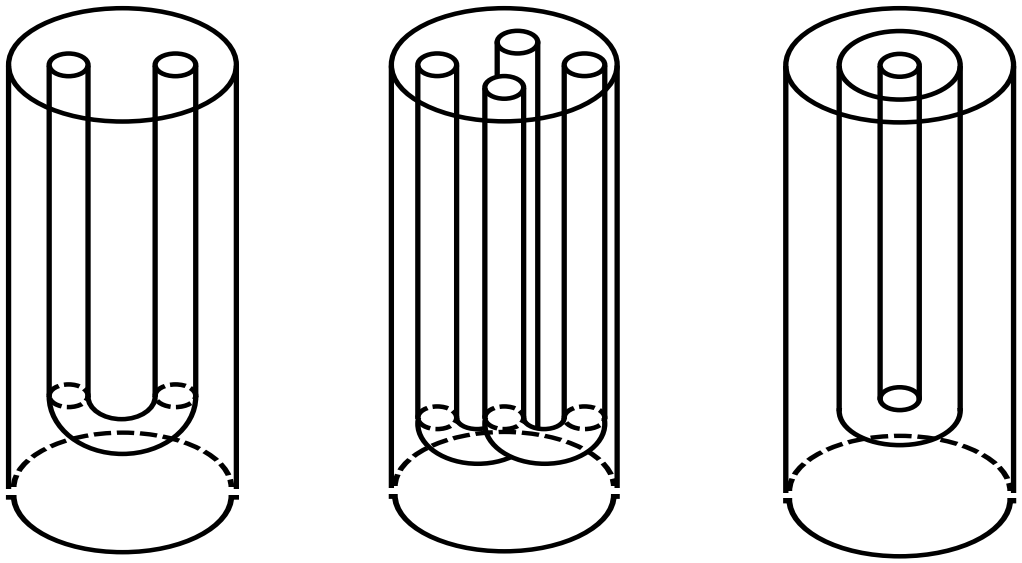

Figure 2.1 Three types of commonly used BHEs. From left to right, single U-tube, double U-tube and concentric tubes.

A BHE is normally 100 – 150 mm in diameter and 50 – 150 m in depth. The transit time of the fluid travelling in the tubes can vary from one minute and half to twenty-five minutes. This can be expected to cause delays in temperature responses. The ground is normally stratified along the depth of the borehole and it is common to have different layers of geological material (clay,

sandstone, gravel etc) along the depth of the borehole. The undisturbed ground temperature profile along the depth of the borehole is not uniform. The surface ground temperature (and up to 10 meters deep) fluctuates daily and annually and is mainly affected by local air temperature and solar radiation. Kasuda and Archenbach (1965) used a sinusoidal function to estimated the daily average soil temperature at different depth at different time of year. The ground temperature below 10 meters deep is sometimes regarded as constant, although a geothermal gradient of 0.01-0.03K/m gives a more accurate description of the ground temperature distribution.

For a grouted BHE, the heat transfer process of a BHE consists of three components: convection heat transfer between the fluid and the inner pipe wall; conduction heat transfer through the pipes and grout, and conduction heat transfer through the ground (and advection if there is ground water flow). For a borehole field with multiple BHEs, over long timescales, thermal interaction among the boreholes develops and this may strongly decrease the heat extraction/rejection capacity after a number of years (e.g. 5 years).

Models of BHEs have been developed to simulate the heat transfer process of BHEs for three principal applications:

1. Analysis of in-situ ground thermal conductivity test data.
2. Design of BHEs. This means sizing the borehole depth, number of boreholes etc.
3. Integration with building system simulation i.e. with the model coupled to HVAC system and building heat transfer models to study overall performance.

Depending upon the methodology used for model development, models of BHEs can be divided into four categories: (I) analytical models; (II) steady state borehole models; (III) response factor models; (IV) discretised numerical models. This chapter reviews models of BHEs according to the four categories. Each model is explained starting with its conceptual modelling, followed by the mathematical formulation, and lastly its implementation and applications. The advantages and limitations of the models are emphasized; thus highlighting some of the current gaps in modelling BHEs and pointing towards the need to better understand the dynamic behaviour of BHEs.

2.1 Analytical Models

There is no analytical solution for the three-dimensional transient heat transfer problem of the complex geometry and boundary conditions found in BHEs. In order to derive analytical models for BHEs, a number of simplifying assumptions need to be made. The simplest one is to consider the whole borehole as an infinitely long line source and ignore the thermal properties of the borehole, for example, the thermal mass of the fluid, pipes, and grout. By making these assumptions, the line source theory propounded by Kelvin (1882) can be applied to develop the so called ' line source model'. The cylinder source solution (Carslaw and Jaeger, 1947) is similar but makes the assumption that the two legs of the U-tube can be considered as a single pipe that is co-axial with the borehole. The thermal mass of the fluid, pipes and grout are also ignored using this approach.

Analytical models allow computationally efficient calculation of BHEs. Their applications include designing the BHEs and analyzing in-situ ground conductivity testing data.

2.1.1 The Line Source Model

The line source model was developed based on Kelvin's line source theory (Kelvin, 1882). If the whole borehole is considered as a semi-infinitely long line source, the temperature of the ground surrounding the borehole at any radius and any point at any time can be obtained. The heat flux at the source point is considered as constant radial heat flow normal to the length of the source, transferring the heat from the line source to an infinite homogenous medium surrounding it.

Assuming a uniform initial temperature and a constant heat flux per unit depth at zero radius, the expression given by Ingersoll (1954) for the temperature at any time at any radius can be written as:

$$T - T_0 = \frac{Q}{2\pi k} \int_X^\infty \frac{e^{-\beta^2}}{\beta} d\beta \equiv \frac{Q}{2\pi k} I(X) \qquad \textbf{(2.1)}$$

and

$$\beta = \frac{r}{2\sqrt{\alpha(t - t')}}$$

$$X = \frac{r}{2\sqrt{\alpha t}}$$

where *T* is the temperature of the ground at radius *r* (°C), T_0 is the initial temperature of the ground (°C), *Q* is the heat flux per unit length of borehole (W/m), *r* is the radius from the line source (m), *k* is the thermal conductivity of the ground (W/mK), α is the thermal diffusivity of the ground (m^2/s), *t* is the time since the start of the operation (s).

For $X < 0.2$, the values of the integral term can be obtained from the following approximation:

$$I(X) = 2.303 \log_{10} \frac{1}{X} + \frac{X^2}{2} - \frac{X^4}{8} - 0.2886 \quad \textbf{(2.2)}$$

Carslaw and Jaeger (1947) used the exponential integral E_1 to approximate the solution of the line source model and derived the most commonly used equation for the estimation of the thermal conductivity of the ground during in-situ thermal response tests. This line source equation can be stated as follows:

$$T - T_0 = \frac{Q}{4\pi k} \int_{r^2/4\alpha t}^{\infty} \frac{e^{-u}}{u} du = \frac{Q}{4\pi k} E_1 \left(\frac{r^2}{4\alpha t} \right) \quad \textbf{(2.3)}$$

The exponential integral E_1 can be approximated as:

$$E_1 \left(\frac{r^2}{4\alpha t} \right) = -\gamma - \ln \left(\frac{r^2}{4\alpha t} \right) - \sum_{n=1}^{\infty} (-1)^n \frac{(\frac{r^2}{4\alpha t})^n}{nn!} \cong \ln \left(\frac{4\alpha t}{r^2} \right) - \gamma \quad \textbf{(2.4)}$$

Where γ is Euler's constant, which is equal to (0.5772…). The natural logarithm approximation of the exponential integral E_1 in equation (2.4) gives errors less than 10% for the time criterion $t_c \geq 5r^2/\alpha$.

The temperature at the borehole wall ($r = r_b$) at time *t* can then be expressed as:

$$T_b = \frac{Q}{4\pi k} \left[\ln \left(\frac{4\alpha t}{r_b^2} \right) - \gamma \right] + T_0 \quad \textbf{(2.5)}$$

with $t_c \geq 5r_b^2/\alpha$, which ranges from 3 to 10 hours in practise.

Assuming the heat transfer within the borehole is in a steady-state, at anytime, the relationship between the mean fluid temperature and the borehole temperature can be defined using a thermal borehole resistance so that:

$$T_f = T_b + Q \cdot R_b$$
$$= \frac{Q}{4\pi k}\ln(t) + Q\left\{R_b + \frac{1}{4\pi k}\left[\ln\left(\frac{4\alpha}{r^2}\right) - \gamma\right]\right\} + T_0 \quad \textbf{(2.6)}$$

where T_f is the mean fluid temperature, T_b is the borehole temperature R_b is the borehole thermal resistance.

For a constant heat flux, the mean fluid temperature varies linearly with the natural logarithm of time and the last two terms in Equation (2.6) do not change with time. In this case, the coefficient of proportionality (slope) is equal to $\frac{Q}{4\pi k}$. During thermal response tests where heat input is constant and the mean fluid temperature over time is measured, plotting the mean fluid temperature versus natural logarithm time, a linear trend can be expected. The conductivity of the ground can be taken to be $\frac{Q}{4\pi m}$ and m is the slope of the linear natural logarithm trend.

There are other solutions developed from Kelvin's line source theory. For example, Hart and Couvillion's approach (1986) and the IGSHPA approach (Bose, 1991).

In the line source model, the geometry of the borehole is necessarily ignored, along with the thermal capacities of the fluid, pipes and grout material within the borehole. Consequently the model is not suitable for short timescale applications where the dynamic response within the borehole should be considered. Furthermore, the borehole is considered as infinitely long so that heat flow is always radial and normal to the borehole. As a result, the heat transfer below the borehole, a.k.a. the end effect, can not be taken into account. Consequently, this model is not suitable for multi-annual simulations, for example, over 20 years, where the end effect becomes important and cannot be neglected.

Despite its limitations, the line source model has been widely used in the analysis of in situ thermal response test data due to its simplicity and efficiency in terms of computing. Moreover, more sophisticated analytical models of BHEs have been developed and contributions have been made to improve such models in recent decades.

2.1.2 Cylinder Source Model

Considering the two pipes as one infinitely long pipe, and coaxial with the borehole with infinite length, the cylinder source solution (Carslaw and Jaeger, 1947) can be used to calculate the temperature distribution of the infinite ground with the initial temperature surrounding

the borehole at any time. Assuming a constant heat flux along the borehole, the governing equation for one dimensional heat transfer problem can be expressed as:

$$\frac{\partial^2\theta}{\partial r^2}+\frac{1}{r}\frac{\partial\theta}{\partial r}-\frac{1}{\alpha}\frac{\partial\theta}{\partial t}=0 \qquad r_0<r<\infty \qquad \textbf{(2.7)}$$

while the boundary conditions and initial condition can be expressed as:

$$-2\pi\cdot r_0\cdot k\frac{\partial\theta}{\partial r}=Q \qquad r=r_0, t>0$$

$$\frac{\partial\theta}{\partial r}=0 \qquad r=0$$

$$\theta=0 \qquad t=0, r>r_0$$

where $\theta=T-T_0$, is the temperature difference between the ground temperature at radial distance r from the cylinder source at time t and the initial temperature (°C).

Taking the Laplace transform and the inverse Laplace transform, the solution can be expressed as:

$$\theta(r,t)=\frac{2Q}{\pi k}\int\left(1-e^{-\alpha u^2 t}\right)\frac{J_0(u,r)Y_1(u\alpha)-Y_0(ur)J_1(u\alpha)}{u^2[J_1^2(u\alpha)+Y_1^2(u\alpha)]}du \qquad \textbf{(2.8)}$$

where J_0, J_1, Y_0, Y_1 are the zero and the first order Bessel functions.

Kavanaugh (1985) developed the cylindrical source approach, and later tested this model using experimental data from two test sites (Kavanaugh, 1992). Due to the fact that the cylinder source solution considers the two pipes as one, the short circuit heat transfer within the borehole introduced by the temperature difference between these two pipes is ignored. Two methods were suggested by Kavanaugh to correct the short circuit effect. The details of the correction can be found in Yavuzturk's thesis (Yavuzturk, 1999).

In a similar way to the line source model, the cylinder source solution assumed the borehole to be infinitely long and the ground to be homogeneous along the depth. The geometry and the thermal properties of the materials inside the borehole were ignored, including the thermal mass of the fluid. A thermal resistance was used to describe the heat transfer between the fluid and the borehole temperatures. This model can be used to calculate the steady state thermal resistance of borehole by superposition. Detailed calculation methods can be found in Young (2004).

2.2 Steady State Borehole Models

Steady state borehole models have been developed mainly for calculating the borehole thermal resistance. The fundamental assumption made in steady state borehole models is that the heat transfer in the borehole is in steady state. The ratio between the heat flux of the borehole and the temperature difference between the fluid and the borehole wall is then a constant value. Thus, a thermal resistance can be used to define the relationship between the heat flux and the temperature difference of the fluid and the borehole wall as follows:

$$R_b = \frac{T_f - T_b}{Q} \tag{2.9}$$

where R_b is the borehole thermal resistance (mK/W), Q is the heat flux per unit length of borehole (W/m), T_f is the average temperature of the fluid (°C) and T_b is the average temperature of the borehole wall (°C).

The borehole thermal resistance includes the convective resistance of the fluid, the conductive resistance of the pipes, and the conductive resistance of the grout. The relationship of the borehole thermal resistance and the thermal resistance of fluid, pipe and grout can be defined as:

$$R_b = \frac{R_f + R_p}{2} + R_g \tag{2.10}$$

where R_f is the convective resistance of the fluid within one pipe, R_p is the conductive resistance of one pipe, and R_g is the conductive resistance of the grout.

The convective resistance of the fluid within one pipe can be calculated by (Incropera et al., 2007):

$$R_f = \frac{1}{2\pi r_1 h} \tag{2.11}$$

where r_1 is the inside diameter of the pipe (m), and h is the convective coefficient of the fluid (W/m^2K).

The conductive resistance of one pipe can be calculated by (Incropera et al., 2007):

$$R_p = \frac{\ln\left(\frac{r_2}{r_1}\right)}{2\pi k_p} \tag{2.12}$$

where r_2 is the outside diameter of the pipe (m), k_p is the conductivity of the pipe (W/mK).

The conductive resistance of the grout can not be calculated as straight forwardly as the thermal resistance of the fluid and the pipe due to its irregular geometry. A number of steady state borehole models have been developed to address this and are discussed below.

2.2.1 Equivalent Diameter Model

The equivalent diameter model developed by Gu and O'Neal (1998) illustrates a very simple way of calculating the borehole thermal resistance in one-dimensional steady-state conditions. Taking the assumption that the thermal influences of the two legs of a U-tube can be represented by the thermal influences of one pipe that is concentric with the borehole, Gu and O'Neal (1998) derived an expression to calculate the equivalent diameter of a concentric pipe (Figure 2.2).

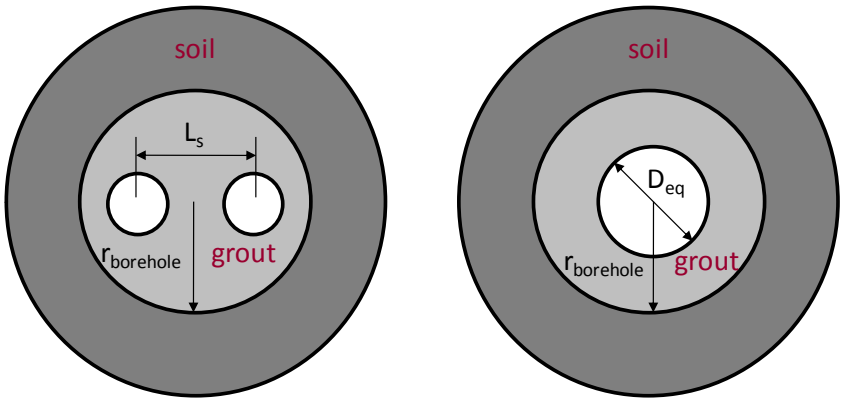

Figure 2.2 Diagram of equivalent diameter of a BHE with single U-tube.

$$D_{eq} = \sqrt{2D_p \cdot L_s} \qquad D_p \leq L_s \leq r_{borehole} \qquad \textbf{(2.13)}$$

where D_{eq} is the equivalent diameter of the pipe (m), D_p is the diameter of the pipe, and L_s is the centre to centre distance between the two legs of the U-tube.

The resistance of the grout, in this case, can be calculated by employing the general equation for radial heat conduction through a cylinder (Incropera et al., 2007).

$$R_g = \frac{ln\left(\frac{D_b}{D_{eq}}\right)}{2\pi k_g} \qquad \textbf{(2.14)}$$

where D_b is the diameter of the borehole (m), k_g is the thermal conductivity of the grout (W/mK).

2.2.2 Paul's Model

Paul's model was developed to calculate the grout thermal resistance by using the so-called 'shape factor correlations', which were created using experimental data from a test apparatus and simulation results from a two dimensional finite element model (Paul, 1996).

Four different configurations classified according to the shank spacing S_1 and S_2 were taken into account in Paul's Model (Figure 2.3).

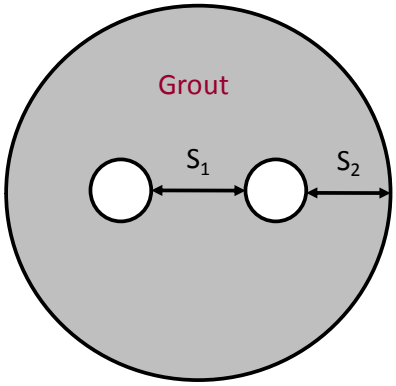

Spacing Condition:

Case A:	$S_1 = 0$
Case B:	$S_1 = 0.3124$ cm
Case C:	$S_1 = S_2$
Case D:	$S_2 = 0.300$ cm

Figure 2.3 Types of shank spacing were considered in Paul's model.

By adding the shape factor, the grout thermal resistance can be expressed as:

$$R_g = \frac{1}{k_g \cdot S} \tag{2.15}$$

where S is the dimensionless shape factor and can be defined by:

$$S = \beta_0 \cdot (\frac{D_b}{D_p})^{\beta_1} \tag{2.16}$$

where β_0 and β_1 are the dimensionless equation fit coefficients and D_p is the outer diameter of the pipe.

Paul derived equation fit coefficients for the four configurations described in Figure 2.3. The values of β_0 and β_1 are given in Table 2.1.

Table 2.1 Equation fit coefficients given by Paul for four different configurations (Paul, 1996).

	Case A	Case B	Case C	Case D
β_0	14.45087	20.10038	17.44268	21.90587
β_1	-0.8176	-0.94467	-0.60515	-0.3796
R	0.997096	0.992558	0.999673	0.969875

where *R* indicates the accuracy of the equation fit with reference to the experimental data or numerical model. An *R* value of 1 indicates a perfect fit.

2.2.3 Multipole Method

The multipole method developed by Bennet et al. (1987) is probably the most rigorous method of calculating the borehole thermal resistance. It represents the pipes in the circular borehole using a series of line heat sources or sinks and can model borehole configurations with more than one U-tube. It can also calculate borehole resistance of U-tubes that are not symmetrically arranged in the borehole. It simulates each pipe by representing it with a line source or line sink, and for each line source or line sink, there is at least one line sink or line source at a mirror point (zero order multipole) (Figure 2.4). More line sinks or line sources are added to account for the non-concentric nature of the geometry (higher order multipoles). The solution can be found limited only by machine accuracy.

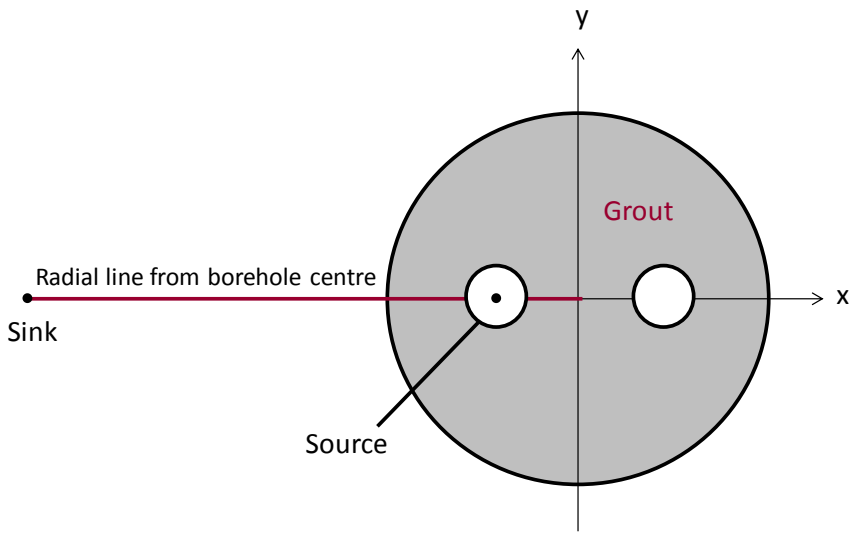

Figure 2.4 A single line source with a single line sink.

By setting a specific temperature for each pipe, the multipole method calculates the heat flux of each pipe and the average temperature of the borehole wall so that the borehole resistance can be derived as follows:

$$R_{borehole} = \frac{T_{fluid} - T_{borehole}}{\sum_{i=1}^{n} Q_i} \quad \textbf{(2.17)}$$

2.3 Response Factor Models

Although analytical models require less computing effort than numerical approaches and are suitable to be used in the analysis of in-situ thermal response test data, they are less suited to design and simulation tasks where one would like to take account of time varying heat transfer rates and the influence of surrounding boreholes over long timescales. Response factor models, on the other hand, have been developed to address these issues.

Response factor models use pre-defined response functions to describe the relationship of temperature changes and heat fluxes of BHE fields/arrays. Hybrid approaches combining analytical and numerical methods are usually adopted in order to derive response functions for pre-defined configurations of BHEs. Response factor models have been proved to be highly efficient and have been implemented in both design and simulation software.

2.3.1 Long time step g-function Model

The long time step g-function model was developed by Eskilson (1987) to model BHEs for thermal storage applications. The g-function is essentially a normalised step-response function that describes the relationship between the average borehole temperature and a step in the extraction/rejection for a defined configuration of BHEs. It is calculated through a combination of analytical and numerical techniques. Firstly, a two-dimensional (radial-axial) finite difference model for a single BHE was constructed to determine its temperature response to a unit step heat pulse. After that, the superposition technique was applied to determine the temperature response to the unit step heat pulse for a pre-defined configuration of multiple BHEs using the temperature distribution of a single borehole obtained previously. These temperature responses are then normalised to the so called g-function. The g-function is usually defined by discrete values that are interpolated in the simulation.

The mathematical expression of the g-function can be derived as follows: given the constant heat extraction rate Q (W/m) and constant far-field ground temperature T_s, the borehole temperature $T_b(t)$ can be written as:

$$T_b(t) = T_s - Q \cdot R_q \tag{2.18}$$

Here R_q can be regarded as a time-dependent thermal resistance for a unit heat extraction step, and is written in the following way:

$$R_q = \frac{1}{2\pi k} \cdot g(\frac{t}{t_s}, \frac{r_b}{H}) \quad \textbf{(2.19)}$$

Where $g(t/t_s, r_b/H)$ denotes the dimensionless step-response function, called the g-function, and t_{ss} is the steady-state time-scale which is defined by the dimensionless time t/t_{ss} and the ratio of borehole radius r_b and depth H.

$$\mathrm{t_s} = \frac{\mathrm{H}^2}{9\alpha} \quad \textbf{(2.20)}$$

where α is the ground thermal diffusivity (m^2/s).

Rearranging Equation (2.18) and (2.19), the g-function can be expressed as:

$$g\left(\frac{t}{t_s}, \frac{r_b}{H}\right) = \frac{2\pi k \cdot (T_b(t) - T_s)}{Q} \quad \textbf{(2.21)}$$

Eskilson (1987)calculated over 200 g-functions for multiple BHEs arranged in different shapes, e.g. in a line, in a rectangle, and in a square, with different distance between two boreholes. The results for each configuration also vary according to the ratio of borehole distance and borehole length (B/H). Four examples are shown in Figure 2.5.

Any heat extraction/rejection varying according to time can be decomposed into a set of unit steps. Consequently, the response to each unit step can be superimposed to calculate the overall response to any heat extraction/rejection time series.

In this approach, the complex geometry of a borehole is simplified as a cylinder with a finite length and diameter. A single temperature is used to represent the borehole wall temperature. The thermal conductivities and capacities of all the different materials inside a borehole, including fluid, pipes and grout, are neglected. For this particular reason, the solution of the equation is only valid for time to be greater than a few hours ($t > \frac{5r_b^2}{\alpha}$). As a result, this g-function is known as a long time step g-function.

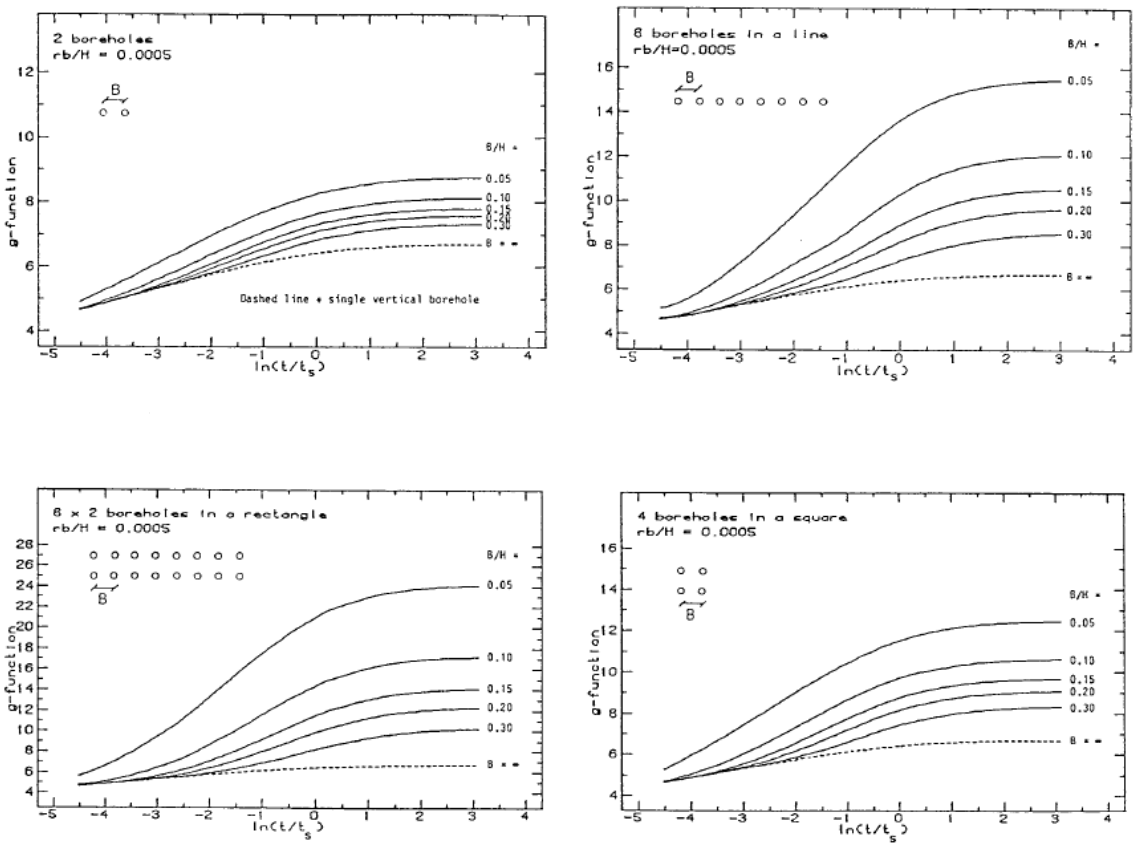

Figure 2.5 Dimensionless g-function for different borehole configurations (Eskilson, 1987).

2.3.2 Short time step g-function Model

The long time step g-function model developed by Eskilson (1987) provides an efficient solution to simulate borehole fields with defined configurations over long timescales, ranging from one month to several years. However, due to the simplification of borehole geometry and the neglect of the thermal properties of all the components inside the borehole, this model is not suitable for simulation of BHEs on shorter timescales (e.g. hourly), which is an essential requirement for system simulation tasks. In order to expand the application of the long time step g-function model, Yavuzturk (1999) developed a two-dimensional numerical model on a polar grid to compute the so-called 'short time step g-function'.

Only half of the borehole was simulated due to its symmetrical geometry. The thermal properties of the materials inside the borehole were modelled, such as the resistance of the pipe and grout due to conduction and the convection resistance due to the flow of the fluid inside the pipes. Figure 2.6 shows the discretization of the borehole geometry on a polar grid.

The pipe was not explicitly modelled but was approximated by cells in a pie-sector. In addition, the fluid inside the pipes was not explicitly modelled so that the heat transfer from the fluid was treated by a heat flux boundary condition at the pipe wall.

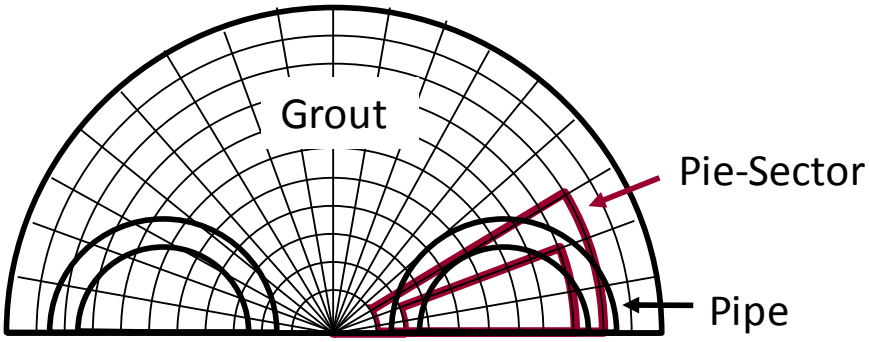

Figure 2.6 Simplified representation of the borehole using the pie-sector approximation of the pipes.

Applying the finite volume method, the temperatures of the fluid can be calculated when there is a heat transfer rate applied to the borehole. Using a borehole resistance to describe the relationship between the fluid temperature and borehole temperature, the borehole temperature can then be subtracted from the fluid temperature.

$$T_b(t) = T_f(t) - R_b \cdot Q \tag{2.22}$$

where R_b can be calculated by Equation (2.10), which is a sum of the convective resistance of the fluid, calculated by Equation (2.11), the conductive resistance of the pipe, calculated by Equation (2.12) and the conductive resistance of the grout, calculated by Paul's method (Equation (2.15) and (2.16)).

Consequently, Equation (2.21) is recast to solve for the g-function and modified to account for the borehole thermal resistance:

$$g\left(\frac{t}{t_s}, \frac{r_b}{H}\right) = \frac{2\pi k \cdot (T_f(t) - R_b \cdot Q - T_s)}{Q} \tag{2.23}$$

For typical ratios of borehole radius to borehole depth, the short time-step g-function data correspond to time steps between 2 ½ minutes and 200 hours. The short time step g-function is implemented as an extension of the long time step g-function. The short time step g-

function generated using the two-dimensional finite volume model extends the long time step g-function smoothly.

The model that combines the short time step g-function and the long time step g-function was implemented in GLHEPro (Spitler, 2000), a design software for vertical borehole ground loop heat exchangers, as well as in EnergyPlus (Crawley et al., 2001), a whole building energy simulation program. Figure 2.7 plots the imbedded short time step g-function and the long time step g-function for four different configurations of borehole fields in GLHEPro.

The biggest disadvantage of this model lies in the fact that the fluid inside the pipes was not explicitly modelled; instead it was treated by a heat flux boundary condition at the pipe wall. Therefore, the dynamics of the fluid transport along the pipe loop cannot be taken into account. In addition, the thermal mass of the fluid is not counted for.

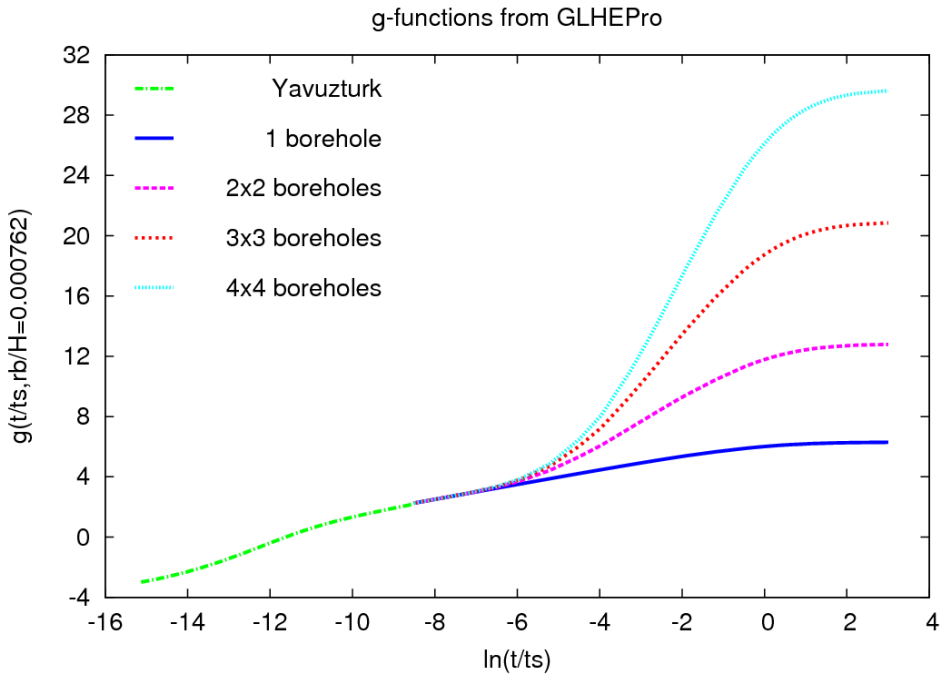

Figure 2.7 The combined short time step g-function by Yavuzturk and long time step g-functions for four different configurations of borehole fields by Eskilson in GLHEPro.

2.3.3 DST Model

Hellström (1991) developed the duct storage (DST) model for ground heat storage systems. The model divides the total volume of the ground for multiple BHEs into two regions: the local region and the global region. The local region is defined as the storage volume assigned to

each individual borehole. Within the local region, there is a heat transfer process between the heat carrier fluid and the borehole wall, which is represented by a borehole resistance. In addition, the BHEs interact with the surrounding ground around each borehole. The global region, on the other hand, is concerned with the heat conduction problem between the bulk of storage volume (sum of the storage volume assigned to each borehole) and the surrounding ground. Figure 2.8 shows a diagram of the division of the local and global region in the DST model.

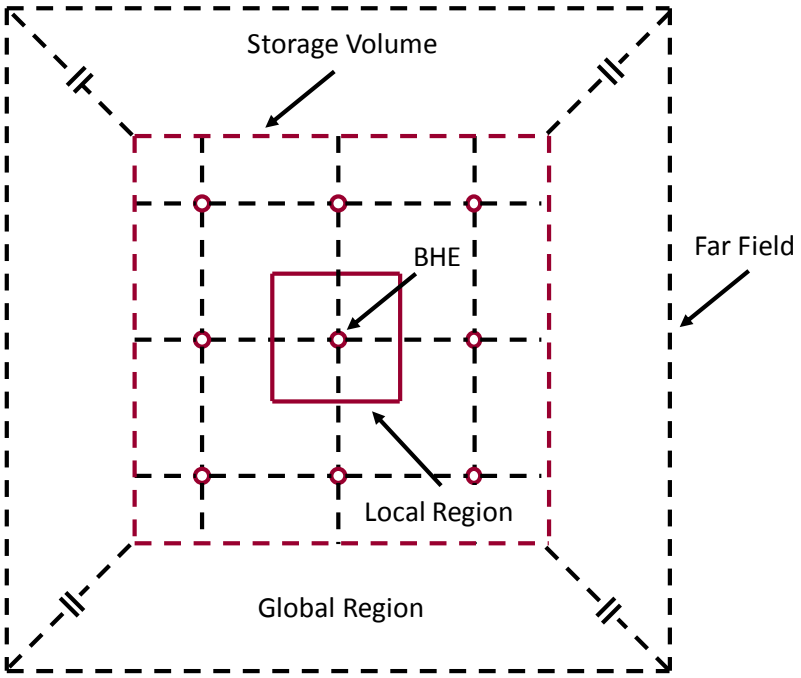

Figure 2.8 The division of the local and global region in the DST model.

The heat transfer process of the local region is simplified as a one-dimensional heat transfer problem, and a one-dimensional radial mesh was constructed to simulate the transient heat transfer process for short timescales. By applying the finite difference method, the temperature change at any point at the local region due to the transient heat transfer process can be calculated. Over longer timescales, when the heat transfer within the local region reaches steady-state, analytical solutions can be applied to simulate this steady-flux process for a BHE with different borehole configurations, e.g. a single U-tube, double U-tube, concentric tubes. There is no heat flux across the border of the local region and the temperature at the border is calculated by superimposing the temperature change due to the two adjacent BHEs that share that border. The global solution is obtained by applying the finite

difference method to a two-dimensional radial-axial mesh to simulate the three-dimensional heat transfer problem. The global thermal process includes three fundamental parts: a transient thermal build-up of the temperature field around the storage volume during the initial years, a steady-state heat loss through the surface of storage volume after the initial thermal build-up years, and a periodic heat loss for the annual storage cycle.

The analysis of the heat transfer process explained in the above paragraph is based on applying a constant heat pulse. For time-varying heat transfer, the load profile needs to be decomposed into a series of heat pulses, and after obtaining the responses to each heat pulse, the results of these responses can then be superimposed in time in order to obtain the final solution.

The DST model is developed based on the assumption that the BHEs are densely packed, with a minimum surface area to volume ratio, which is typical for heat storage; however this assumption is not ideal for other applications, for example, multi-year simulations of ground source heat pump systems where the boreholes are more widely spaced.

The DST model has been implemented in TRNSYS (SEL, 2005), a transient systems simulation program with a modular component based structure. This model implementation is able to deal with relatively short time steps.

2.4 Discretised Three-Dimensional Numerical Models

Discretised three-dimensional (3D) numerical models can provide a complete description of the borehole geometry and fully capture the complex transient 3D heat transfer of BHEs and fluid transport effects.

2.4.1 Vertical BHE EWS Model

Wetter and Huber (1997) developed the vertical BHE EWS model for BHE with double U-tubes and implemented it in TRNSYS (Type 451) in order to simulate the short time step transient behaviour of the BHE. The model was constructed by solving the one-dimensional heat transfer equation in radial direction using the Crank-Nicholson algorithm. The equation can be expressed as follows:

$$\frac{\partial^2 T}{\partial r^2} + \frac{\partial T}{\partial r} - \frac{1}{\alpha}\frac{\partial T}{\partial t} = 0 \qquad \textbf{(2.24)}$$

In order to solve this equation, the BHE is divided into different layers with variable distances in radial direction (Figure 2.9).

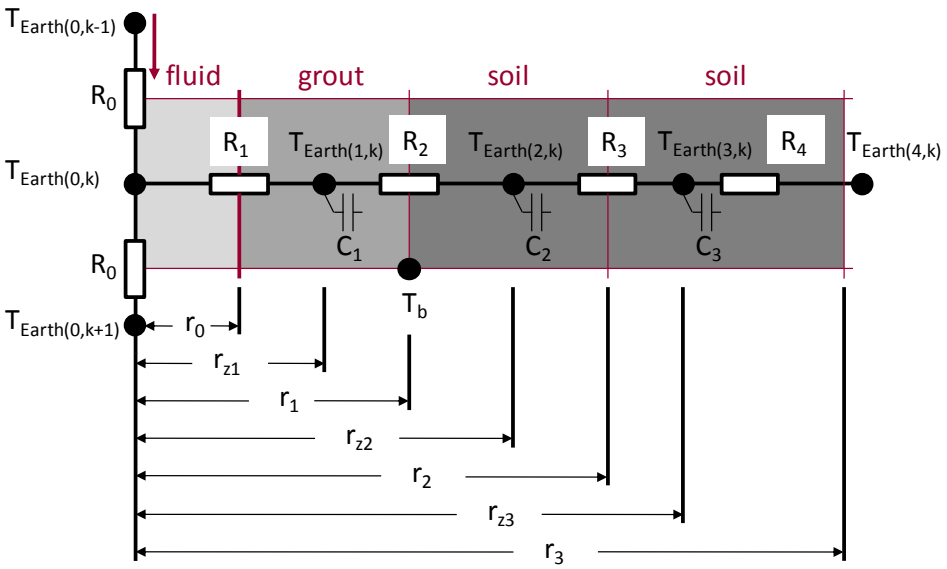

Figure 2.9 Diagram of different layers with variable distances in radial direction of the BHE.

$r_0 = D_{in}/2$ = inner radius of the pipes

$r_1 = D_b/2$ = radius of the borehole

$j \geq 2$:
$$r_j = r_{j-1} + (r_m - r_1)\frac{1-f}{1-f^{m-1}} f^{j-2} \tag{2.25}$$

where r_m is the maximum radius of the simulation area, and f is the grid factor which is defined as:

$$f = \frac{r_{j+1} - r_j}{r_j - r_{j-1}} \tag{2.26}$$

Applying the Crank-Nicholson scheme for discretization in time, Equation (2.24) can be re-written implicitly:

$$\begin{aligned} T_{n+1,j} - \frac{dt}{2}\frac{L_j}{C_j}\left(T_{n+1,j-1} - T_{n+1,j}\right) - \frac{dt}{2}\frac{L_{j+1}}{C_j}\left(T_{n+1,j+1} - T_{n+1,j}\right) \\ = T_{n,j} + \frac{dt}{2}\frac{L_j}{C_j}\left(T_{n,j-1} - T_{n,j}\right) \\ + \frac{dt}{2}\frac{L_{j+1}}{C_j}\left(T_{n,j+1} - T_{n,j}\right) \end{aligned} \tag{2.27}$$

where subscript n indicates the time coordinate and j indicates the radial coordinate. C is the capacity which is described below:

$$\begin{aligned} C_1 &= c_{p,grout}\rho_{grout}\pi(r_1^2 - 4r_0^2)dl \\ C_2 &= c_{p,soil}\rho_{soil}\pi(r_2^2 - r_1^2)dl \\ C_3 &= c_{p,soil}\rho_{soil}\pi(r_3^2 - r_2^2)dl \end{aligned} \quad \textbf{(2.28)}$$

L is the conductance, which is the reciprocal of a thermal resistance:

$$L = \frac{1}{R} = \frac{Q}{\Delta T} \quad \textbf{(2.29)}$$

And the thermal resistance of the grout and the ground are:

$$\begin{aligned} R_1 &= \frac{1}{4}\frac{1}{2\pi dl}\left(\frac{1}{\alpha r_0} + \frac{1}{k_{grout}} ln\frac{r_1 - r_{z1}}{r_0}\right) \\ R_2 &= \frac{1}{2\pi dl}\left(\frac{1}{k_{grout}} ln\frac{r_1}{r_{z1}} + \frac{1}{k_{soil}} ln\frac{r_{z2}}{r_1}\right) \\ R_3 &= \frac{1}{2\pi dl}\frac{1}{k_{soil}} ln\frac{r_{z3}}{r_{z2}} \\ R_4 &= \frac{1}{2\pi dl}\frac{1}{k_{soil}} ln\frac{r_3}{r_{z3}} \end{aligned} \quad \textbf{(2.30)}$$

In the vertical direction, the BHE is divided into layers with equal distance (Figure 2.10).

$$dl = \frac{borehole\ length}{DimAxi} \quad \textbf{(2.31)}$$

The fluid temperature is calculated from the energy balance from the upward and downward flowing fluid in each vertical layer. The temperature of the fluid is then used as the boundary condition for the simulation of the heat transfer in the radical direction from the fluid to the ground as described above.

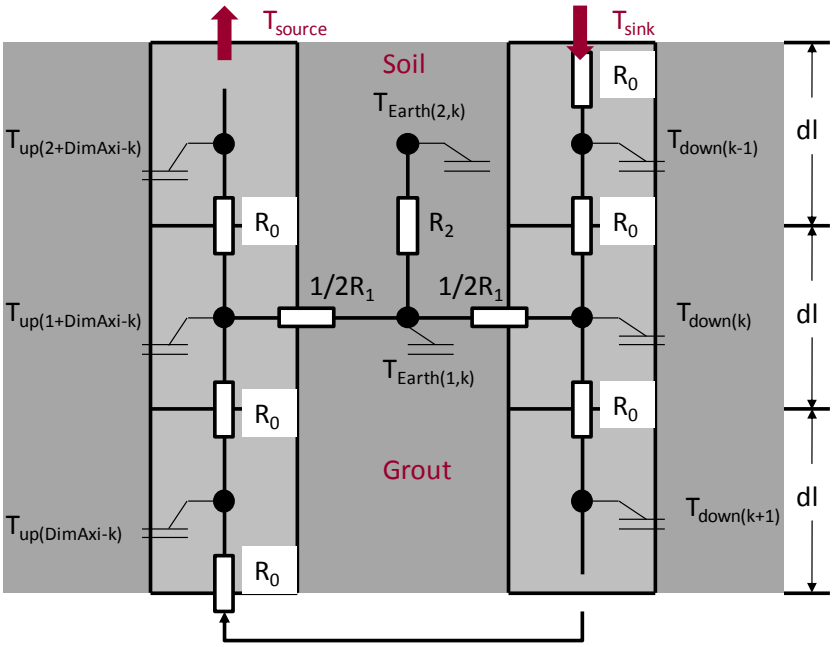

Figure 2.10 Diagram of different layers with equal distance in vertical direction of the BHE.

The energy balance for each element gives:

$$T_{down(k,n)} = T_{down(k,n-1)} + \left(T_{down(k-1,n)} - T_{down(k,n-1)}\right)\frac{L_0 dt}{mc_p} + \left(T_{Earth(k,n-1,1)} - T_{down(k,n-1)}\right)\frac{L_1 dt}{2mc_p} \quad \textbf{(2.32)}$$

and

$$T_{up(k,n)} = T_{up(k,n-1)} + \left(T_{up(k-1,n)} - T_{up(k,n-1)}\right)\frac{L_0 dt}{mc_p} + \left(T_{Earth(1+DimAxi-k,n-1,1)} - T_{up(k,n-1)}\right)\frac{L_1 dt}{2mc_p} \quad \textbf{(2.33)}$$

With the boundary condition

$$\begin{aligned} T_{down(0,n)} &= T_{sink} \\ T_{up(0,n)} &= T_{down(DimAxi,n)} \\ T_{source} &= T_{up(DimAxi,n)} \end{aligned} \quad \textbf{(2.34)}$$

Where L_0 is defined as:

$$L_0 = c_{p,f}\dot{m} = 2\pi r_0^2 v \rho_f c_{p,f} \quad \textbf{(2.35)}$$

By solving these equations in direction of the flow, the temperature of the fluid can be calculated.

With the pre-defined boundary for the simulation area, i.e. at a radius of about 2 meters around the borehole, the temperature profile at the outer boundaries can be calculated by superposing constant heat fluxes, starting at different time steps, using the analytical line source solution (Ingersoll et al., 1954). Figure 2.11 demonstrates the discretization process graphically.

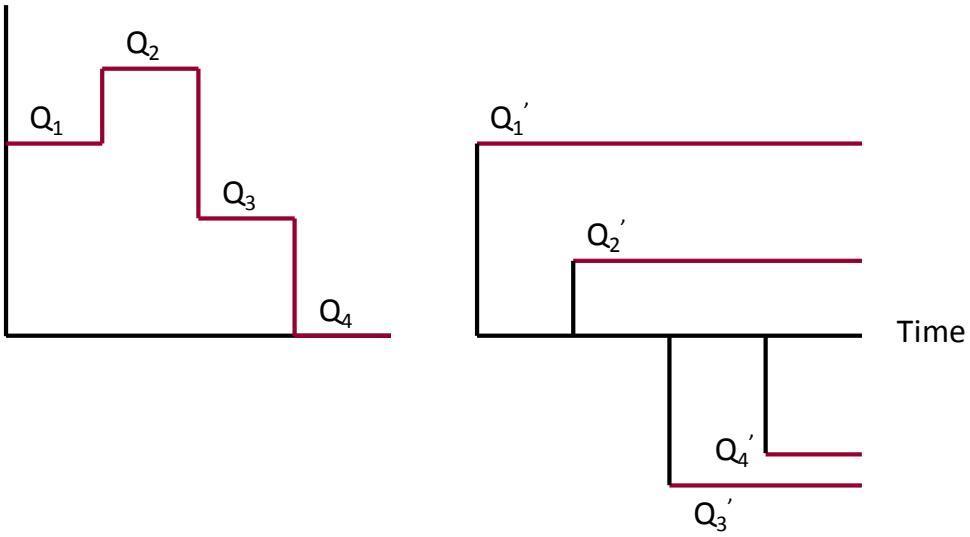

Figure 2.11 Discretization of variable heat flux in time series into constant heat fluxes starting at different time steps.

The temperature at the outer boundary of the simulation area is calculated for each vertical layer with its own specific heat flux. The outer boundary conditions are calculated weekly and then held constant during the whole week.

The EWS model can only simulate a single BHE. The end effect is neglected. The grout is regarded as one element.

2.4.2 MISOS Model

In order to improve the accuracy of the representation of borehole geometry in the EWS model (Wetter and Huber, 1997), Oppelt et al (2010) developed a new model called MISOS that allows a more detailed consideration of the grout. Instead of representing the grout using only one element, as shown in the EWS model in previous section, the MISOS model divides

the grout into three elements according to different temperature zones. Figure 2.12 illustrates the three divided elements of the grout of a BHE with double U-tubes. In the centre of the borehole lies the core element (Element 1), which encloses a quarter of the circumference of each tube. Assuming both inlet pipes are next to each other (on the left-hand side) and both outlet pipes are next to each other (on the right-hand side), the remaining grout enclosed within the borehole can be divided into two halves, which are called the semi-annulus element around the inlet tubes (Element 2) and the semi-annulus element around the outlet tubes (Element 3).

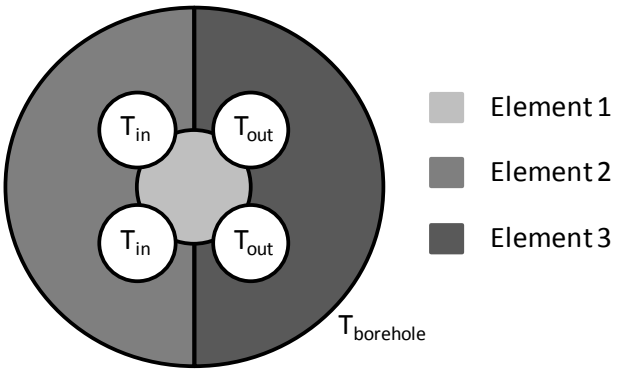

Figure 2.12 A diagram of three divided elements of the grout of a BHE with double U-tubes.

The MISOS model calculates the temperature of each element of the grout based on the energy balance of each element. For the calculation of the temperature distributions of the fluid inside the pipes and the ground surrounding the borehole, this model needs to be combined with the EWS model (Wetter and Huber, 1997).

BHEs with different distances between pipes were tested out using the combined MISOS model and EWS model. For example, pipes in the centre of the borehole (with no or minimum spacing), pipes against to the borehole wall (with maximum spacing) and pipes in the middle between the centre of the borehole and its wall (with equal spacing). Figure 2.12 shows a BHE with pipes of equal spacing. Results were then compared to those from a 3D CFD simulation carried out with ANSYS CFX. It was found that a very good agreement can obtained for BHEs with pipes of equal spacing from the combined model and CFX. For BHEs with pipes of minimum spacing, the temperature difference between the inlet and outlet fluid is slight over predicted (about 5%) by the combined model, when comparing to the simulation results from

CFD simulation. A maximum of 15% under prediction can be expected for BHEs with pipes of maximum spacing.

2.4.3 Capacity Resistance Model

The Capacity Resistance Model (CaRM) was developed by De Carli et al. (2010) by adopting the electrical analogy with lumped capacities and thermal resistances to simulate the thermal behaviour of BHEs.

The surrounding ground of the BHE is divided into a number of annular regions (n) in the radial direction and a number of slices (m) in the vertical direction. It is assumed that the heat transfer of the ground only exists in the radial direction and there is no heat flux in the vertical direction between layers. Therefore, the heat transfer of the ground can be considered as one-dimensional heat conduction problem in each layer.

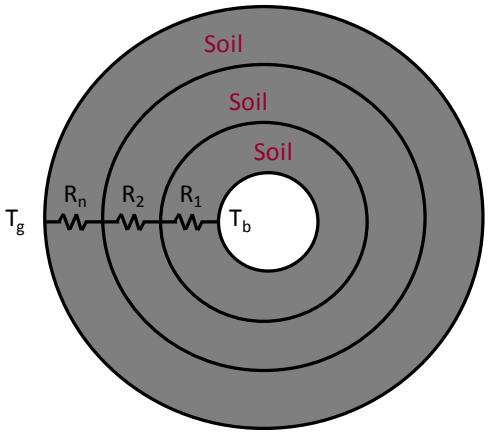

Figure 2.13 Diagram of heat transfer in the ground.

For each slice, the heat conduction equation can be written as:

$$\frac{T_{t,k,j-1} - T_{t,k,j}}{R_{k,j-1}} + \frac{T_{t,k,j+1} - T_{t,k,j}}{R_{k,j}} = \mathrm{C_{k,j}} \cdot \frac{T_{t,k,j} - T_{t-1,k,j}}{\Delta\tau} \qquad \textbf{(2.36)}$$

with the boundary condition: $T_{t,k,n} = T_g$; where $R_{k,j}$ is the thermal resistance between two adjacent annular regions , which can be calculated:

$$R_{k,j} = \frac{1}{2\pi L \cdot k} \ln \frac{\sqrt{(r_{k,j}^2 - r_{k,j-1}^2)/2}}{\sqrt{(r_{k,j-1}^2 - r_{k,j-2}^2)/2}} \qquad \textbf{(2.37)}$$

and $C_{k,j}$ is the thermal capacity, which can be calculated:

$$C_{k,j} = \rho c_p \cdot \pi \cdot (r_{k,j}^2 - r_{k,j-1}^2) \cdot \Delta z_k \qquad \textbf{(2.38)}$$

where r is the radius. The subscript k denotes the number of the slice at the vertical direction, j denotes the number of the annular region in the radial direction, and t denotes the number of time step.

Different arrangements of the pipes within the borehole can be simulated, i.e. single U-tube, double U-tubes and coaxial pipes. The equations of heat balance between the fluid and the borehole wall are described by thermal resistances between pipe and pipe and between pipe and borehole wall (Figure 2.14). The thermal resistances of the BHEs with different configurations can be represented in the CaRM model but need to be calculated from another finite element model.

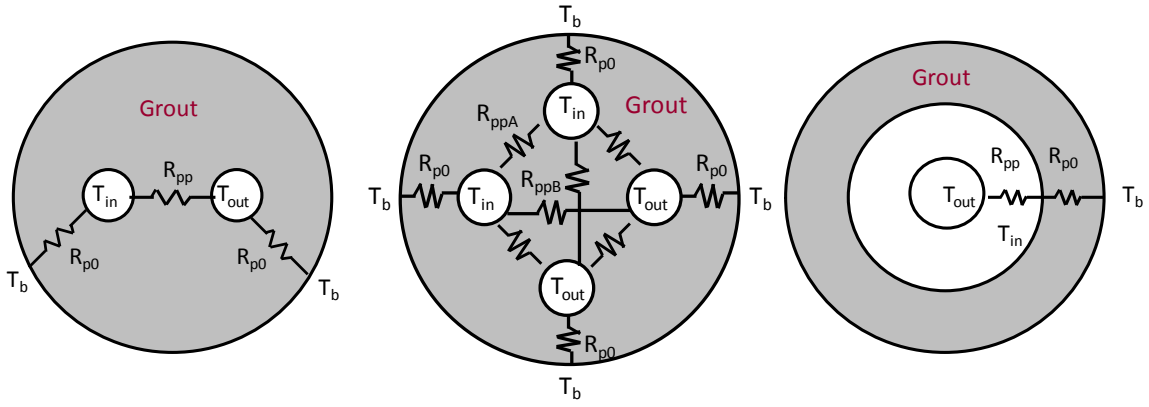

Figure 2.14 Borehole resistance of single U-tube, double U-tubes, and coaxial pipes.

Neglecting the fluid thermal capacity, the fluid temperature can be easily calculated from the energy balance inside each cell.

$$m_w c_{pw} \cdot [T_{w,in(k)} - T_{w,out(k)}] = 2\pi r_i \cdot h \cdot \Delta z_k [T_{w(k)} - T_{p(k)}] \qquad \textbf{(2.39)}$$

where *h* is the convective heat transfer coefficient, $T_{w,in(k)}$ is the fluid temperature entering the cell k, $T_{w,out(k)}$ is the fluid temperature leaving the cell k, $T_{w(k)}$ is the mean fluid temperature in the cell k, which is taken as the fluid temperature leaving the cell k. The error introduced by taking the fluid temperature leaving the cell k as the mean fluid temperature in the cell k is said to be limited, as the cell is small and the temperature difference between the fluid entering the cell and leaving the cell is limited.

Zarrela et al (2011) improved the model by taking into account the borehole thermal capacity, i.e. the thermal capacity of the circulating fluid and the thermal capacity of the grout. The

grout is divided into two zones, the core, which is the central zone between the pipes, and the shell, which is the external part between the pipes and the borehole wall (Figure 2.15). By adding the thermal capacities of the core zone and shell zone of the grout, the heat transfer within the borehole for a BHE with double U-tubes can be illustrated in Figure 2.16.

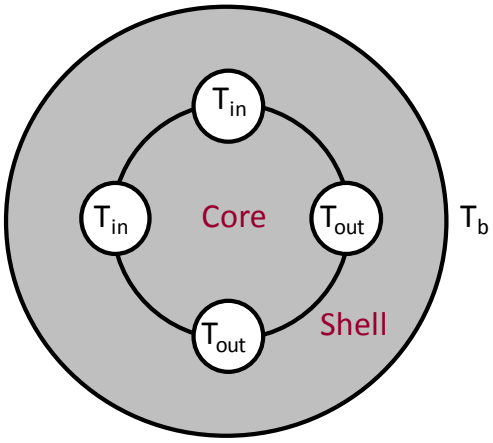

Figure 2.15 Diagram of divided two zones of the grout, the core and the shell.

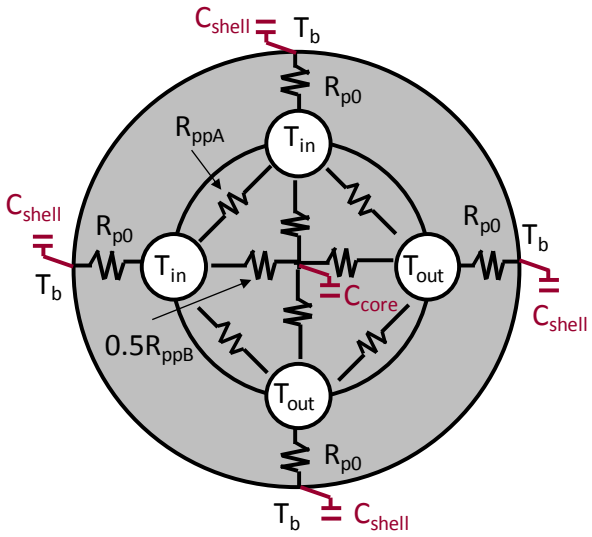

Figure 2.16 Borehole resistance and thermal capacity of BHE with double U-tubes.

Adding the thermal capacity of the fluid, Equation (2.39) can be re-written as:

$$m_w c_{pw} \cdot \left[T_{w,in(t,k)} - T_{w,out(t,k)}\right] - 2\pi r_i \cdot h \cdot \Delta z_k \left[T_{w(t,k)} - T_{p(t,k)}\right] = \rho_w c_{pw} \cdot \pi r_{p,k}^2 \cdot \Delta z_k \cdot \frac{T_{w(t,k)} - T_{w(t-1,k)}}{\Delta \tau} \quad \textbf{(2.40)}$$

The heat transfer rate of the circulating fluid due to the temperature variation along the pipe loop can be calculated by:

$$q = \rho_w c_{pw} \cdot \pi r_p^2 \cdot L \cdot \frac{T_{w(t)} - T_{w(t-1)}}{\frac{L}{v_w}} \quad \textbf{(2.41)}$$

where L is the length of the pipe loop and v_w is the circulating fluid velocity. The ration L/v_w is the circulation time of the fluid.

It is important to take into account this heat transfer rate when simulation time step is shorter than the circulation time. Measurement data from a ground thermal response test were used to verifying the CaRM model and the improved CaRM model. This improvement was proved to be able to predict more realistic temperature response of the fluid than the model of its original form when the simulations run at short time step, i.e. 60 s. The errors introduced by neglecting the thermal capacity of the grout in short time step simulations were also highlighted.

2.4.4 Finite Element Model

Al-Khoury *et al.* developed a three-dimensional finite element model to simulate a BHE with single or double U-tubes for steady state and transient heat flow (Al-Khoury *et al.*, 2005, Al-Khoury and Bonnier, 2006). This model used two types of elements: a one-dimensional heat pipe element along the depth of the borehole to simulate a pseudo three-dimensional heat flow within the borehole, and a three-dimensional element to model coupled heat and groundwater flow surrounding the borehole.

Figure 2.17 shows the schematic heat flow in a borehole heat exchanger with a single U-tube for Al-Khoury's model. Within the borehole, three components were taken into account, one pipe in, one pipe out, and grout. Energy conservation equations were used to formulate the heat transfer processes within the borehole. Considering a control volume of BHE with a finite length dz, the net energy flow into each component must equal to the increase in the amount of energy stored in that component. The heat transfer processes of the ground, therefore, can be coupled with the heat transfer processes within the borehole via the heat transfer across the borehole wall.

The finite element method was applied to solve the partial differential equation of heat conduction and convection which describes the heat transfer processes of the ground. A sequential numerical algorithm was adopted to solve the two non-linear systems of equations generated due to the coupling of the one-dimensional heat pipe element and the three-dimensional ground element.

Using a one-dimensional representation of heat flow within the borehole instead of a three-dimensional full discretisation allows a spatial discretisation of the surrounding ground. As a result, the size of the mesh required for simulating the BHE reduces significantly which

according to the authors, makes the solution much more efficient. However, the one-dimensional representation of heat flow within the borehole neglects the thermal mass of the pipes and assumes a uniform temperature distribution in the grout. Although this assumption is reasonable considering the ratio of the borehole diameter and borehole depth is under 1/500 (extremely slender), the solution is not accurate enough and is insufficient for transient computations.

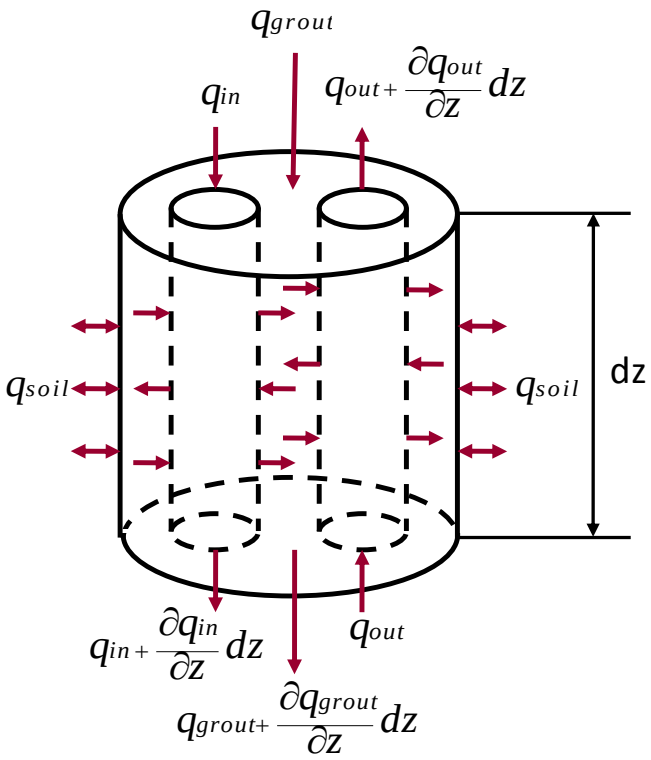

Figure 2.17 Schematic heat flow in a BHE with a single U-tube for Al-Khoury's model (Al-Khoury et al., 2005).

Diersch et al. (2011a, 2011b) extended Al-Khoury's model (Al-Khoury et al., 2005, Al-Khoury and Bonnier, 2006) by using multiple grout points in single and double U-tube BHEs and including coaxial pipe configurations. The improved thermal resistance and capacity model (TRCM) approach was adopted to simulate the transfer within the borehole, i.e. fluid to grout and grout to borehole. Instead of only using one single capacity point for the grout (Al-Khoury et al., 2005, Al-Khoury and Bonnier, 2006), this model divides the grout into different zones according to the number of pipes within the borehole. For instance, for BHEs with single U-tub (two pipes), the grout is divided into two zones and for BHEs with double U-tube (four pipes),

the grout is divided into four zones (Figure 2.18 and Figure 2.19). Consequently, the capacity of each zone of the grout can be taken into account. By using more than a single capacity point for the grout, the heat transfer within the borehole can be modelled more accurately.

Due to the differences in the separated zones of the grout, the thermal resistances for different types of BHEs are also different. The detailed presentation of the thermal resistances and capacities for BHEs with different tube arrangements are shown in Figure 2.18 - Figure 2.21.

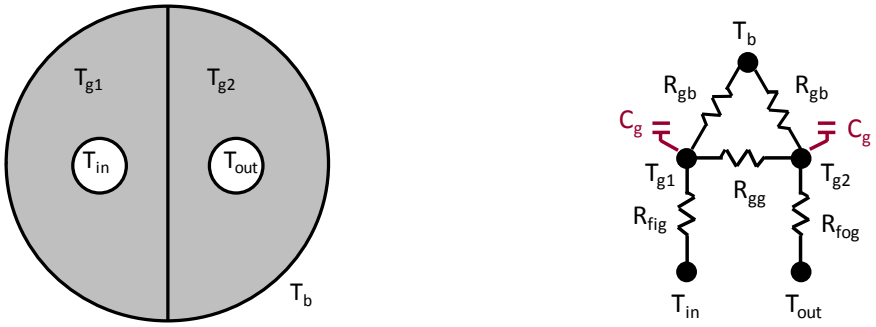

Figure 2.18 Two divided zones of the grout for single U-tube and the representation of thermal resistances and thermal capacities (Diersch et al., 2011a).

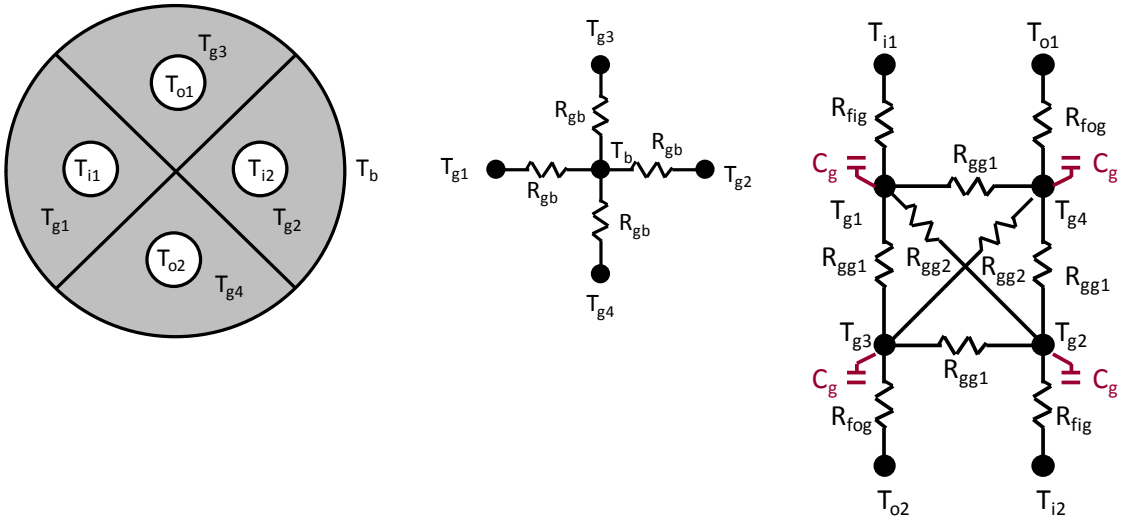

Figure 2.19 Four divided zones of grout for double U-tubes and the representation of thermal resistances and thermal capacities (Diersch et al., 2011a).

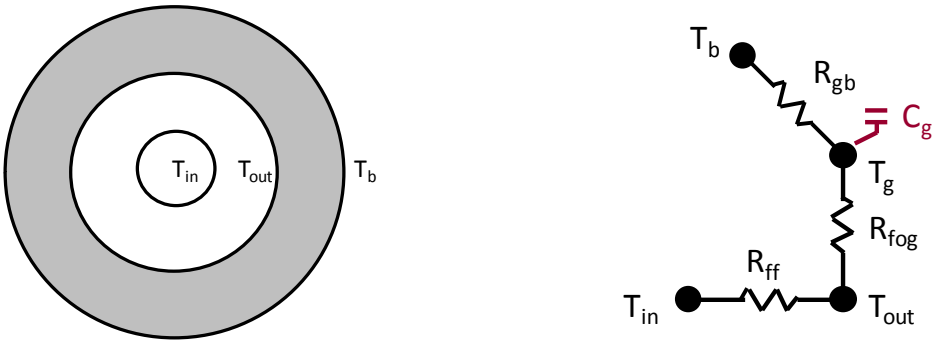

Figure 2.20 One zone of grout for coaxial pipes with centred inlet, and the representation of thermal resistances and thermal capacities (Diersch et al., 2011a).

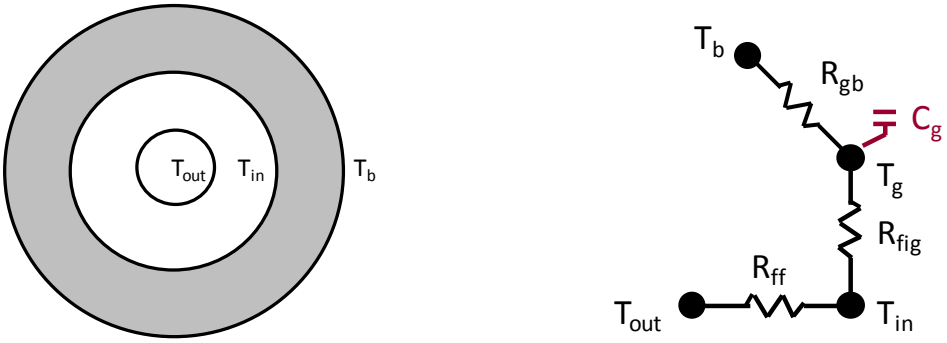

Figure 2.21 One zone of grout for coaxial pipes with annular inlet, and the representation of thermal resistances and thermal capacities (Diersch et al., 2011a).

Diersch et al. (2011a, 2011b) implemented this solution and the analytical line source solution (Eskilson, 1987) in the FEFLOW solver (DHI-WASY, 2010). A direct and non-sequential coupling strategy was developed for the numerical model, which reduces the mesh dependency, especially for the ground elements close to the borehole.

In the study carried out by Diersch et al (2011b), both the analytical and numerical approaches were applied to simulate a single BHE for both short-term and long-term period. The results have been compared to a fully discretized 3D model. A good agreement was found between different solutions. The numerical solution was proved to be more accurate for both short-term and long-term simulations, while the analytical solution was highly efficient, precise and robust, although might not be applicable for short term simulations.

For simulating the arrays of BHEs, a module using FEFLOW's open programming interface IFM were developed for thermally interacting BHEs. This module also allows the coupling between the FEFLOW and TRNSYS to carry out systematic simulations with BHEs. A real-site borehole

field with 80 BHEs in Germany was simulated and the results indicated groundwater flow in that regime can affect efficiency and reliability of the system.

2.5 Summary

This chapter has provided an overview of literature regarding BHEs models. These models have been reviewed according to four categories: (I) analytical models; (II) steady state borehole models; (III) response factor models; (IV) discretised numerical models.

Analytical models have been developed by making a number of simplifying assumptions and applied to both the design of BHEs and analysis of in situ test data. One of the most common assumptions is ignoring the geometry and thermal capacity of the components in the borehole. Analytical models, therefore, are not suitable for short timescale applications where the transient heat transfer within the borehole can dominate the heat transfer process. The other common assumption is to consider the borehole to be infinitely long. The heat transfer below the BHEs, as a result, cannot be taken into account. This assumption makes analytical models unsuitable for multi-annual simulations either. For simulations over 5-10 years, the heat transfer through the bottom of the BHEs in large arrays accounts for a high percentage over the total heat transfer rate. Ignoring the end effect will result an inaccurate representation of BHEs.

Although analytical solutions require less computing effort, they are less suited to design and simulation tasks where one would like to take account of time varying heat transfer rates and the influence of surrounding boreholes on long timescales. A number of approaches that have combined analytical and numerical methods have been developed with design tasks in mind, e.g. Eskilson' g-function model. Heat transfer within a borehole was not represented explicitly but instead a thermal resistance was used to define the relationship between the fluid and borehole wall temperatures. The thermal mass of the fluid, pipes and grout were neglected. Response to heat flux over timescales of approximately 1 month to more than 10 years were derived from application of the model and integration of the response according to the number of boreholes and the relationship to those neighbouring. The responses were normalized and can be applied to ranges of BHE configurations.

Application of models for system simulation tasks – unlike design tasks – requires the ability to operate at much shorter timescales than 1 month. Yavuzturk extended Eskilson's g-function

model to short timescales, between $2\,{}^{1}/_{2}$ minutes and 200 hours for typical ratios of borehole radius to borehole depth, through applying a two-dimensional numerical model to discretise the material inside the borehole so that the thermal mass of the pipes and grout can be taken into account.

Two-dimensional discretised models provide detailed representation of the borehole geometry and allow the thermal properties of pipes and grout to be considered precisely. However, as variation in fluid temperature with depth cannot be simulated explicitly, assumptions have to be made about the fluid temperatures in the two pipes and the associated boundary conditions.

Three-dimensional discretised models, on the other hand, can avoid these assumptions. Several three-dimensional discretised models were developed to offer a more general and more accurate representation of heat transfer of BHEs, for example, Wetter and Huber's EWS model, De Carli et al.'s capacity resistance model, Al-Khoury's finite element model and its further extended version by Diersch et al. All these models were developed using the 'de-coupling and coupling' approach. The heat transfer within the borehole and the heat transfer of the ground surrounding the borehole were described separately using different models. While it is easy and straight forward to have a three-dimensional discretised model to simulate the heat transfer of the surrounding ground, some simplifications were made for the heat transfer within the borehole so that a one-dimensional model can be used. These two models were then coupled, using the temperatures of the borehole wall obtained from the model that describes the heat transfer within the borehole as the boundary condition for the model to simulate the surrounding ground, and solved simultaneously. Doing this allows a spatial discretisation of the surrounding ground and reduces the size of the mesh required for simulating the BHE. The solution, as a result, is more efficient and more practical for design and simulation purposes.

Several advantages of a three-dimensional model for BHEs can be found, including: i) fluid transport along the pipe loop can be represented; ii) fluid, borehole and ground temperature variation along the borehole depth can be modelled; iii) different layers of rock and soil can be explicitly represented; iv) climate dependent boundary conditions at the surface can be

applied; v) initial vertical ground temperature gradients can be imposed; vi) heat transfer below the borehole can be explicitly considered.

In this study, a fully-discretised three-dimensional model for BHEs has been developed with the purposes:

- Investigate the effects of the dynamics of the fluid transport along the pipe loop;
- Study the three-dimensional characteristics of heat transfer around a BHE;
- Develop insight into the limitations of two-dimensional models and suggest ways in which they can be improved;
- Examine the significance of applying a dynamic BHE model on domestic GSHP systems;
- Investigate the thermal interferences of multiple BHEs with different configurations;
- Evaluate the accuracy of applying line source model in the analysis of thermal response tests

In the next chapter, the development of the 3D numerical model is presented. The finite volume method applied to the model development is introduced. The validations of the model against analytical models and experimental data are demonstrated.

Chapter 3 Model Development and Validation

In this chapter, a three-dimensional (3D) model for Borehole Heat Exchangers (BHEs) and arrays has been proposed. The intention is to model the BHEs explicitly using the least possible assumptions. The aims of the model development are to investigate the three-dimensional effects on the model predictions and their implications on system simulations. In order to highlight the effects caused purely by three dimensional modelling, a two-dimensional (2D) model has been implemented using the same numerical method. This 2D model necessarily employed some of the assumptions that are generally applied to all 2D models, but can be avoided in a 3D model. Comparing the simulation results obtained from the 3D and 2D models under the same testing conditions allows the three dimensional effects to be identified and quantified.

One important feature of the 3D model is the simulation of the circulating fluid flow along the pipe loop. By taking into account the transit time of the fluid travelling in the pipe and the thermal capacity of the fluid, this 3D model is expected to be more accurate and realistic than those models that do not simulate the fluid transport, for example, all 2D models. The ground underneath the BHEs is also simulated, allowing the heat transfer below to be explicitly considered. Other advantages of the 3D model include: i) temperature variation along the depth of the borehole can be modelled; ii) different layers of rock and soil can be represented; iii) climate dependent boundary conditions at the ground surface can be applied; iv) initial vertical ground temperature gradients can be imposed.

The validations of the models are presented at the last section of this chapter. The thermal resistances of a single BHE calculated by the 2D model are compared to a highly accurate analytical solution, with various configurations and thermal properties. The characteristics of the fluid transport in the 3D model are validated against a widely used analytical solution for fluid transport. Both the 3D and 2D models are further validated against to the experimental data obtained from the testing facility at Oklahoma State University.

3.1 Model Development

Model developments for BHEs have been reviewed in Chapter 2. Analytical models have been developed with tasks of designing BHEs and analyzing in situ thermal response test data in mind. The geometry and thermal capacity of the components in the borehole are neglected.

They require less computing effort but are less suited to design and simulation tasks where time varying heat transfer rates and the influence of surrounding boreholes over long timescales need to be considered. A number of approaches that have combined analytical and numerical methods have been developed to be better suited for the design task. Application of models for system simulation task also requires the ability to operate over short timescales. Furthermore, the geometry and thermal capacity of the components in the borehole need to be taken into account.

Discretising the geometry and material inside and outside the borehole has been proved to be an effective and accurate method that can explicitly simulate the complex geometry of BHEs and the thermal capacities of all BHE components – fluid, pipes, grout and ground. This approach has been applied widely in recent development of BHE models, both 2D and 3D. Although 2D discretised numerical models are much more efficient in computation, 3D discretised numerical models offer a more general and accurate representation of the heat transfer processes.

A dynamic 3D numerical model of BHEs is developed, built upon a finite volume solver known as GEMS3D (General Elliptical Multi-block Solver in 3 Dimensions), which is an in-house code that has been implemented in Fortran 90. The GEMS3D solver has been used to model ground heat exchanger problems in a number of earlier projects and further details are given in Rees et al. (2002, 2004). This solver applies the finite volume method (Patankar, 1980) to solve the partial differential advection-diffusion equation for heat transfer on 3D boundary fitted grids.

Due to the symmetrical geometry of a BHE, only half of the borehole is modelled in the initial development of a single BHE. Figure 3.1 shows a representation of the numerical simulation domain of half a BHE with a diameter of 150 mm and a depth of 100 m. The simulation domain extends 20x20x200m. The Cartesian coordinate system and multi-block boundary fitted mesh are applied to discretise the simulation domain, by which the complex geometry of BHEs can be modelled explicitly. A number of blocks of cells are assigned to simulate different materials, e.g. fluid, pipe, grout, and ground. The thermal properties or velocities of each material are specified according to the corresponding block.

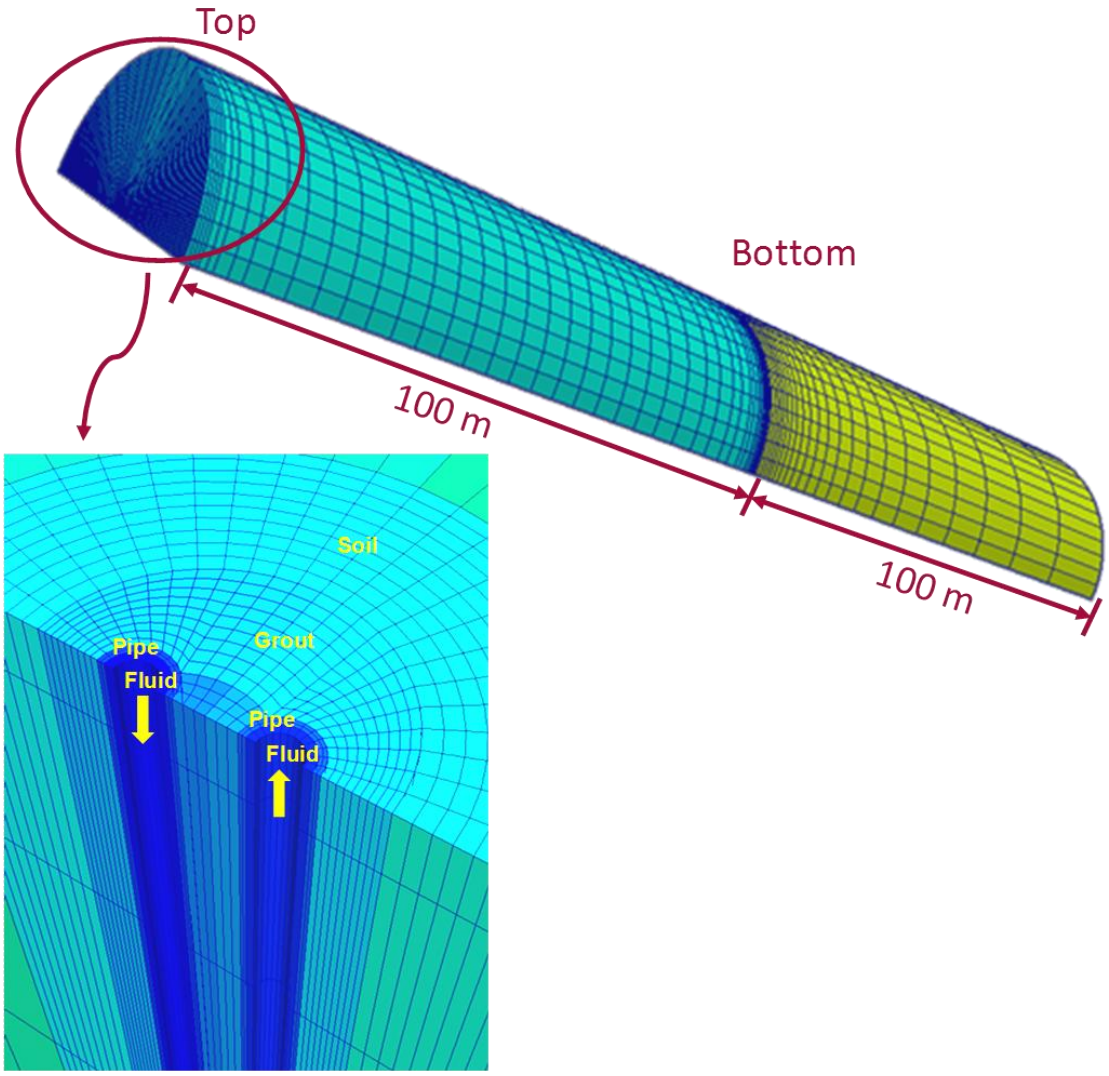

Figure 3.1 A representation of the numerical simulation domain of half a BHE (20x20x200m).

3.1.1 Finite Volume Method

The finite volume method starts from the integral form of the partial differential equation for the generic advection-diffusion equation:

$$\frac{\partial}{\partial t}\int_{V} T d\mathbf{V} + \int_{S} \rho T \mathbf{v}\cdot\mathbf{n} d\mathbf{S} = \int_{S} \Gamma \nabla T \cdot \mathbf{n} d\mathbf{S} \qquad (3.1)$$

The advection flux term in discrete form is the sum of the advection fluxes through each cell face:

$$\int_S \rho T \mathbf{v} \cdot \mathbf{n} d\mathbf{S} \approx \sum_i F_i^C \quad \textbf{(3.2)}$$

where i = n,s,w,e,t,b for a 3D cell. If the advection flux on a particular face of a prototype cell is considered, for example, the east face, then:

$$F_e^C = (\rho T \mathbf{v} \cdot \mathbf{n})_e S_e \quad \textbf{(3.3)}$$

where S_e is the surface area of the east face. This assumes that the value of the temperature T at the face can be approximated by the value at the centroid (midpoint) of the face. The same assumption applies to the velocity v. Each component of the velocity vector makes a contribution to the advection flux passing through the cell face.

In this 3D model, the advection flux term is only used for simulating the fluid flows in the pipes and only the velocity at the z direction along the depth of the borehole is specified. The advection flux term can be extended to simulate the ground water flow by specifying the Darcy velocities at the x,y, and z directions.

In the same way as the advection flux, assuming that the value of the temperature T on a particular face is well represented by the value at the centroids, for the east face, the diffusion heat flux can be expressed as:

$$F_e^D = \int_{S_e} \Gamma \nabla T \cdot \mathbf{n} d\mathbf{S} \approx (\Gamma \nabla T \cdot \mathbf{n})_e S_e \quad \textbf{(3.4)}$$

The main task is to calculate the gradient of the temperature (∇T) at each cell face. Local coordinates at each cell face can be defined (Figure 3.2). The coordinate *n* is defined in the direction normal to the face at its centroids, and the coordinate ξ is defined on the line between neighbouring centroids which passes through the face at point *e'*.

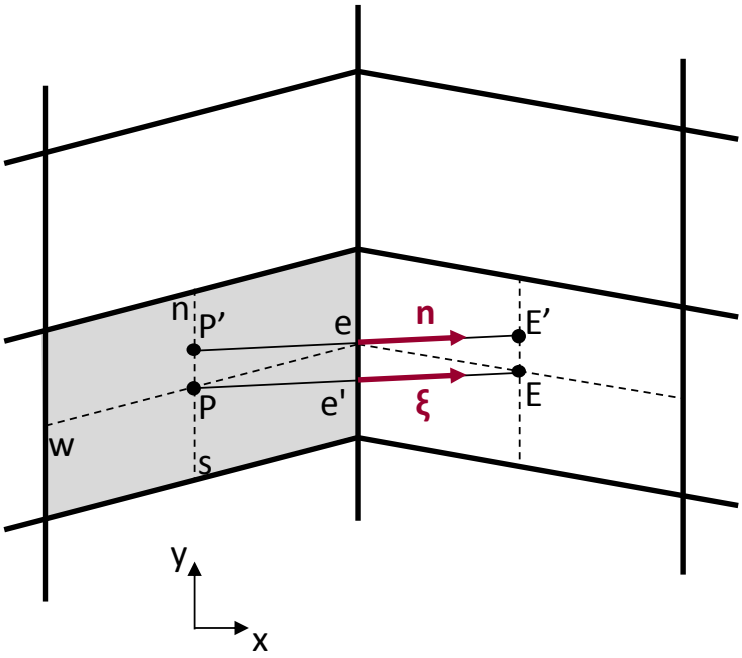

Figure 3.2 An diagram for the definition of local coordinates at the cell face.

In order to calculate the gradient of the variable at the cell face, the values of the variable at the cell centroids are used as they are calculated implicitly. The gradient is calculated using the values at T_P and T_E and the distance between these points, $L_{P,E}$. In this case $F_e^D \approx \Gamma_e S_e (\partial T/\partial \xi)_{e'}$, this is only accurate if the grid is orthogonal. In order to preserve second order accuracy, the calculation of the gradient along the normal to the face and at the centroids of the face is made by using the values of the temperature at points P' and E'. However, the values of the temperature are not calculated implicitly; instead, a 'deferred correction' approach is used to calculating the flux as follows:

$$F_e^D = \Gamma_e S_e \left(\frac{\partial T}{\partial \xi}\right)_{e'} + \Gamma_e S_e [\left(\frac{\partial T}{\partial n}\right)_e - \left(\frac{\partial T}{\partial \xi}\right)_{e'}]^{old} \quad \textbf{(3.5)}$$

where the central differencing is used to get the gradients:

$$\left(\frac{\partial T}{\partial \xi}\right)_{e'} = \frac{(T_E - T_P)}{L_{P,E}} \quad \text{and} \quad \left(\frac{\partial T}{\partial n}\right)_e = \frac{(T_{E'} - T_{P'})}{L_{P',E'}} \quad \textbf{(3.6)}$$

The terms in the square brackets on the right of Equation (3.5) are calculated explicitly, i.e. using the previous values of the variable. As the solution approaches convergence, the terms $(\partial T/\partial \xi)_{e\prime}$ and $(\partial T/\partial \xi)_{e\prime}^{old}$ cancel out.

Finally the discrete equation can be written as:

$$F_e^D = \Gamma_e S_e \frac{(T_E - T_P)}{L_{P,E}} + \Gamma_e S_e [\frac{(T_{E\prime} - T_{P\prime})}{L_{P\prime,E\prime}} - \frac{(T_E - T_P)}{L_{P,E}}]^{old} \quad \textbf{(3.7)}$$

where the right hand terms are calculated as a deferred correction. If the grid is orthogonal then this deferred correction becomes zero and this equation becomes equivalent to that for orthogonal grids.

3.1.2 Mesh Generation

Three-dimensional multi-block boundary fitted structured meshes for BHEs are generated using an in-house developed program. After defining the edges by a sequence of lines and arcs, a 2D mesh is first generated in Cartesian coordinate before being extruded in the Z direction. The number of cells in each block can be specified individually to allow for flexible control of cell distribution. The cells can either be distributed equally or exponentially. In this way, more cells can be included in places where greater temperature gradients are expected, e.g. close to the borehole wall, and less cells where temperature gradients are smaller, e.g. far away from the borehole. Moreover, using multi-block boundary fitted structured meshes enables good control of the orthogonality of the cells. For a single BHE, only half of it is meshed due to the symmetry of the borehole. Figure 3.3 shows a half cross-section of a BHE.

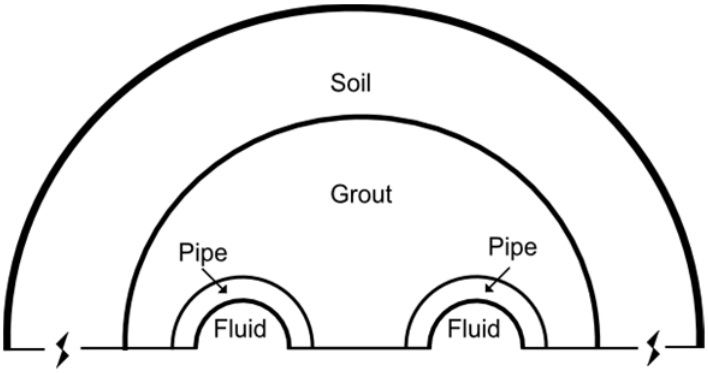

Figure 3.3 A half cross-section of a BHE.

The multi-block structured mesh creates a discrete representation of the geometric domain of BHEs. Figure 3.4 shows the discrete representation of half of a borehole by the multi-block structured boundary-fitted mesh.

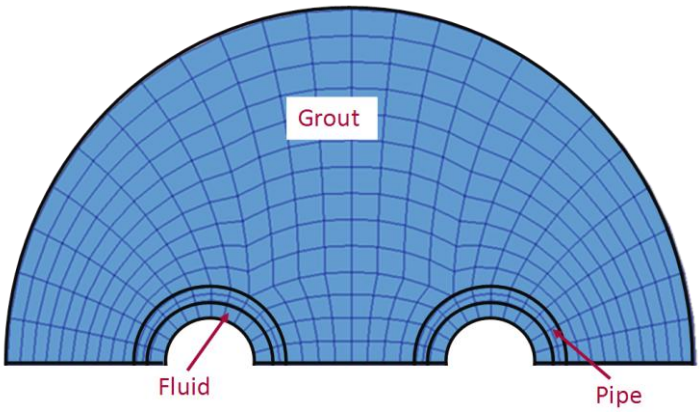

Figure 3.4 A horizontal cross-section of the multi-block structured boundary-fitted mesh representing half a borehole (344 cells).

The downward and upward fluid flow domains are represented by semi-cylindrical blocks with a single layer of cells. Two pipes are represented by semi-cylindrical blocks with two layers of cells, adjacent to the fluid blocks. And the grout is represented by a block enclosed by half of the borehole wall. In this way, the complex geometry of the BHE can be modelled explicitly and accurately. The thermal properties of the materials, e.g. fluid, pipe and grout, and the fluid velocity, can be assigned to the corresponding blocks. By adjusting the number of cells in each block a coarser or a finer mesh can be easily obtained. Figure 3.5 shows a finer mesh with 1232 cells on a horizontal plan. Equally distributed cells are constructed in each block.

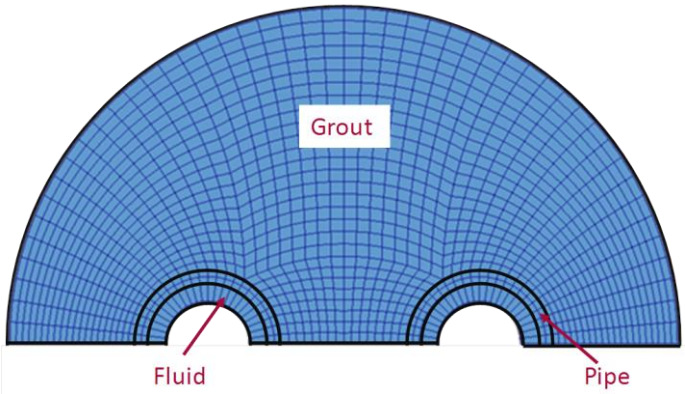

Figure 3.5 Mesh for half a borehole in a horizontal plan (1232 cells).

Figure 3.6 shows an additional block representing the surrounding ground adjacent to the grout block where exponential distributed cells have been added. More cells are pushed near to the borehole where the temperature gradient is expected to be greater while fewer cells near the outer boundary of the simulation domain where the temperature gradient is expected to be smaller.

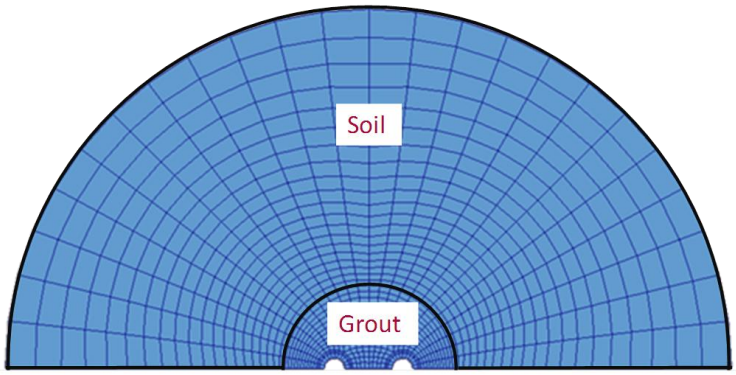

Figure 3.6 Mesh for half a BHE including ground in a horizontal plan.

To represent a BHE in three dimensions, the mesh is essentially extruded in the third dimension (z) along the depth of the borehole. In this dimension, the mesh can be divided into a number of layers and the distance between each layer can vary. In general, more cells are included at the top and at the bottom of the BHE where temperature gradients are usually larger and less cells in the middle of the BHE due to smaller temperature gradients. Additional blocks are added to the bottom, to allow the region below the borehole to be simulated.

3.1.3 Simplifications of the Fluid

Although multi-block boundary-fitted structured meshes enable detailed representation of the geometry of the borehole in the Cartesian coordinate system, special adjustment needs to be made to allow for the orthogonal representation of the fluid. Figure 3.7 shows the simplified representation of the fluid. The shaded area is used to represent all the fluid contained within half of a pipe. One layer of cells is used to represent the fluid.

The mesh is constructed so that the cell area is half that of the half pipe. The density of the fluid in each cell has to be correspondingly double in order to take into account the total fluid thermal capacity.

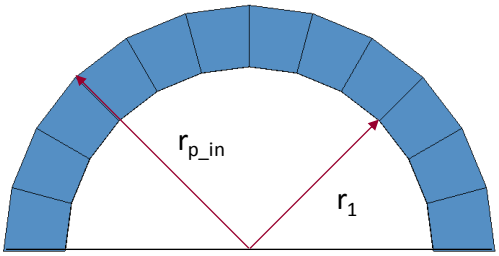

Figure 3.7 The simplified representation of the fluid contained within half of a pipe (cross section).

The discretisation along the depth of the borehole allows for fluid velocity to be imposed in the layer of cells that are used to represent the fluid inside the pipe. The fluid flow inside the whole pipe is considered as fully developed turbulent flow. The transport of heat from one cell to the next one along the pipe can be represented by an advection flux term in the advection-diffusion pde (Equation (3.1)). Each cell can be considered as a well-mixed node that is defined by a single temperature, and is transported at a uniform velocity. Figure 3.8 demonstrate the diagram of modelling fluid transport along the pipe loop.

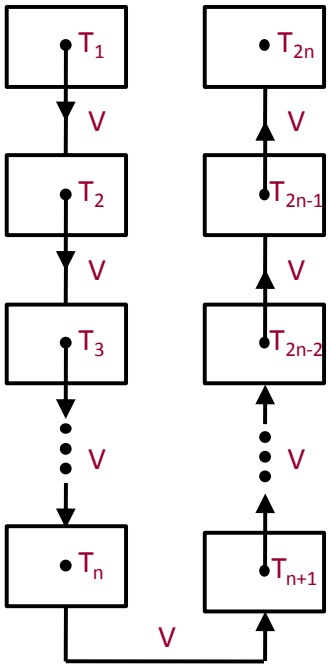

Figure 3.8 A diagram of modelling fluid transport along the pipe loop.

Simultaneously, in the horizontal direction, there is convection heat transfer between the fluid and inner surface of the pipe wall. The convective heat flux of this process can be calculated by:

$$q_{conv} = h(T_f - T_{p\_s}) \quad \textbf{(3.8)}$$

where h is the convection heat transfer coefficient (W/m^2.k), T_f is the fluid temperature (°C), and T_{p_s} and the surface temperature of the inner pipe wall (°C).

The convection coefficient is related to the Nusselt number according to Equation (3.9):

$$Nu = \frac{hD}{k} \quad \textbf{(3.9)}$$

where Nu is the dimensionless Nusselt number, D is the diameter of the pipe (m), and k is the thermal conductivity of the fluid (W/m.K).

The Nusselt can be calculated by the Dittus-Boelter equation (Equation (3.10)).

$$Nu = 0.023Re^{4/5}Pr^n \quad \textbf{(3.10)}$$

where n = 0.4 for heating and 0.3 for cooling. Pr is the Prandtl number. Re is the Reynolds number and can be calculated by:

$$Re = \frac{4m}{\pi D\mu} \quad \textbf{(3.11)}$$

where m is the mass flow rate (kg/s), D is the pipe diameter (m) and μ is the viscosity (kg/s.m).

Rearranging Equation (3.9) and substituting the Nusselt number with Equation (3.10), the convection heat transfer coefficient can be expressed as:

$$h = \frac{0.023Re^{4/5}Pr^n \cdot k}{D} \quad \textbf{(3.12)}$$

In order to incorporate the convection heat transfer between the fluid and the inner pipe wall into the general convective-diffusive pde (Equation (3.1)), an effective conductivity has to be derived to allow the equation to be used to describe the convection heat transfer process.

Figure 3.9 shows a diagram for the heat transfer process between the fluid and the pipe. The surface AB represents the inner pipe wall.

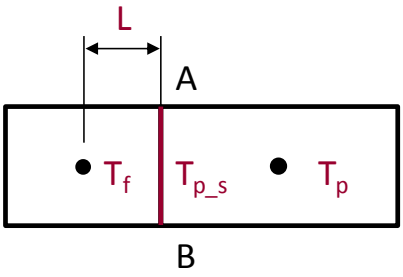

Figure 3.9 A diagram for the heat transfer process between the fluid and pipe.

Assuming the heat transfer process between the fluid and the inner pipe wall is conduction heat transfer, the conductive heat flux of this process can be calculated by:

$$q_{cond} = \frac{k_{eff}(T_f - T_{ps})}{L} \tag{3.13}$$

where k_{eff} is the effective conductivity (W/m.K), and L is the distance between the fluid cell and inner pipe wall.

Since both Equation (3.8) and (3.13) are describing the same heat transfer process, the conductive heat flux should be equal to the convective heat flux. Rearranging Equation (3.8) (3.9)and (3.13), the effective conductivity can be written as:

$$k_{eff} = h \cdot L \tag{3.14}$$

The conductivity of the fluid cell can then be adjusted using this effective conductivity.

3.1.4 Boundary Conditions

Different types of boundary conditions can be applied to the whole boundary of the simulation domain. These boundary conditions can be classified according to three basic types:

1. Dirichlet boundary conditions, or constant temperature boundary conditions, where the constant temperature is specified ($T = T_B$).
2. Neumann boundary conditions, or constant heat flux boundary conditions, where the constant heat flux is specified ($T = \frac{\partial T}{\partial n}\Big|_B$).
3. Robins boundary conditions, or mixed boundary conditions, where the relationship between the temperature and the heat flux is specified ($k\frac{\partial T}{\partial n}\Big|_B = h(T_\infty - T_B)$).

The default boundary condition is zero heat flux (adiabatic surface), where $\left.\frac{\partial T}{\partial n}\right|_B = 0$ is specified on the boundary.

The undisturbed ground temperature is normally assigned to each cell of the semi-circular simulation domain as the initial temperature when the simulation starts. A zero heat flux boundary condition is assigned to the symmetry plane and the top and bottom surfaces. Either a constant far-field temperature or a zero heat flux condition can be assigned to the outer boundary of the simulation domain. The simulation domain needs to be large enough to allow for boundary conditions to be specified to the outer boundary of the simulation domain which should not have any influence on the simulation results over the simulation period. Therefore, if a constant far-field temperature condition is specified on the outer boundary, the boundary temperature should be monitored and there should be no heat flux across this boundary. If a zero heat flux condition is specified on the outer boundary, the temperature of the outer surface should not change but remain at the far-field temperature at the end of the simulation.

In the 3D model, the circulating fluid along the pipe loop is modelled explicitly. Therefore, the inlet temperature of the fluid is assigned to the top surface of the block which represents the inlet (downward flow).

3.1.5 Implementation of a 2D Model

A 2D model (equivalent to the 3D model of one metre depth and adiabatic upper and lower surfaces) was implemented precisely using the same numerical method. The fluid transport is not explicitly modelled; instead, the heat transfer from the fluid is treated by a mixed boundary condition at the pipe walls. This model was initially used in this study to highlight the differences between model predictions that are due solely to three-dimensional effects and dynamic fluid transport, which cannot be simulated by 2D models. Improvements to this model, based on the findings of the differences between the 3D and 2D models, are described later in Chapter 5.

This two-dimensional model necessarily employs some of the simplifications that have been made by other two-dimensional models.

- The ground is assumed to be homogeneous along the depth of the borehole;
- The heat transfer at the ground surface and the end of the borehole is neglected;

- The dynamic fluid transport along the pipe loop and the thermal mass of the fluid are neglected;
- The temperatures and fluxes of the pipes along the depth of the borehole are assumed to be uniform.

The mesh in this initial 2D model is similar to that of the 3D model but is one cell deep and does not include the layer (block) of cells representing the fluid. One important issue in defining a two-dimensional model is to relate the model boundary conditions to the inlet and outlet fluid temperatures. One common approach is to use a mixed boundary condition to take into account of the convection between the fluid and the pipe surface. One pipe of the model is assumed to have convection heat transfer with the fluid that has the same temperature as the inlet, and the other pipe is assumed to have convection heat transfer with the fluid that has the same temperature as the outlet. The temperature applied to the second pipe, which represent the outlet temperature of the fluid, is calculated in an iterative manner so that the fluid heat balance is consistent with the heat flux. Figure 3.10 illustrates the iterative procedure used to calculate the outlet temperature.

When the calculation starts, the inlet temperature (T_{in}) is applied to one pipe as the boundary condition, and an initial guess of the value of the outlet temperature (T_{out}) is applied to the other. By running GEMS3D, a total heat flux across the boundary of the pipes can be defined. According to the energy balance of the BHE, this total heat flux should be the same as the total heat flux defined by the temperature difference between the inlet and outlet fluid temperatures. If this temperature difference is not sufficiently close to that of the previous iteration, an improved estimation of the outlet temperature is calculated and applied to start the next iteration, until the temperature difference is sufficiently close to that of the previous iteration and the calculation is stopped. The final output of the outlet temperature is equal to the inlet temperature minus the temperature difference.

It is important to point out that the iterative procedure is not guaranteed to be numerically stable. This formulation does not guarantee that the outlet temperature is consistent with the second law of thermodynamics – at least during the iteration process if not at the end. This is not generally a problem when the time steps are large. However, with short time steps, and when there is a sudden change in inlet temperature, the model can become unstable. This is problematic if the interest is in control system interaction, for example. This issue is common

to all models that take the mixed boundary conditions to have the same temperatures as the inlet and outlet temperatures and try to calculate the outlet temperature. Even though this is not usually an issue with such models in design tool applications, it can be an issue in models used to simulate system operation.

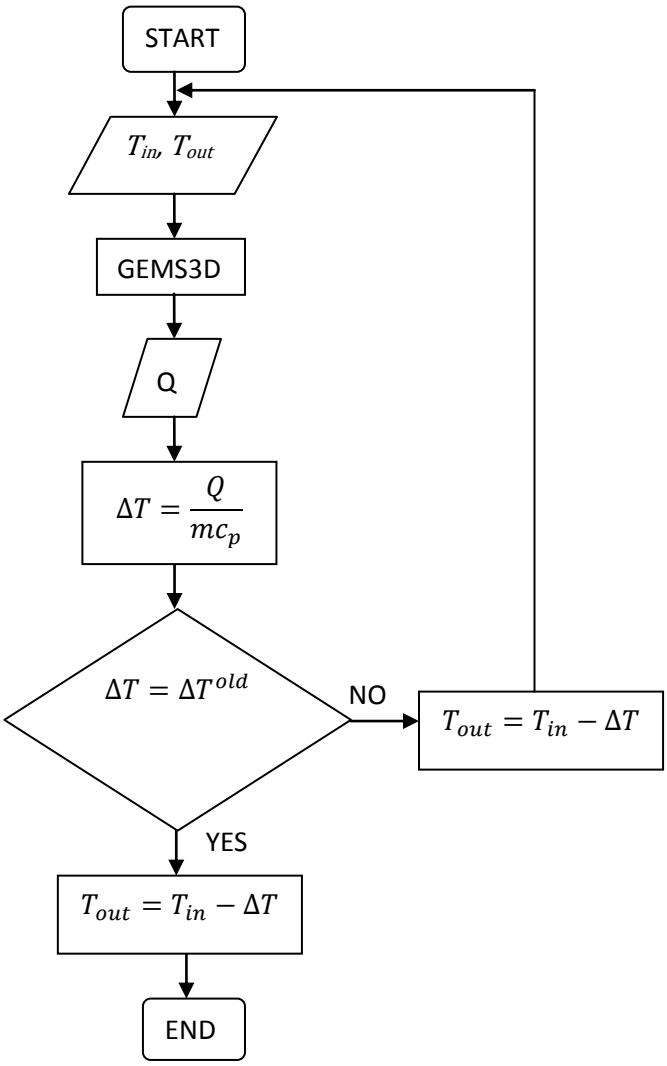

Figure 3.10 An illustration of the first iterative procedure used to calculate the outlet temperature of a two-dimensional BHE model.

In reality, and potentially in 3D numerical models, the fluid and pipe temperatures change along the pipe loop. However, in the two-dimensional model the temperatures of the two pipes have to be assumed to be constant along the depth of the borehole. One pipe represents the inlet and the other pipe represents the outlet. In this case, the pipe temperatures reflect conditions near the top of the borehole where the difference in temperature between the

pipes is greatest. This can be expected to result in over estimation of the heat fluxes between the two pipes, the so called short circuit fluxes. This is discussed further in Chapter 4 Section 4.2.2 and Section 4.3.2.

3.2 Model Validations

There is no exact analytical solution for three-dimensional heat transfer in a borehole geometry that can be applied to try to validate the numerical model. However, if only conduction in two dimensions is considered, steady-state borehole thermal resistance can be used as an index to validate the model. Young (2004) carried out an intensive study to compare the steady state borehole resistances calculated by different models, including the Paul's method (1996), the Gu and O'Neal's approximate diameter method (1998), the cylinder source (Carslaw and Jaeger, 1947), and the multipole method (Bennet et al., 1987). The multipole method can be regarded as a reference method and accurate to within machine precision. The steady-state borehole resistances calculated by the multipole method in Young's study are used to validate the values calculated by the 3D model.

The fluid transport, which only occurs in the third dimension, can be validated separately using an analytical model for fluid transport (Bosworth, 1949). The transport characteristics of the fluid in pipes can be quantified using the Residence Time Distribution (RTD).

3.2.1 Borehole Thermal Resistance

Assuming the heat transfer of BHEs is in steady-state, the total amount of heat transfer rate per unit length between the fluid and the ground can be expressed as:

$$\mathrm{Q} = \frac{T_f - T_b}{R_b} \tag{3.15}$$

where, Q is the steady-state heat transfer rate between the fluid and the borehole wall (W), T_f is the average fluid temperature (°C), T_b is the average borehole wall temperature (°C), and R_b is the borehole thermal resistance (mK/W).

The borehole resistance defined here includes the convective resistance between the fluid and the inner side of the pipes, the conductive resistance of the pipes, and the conductive resistance of the grout. The concept of borehole thermal resistance has been widely used in development of analytical BHE models, as well as development of some numerical models and is therefore a useful metric when trying to compare the accuracy of different models.

By making a 2D steady-state calculation of the heat flux across the borehole wall and borehole temperature for a given fluid and far field temperature in the 3D model, and by applying Equation (3.15), an overall borehole thermal resistance can be calculated. Two single BHEs with different borehole diameters, 114 and 152 mm and two different grout types, one with the thermal conductivity of 0.75 W/mK and the other with 1.5 W/mK, have been studied (Young, 2004). The borehole configurations and thermal properties are shown in Table 3.1.

Table 3.1 BHE configuration and thermal properties for validation of borehole thermal resistances.

Borehole Diameter		D	114.3/152.4	mm
Pipe Inner Diameter		D_{in}	27.4	mm
Pipe Outer Diameter		D_{out}	33.4	mm
Spacing between pipes		L_s	15.8/28.5	mm
Pipe	Conductivity	k_{pipe}	0.39	W/mK
	Thermal Capacity	ρc_p	1.77	MJ/m^3K
Grout	Conductivity	k_{grout}	0.75/1.5	W/mK
	Thermal Capacity	ρc_p	3.9	MJ/m^3K
Ground	Conductivity	k_{ground}	2.5	W/mK
	Thermal Capacity	ρc_p	2.5	MJ/m^3K
Fluid	Convection Coefficient	H	1690	W/m^2K

The U-tube shank spacing denotes the distance between the outside walls of the two pipes. Variation of the calculated borehole thermal resistance with mesh density has also been examined. The calculated borehole thermal resistances are shown in Table 3.2. The model can be seen to be capable of matching with the analytical values by the multipole method (Bennet *et al*., 1987) extremely closely. Variation of mesh density from 656 to 40,448 cells shows very small changes in terms of borehole thermal resistance. In practical calculations, using coarser meshes to reduce computation times would be reasonable.

Table 3.2 Borehole thermal resistances by the numerical model and multipole method.

Borehole Diameter	No. of Cells	k_{grout} (W/mK)	R_b (mK/W)		k_{grout} (W/mK)	R_b (mK/W)	
			Numerical	Multipole		Numerical	Multipole
114.3 mm	656	0.75	0.1827	0.1823	1.5	0.1160	0.1158
	2,528		0.1825			0.1161	
	5,688		0.1824			0.1160	
	10,112		0.1824			0.1160	
	40,064		0.1824			0.1160	
	40,448		0.1824			0.1160	
152.4 mm	656	0.75	0.2221	0.2216	1.5	0.1347	0.1345
	2,528		0.2218			0.1347	
	5,688		0.2217			0.1346	
	10,112		0.2217			0.1346	
	40,064		0.2216			0.1346	
	40,448		0.2216			0.1346	

3.2.2 Fluid Transport

The circulating fluid has been modelled using a single layer of cells inside the pipe. Dividing the length of the pipes into finite number of cells allows the fluid to be discretised in effectively a one-dimensional manner. A fluid velocity is imposed in these cells in accordance with the system flow rate and the transport of heat from one cell to the next along the pipe can then be represented by the advection flux term in the temperature partial differential equation. This is effectively a one-dimensional representation of fluid flow in the pipe, in which each finite volume cell can be considered as a well-mixed node that is defined by a single temperature T and is transported at a velocity V. This arrangement of fluid cells in the pipe model can be considered similar to a Compartments-In-Series model (Wen and Fan, 1975), as illustrated in Figure 3.11.

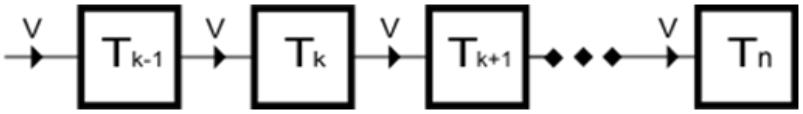

Figure 3.11 Diagram of the 'Compartments-In-Series' representation of the fluid flow along a pipe.

Fluid transport models of this type have been widely used in process engineering and their characteristics are well known. The thermal response of the pipe inside the borehole will be

different from this simple model by virtue of heat transfer to the pipe wall. However, it is worth testing the model without this heat transfer for the purpose of validation. The transport properties of the pipe (be it heat or a chemical species that travels along the pipe) can be thought of in terms of residence time distribution, which is commonly expressed as a function of dimensionless time F(τ), and often illustrated in an 'F-Diagram'. When a steady flow fluid undergoes a step change in temperature at time t=0, the variable F(t) represents the proportional change at the outlet at later time t. The analysis is simplified by using dimensionless time given by

$$\tau = \frac{\dot{v}t}{V} \tag{3.16}$$

where, τ is the dimensionless time, $\dot{v}$ is the volume flow rate (m^3/s), and V is the system volume (m^3).

The actual shape of the F-diagram depends primarily on the velocity profile (and hence turbulence), in which case the faster-moving fluid near the centreline will arrive at the end of the pipe more quickly than the average. Fluid undergoes a diffusion process as it travels along the pipe, by virtue of the non-uniform velocity profile, so that step changes in inlet condition appear smoothed at the outlet. The solution, given by a one-dimensional model such as the compartments-In-Series model, depends to some extent on the number of cells that are discretized along the pipe length. This is also true in the representation of fluid flow in the pipe in the 3D numerical model, where the response is also subject to the limitations of the temporal discretisation scheme (representing the left-hand term in Equation (3.1).

Effectively insulating the pipes by setting zero heat flux across the pipe wall in the 3D model make it possible to calculate the RTD of the circulating fluid by examining the response of the outlet temperature to a step change in inlet temperature. Figure 3.12 shows the F-Diagram generated using the first-order backward implicit temporal discretisation scheme with different numbers of cells, compared with the analytical solution derived by Hanby et al. (2002), which is similar to Bosworth's solution (Bosworth, 1949). The shape of the F-Diagrams varies in accordance to the number of cells. As the number of cells increases, the response gets steeper, and as the number of cells approaches infinity, the response approaches that of plug flow, in which case all the fluid arrives at the exit of the pipe at the same time (τ=1).

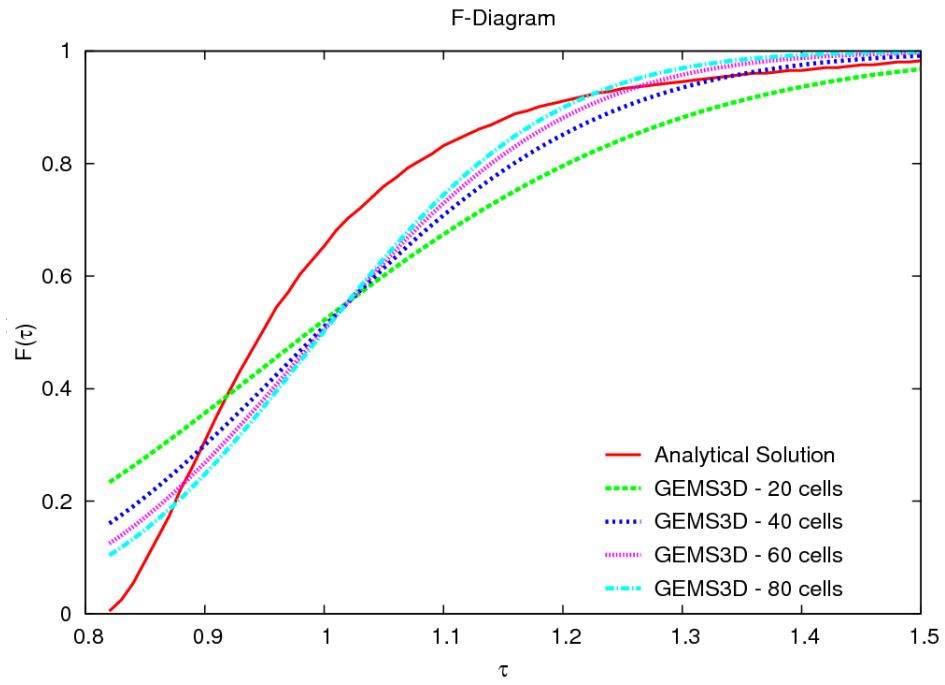

Figure 3.12 F-Diagram calculated using different numbers of cells compared with the analytical solution.

Figure 3.13 shows the F-Diagram generated using 60 cells along the pipe length and using two different temporal discretisation schemes, the first order backward implicit scheme and the second order three time level scheme. The solutions are compared with the analytical solution derived by Hanby et al. (2002). The first order differencing scheme over-predicts the diffusion of the flow and the second order scheme less so.

The effect of different numbers of cells for discretisation along the pipe and different temporal discretisation schemes has been studied. The root mean square error (RMSE) of the F-diagram for the two discretisation schemes over the range $0.8 < \tau < 1.5$ for different numbers of cells is shown in Figure 3.14. It has been found that there is no optimal number of cells by the backward implicit scheme. The RMSE drops quickly from 20 to 60 cells, and levels at around 0.08 for more than 60 cells. The optimal number of cells is 47 using the three time level scheme, but given lengths of the pipes and uniform distributions of the fluid along the pipe length are required, 60 gives a reasonable accurate approximation. These results are consistent with the findings by Hanby et al. (2002) who used the equivalent 'Well-Mixed Nodal' model to examine the RTD for turbulent flow in a conduit.

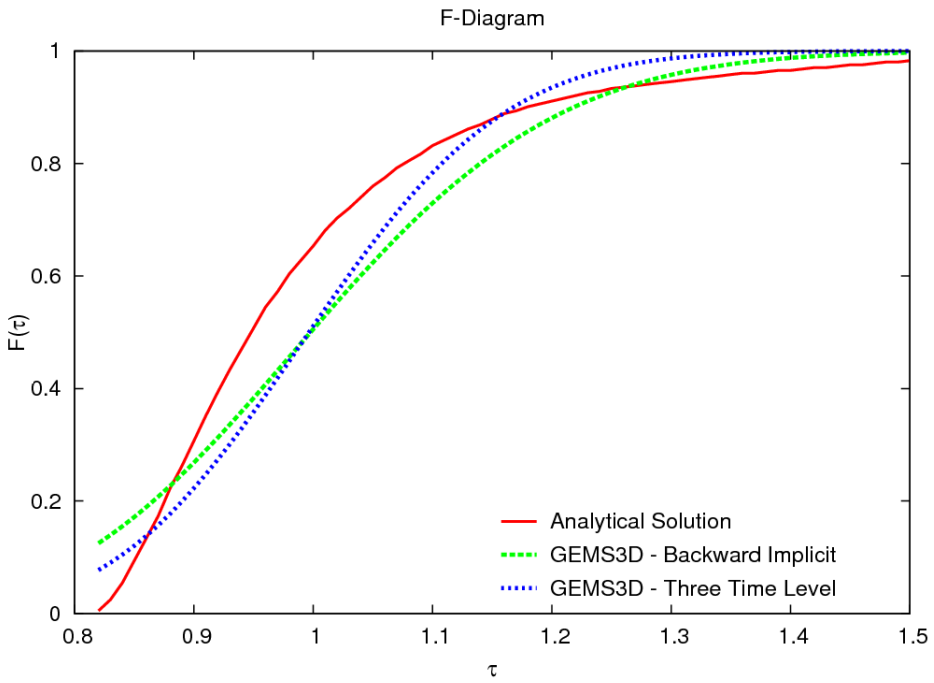

Figure 3.13 F-Diagram calculated using different discretization schemes compared with the analytical solution (60 cells).

The model always tends to over-predict the degree of diffusion. Although the error is greater than one would like, it should be noted that this could not be addressed to any great degree by higher order differencing schemes. The model accuracy is limited primarily by the fact that the 2D flow in the pipe is simplified to be 1D. This might be addressed by computational fluid dynamics (CFD) calculation of the pipe fluid flow but this would add unreasonable computational burden. Some overestimation of the diffusion process is not unreasonable as additional diffusion occurs in practice by virtue of the horizontal header pipes in a typical borehole array.

Despite the smaller error using the higher order three time-level differencing, unphysical results can sometimes occur (wiggles in the temperature prediction). This is a known issue with higher order schemes. Consequently, the first order backward implicit differencing scheme has been selected in the remaining work due to its greater robustness.

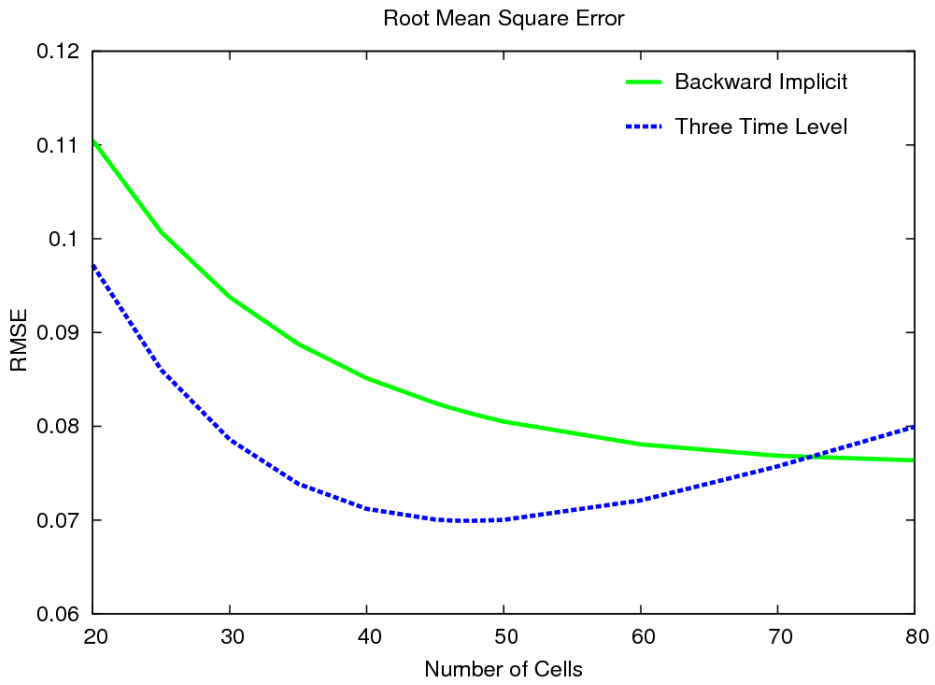

Figure 3.14 Root mean square error by two different time discretization schemes compared with the analytical solution.

3.2.3 Comparison with Experimental Data

Experimental data obtained from an experimental facility at Oklahoma State University are used to validate the numerical models. The experimental facility was designed and constructed to study hybrid ground source heat pump systems (Hern, 2004). Only the measured data from the ground loop are taken for the validation. The same set of data have been used in a study carried out by Spitler et al. (2009) for inter-model comparison of ground heat exchangers.

The ground loop consists of three BHEs, and each borehole is approximately 75 meters in depth and 114 mm in diameter. A single U-tube made of ¾ inch IPS DR 11 high-density polyethylene pipes was inserted into each borehole and backfilled with bentonite grout. Water is used as the working fluid and the nominal fluid flow rate of the system is 0.631l/s. Details of a single BHE configuration are shown in Table 3.3. The undisturbed ground temperature was measured at 17.3 ^{o}C (Hern, 2004). The flow rate of each borehole was assumed to be the same.

The inlet and outlet fluid temperatures of the BHEs were measured at 1 minute intervals and continuously for 18 months. During this period, there is no thermal interaction taking place among these three BHEs. The experimental data have been used in two ways. Firstly, the

measured inlet and outlet temperatures and flow rates at 1 minute intervals of the first month are chosen for validating the numerical models over short timescales. Secondly, hourly average data from the measurement of the first 16 months are chosen for validating the models over long timescales.

Table 3.3 BHEs configurations of OSU experimental facility.

Borehole Depth		L	74.68	m
Undisturbed ground temp		$T_{initial}$	17.3	°C
Fluid flow rate		m	0.212	l/s
Borehole Diameter		D	114.330	mm
Pipe Inner Diameter		D_{in}	21.820	mm
Pipe Outer Diameter		D_{out}	26.670	mm
Borehole Shank Spacing		L_s	20.320	mm
Pipe	Conductivity	k_{pipe}	0.3895	W/m.K
	Thermal capacity	ρc_p	1770	$KJ/m^3.K$
Grout	Conductivity	k_{grout}	0.744	W/m.K
	Thermal capacity	ρc_p	3900	$kJ/m^3.K$
Ground	Conductivity	k_{ground}	2.550	W/m.K
	Thermal capacity	ρc_p	2012	$KJ/m^3.K$
Water	Conductivity	k_{water}	0.598	W/m.K
	Thermal capacity	ρc_p	4184	kJ/kg.K
	Convection Coefficient	h	2260	$W/m^2.K$

A single BHE with the configurations shown in Table 3.3 is simulated using both the 2D and 3D models. The average inlet temperature of the three BHEs is taken as the input for the 2D and 3D models, and the outlet temperatures calculated from the 2D and 3D models are compared with the average outlet temperature of the three BHEs.

3.2.3.1 Validation over Short Timescales

All simulations run at two different time intervals to optimise the computational time and the accuracy of simulation results. Firstly, the simulations have been run on 1-hour intervals for 14 days (1 – 14 March) and the hourly average inlet temperatures and flow rate have been taken as the inputs for the 2D and 3D models, in order to build up the thermal history of the ground. After that, the models use 1-minute interval inlet temperatures out of 1 day (15 March) as the

input, and the outlet temperatures calculated from the models are compared to the average outlet temperature measured data.

Figure 3.15 and Figure 3.16 show the predicted outlet temperatures by the 2D and 3D models, compared to the experimental outlet temperature, from 15:00 to 16:30 and from 17:00 to 18:30, respectively. Over these periods, the outlet temperatures predicted by the 2D and 3D models show a good match to the measured outlet temperature, but the 3D model gives a closer fit. The most significant differences are shown when there is a sudden change in the inlet temperature. It can be seen from the experimental measurements that when this happens the outlet temperature does not change instantly, but instead, a delayed response of the outlet temperature is shown. The 3D model is able to capture the delayed responses of the outlet temperatures, due to the explicit modelling of the fluid transport in the pipes in the 3D model. The 2D model, on the other hand, is not able to demonstrate such a delay and predicts a sharp decrease or increase in outlet temperature. In Figure 3.15, the Root Mean Square Error (RMSE) for the 2D model is 0.464 K and for the 3D model is 0.324 K; and in Figure 3.16, the RMSE for the 2D model is 0.466 K and for the 3D model is 0.320 K.

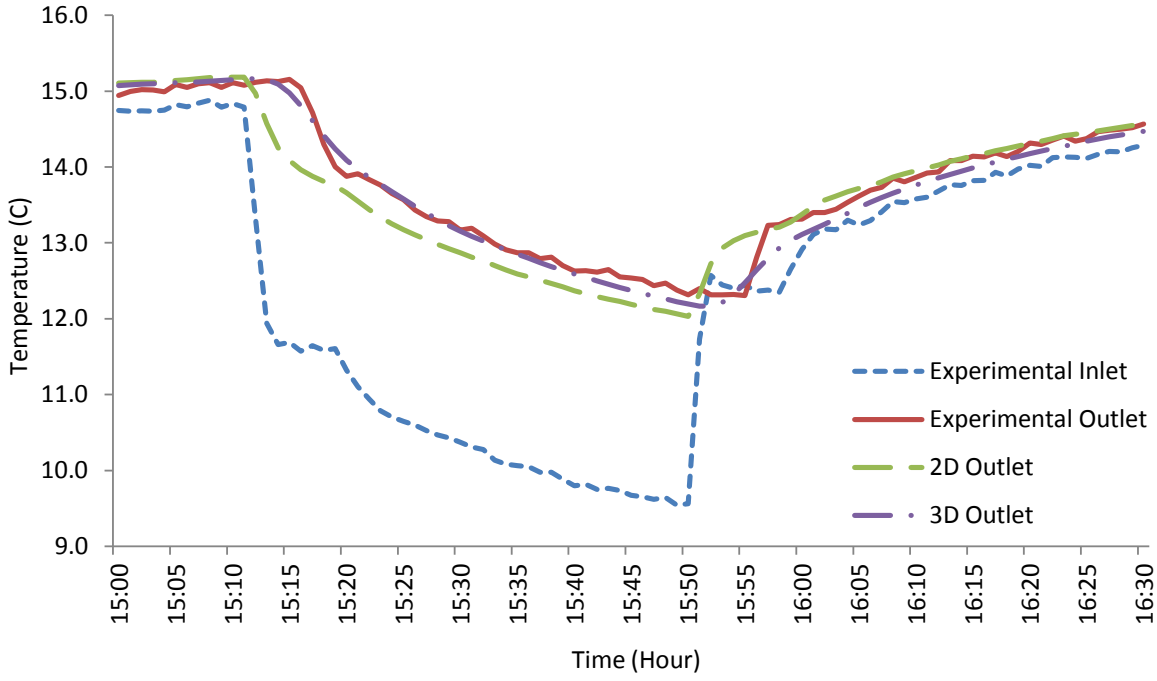

Figure 3.15 Predicted outlet temperatures by the 2D and 3D models, compared to the experimental outlet temperature (15:00 – 16:30).

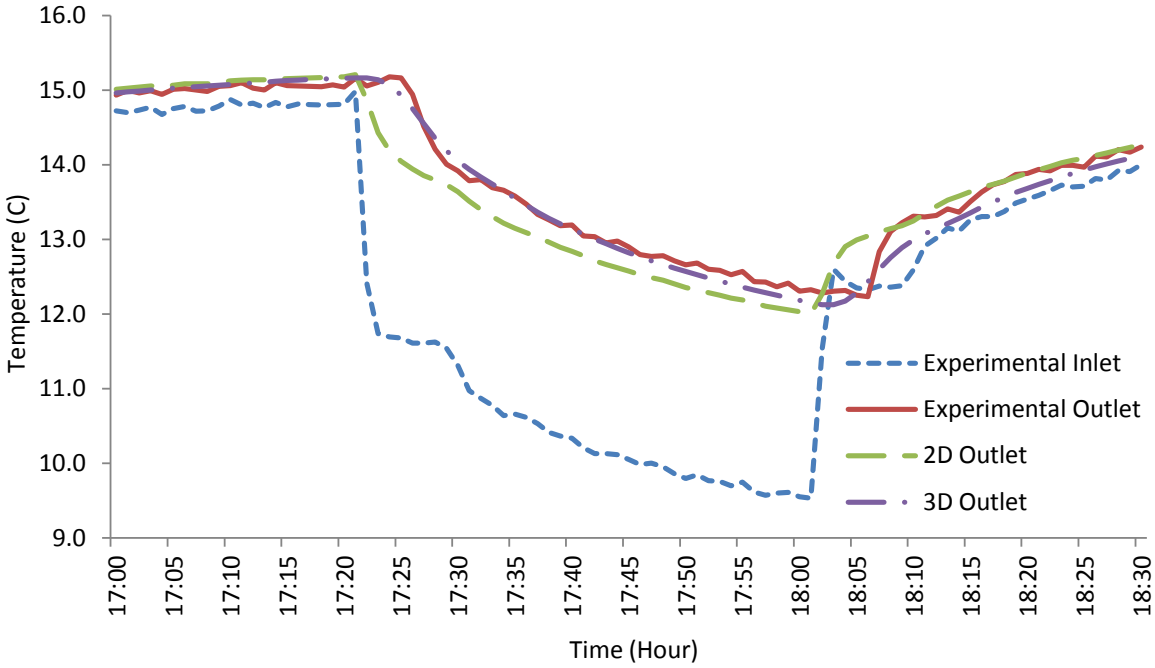

Figure 3.16 Predicted outlet temperatures by the 2D and 3D models, comparing with the experimental outlet temperature (17:00 – 18:30).

3.2.3.2 Validation over Long Timescales

The hourly average inlet temperatures and flow rates taken from the experimental data are used as the input for both the 3D and 2D models. By running the simulations, the outlet temperatures and heat transfer rates calculated by the 3D and 2D models can then be compared to the measurements using monthly average values over 16 months.

Figure 3.17 shows the monthly average outlet fluid temperatures calculated by the 3D and 2D models, comparing to the experimental outlet fluid temperatures for 16 months (from 03/05 to 06/06). Both the predictions by 3D and 2D models are a close fit with the experimental outlet temperatures. The biggest error occurs at December 2005, when the heating load is highest.

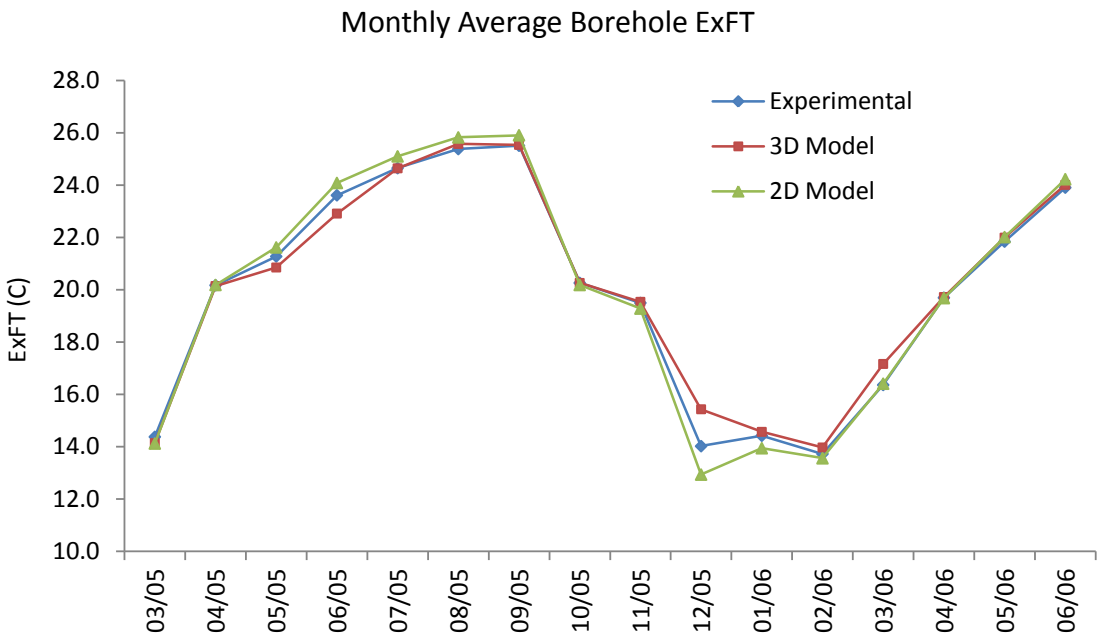

Figure 3.17 Monthly average borehole ExFT predicted by the 2D and 3D models, comparing to the experimental ExFT for 16 months (03/05 to 06/06).

Figure 3.18 shows monthly average heat extraction/rejection predicted by the 3D and 2D models, comparing to the experimental data for 16 months (from 03/05 to 06/06). Heat extraction is shown as positive; heat rejection as negative. In general, the predictions by the two models follow the general trend of the measurement quite closely. During the months with high cooling demand (from 05/05 to 09/05), the heat rejection predicted by the 3D model is closer to the experimental data than the prediction by the 2D model. But during the high demand heating months (from 12/05 to 02/06), both the predictions by the 3D and 2D models are much lower than the experimental measurement.

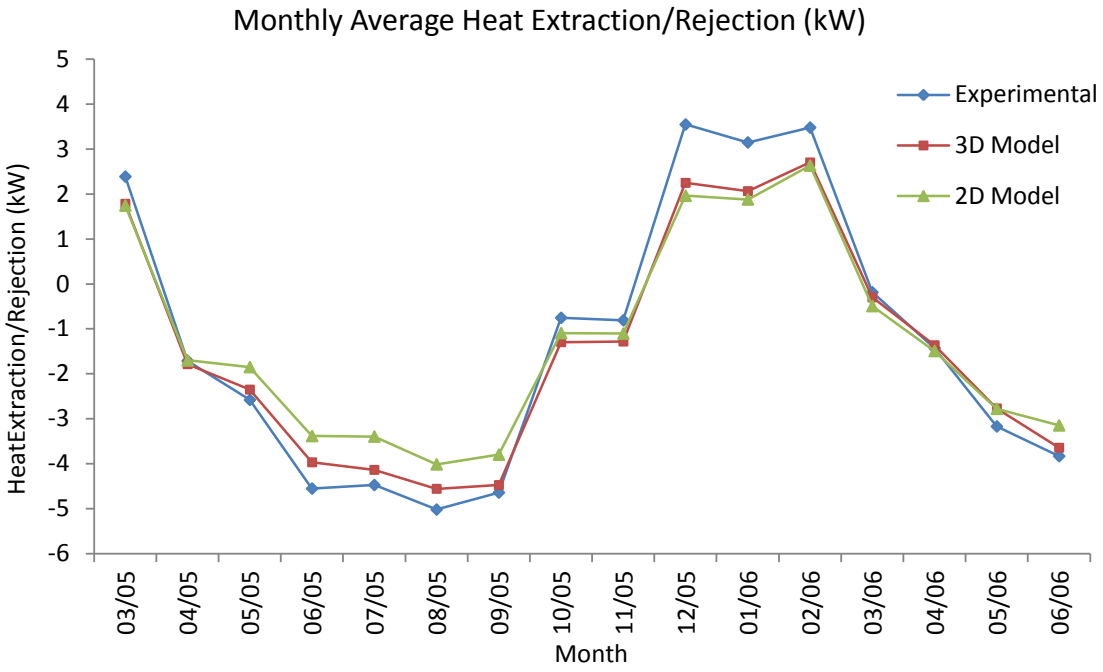

Figure 3.18 Monthly average heat extraction/rejection rates predicted by the 2D and 3D models, compared to the experimental data for 16 months (03/05 to 06/06).

The same set of data were used in a study carried out by Spitler et al. (2009) for comparing models for BHEs developed for different software programs. In their study, the monthly average heat extraction/rejection rates calculated by TRNSYS, HVACSIM+, and EnergyPlus have also been compared to the experimental data. Figure 3.19 shows the monthly average heat extraction/rejection rates calculated by TRNSYS, HVACSIM+, and EnergyPlus (Spitler et al., 2009), combining with the predictions by the 3D and 2D model (Figure 3.18), compared to the experimental data. In a similar way to the predictions by the 3D and 2D model, the predictions by the three models (TRNSYS, HVACSIM+ and EnergyPlus) also follow the trend of the experimental data closely, although relatively large differences are shown for months with high cooling and heating demands. It was pointed out that the differences might have been exacerbated by the operating schedule during those months, when the system was shut down for several multi-day periods.

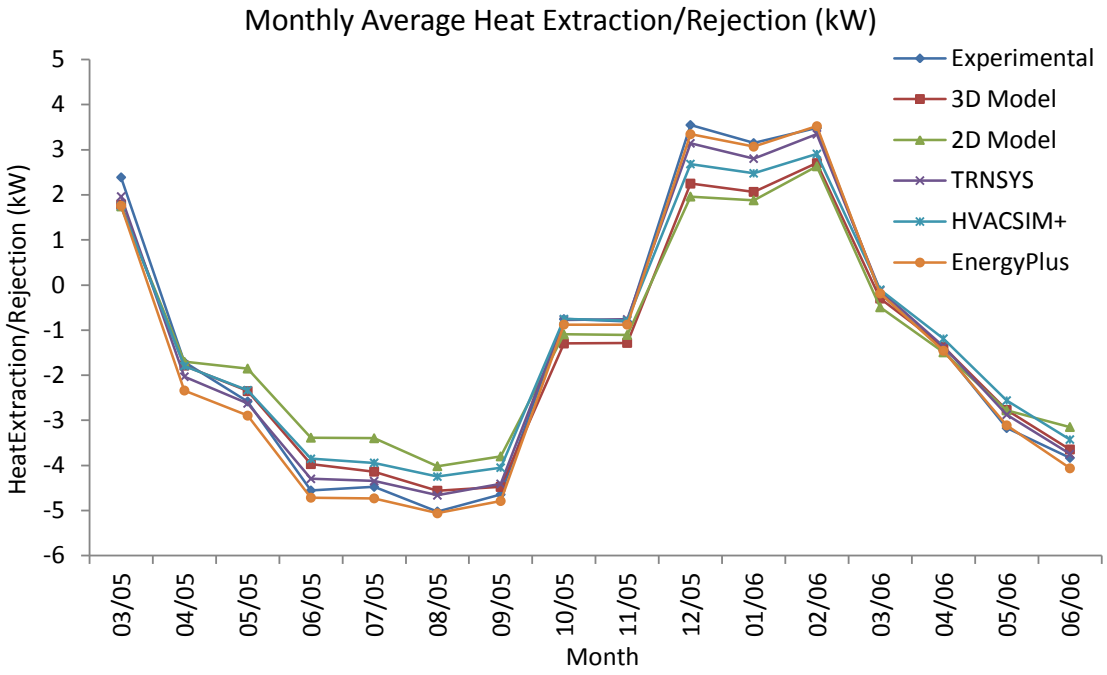

Figure 3.19 Monthly average heat extraction/rejection rates predicted by the 2D and 3D models, compared to predictions by TRNSYS, HVACSIM+, EnergyPlus and experimental data (03/05-06/06).

3.3 Summary

A dynamic 3D finite volume numerical model has been developed for simulation of transient heat transfer in and around BHEs in three dimensions. Multi-block boundary fitted structured meshes have been employed to discretise the simulation domain and allow the complex geometries of BHEs and the surrounding ground to be represented exactly. This type of mesh also allows a close control of the cell distribution and its orthogonality. A 2D model has been implemented using the same numerical method for comparison purposes.

The validations of the 3D model have been done by reference to analytical models of borehole thermal resistance and fluid transport in pipes. By making a 2D steady-state calculation of a single BHE, borehole thermal resistances have been calculated with meshes of different density. The values of borehole thermal resistance calculated by the numerical 3D model match the analytical results extremely well. In practice, calculation using coarser meshes to reduce computation time would be reasonable. Furthermore, representing the fluid transport in pipes in a 1D manner, the characteristics of the fluid transport have been validated against an analytical RDT solution.

Both the 3D and 2D models are further validated against experimental data obtained from an experimental facility at Oklahoma State University. The outlet temperatures predicted by the 2D and 3D models show a close match to the measured outlet temperature over the simulation period. The 3D model, due to the explicit modelling of the fluid transport in the pipes, is able to capture the delayed responses that were demonstrated in the experimental data, but not the 2D model.

In the following chapters, this 3D numerical model is used for different applications:

- Chapter 4 focuses on the investigation of transient heat transfer in and around BHEs in three dimensions in short timescales (up to one minute), which includes the predictions for fluid temperature profiles, inter-tube heat flux profiles and borehole wall heat flux profiles along the depth of a borehole and the comparisons of simulation results by the 2D and 3D models;
- Chapter 5 suggests methods to improve the 2D model based on the differences in model predictions by the 2D and 3D models highlighted in Chapter 4;
- Chapter 6 presents a study of simulating a ground source heat pump system for a domestic building using both the 2D and 3D models. The simulation results have been compared with other models;
- Chapter 7 investigates the thermal interactions of multiple BHEs arrays;
- Chapter 8 evaluates applying line source model in thermal response tests.

Chapter 4 Simulation Results

A dynamic three-dimensional (3D) finite volume model for BHEs has been developed and presented in Chapter 3. This model not only provides a detailed representation of borehole geometry, taking into account the thermal mass of the fluid, pipes and grout, but also simulates the fluid transport in pipes explicitly. A two-dimensional (2D) model was implemented using the same numerical method applied in the 3D model development. The main purpose of the 2D model implementation has been to investigate the differences caused by modelling the heat transfer in and around BHEs in three dimensions as opposed to two.

This chapter presents results of simulating a single BHE using the 3D model in both steady-state and transient simulations. These practical test calculations have been made to characterise the behaviour of the model. They have also allowed some of the three-dimensional behaviour of BHE to be examined. Applying the 3D model to simulate a BHE under a step change test, it is possible to examine the variations of the temperature and heat transfer profiles along the borehole depth in detail at short timescales.

This chapter also presents studies of a single BHE made by applying the 3D and 2D models in different test cases. The aims have been to:

- Examine the temperature and heat balances predicted by the 2D and 3D models in steady-state conditions;
- Compare the responses of the 2D and 3D models by applying a step change in inlet temperature;
- Investigate heat transfer rates across the pipe and borehole walls predicted by the 2D and 3D models at short timescales;
- Study predicted heat pump operations using the 2D and 3D models;
- Characterise the frequency response of the 2D and 3D models.

The significance of the findings is highlighted.

4.1 Borehole Heat Exchanger Configurations

In this chapter, a single BHE with a borehole diameter of 150 millimetres and a depth of 100 meters has been simulated. The surrounding ground to a diameter of 4 meters has been

included in the simulation domain. The configurations and thermal properties of the borehole are shown in Table 4.1.

Table 4.1 BHE configurations and thermal properties.

Borehole Diameter		D	152.4	mm
Pipe Inner Diameter		D_{in}	27.4	mm
Pipe Outer Diameter		D_{out}	33.4	mm
U-tube Shank Spacing		L_s	28.53	mm
Pipe	Conductivity	k_{pipe}	0.39	W/mK
	Thermal Capacity	ρc_p	1.77	MJ/m^3K
Grout	Conductivity	k_{grout}	0.75	W/mK
	Thermal Capacity	ρc_p	3.9	MJ/m^3K
Ground	Conductivity	k_{ground}	2.5	W/mK
	Thermal Capacity	ρc_p	2.5	MJ/m^3K
Water	Conductivity	k_w	0.6	W/mK
	Thermal Capacity	ρc_p	4.18	MJ/m^3K

Five different velocities of the circulating water along the pipe loop have been tested: 1.0 m/s, 0.8 m/s, 0.6 m/s, 0.4 m/s, and 0.2 m/s. These velocities are chosen to represent a wide range of applications of BHEs. A velocity of 0.6 m/s is a reasonable design velocity for a normal BHE, while relative high velocity of 1.0 m/s and relative low velocity of 0.2 m/s might occur in variable flow systems. The corresponding flow rates, Reynolds numbers, convection coefficients and nominal transit time are listed in Table 4.2.

Table 4.2 Fluid properties at a range of circulating velocities.

Velocity (m/s)	1.0	0.8	0.6	0.4	0.2
Flow Rate (l/s)	0.590	0.472	0.354	0.236	0.118
Reynolds Number	25,400	20,320	15,240	10,160	5,080
Convection Coefficient (W/m^2K)	3,400	2,850	2,260	1,640	940
Nominal Transit Time (s)	200	250	333	500	1,000

In the analysis, the simulation results are normalised according to the advancing dimensionless depth *D**, which is the ratio of depth of the fluid and the total depth of the borehole (Equation (4.1)); dimensionless temperature *T**, which is the ratio of temperature difference between the fluid and initial temperatures and inlet and initial temperatures (Equation (4.2)); and dimensionless transit time τ (Equation (4.3)).

$$D^* = \frac{D}{D_{total}} \tag{4.1}$$

$$T^* = \frac{T - T_{initial}}{T_{in} - T_{initial}} \tag{4.2}$$

$$\tau = \frac{vt}{L} \tag{4.3}$$

where D is the depth of the fluid (m), D_{total} is the total depth of the borehole (m), T is the temperature of the fluid (°C), T_{in} is the inlet temperature of the fluid (°C), $T_{initial}$ is the initial temperature of the fluid (°C), v is the velocity of the circulating fluid (m/s), t is the time (s), and L is the total length of the pipes (m).

4.2 Steady-State Simulations

Steady-state simulations have been carried out in order to characterise the behaviour of a BHE in three dimensions at long timescales, and in particular to examine the temperature and heat flux profiles along the borehole and to quantify the 'short-circuit' inter-tube heat transfer.

All the steady-state simulations have been made using two constant temperature boundary conditions: the inlet fluid temperature was 20 ^{o}C, and the far-field ground temperature was 10 ^{o}C. The initial temperature of the whole simulation domain of the BHE (including the fluid, pipes, grout and ground) was 10 ^{o}C.

4.2.1 Vertical Temperature Profiles

One of the advantages of the 3D model is that it can predict temperature profiles along the borehole depth. Five different velocities are tested, and the resulting fluid temperature profiles are illustrated in Figure 4.1.

For relatively high velocities (1.0 m/s and 0.8 m/s), the temperature profiles are approximately linear; for mid-range velocities (0.6 m/s and 0.4 m/s), the temperature profiles are noticeably non-linear; and for relatively low velocity (0.2 m/s), the non-linearity of the temperature profile is very significant.

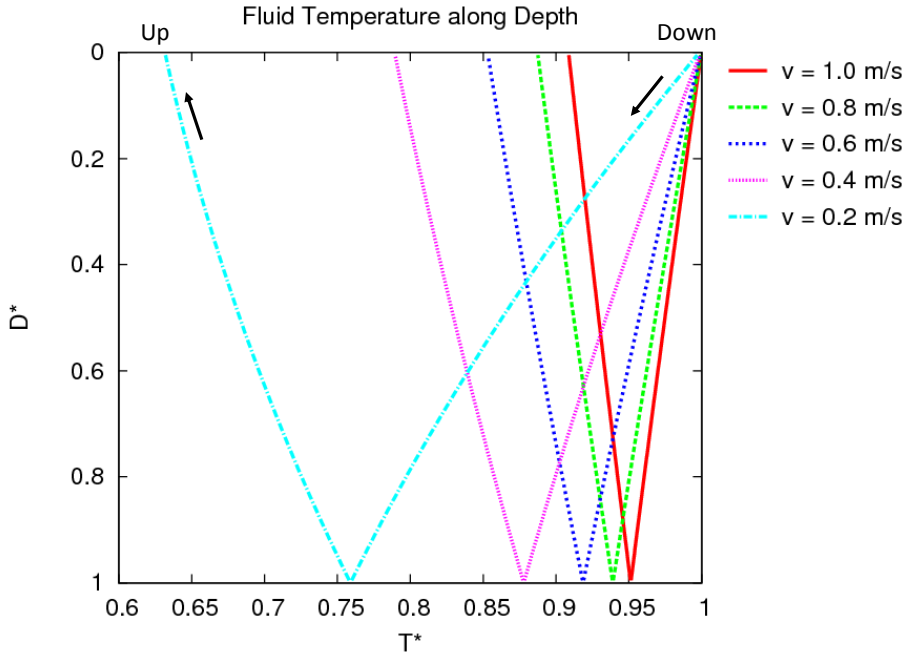

Figure 4.1 Fluid temperature profiles along borehole depth at different fluid velocities.

Figure 4.2 shows the borehole temperature profiles along the borehole depth at different fluid velocities in steady-state simulations.

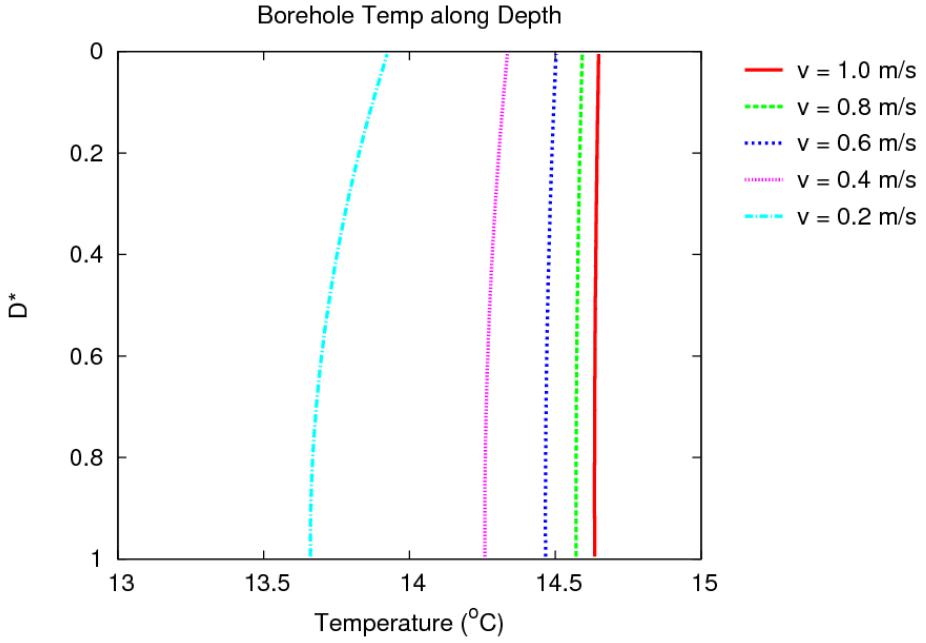

Figure 4.2 Borehole temperature profiles along borehole depth at different fluid velocities.

This is the temperature of the borehole wall. In a similar way to the fluid temperature profiles, for relatively high velocities (1.0 m/s and 0.8 m/s), the profile is linear and reasonably constant along the depth; for mid-range velocities (0.6 m/s and 0.4 m/s), the profile varies slightly and non-linearly; and for a relatively low velocity (0.2 m/s), the non-linearity is more significant.

4.2.2 Heat Flux Profiles

Another advantage of the 3D model is that it can predict heat flux profiles along the borehole depth. Figure 4.3 illustrates the definition of the borehole heat flux (Q_b) and inter-tube heat flux (Q_{int}). The borehole heat flux is defined as the heat transfer across the borehole surface, and the inter-tube heat flux is defined as the heat transfer between the two pipes. In the 3D model, patches of borehole and inter-tube surface can be specified, which allows the heat fluxes across these surfaces to be examined.

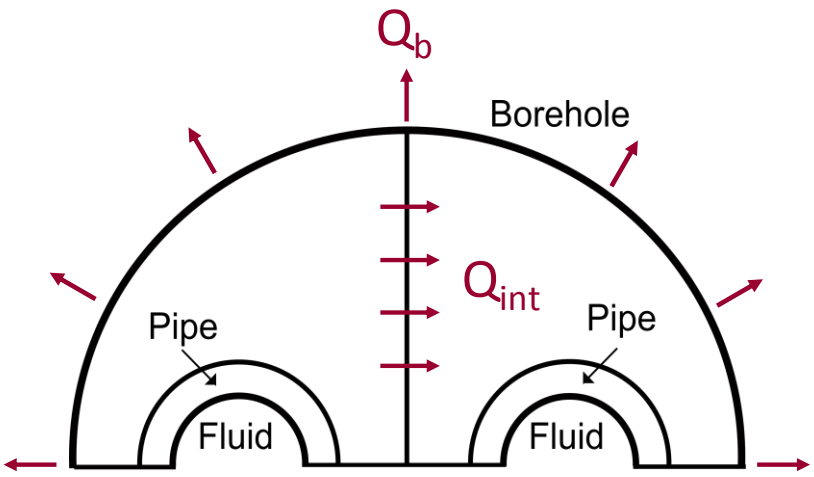

Figure 4.3 A diagram of defining borehole heat transfer and inter-tube heat transfer.

Figure 4.4 illustrates the heat flux across borehole wall along the borehole depth at different fluid velocities in steady-state. The borehole heat flux profiles vary in accordance with the borehole temperature profiles at each velocity. This is because, in steady-state simulations, the heat flux across the borehole wall is proportional to the temperature difference between the borehole temperature and the far-field temperature.

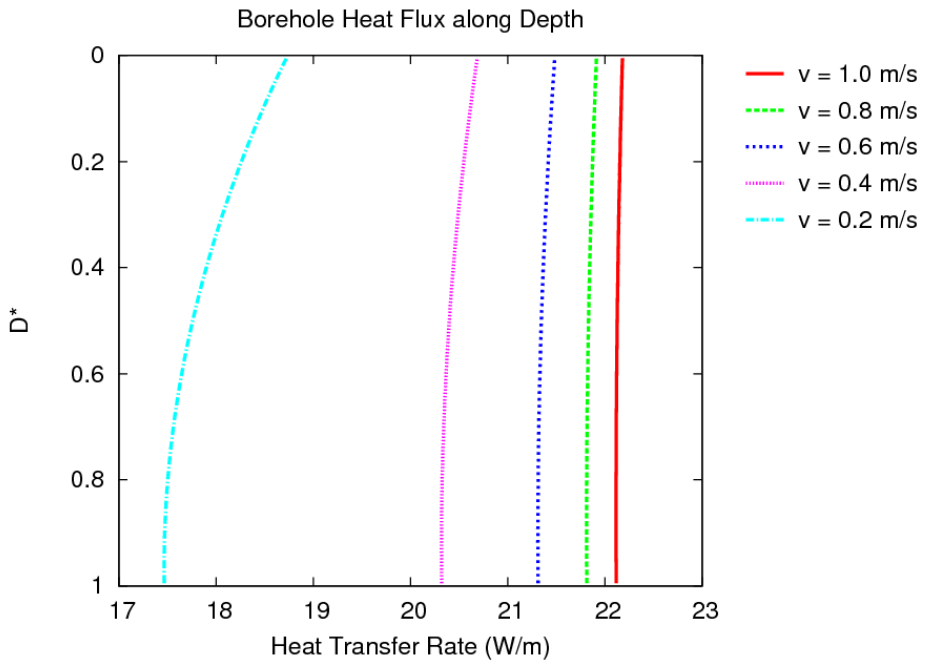

Figure 4.4 Borehole wall heat flux along borehole depth at different fluid velocities.

Due to the temperature difference between the upward and downward fluid in adjacent pipes, heat is transferred directly from one pipe to the other, rather than the borehole wall. This inter-tube heat flux is also called the 'short-circuit' heat flux. The inter-tube heat flux is proportional to the temperature difference between the upward and downward flowing fluids at a given depth. It is highest at the top of the borehole where this fluid temperature difference is greatest and lowest at the bottom. Accordingly there is a correspondence between the temperature profiles in Figure 4.1 and fluxes shown in Figure 4.5. In any BHE, the pipes of the u-tube are necessarily close together and this 'short-circuit' heat flux cannot be avoided. This heat flux is detrimental to overall performance. It is interesting to examine this flux in the 3D model as this is often ignored by many other models. Depending upon the way in which 2D models associate the inlet and outlet temperatures with the temperatures of the pipes, 2D models either overestimate or underestimate the inter-tube heat flux.

Figure 4.5 shows the inter-tube heat flux profiles along the borehole depth at different circulating fluid velocities. And Figure 4.6 shows the ratio between the inter-tube and the borehole heat fluxes along the borehole depth at different velocities. The inter-tube heat flux profiles are approximately linear. The inert-tube heat flux is inversely proportional to flow velocity.

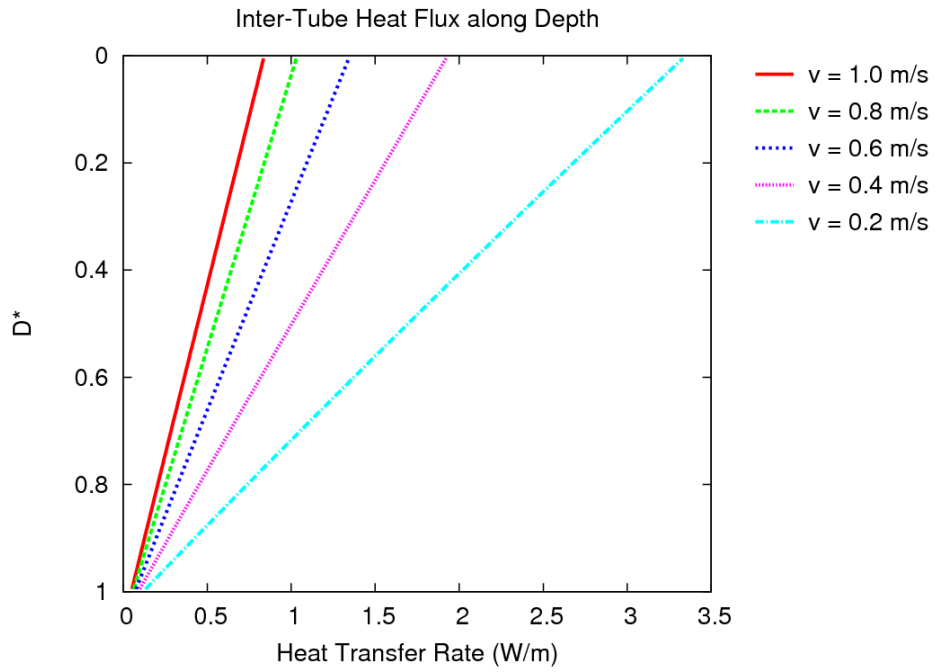

Figure 4.5 Inter-tube heat flux along borehole depth at different velocities.

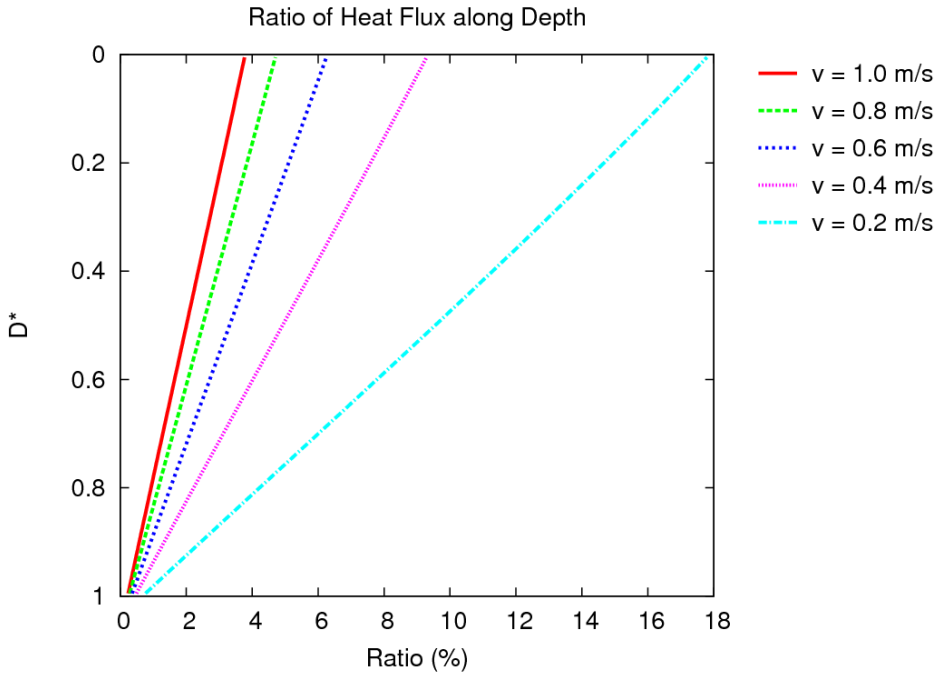

Figure 4.6 Ratio between the inter-tube and borehole heat fluxes along borehole depth at different velocities.

The effect of the inter-tube heat transfer on the borehole heat transfer can be assessed by examining the ratio between the total inter-tube heat transfer and the total borehole heat

transfer. Figure 4.7 shows the ratio between the total inter-tube heat transfer and the borehole heat transfer against the fluid velocity. The variation of the ratio is not linear with velocity. The inter-tube heat transfer is nearly 10% of the borehole heat transfer for fluid flow circulating at a low velocity of 0.2 m/s, and the ratio is much lower (2%) for fluid flow circulating at a high velocity of 1 m/s. This is because, for fluid flow circulating at a low velocity, the inter-tube heat transfer is high due to the large temperature difference between the upward and downward fluid flows, but the borehole heat transfer is low due to the low average fluid temperature. For fluid flow circulating at a high velocity, a low inter-tube heat transfer but a high borehole heat transfer can be expected due to the small temperature difference between the upward and downward fluid flows and high average fluid temperature. Consequently, the ratio between the inter-tube heat transfer and the borehole heat transfer for fluid flow circulating at a low velocity is much higher than that for fluid flow circulating at a high velocity.

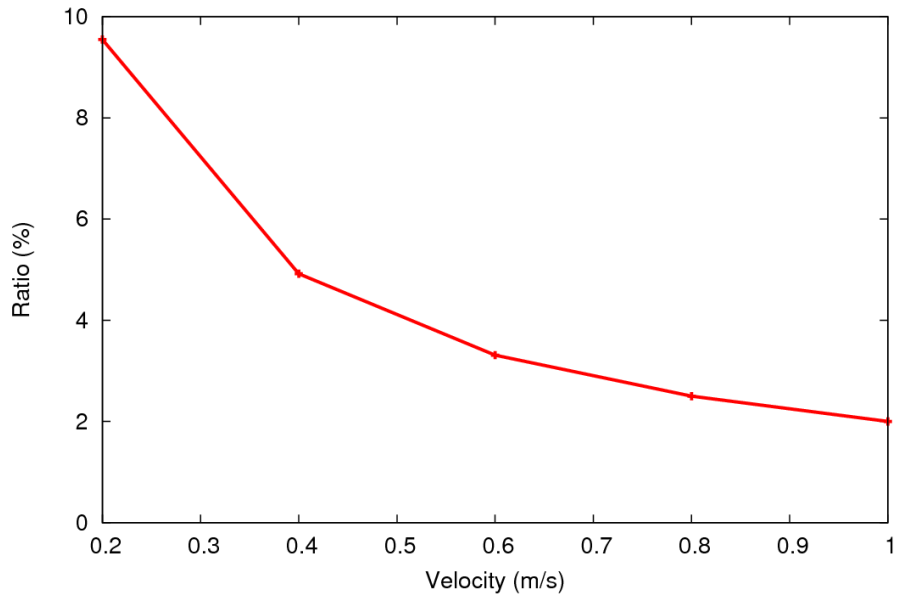

Figure 4.7 Ratio between the total inter-tube heat transfer and the total borehole heat transfer at different velocities.

4.3 Transient Simulations

Steady-state simulations of a BHE can give some insight into the responses of the BHE over long timescales. The dynamic response of BHEs over short timescales, in many applications, can be of greater interest. Transient simulations are reported in this section and have been

used to examine the dynamic responses of a single BHE over short timescales. The variations of fluid temperature profiles, borehole heat flux profiles, and inter-tube heat flux profiles along the borehole depth in short timescales under a step change in inlet temperature are discussed.

4.3.1 Fluid Temperature Profiles

A step change in inlet temperature is applied to examine the fluid temperature profiles along the borehole depth in short timescales. Figure 4.8, Figure 4.9, and Figure 4.10 show the fluid temperature profiles along the borehole depth with fluid circulating at the velocities of 1.0 m/s, 0.6 m/s, and 0.2 m/s, respectively.

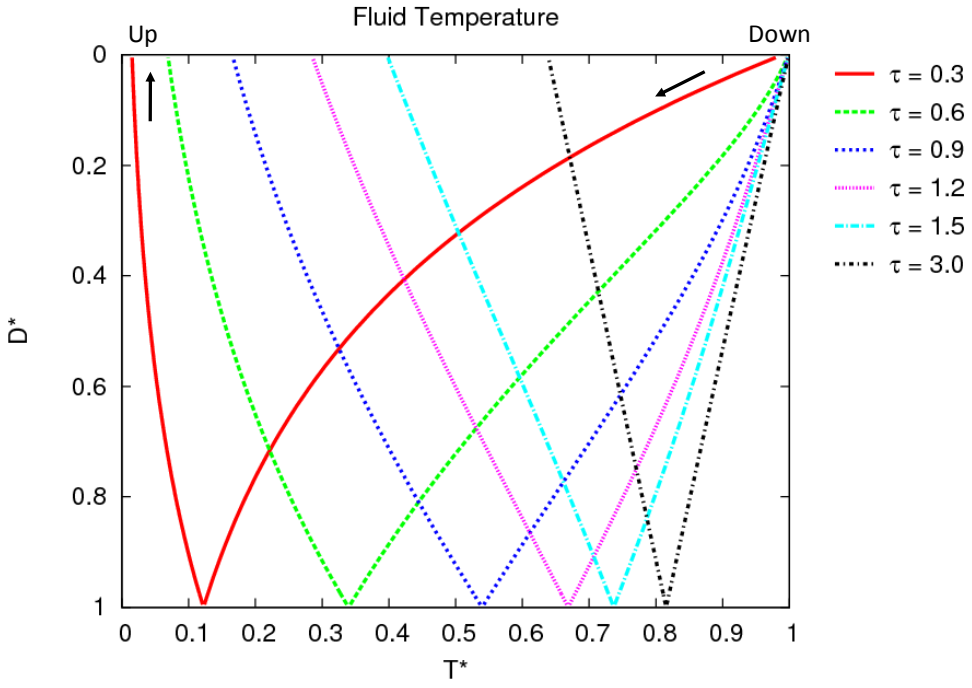

Figure 4.8 Fluid temperature profile along the borehole depth (v=1.0m/s, Re = 25,400).

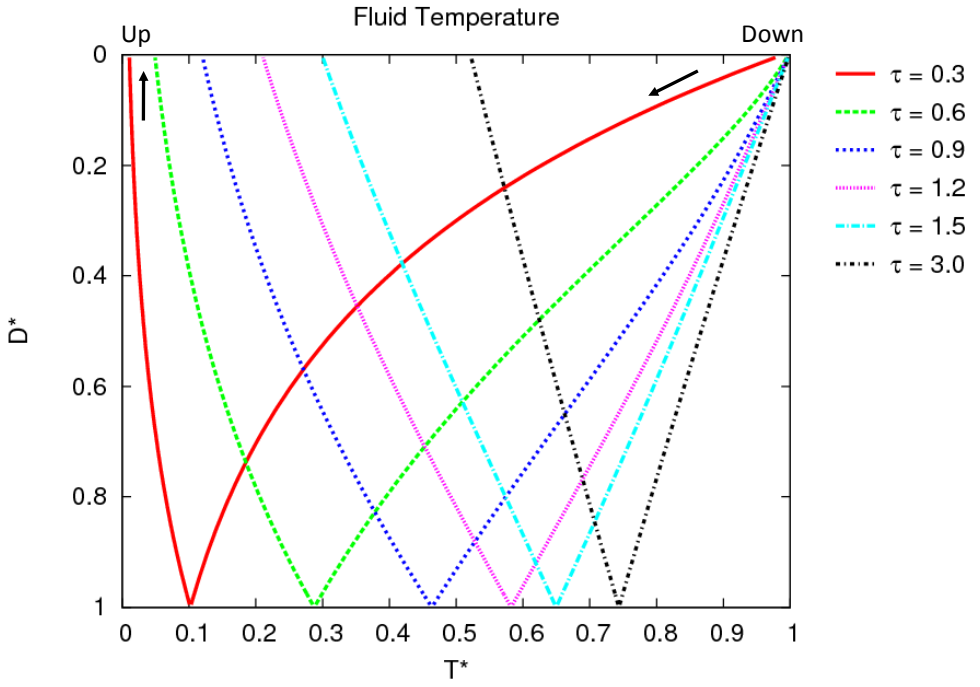

Figure 4.9 Fluid temperature profile along the borehole depth (v=0.6m/s, Re = 15,240).

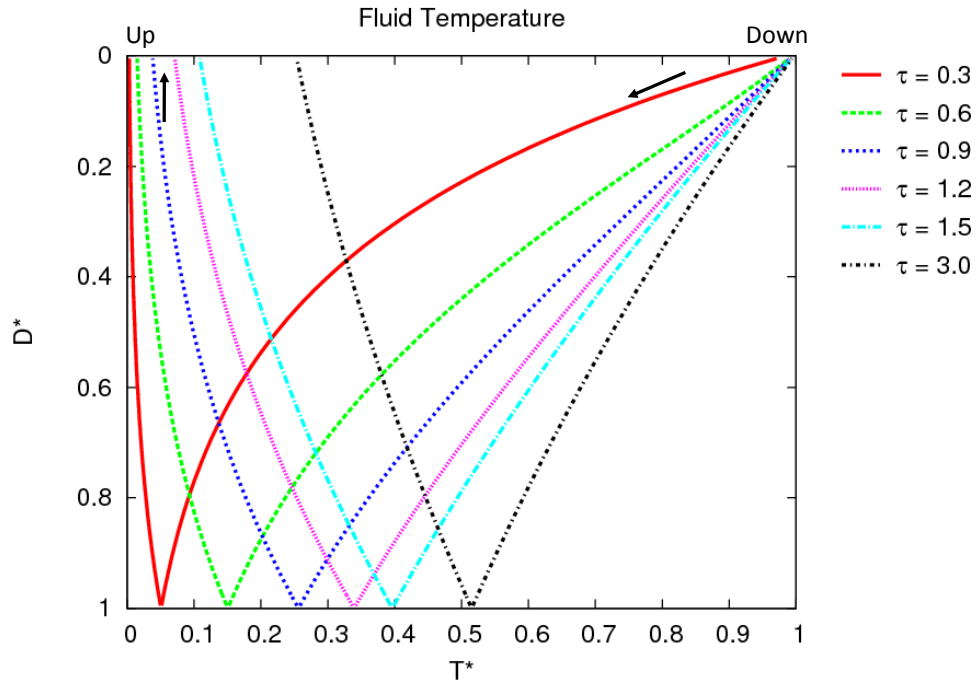

Figure 4.10 Fluid temperature profile along the borehole depth (v=0.2m/s, Re = 5,080).

For the same dimensionless transit time τ, the fluid temperature profiles differ for fluid circulating at different velocities. This is because the fluid temperature profile is not only

dependent upon the circulating velocity of the fluid but also the convection heat transfer introduced by the circulating fluid, as well as the conduction heat transfer through the grout and ground. Nevertheless, the non-linearity of the temperature profiles along the depth of the borehole for smaller τ is clearly demonstrated, although they are approaching linear distribution for τ larger than 3 in the first two cases (v = 1.0m/s and v = 0.6m/s). In the case of the smallest velocity (v = 0.2m/s), the non-linearity remains after τ gets larger than 3 and seems continue even when the simulation approaches steady-state.

4.3.2 Inter-Tube Heat Flux Profiles

Figure 4.11, Figure 4.12 and Figure 4.13 show the inter-tube heat flux profiles along the borehole depth with fluid circulating at the velocity of 1.0 m/s, 0.6 m/s, and 0.2 m/s, respectively. This inter-tube heat flux is caused by the temperature difference between the two adjacent pipes inside the borehole. The non-linearity of the profiles can be observed for smaller dimensionless transit time. For τ with higher values, the inter-tube heat flux profiles along the borehole depth approach a linear distribution.

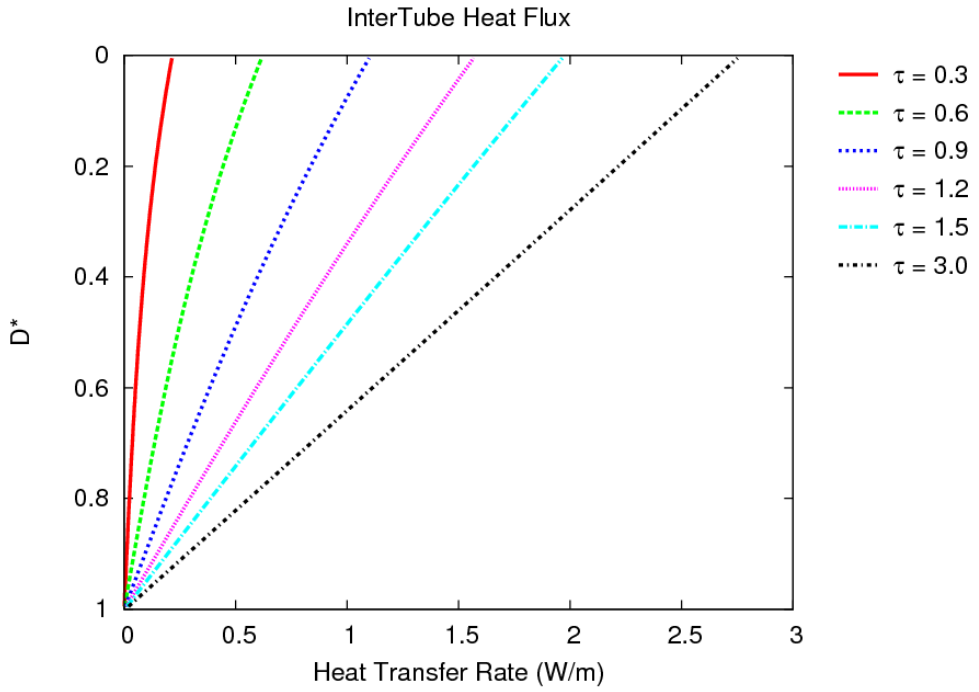

Figure 4.11 Inter-tube heat flux along the borehole depth (v=1.0m/s, Re = 25,400).

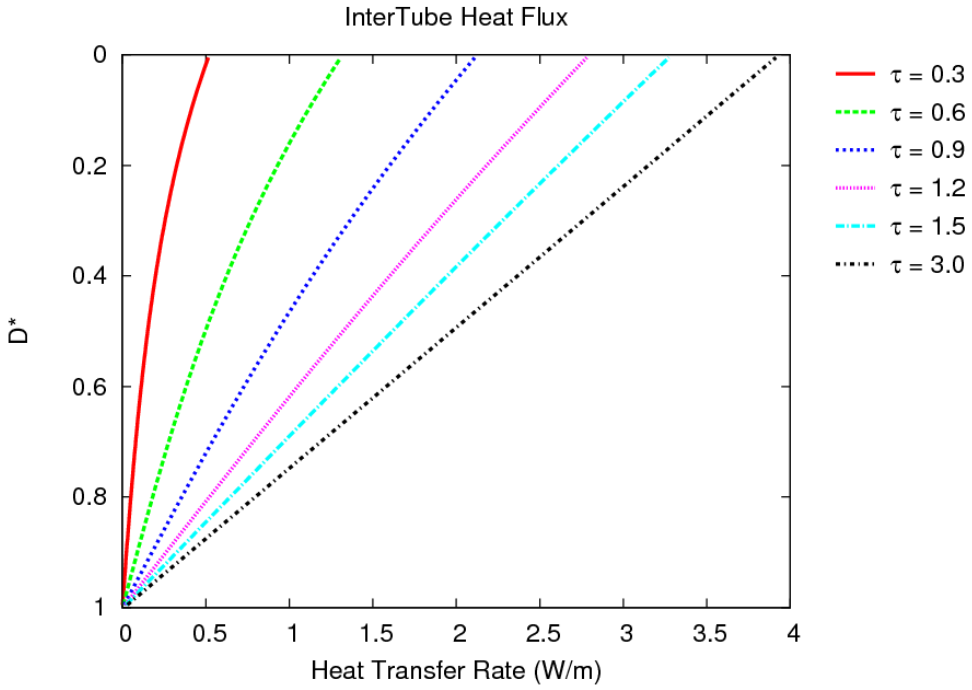

Figure 4.12 Inter-tube heat flux along the borehole depth (v=0.6m/s, Re = 15,240).

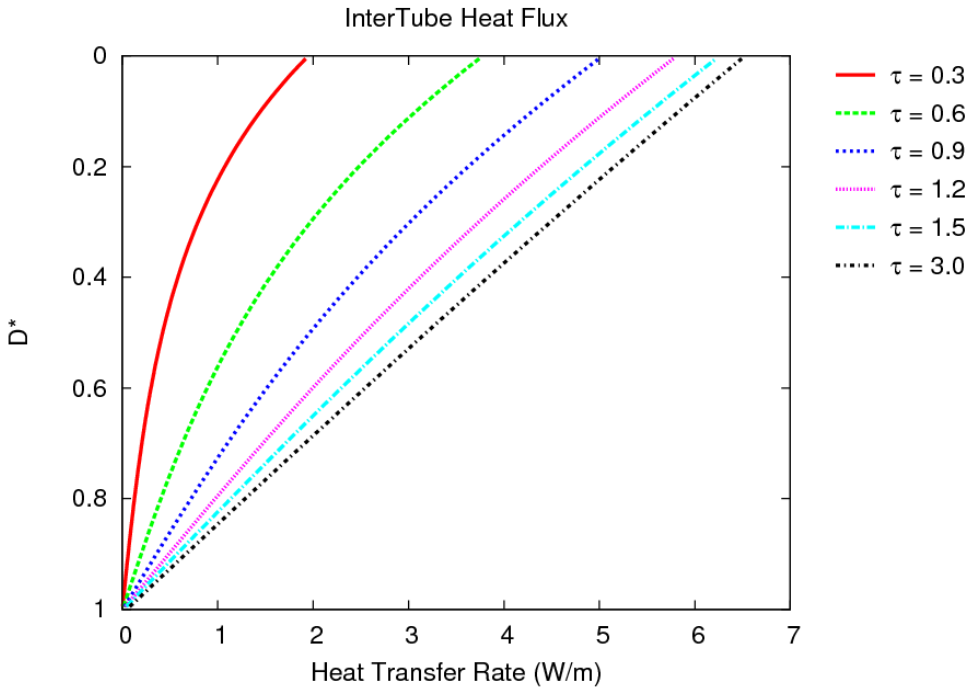

Figure 4.13 Inter-tube heat flux along the borehole depth (v=0.2m/s, Re = 5,080).

4.3.3 Borehole Heat Flux Profiles

Figure 4.14, Figure 4.15, and Figure 4.16 show the borehole heat flux profiles along the borehole depth.

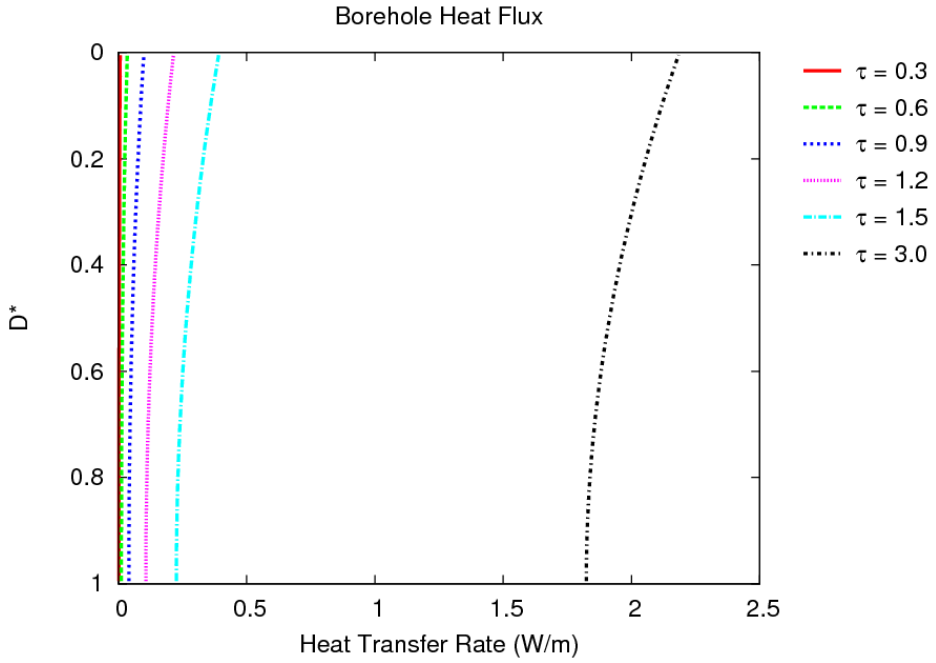

Figure 4.14 Heat flux along the borehole depth (v=1.0m/s, Re = 25,400).

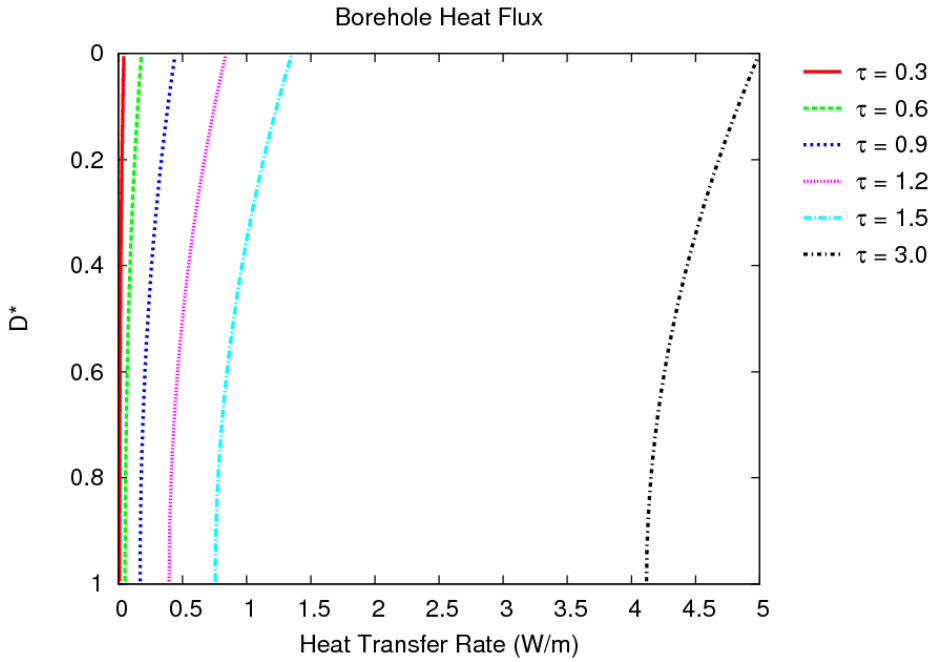

Figure 4.15 Heat transfer along the borehole depth (v=0.6m/s, Re = 15,240).

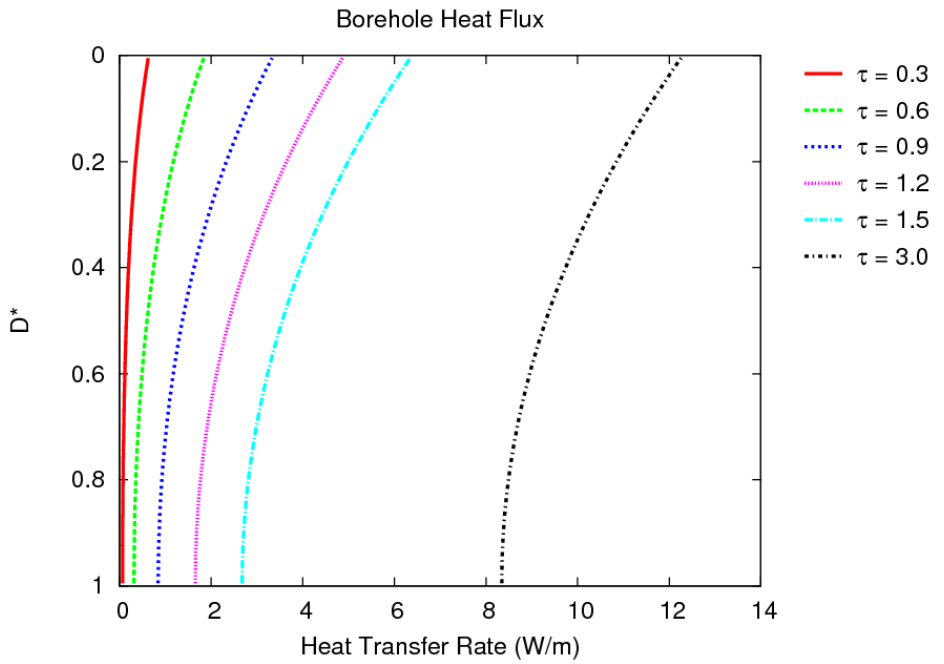

Figure 4.16 Heat transfer along the borehole depth (v=0.2m/s, Re = 5,080).

This heat flux is caused by the temperature difference between the borehole wall and the far-field temperature. The borehole heat flux increases as the transit time τ increases. The non-linearity for large dimensionless transit time τ can be easily observed.

4.3.4 Comparison of Inter-Tube and Borehole Heat Transfer Rates

The heat transfer process within the borehole at short timescale can be examined by comparing the total inter-tube heat transfer – which indicates the 'short-circuit' heat transfer from one pipe directly to the other pipe – and the total heat transfer across the borehole surface.

Figure 4.17 shows the comparisons of inter-tube and borehole heat transfer rates for fluid circulating at three different velocities, v = 1.0 m/s, 0.6 m/s, and 0.2 m/s. The dimensionless transit time τ varies from 0 to 3.

The inter-tube heat transfer is higher than the borehole heat transfer up to τ = 2.5 for the case with the fluid circulating at a velocity v = 1.0 m/s; up to τ = 2 for v = 0.6m/s; and up to τ = 1.2 for v = 0.2 m/s. In this step change test, the inter-tube heat transfer increases rapidly but approaches a steady value quickly as τ approaches 3. The borehole heat transfer, on the other hand, increases slowly at the beginning but increases rapidly (linearly) as τ increases to 3. The

borehole heat transfer will approach to stable as simulation continues, and the timescale of this will be examined in Section 4.4.3. Low inter-tube heat transfer can be expected for cases with high fluid velocity due to the small temperature difference between the downward and upward fluid flows, and high inter-tube heat transfer for cases with low fluid velocity due to the large temperature difference between the downward and upward fluid flows.

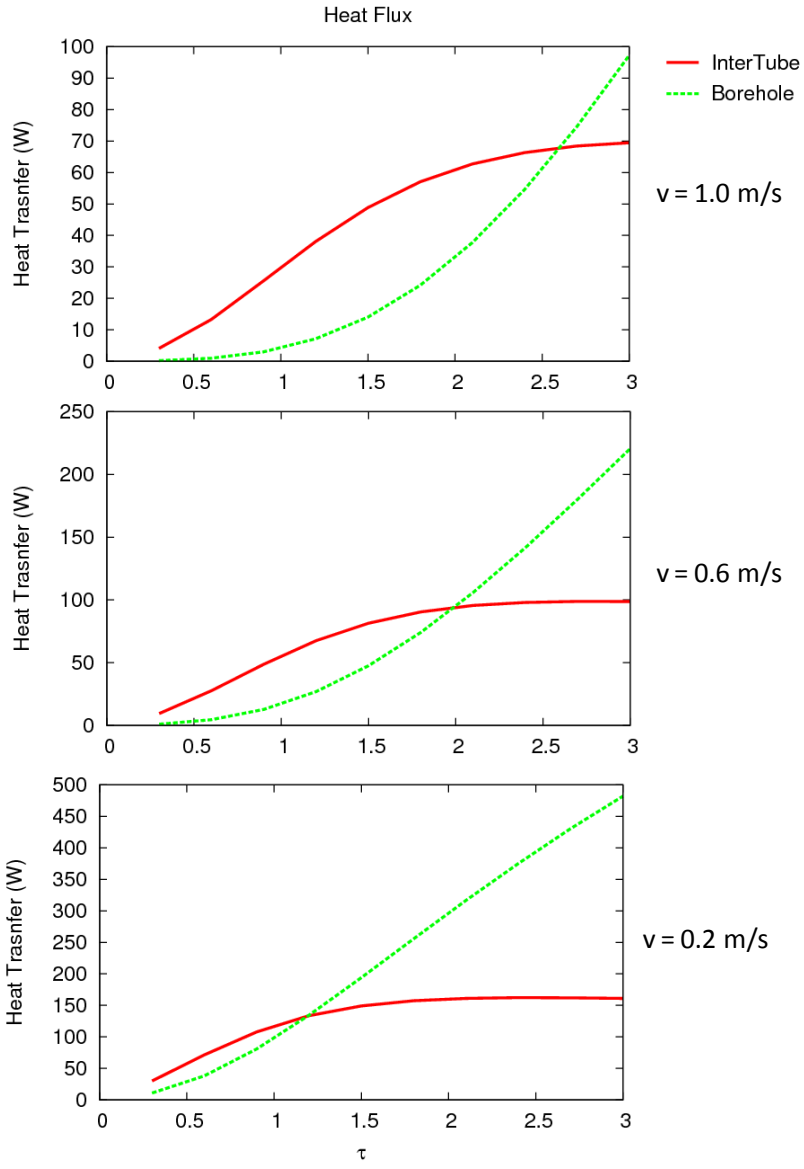

Figure 4.17 Comparisons of inter-tube and borehole heat transfer rates for fluid circulating at different velocities.

4.4 Comparisons between the 2D and 3D models

Both the 3D and 2D models have been applied to simulate the BHE defined in Table 4.1. Steady-state temperatures and heat transfer for fluid flows at various velocities are examined. Transient simulations under a step change in fluid inlet temperature are applied to investigate the outlet temperature responses of the 3D and 2D model over short timescales. Various circulating fluid velocities have been studied. The implications of differences in predictions by the 3D and 2D models are further examined through simulating synthetic heat pump cyclic operation. Furthermore, different responses of the 3D and 2D models has been characterised in terms of frequency response.

4.4.1 Steady-state Temperature and Heat Balance

The difference in terms of model predictions by the 3D and 2D model is firstly examined through comparisons of outlet temperatures, inter-tube heat transfer, and borehole heat transfer in steady-state conditions. The results of the comparisons for fluid circulating at different velocities are shown in Table 4.3. The outlet fluid temperatures (T_{out}) predicted by the 3D model are slightly lower than that predicted by the 2D model except the case with the lowest velocity (0.2 m/s) in which the outlet temperature predicted by the 3D model is relatively higher than that predicted by the 2D model. Due to the way that the inlet and outlet temperatures are associated with the boundary conditions in the 2D model (as explained in Chapter 3), the inter-tube heat transfer (Q_{int}) predicted by the 2D model is nearly double that predicted by the 3D model. The heat transfer across the borehole surface (Q_b) predicted by the 3D model is slightly lower than that predicted by the 2D model.

The predictions of the fluid temperature profiles and heat flux profiles along the borehole depth by the 3D model in steady-state simulations have been examined in Section 4.2. It has been demonstrated that the non-linearity of these profiles along the borehole depth is very significant for fluid circulating at low velocity (0.2 m/s), although for fluid circulating at high velocity (1.0 m/s), these profiles can be regarded as linear. However, the variations of the fluid temperature and heat transfer along the depth of the borehole cannot be simulated explicitly in the 2D model. It is always assumed that the fluid temperature and heat transfer profiles along the depth of the borehole are linear. This partially explains the differences in the outlet temperatures and borehole heat transfer rates calculated by the 3D and 2D model, as the difference is larger when the flow velocity gets lower.

Table 4.3 Comparisons of temperature and heat transfer calculated by the 3D and 2D model in steady-state simulations.

Velocity (m/s)	Model	T_{in} (°C)	T_{out} (°C)	Q_{int} (W)	Q_b (W)	Ratio (%)
1.00	3D	20.0	19.09	44	2210	2.0
	2D	20.0	19.10	87	2215	3.9
0.80	3D	20.0	18.87	55	2181	2.5
	2D	20.0	18.89	107	2188	4.9
0.60	3D	20.0	18.53	71	2132	3.3
	2D	20.0	18.55	139	2144	6.5
0.40	3D	20.0	17.89	100	2038	4.9
	2D	20.0	17.91	199	2062	9.6
0.20	3D	20.0	16.32	169	1780	9.5
	2D	20.0	16.25	348	1852	18.8

4.4.2 Outlet Temperature Responses

The dynamic characteristics of the 3D model can be illustrated in terms of outlet temperature response by applying a step change in inlet temperature. The outlet temperature response can be normalised by considering the ratio of temperature changes between the outlet and initial temperatures and the inlet and initial temperatures, which can be expressed as:

$$T_{out}{}^{*} = \frac{T_{out} - T_{initial}}{T_{in} - T_{initial}} \tag{4.1}$$

where T_{in} is inlet fluid temperature, T_{out} is outlet fluid temperature, and $T_{initial}$ is initial fluid temperature.

Figure 4.18 shows the outlet temperature responses predicted by the 2D and 3D models for fluid circulating inside the pipes at a velocity of 1 m/s. The responses are shown on a logarithmic timescale (x axis) for a simulation of 120 minutes. In the case of the 3D model, the nominal fluid transit time is 200 seconds, but the differences in the responses by these two models prevail over the first 10 minutes. The response predicted by the 3D model is much slower than that by the 2D model in this period. This is because; the response of the 2D model is governed entirely by the transient conduction of heat through the pipe wall and grout. But in the 3D model, not only are the thermal mass of the pipes and grout taken into account but also the effect of the dynamics of the circulating fluid. This is a question of both the thermal

mass of the fluid itself as well as its transport along the pipe and heat loss through the pipe wall. The response is not just delayed according to the nominal transit time, which is 200 second in this case, but can be seen to be significant for several times this period – up to approximately 10 minutes in this case. Beyond this timescale, the response predicted by the 2D model is very similar to that of the 3D model.

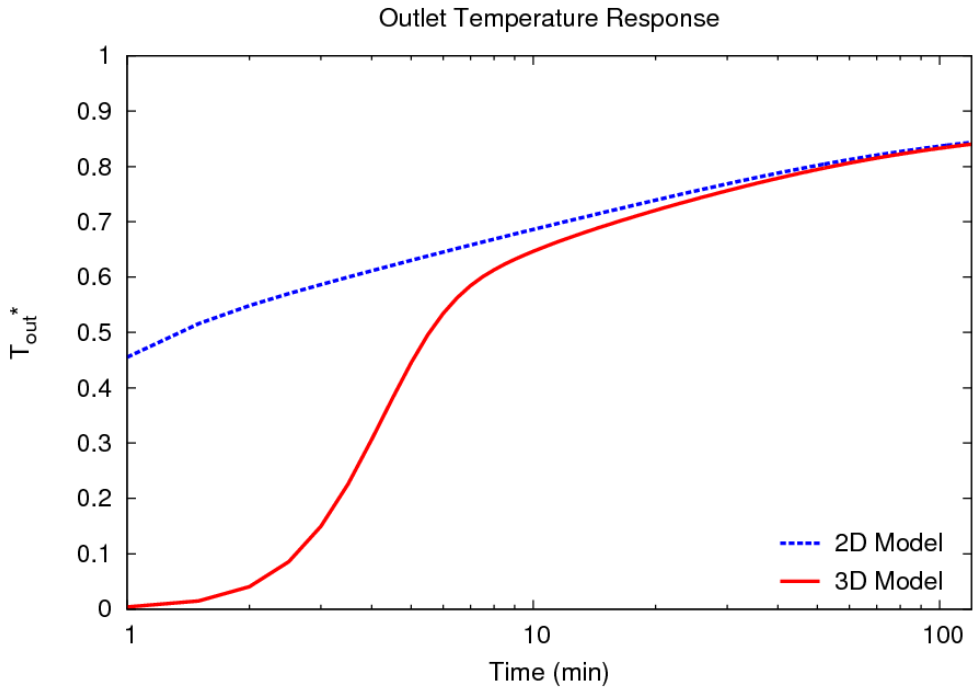

Figure 4.18 Outlet temperature responses predicted by the 2D and 3D models at v = 1.0 m/s.

The outlet temperature responses by the 2D and 3D models at different velocities, 1.0 m/s, 0.8 m/s, 0.6 m/s and 0.4 m/s, are shown in Figure 4.19. As expected, the 2D model predicted a much faster response compared to that predicted by the 3D model. The lower the velocity, the longer period the difference prevails. The difference of the responses predicted by the 2D and 3D models for all fluid velocities studied are similar in the calculations by the 2D and 3D models after approximately 2 hours.

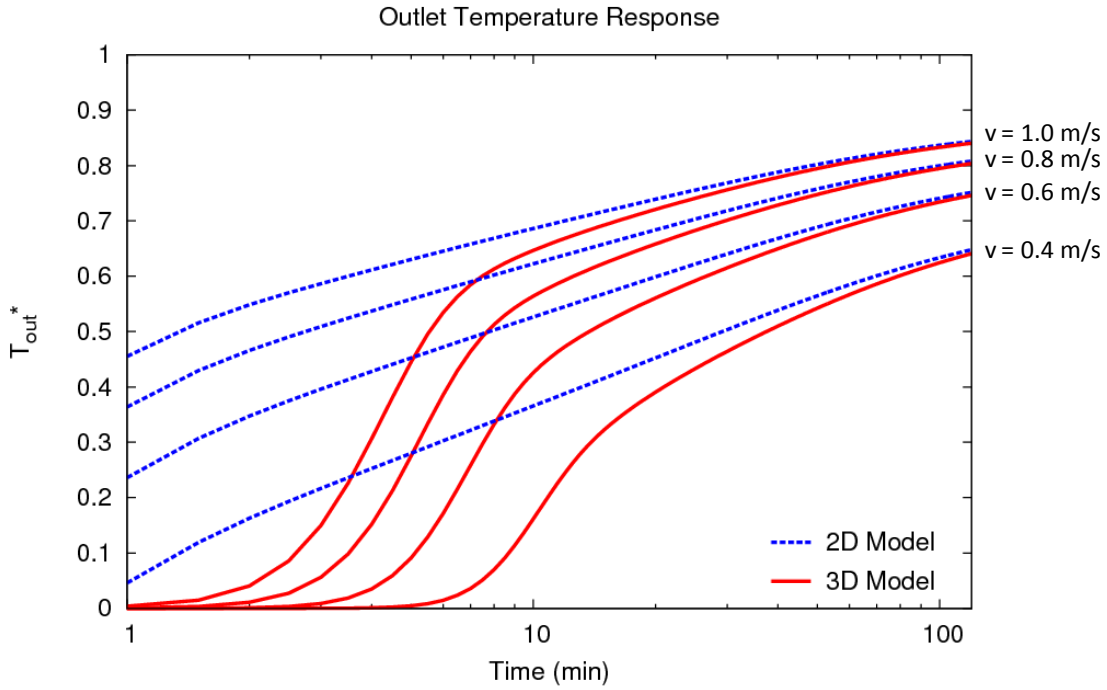

Figure 4.19 Outlet temperature responses predicted by the 2D and 3D models at different velocities.

In the 2D model, where only the BHE of one metre depth is simulated, the outlet temperature is calculated in an iterative manner to ensure the fluid heat balance is consistent with the heat transfer across the inner surface of the pipes.

$$T_{out} = T_{in} - \frac{Q}{mc_p} \qquad \textbf{(4.4)}$$

where Q is the total heat transfer across the inner surface of the pipes (W/m), m is the mass flow rate (kg/s), c_p is the specific heat capacity (J/kg.K), T_{in} is the inlet temperature (°C) and T_{out} is the outlet temperature (°C).

Figure 4.20 shows heat transfer rates across the inner surface of the pipes calculated by the 2D model at different fluid velocities. Unrealistically high heat transfer rates are predicted by the 2D model at the start of the simulations in very case. This explains the different responses of the outlet temperatures at the beginning of the simulations shown in Figure 4.19.

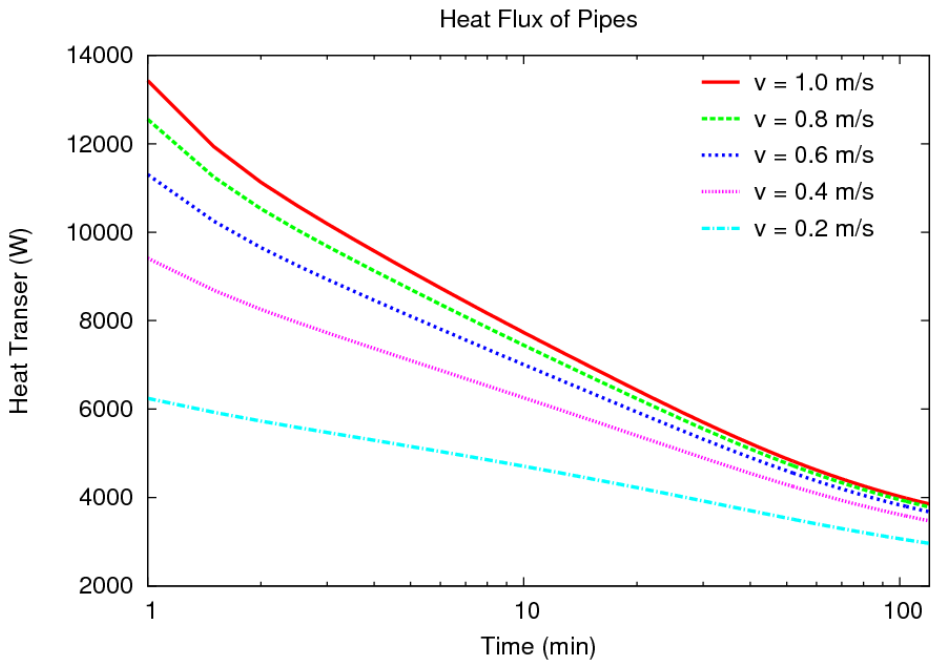

Figure 4.20 Heat transferes across the inner boundary of the pipes calculated by the 2D model at different fluid velocities.

Figure 4.21 shows the outlet temperature responses predicted by the 2D and 3D models for fluid circulating inside the pipes at a velocity of 0.2 m/s.

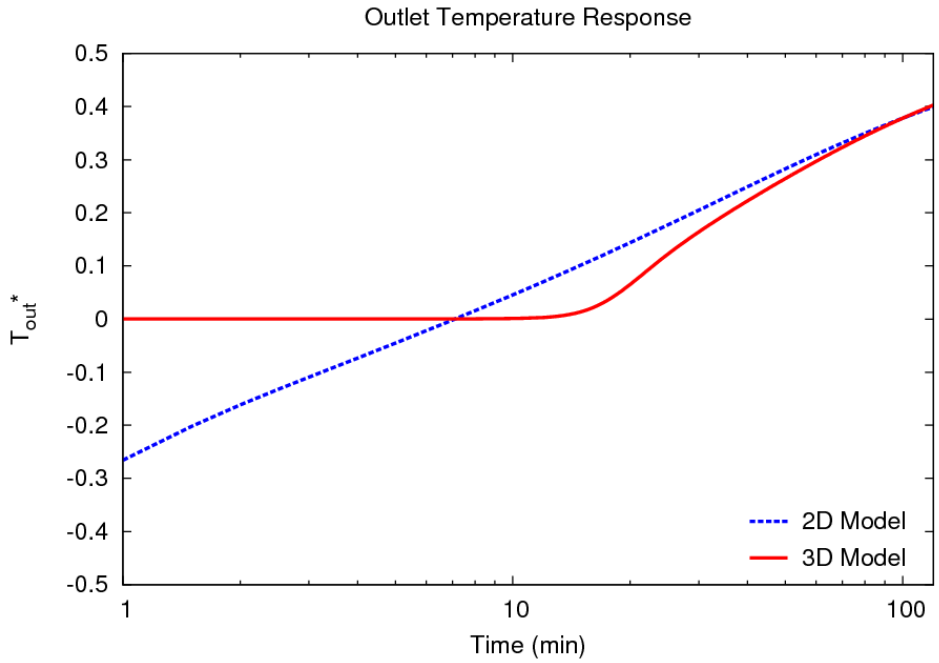

Figure 4.21 Outlet temperature responses by the 2D and 3D models at v = 0.2 m/s.

The negative T_{out*} indicates an unrealistic outlet temperature response calculated by the 2D model for the first few minutes (up to 8 minutes). This is because the iteration process used in the 2D model gives an outlet temperature that is mathematically correct but is not physically possible. This means the 2D model cannot be used to simulate BHEs with low fluid velocity at very short timescales. It is also possible that the iterative procedure will not converge. These issues are found with other 2D models that use this iterative procedure (Yavuzturk, 1999).

4.4.3 Pipe and Borehole Short Timescale Response

Assuming the initial temperature to be 10 ^{o}C and applying a step change at the inlet temperature from 10 ^{o}C to 20 ^{o}C at the start of the simulation (t=0) and maintaining it at 20 ^{o}C during the simulation time t for 24 hours, makes it possible to examine the heat transfer process within the borehole. Figure 4.22 shows the total heat transfer across the inner surface of the pipes and the borehole surface predicted by the 3D model using a log timescale. The fluid is circulating at 1 m/s.

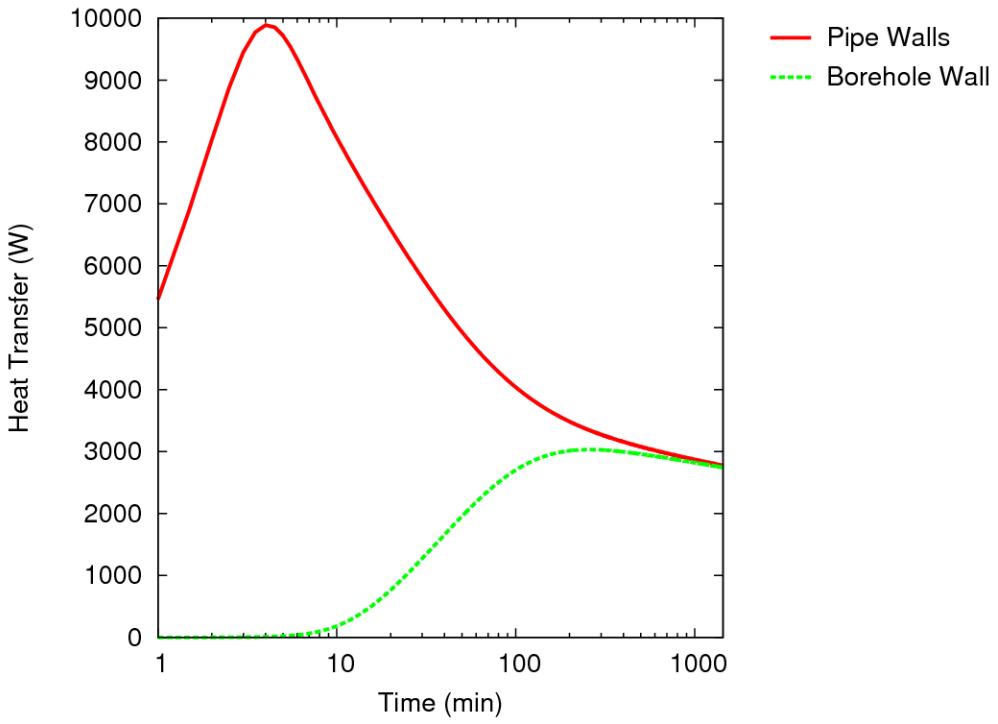

Figure 4.22 Heat Transfer across the pipe walls and borehole wall predicted by the 3D model.

The total heat transfer across the inner surface of the pipes starts at around 5.5 kW and hits a peak of nearly 10 kW at around 4 minutes. This is due to the fluid transport and the thermal

mass of the fluid that have been simulated in the 3D model. The total heat transfer across the inner surface of the pipes starts to decrease since then and approaches to a stable value of around 2.8 kW at the end of 24 hours.

The variation of the heat transfer across the borehole surface is very different over this same timescale. For the first 10 minutes, the heat transfer across the borehole wall is nearly zero. This is due to the thermal mass of the fluid, pipes and grout that have been simulated in the 3D model. The heat transfer at the borehole wall starts to increase after 10 minutes and approaches a maximum value of approximately 3 kW after nearly 2 hours, and decreases to the same value as that predicted at the pipe surface.

Figure 4.23 shows the comparison of heat transfer at the pipe and the borehole surfaces predicted by the 3D and 2D models. The heat transfer predicted at the borehole wall by the 3D and 2D models are very similar except that between the 10th and the 11th minute, the heat transfer predicted by the 3D model is slightly lower than that predicted by the 2D model.

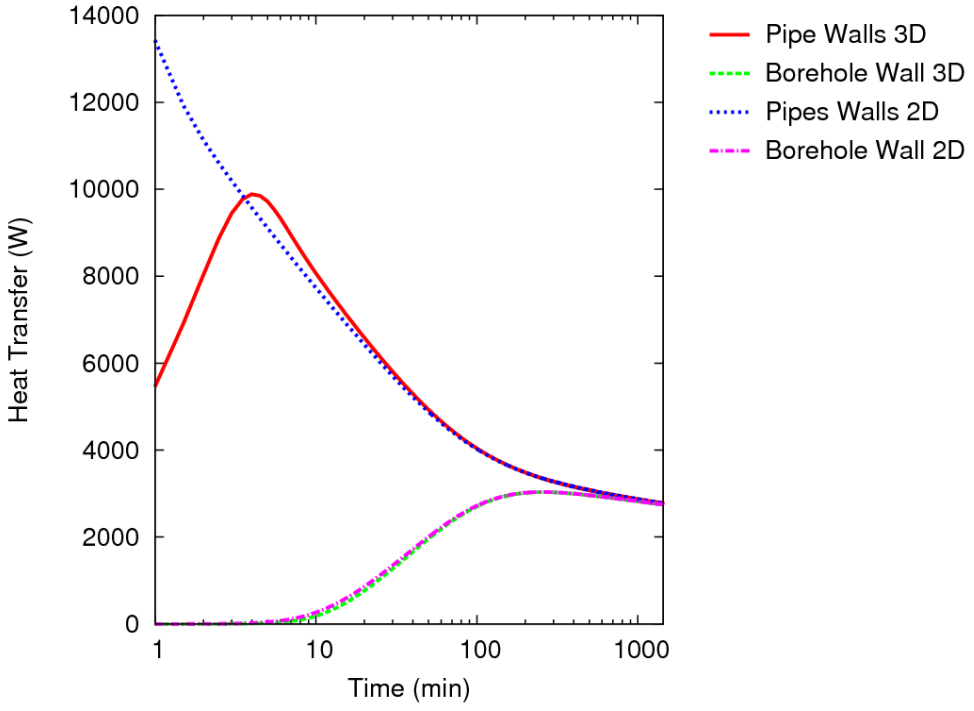

Figure 4.23 Comparison of heat transfer rates of pipes and borehole by the 3D and 2D models.

The heat transfer across the inner surface of the pipes predicted by the 3D and 2D models are significantly different during the first 4 minutes. The heat transfer at the pipe surface predicted

by the 2D model is at its highest value at the very beginning of the simulation: approximately 13.6 kW. As the simulation time increases, the heat transfer at the pipe surface decreases and approaches to the same value as that predicted by the 3D model.

The different predictions of the heat transfer at the pipe surface by the 3D and 2D model at short timescales are mainly due to the transport and the thermal mass of the fluid that have been simulated in the 3D but not the 2D model. In the 3D model, due to the transport delay, not all the pipe is exposed to the warm fluid at the same time, and the heat transfer across the surface of the pipes does not correspond to the overall heat balance of the BHE. In the 2D model, an iterative procedure is used to calculate the outlet temperature according to the overall heat balance. As a result, the heat transfer across the surface of the pipes always corresponds to the overall heat transfer of the BHE, which is not accurate and realistic at short timescales. In some cases, especially with low fluid flow velocities, this unrealistic heat transfer across the surface of the pipes can result in unrealistic outlet temperature calculated at the beginning of the simulation, as illustrated in Figure 4.21.

4.4.4 Simulated Heat Pump Operation

A square wave function has been applied to study the practical significance of transient fluid transport and the resulting delayed responses. This has been studied using repeating step changes that might be typical of the on-off operating cycle of a domestic heat pump. It is assumed that the heat pump cycles twice per hour with the inlet temperatures changing suddenly between 25 ^{o}C and 15 ^{o}C. The far-field ground temperature is assumed to be 10 ^{o}C. A steady-state simulation, with the inlet temperature of 20 ^{o}C and far-field temperature of 10^{o}C, has been carried out to build up the thermal history i.e. many years of excitation. The inlet and outlet temperatures predicted by the 2D and 3D models are shown in Figure 4.24. This study has also been reported in He *et al.* (2010).

The outlet temperature predicted by the 2D model necessarily shows an instant response to changes in the inlet temperature. This is representative of many models that are formulated on a one or two-dimensional basis. In contrast, the outlet temperature predicted by the 3D model shows a delay in response to the step changes and this could significantly change overall system behaviour when interaction with heat pump control system (i.e. fluid and room thermostats) is considered (Kummert and Bernier, 2008).

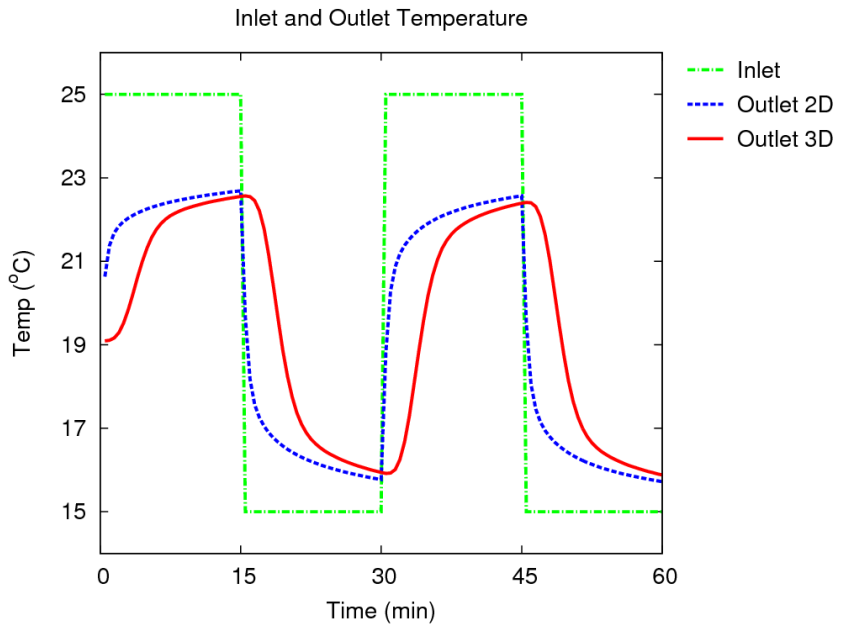

Figure 4.24 Fluid inlet and outlet temperatures for a step change function.

The dynamic behaviour of the BHE also depends upon the velocity of the circulating fluid. Figure 4.25 shows the outlet temperature variations that are predicted by the 3D model at different velocities. The smaller the velocity is, the longer the delayed response can be expected.

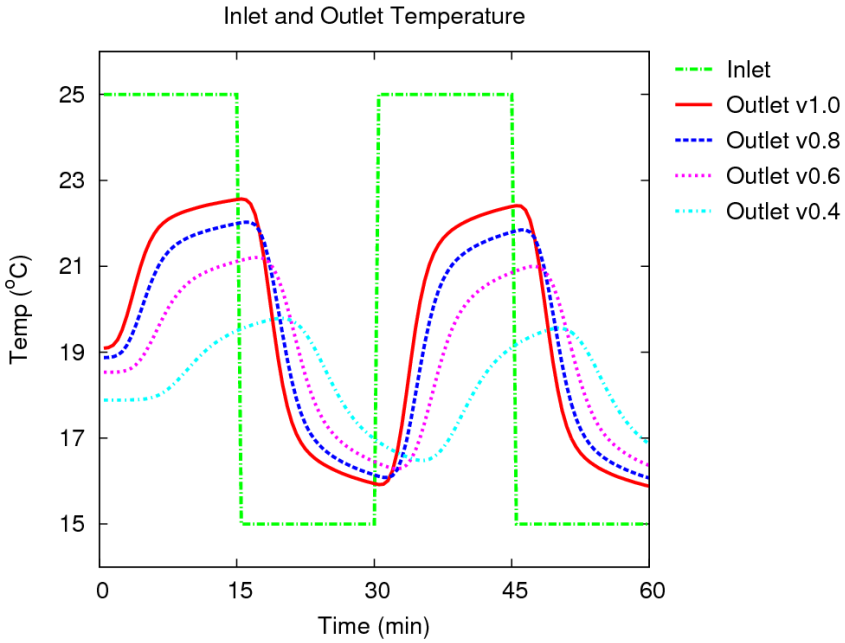

Figure 4.25 Fluid inlet and outlet temperatures for a step change function at different velocities.

4.4.5 Frequency Response Test

BHE arrays experience periodic variations in system temperatures on a wide range of timescales varying from annual, daily and sub-minutely. Response is often analysed as that of a superposition of steps of different magnitude and duration. It is equally valid to think of the overall response in terms of superposition of sinusoidal variations. A useful way to characterise the response of the BHE and the models is, accordingly, to impose a periodic excitation of the inlet temperature and compare this with that of the outlet over a range of frequencies. In this case, a sinusoidal variation in inlet temperature with the same amplitude (A_{in}) but different frequencies (f), or periods (P) have been applied. The dynamic responses of the BHE models can then be characterised by examining the amplitude and phase (θ) of the predicted outlet fluid temperature.

The variation of the inlet fluid temperature in this study can be expressed as:

$$T_{in} = T_i + A_{in} \sin\left(\frac{2\pi}{P} t\right) = T_i + A_{in} \sin(2\pi f t) \tag{4.2}$$

And the variation of the outlet fluid temperature can be expressed as:

$$T_{out} = T_o + A_{out} \sin\left(\frac{2\pi}{P} t + \frac{2\pi}{\Delta P}\right) = T_o + A_{out} \sin(2\pi f t + \theta) \tag{4.3}$$

where ΔP is the time shift or delay between peak inlet and outlet temperatures. This can also be expressed as a phase shift θ.

All the simulations are started from the steady-state condition (i.e. representative of operation over a long period) with an initial and far-field temperature of 10 ^{o}C and a constant inlet temperature of 20 ^{o}C to enable a consistent and generic comparison. All the simulations are run for 2 hours. The responses of the 2D and 3D models are quantified using the amplitude ratio (A_{out}/A_{in}) and phase shift (θ or $2\pi/\Delta P$). ΔP is the time shift and is estimated by the time delay between the appearance of peak in the inlet temperature and the appearance of the corresponding peak in the outlet temperature.

Figure 4.26 shows the outlet temperature variations by the 2D and 3D model in response to the inlet temperature of a sine wave with the amplitude of 5 K and the frequency of 1/600 Hz (a 10 min period).

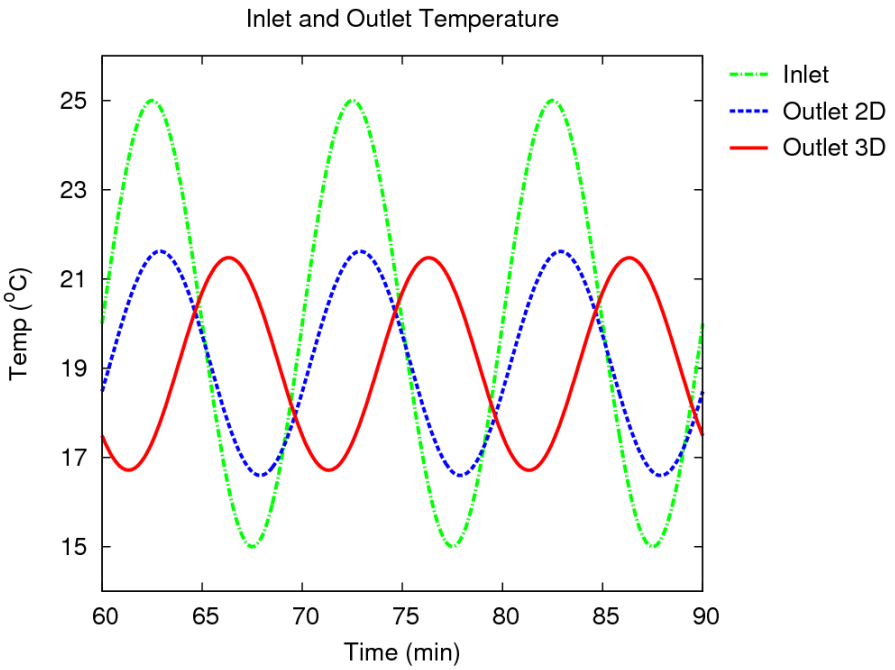

Figure 4.26 Inlet and outlet temperatures by the 2D and 3D models at a frequency of 1/600 Hz.

At this particular frequency, the outlet temperature calculated by the 3D model shows an amplitude (A_{out}) of 2.38 K and a phase shift (ΔP) of 230 s. The amplitude of the outlet fluid temperature predicted by the 2D model is similar to the one predicted by the 3D model at this particular frequency although the phase shift is much smaller than that predicted by the 3D model. A range of frequencies have been applied to the inlet fluid temperature in order to obtain the full frequency response, and a sample of the predicted outlet fluid temperatures are shown in Figure 4.27 to Figure 4.31.

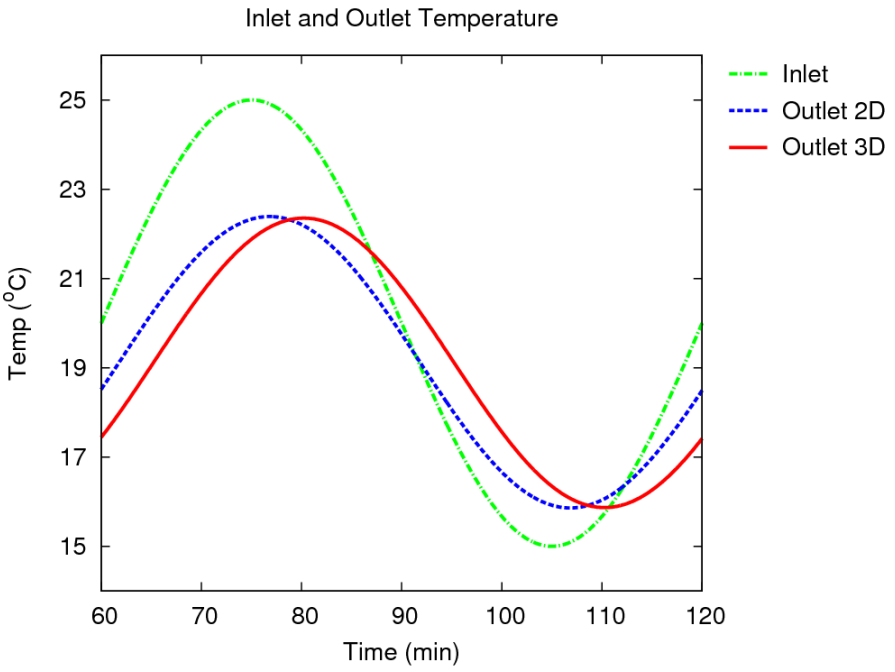

Figure 4.27 Inlet and outlet temperatures by the 2D and 3D models at a frequency of f=1/3600 Hz.

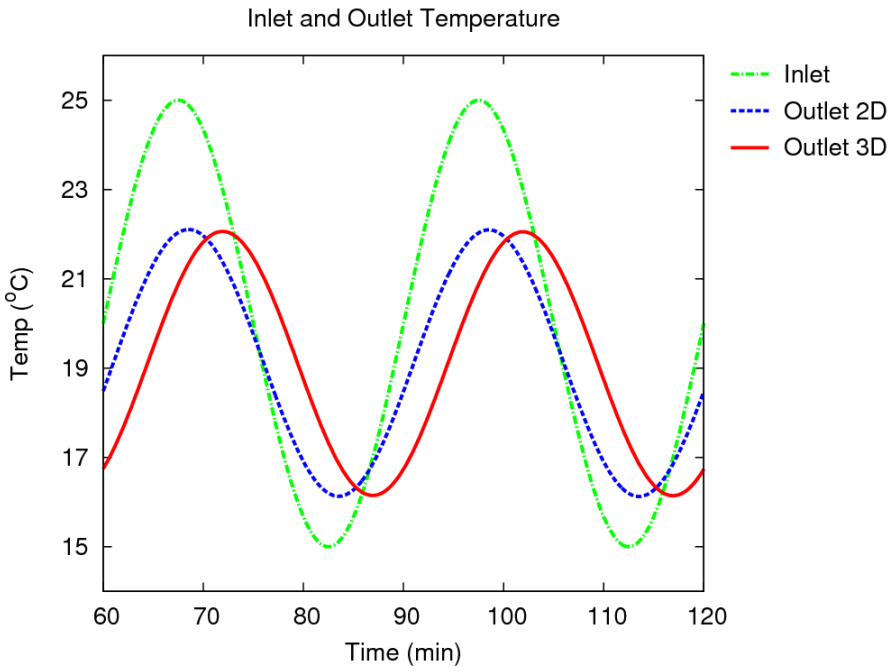

Figure 4.28 Inlet and outlet temperatures by the 2D and 3D models at a frequency of f=1/1800 Hz.

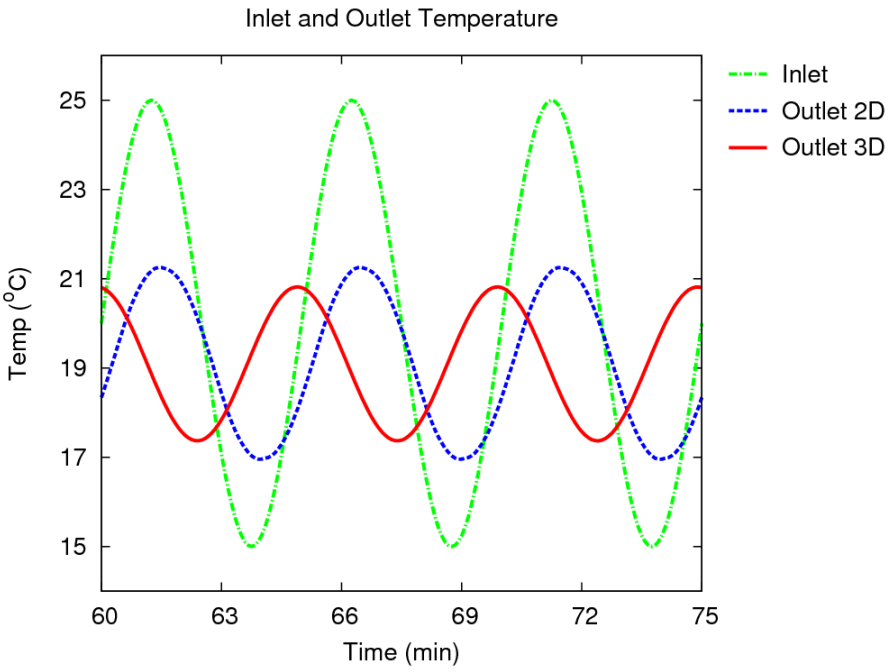

Figure 4.29 Inlet and outlet temperatures by the 2D and 3D models at a frequency of f=1/300 Hz.

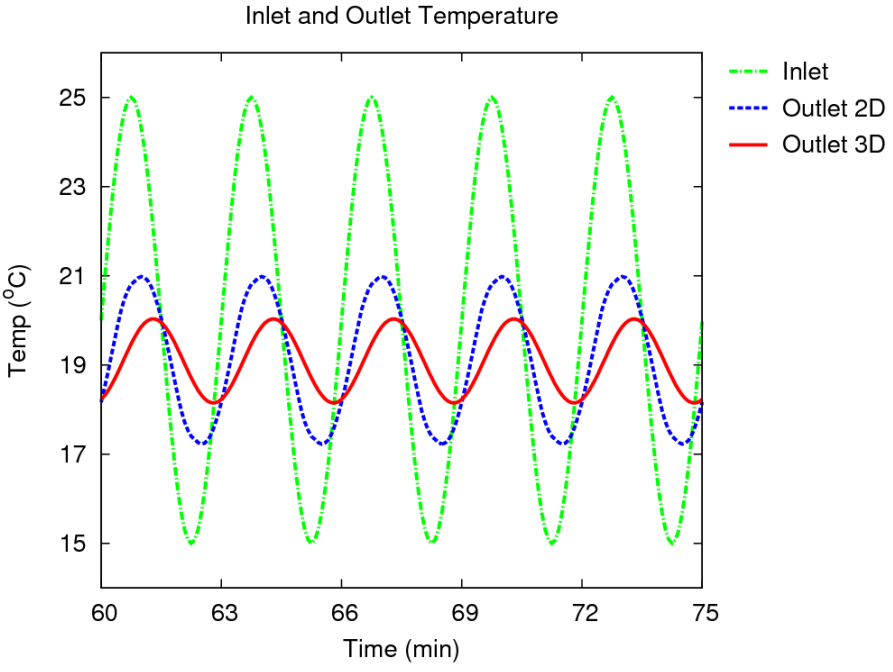

Figure 4.30 Inlet and outlet temperatures by the 2D and 3D models at a frequency of f=1/180 Hz.

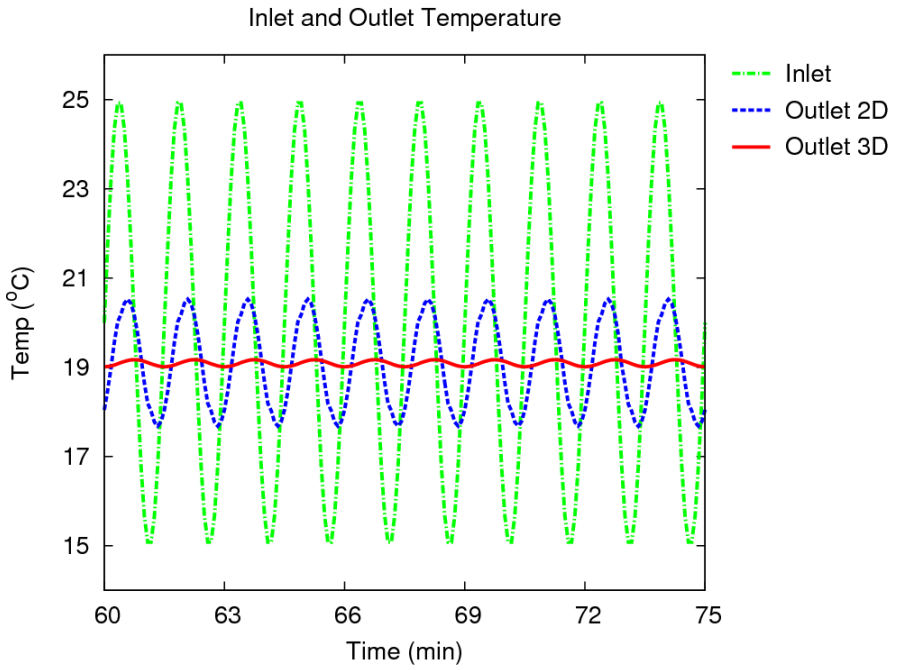

Figure 4.31 Inlet and outlet temperatures by the 2D and 3D models at a frequency of f=1/90 Hz.

Figure 4.32 shows the amplitude ratio (A_{out}/A_{in}) calculated by the 2D and 3D models on a logarithmic frequency scale. It can be seen that the amplitude ratio calculated by the 2D model decreases almost linearly as the frequency increases. This is because, in the 2D model, the damping effect on the amplitude of the outlet is only due to diffusion of the heat into and out of the pipes and adjacent grout. However, in the 3D model, the response is damped not only by the heat diffusion in and out of the pipes and adjacent grout, but also by the transport of the fluid as well as the heat transfer into and out of the fluid. Accordingly, a much reduced response is predicted by the 3D model when the frequency gets higher than 0.28 mHz. At lower frequencies, the predictions of the 2D and 3D models are similar. At high frequencies, the variation in inlet temperature results in no change in outlet temperature suggesting that the fluctuations are damped out the heat transfer relatively close to the pipe inlet.

Figure 4.33 shows the variation of phase shift according to the change of frequency for the 3D model. The phase shift can be more than 2π, and in this case the outlet temperature comes to the peak after the corresponding peak in the inlet temperature (Figure 4.30). When the frequency gets higher, the phase $\rightarrow\infty$, which means the outlet temperature becomes constant (Figure 4.31) and the fluctuation in the inlet temperature has no effect on the outlet temperature.

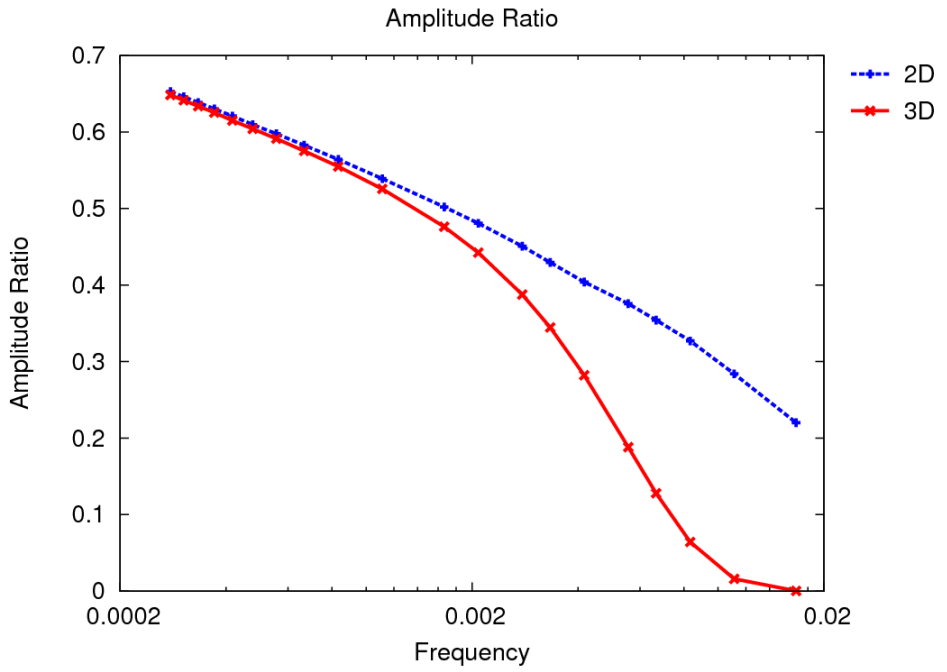

Figure 4.32 Amplitude ratio predicted by the 2D and 3D models across a range of frequencies.

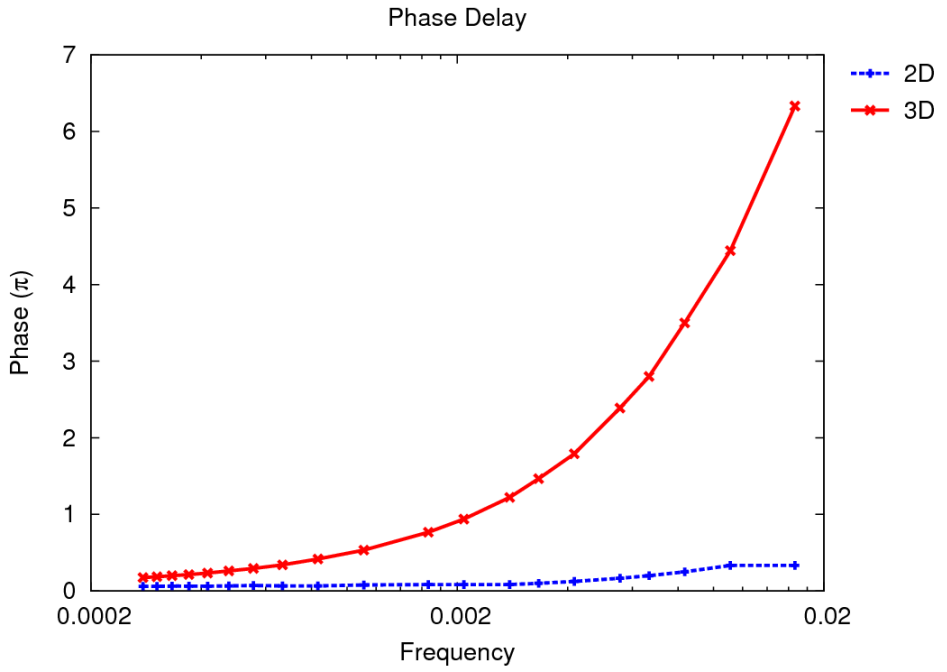

Figure 4.33 Phase delay predicted by the 2D and 3D models cross a range of frequencies.

4.5 Summary

The dynamic 3D model has been applied to simulate a single BHE in both steady-state and transient simulations. The variations of the fluid temperature profiles, borehole heat flux profiles and inter-tube heat flux profiles along the borehole depth in both long and short timescales have been examined. Velocities of the circulating fluid have been chosen to represent the full range of possible BHE fluid flow conditions.

In steady-state simulations it was found that the fluid temperature profiles and borehole heat flux profiles along the depth of the borehole were dependent upon the velocity of the circulating fluid and these two profiles were correspondent with each other. For relative high velocity the profiles were approximately linear; for mid-range velocity the profiles were noticeably non-linear; and for relatively low velocity the non-linearity of the profile was very noticeable. Therefore, in models which assume linear fluid temperature profiles or borehole heat transfer profiles some errors in overall heat transfer can be expected. The total inter-tube heat transfer rates varied in a similar non-linear manner and were found to be as much as 10% of the overall heat transfer at low fluid velocities.

For transient simulations, the non-linearity in fluid temperature profiles and borehole heat flux profiles could be clearly observed at short timescales, regardless of the fluid velocity. Although in cases with high fluid velocity the fluid temperature profiles and borehole heat flux profiles approach a linear profile as the simulation time increased, in cases with low fluid velocity, the non-linearity of these profiles remained.

The 2D model, implemented using the same numerical method applied for the 3D model, has also been applied to simulate the same single BHE. Comparisons of outlet temperature responses predicted by the 3D and 2D model have been made through transient simulations of step changes in inlet temperature. A delayed response in outlet temperature, associated with the transit of fluid along the pipe loop, was predicted by the 3D model, while an instant change was predicted by the 2D model. The response is not just delayed according to the nominal transit time but can be seen to be significant for several times this period.

The practical implications of this delayed response were further investigated through simulating a step change function in inlet temperature, which might be typical of a domestic heat pump operation and the on-and-off operating intervals. Comparing to the outlet

temperature predicted by the 2D model, the outlet temperature predicted by the 3D model showed a slightly delayed and decreased peak when the heat pump was on. This indicated the delayed response could be of some significance in moderating swings in temperature during heat pump operations.

Frequency response tests have been carried out to further investigate the modelling of the damping of temperature swings. The results showed that it was possible if the variation in inlet temperatures was at high frequencies, the fluctuations could be damped out completely, which resulted in no change in outlet temperatures.

To conclude, it is important to consider the variation of temperature and heat transfer along the depth of the borehole when modelling a BHE, as the non-linearity in those profiles could affect the accuracy of the model prediction both at short and long timescale, especially for fluid circulating at low velocities. It is also important that the transport and thermal mass of the fluid are considered in the BHE model, as the effects of the delayed response associated with the transport and thermal mass of the fluid on the model prediction can very significant at short timescales.

The findings reported in this chapter have highlighted some of the limitations of 2D models. In the next chapter, methods to improve a 2D model are tested and validated.

Chapter 5 Development of an Improved Two-Dimensional Model

The previous chapter presented a number of studies of a single BHE to characterise the predictive abilities of a two-dimensional (2D) and a three-dimensional (3D) model. The significance of delayed responses to fluid temperature changes were highlighted in the 3D model results. The delayed response associated with the thermal mass and transport of the fluid was demonstrated to be more accurate and realistic when compared to the experimental data. However, the 3D model is computationally expensive and therefore impractical to integrate into system simulations that normally run on hourly basis for long simulation periods (daily, monthly, yearly, or 10 years). For a mesh ratio of 100:1 between the 3D and 2D models, running an hourly annual simulation using the 3D model on a 3.8GHz Intel Pentium computer takes about 6 hours, while running the same simulation using the original 2D model takes less than 10 minutes, resulting the ratio of the computation time between the 3D and 2D models to be 36:1.

In this chapter, methods are proposed to improve the accuracy of the original 2D model while retaining its computational speed. Representations of the delayed response associated with the thermal mass and transport of the fluid are introduced into the original 2D model in a number of ways. These methods are tested by implementing BHE with the same configuration as that specified in Chapter 4 and comparing the simulation results to those predicted by the original 2D and 3D Finite Volume Models.

5.1 Method I – 2D + Tank Model

One way to include the thermal mass of the fluid and introduce some damping of the fluid temperature response is to add a model of a single tank to the 2D numerical model. It is assumed the volume of fluid inside the tank is equivalent to the volume of the fluid inside the borehole pipes and there is no heat loss from the tank. A diagram of the coupling of the 2D model and the tank is shown in Figure 5.1.

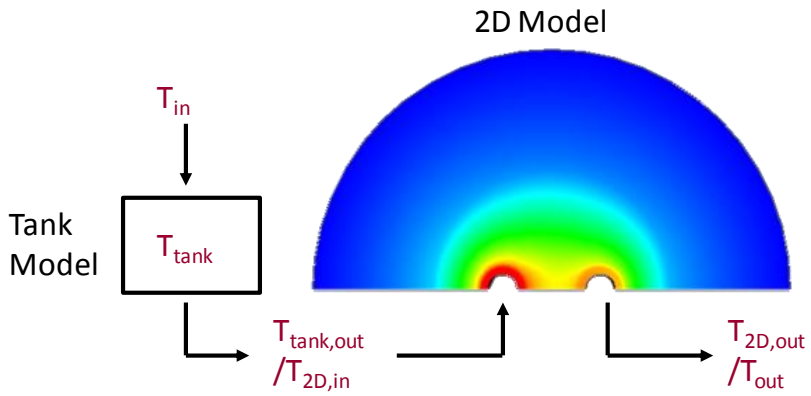

Figure 5.1 A diagram of the coupling between the 2D Finite Volume and Tank models.

The state of the tank is defined by the differential equation:

$$Mc_p \frac{dT}{dt} = mc_p(T_{in} - T) \tag{5.1}$$

Integrating Equation (5.1) over time interval Δt, it can be written as:

$$Mc_p \frac{T^n - T^{n-1}}{\Delta t} = mc_p(T_{in} - T^n) \tag{5.2}$$

where M is the total mass of fluid in the tank (kg), m is the mass flow rate of the incoming fluid (kg/s), T_{in} is the temperature of the incoming fluid, T^n is the temperature of the tank at current time step and T^{n-1} is the temperature of the tank at previous time step.

Assuming the incoming fluid flow into the tank at a mean velocity v, the total length of the pipes is L and the cross sectional areas of the pipe is A, the total mass of the fluid in the tank and the mass flow rate of the incoming fluid can be expressed as:

$$\begin{aligned} M &= \rho LA \\ m &= \rho vA \end{aligned} \tag{5.3}$$

Substituting Equation (5.3) into Equation (5.2) and rearranging the equation, the well-mixed temperature of the tank can be expressed as:

$$T^n = \frac{v\Delta t \times T_{in} + L \times T^{n-1}}{v\Delta t + L} \tag{5.4}$$

The tank temperature is treated as the input temperature for the 2D model and the heat transfer calculation process of the ground conductions is the same as the original 2D model. Adding this tank model slows down the change in the inlet temperature whenever a step change happens due to the thermal mass of the fluid, and as a result, it also makes the 2D model more stable.

In a similar way to section 4.4.2, applying a step change in the inlet temperature, it is possible to examine the dynamic responses of the outlet temperature calculated by the 2D+Tank model. Figure 5.2 shows the normalised outlet temperature response (T_{out}*), defined by Equation (4.1), of the 2D+Tank model, compared to those predicted by the original 2D and 3D numerical models. This data shows that adding a tank model results in a delayed response during the first 10 minutes. This is more similar to the prediction of the 3D numerical model. Although the response of the 2D+Tank model shows an improvement, the response, in this case, is still quite different from that of the 3D model during the first 5 minutes.

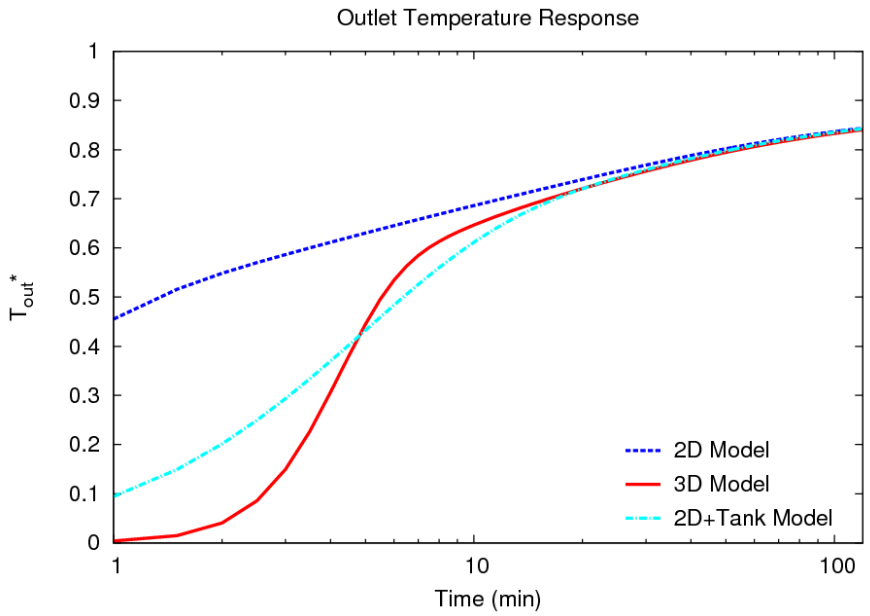

Figure 5.2 The outlet temperature response of the 2D+Tank model, compared to that of the original 2D and 3D numerical models.

5.2 Method II – 2D + 2Tank Model

An alternative way to simulate the effects of the fluid is to add two tanks, one tank to simulate the thermal capacity of the downward flowing fluid and the other to simulate the thermal

capacity of the upward flowing fluid. The coupling of the 2D Finite Volume and 2Tank models is shown in Figure 5.3.

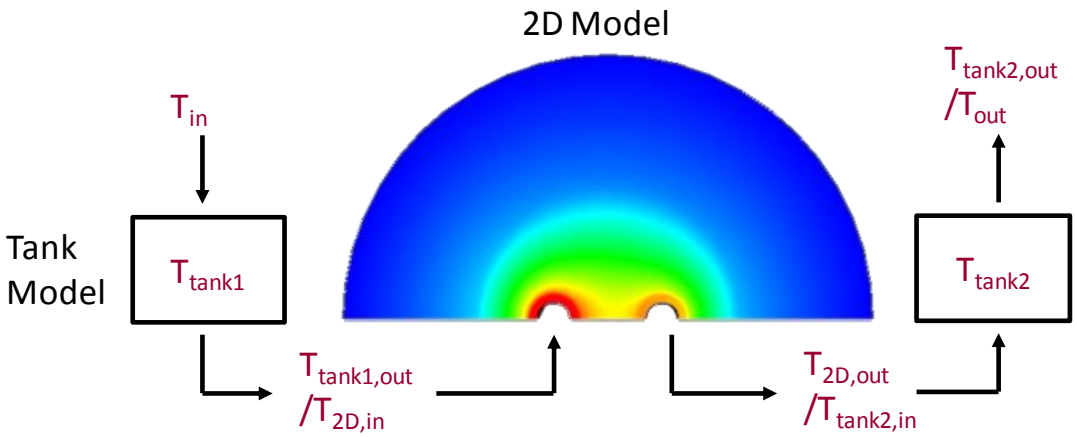

Figure 5.3 A diagram of the coupling of the 2D Finite Volume and 2Tank models.

The volume of each tank is the same as the volume of the fluid inside each pipe of the u-tube. In this case, the incoming fluid with the temperature T_{in} goes into one tank and mixes with the fluid inside that tank with the temperature of $T_{tank1,old}$, and the same amount of fluid comes out of the tank at the temperature of $T_{tank1,new}$. This new tank temperature is then taken as the input temperature of the 2D model. The 2D model calculates the output temperature by iteration to reach a heat balance inside the borehole. Fluid with the calculated outlet temperature $T_{2D,out}$ mixes with the fluid inside the second tank with the temperature of $T_{tank2,old}$. The new temperature of the second tank $T_{tank2,new}$ is the BHE outlet temperature predicted by the 2D+2Tank model.

Assuming the incoming fluid flows at a mean velocity of v, the length of one pipe is L and the inner area of the pipe is A, the amount of fluid flows in over time interval Δt can be expressed as $vA\Delta t$. Since the volume of one tank is equal to the volume of one pipe, the tank volume can be expressed in LA. The new tank temperature can be calculated using Equation (5.4).

Again, by applying a step change in the inlet temperature, it is possible to examine the dynamic responses of the outlet temperature calculated by the 2D+2Tank model. The responses predicted by the original 2D, 3D, 2D+Tank and 2D+2Tank models are shown in Figure 5.4. It can be seen that using two tanks damps the response more than using one tank during the first 10 minutes and more closely resembles to the prediction of the 3D model. The

predicted response is still not well matched to that of the 3D model during the first few minutes.

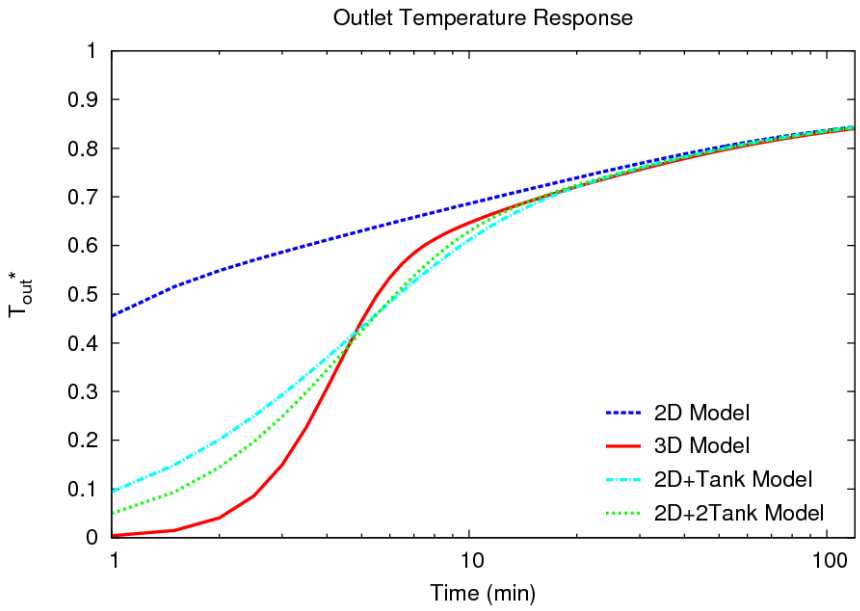

Figure 5.4 Outlet temperature response of the 2D+2Tank model, compared to that of the original 2D, 3D and 2D+Tank models.

5.3 Method III – 2D + Pipe Model

In the approach denoted as method III, a simple pipe model is used to simulate the fluid transport and the thermal mass of the fluid in each pipe of the borehole. The transient heat transfer between the fluid, pipes, grout and the surrounding ground is simulated by the 2D finite volume model.

The pipe model applies a similar method to that of the 3D model to simulate the fluid transport along the pipe loop. The total length of the pipe is discretised into a finite number of cells, and fluid velocity is imposed in these cells in accordance with the system flow rate. Assuming the fluid is well-mixed in each cell, each fluid cell can be represented by a single temperature T and is connected by a mean velocity v. This model can be considered similar to a Compartment-In-Series model (Wen and Fan, 1975), which is widely used in processing engineering.

Although both the 3D model and the 2D+Pipe model use the same pipe model to simulate the fluid transport inside the pipe, there is a significant difference between these two models. In

the 3D model, the dynamics of the fluid transport and the transient heat transfer between the fluid, pipes, grout and the surrounding ground are simulated simultaneously in three dimensions. In the 2D+Pipe model, the fluid transport is simulated in one dimension and the heat transfer is simulated in two dimensions, separately. In this way, the computing time required by the 2D+Pipe model can be reduced dramatically compared to the 3D model.

The coupling between the 2D and pipe model can vary according to ways these two models are connected. Findings from the previous sections 5.1 and 5.2 indicate that using one tank model to simulate the downward fluid flow and the other tank model to simulate the upward fluid flows generates closer agreement to the 3D model. Subsequently, in this approach, there are two instances of the pipe model to simulate the downward and upward fluid flows in turns, connected with the 2D finite volume model, such that the incoming fluid enters one pipe, and the temperature of the outgoing fluid from that pipe will be the inlet temperature for the 2D finite volume model. The 2D finite volume model is used to calculate the outlet temperature, and by iteration establish the heat balance of the borehole and its outlet temperature. Same amount of fluid of this outlet temperature defines the inlet conditions to the second pipe, and the BHE outlet condition is taken to be that at the outlet to the second pipe. The coupling of the 2D Finite Volume model and the pipe model is illustrated in Figure 5.5.

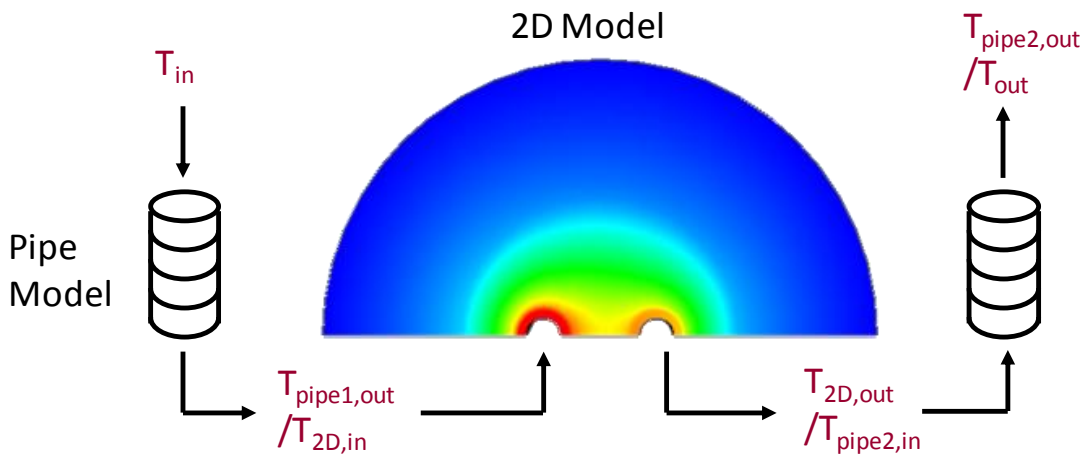

Figure 5.5 A diagram of the coupling of the 2D Finite Volume and the Pipe models.

Assuming the length of the pipe is *L* and the cross section area of the pipe is *A* and the fluid is transporting at a mean velocity of *v*, the total amount of the incoming fluid over time step Δt can be expressed as $vA\Delta t$. If the pipe is discretised into a number of cells (n), the volume of the

fluid in each cell can be expressed as *LA/n*. At time step *t* and in cell *k*, the temperature of the cell is denoted by $T_{t,k}$ such that the entering fluid temperature can be expressed as $T_{t,k-1}$, and the temperature of the cell *k* at previous time step can be expressed as $T_{t-1,k}$. Assuming the incoming fluid is well-mixed with the fluid in cell *k*, according to the energy balance, the temperature of cell *k* at current time step *t* can be express as:

$$T_{t,k} = \frac{vA\Delta tT_{t,k-1} + LA/nT_{t-1,k}}{vA\Delta t + LA/n} \tag{5.5}$$

This formula can be applied recursively to find the pipe outlet temperature at a given time step. An illustration of the recursive procedure used to calculate the pipe outlet temperature at a given time step is shown in Figure 5.6. The solution of the pipe model is partly dependent upon the number of cells that the pipe is discretised by. Simulation results with different numbers of cells will be examined in the following section.

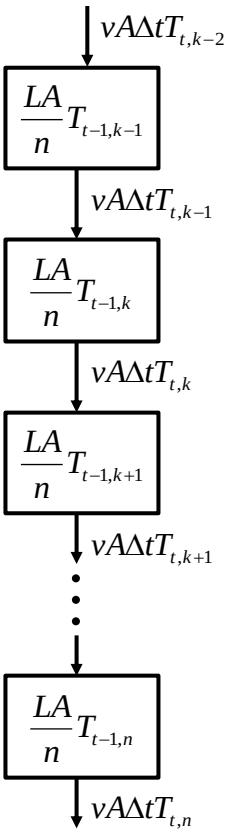

Figure 5.6 An illustration of the recursive procedure used to calculate the pipe outlet temperature at a given time step.

The dynamic characteristics of the 2D+Pipe model can be illustrated in terms of outlet temperature response when applying a step change in inlet temperature. For fluid circulating along the pipe loop at a velocity of 1m/s, the outlet temperature response predicted by the 2D+Pipe model with different numbers of cells of each pipe model is shown in Figure 5.7, compared to those of the original 2D and 3D numerical models. The number after *P* in the key of this figure denotes the number of cells by which the fluid inside each pipe has been discretised.

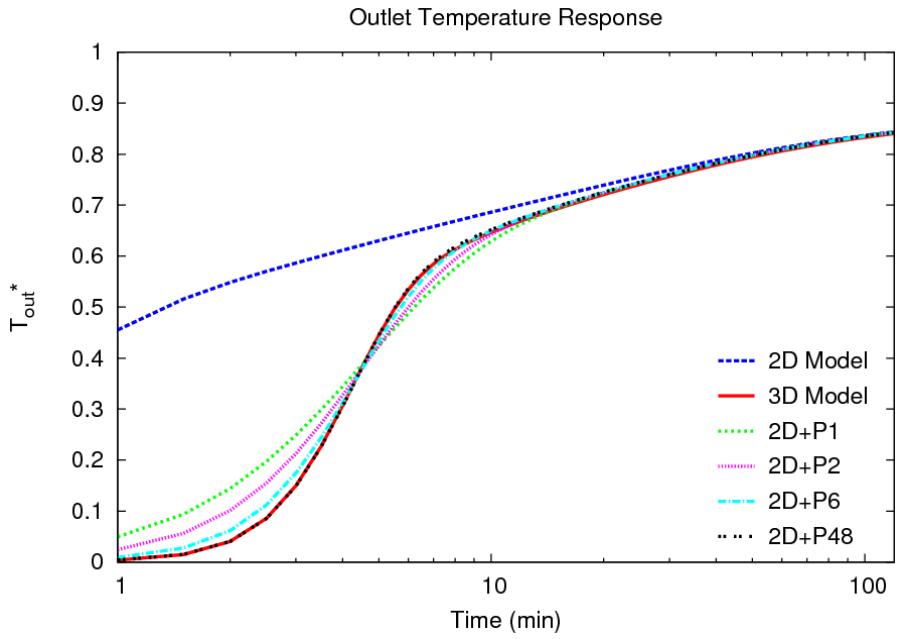

Figure 5.7 Outlet responses predicted by the 2D+Pipe model with different numbers of cells, compared to the original 2D and 3D finite volume models.

The results indicate that by using the pipe model to simulate the dynamics of fluid transport, the 2D+Pipe model is able to show a response similar to that of the 3D model. In the case that the whole pipe is considered as only one cell (2D+P1), the 2D+Pipe model behaves the same as the 2D+2Tank model, and the temperature of the fluid inside each pipe can be represented by a single temperature. As the level of discretisation increases, the prediction of the 2D+Pipe model gets closer to that of the 3D model. Using 48 cells for each pipe model, the outlet temperature response predicted by the 2D+Pipe model matches the response predicted by the 3D model very closely. However, further increasing the number of cells has little or no effect on improving the agreement in terms of outlet temperature response between the 2D+Pipe model and the 3D model. Accordingly the number of 48 has been chosen to discretise the pipe

model in the rest of this study. This is also the number chosen in the 3D model by which the BHE is discretised along the borehole depth.

The effects of different fluid velocities are studied and the results are shown in Figure 5.8. For relatively high flow velocities (v = 1.0 m/s and v = 0.8m/s), the outlet temperature responses predicted by the 2D+Pipe model match very well with that predicted by the 3D model. At lower velocities (v = 0.4m/s), the difference between the outlet temperature responses predicted by the 2D+Pipe and 3D model is more significant.

The key difference in the modelling of the pipes in the 2D+Pipe model and 3D finite volume model is that in the 2D+Pipe model, the transport of the fluid is modelled separately, followed by the simulation of the pipe transfer. But in the 3D finite volume model, the transport of the fluid and the pipe heat transfer are simulated simultaneously.

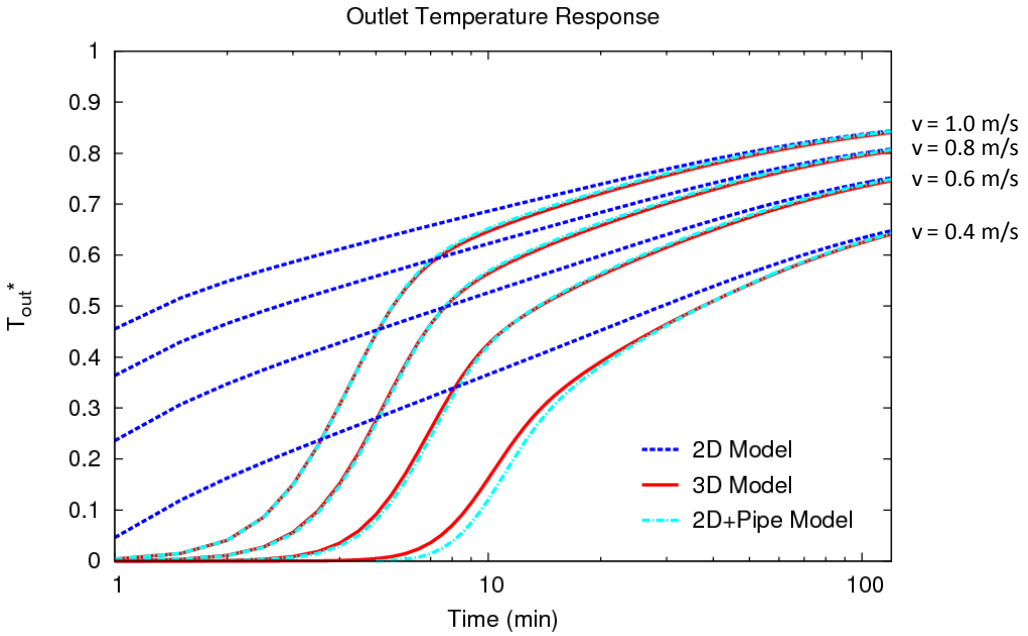

Figure 5.8 Outlet temperature responses predicted by the 2D, 3D and 2D+Pipe models at different velocities.

5.4 Model Step Change Function Characteristics

The same step change function as that in section 4.4.4 has been applied to the 2D+Pipe model, in order to simulate the on-and-off operation of a heat pump. It is assumed that the heat pump cycles twice per hour with the inlet temperatures changing suddenly between 25 ^{o}C and

15 °C. The far-field ground temperature is assumed to be 10 °C. A steady-state simulation, with the inlet temperature of 20 °C and far-field temperature of 10°C, has been carried out to develop the simulation of ground conditions representing many years of excitation.

Figure 5.9 to Figure 5.12 shows the comparison of outlet temperatures predicted by the original 2D, 3D, and 2D+Pipe models at v=1.0 m/s, 0.8 m/s, 0.6 m/s, and 0.4 m/s, respectively. For fluid flow with the velocities of 1.0 m/s, 0.8 m/s, and 0.6 m/s, the outlet temperatures in response to the step change function in the inlet temperature predicted by 2D+Pipe model closely match the outlet temperatures predicted by the 3D model.

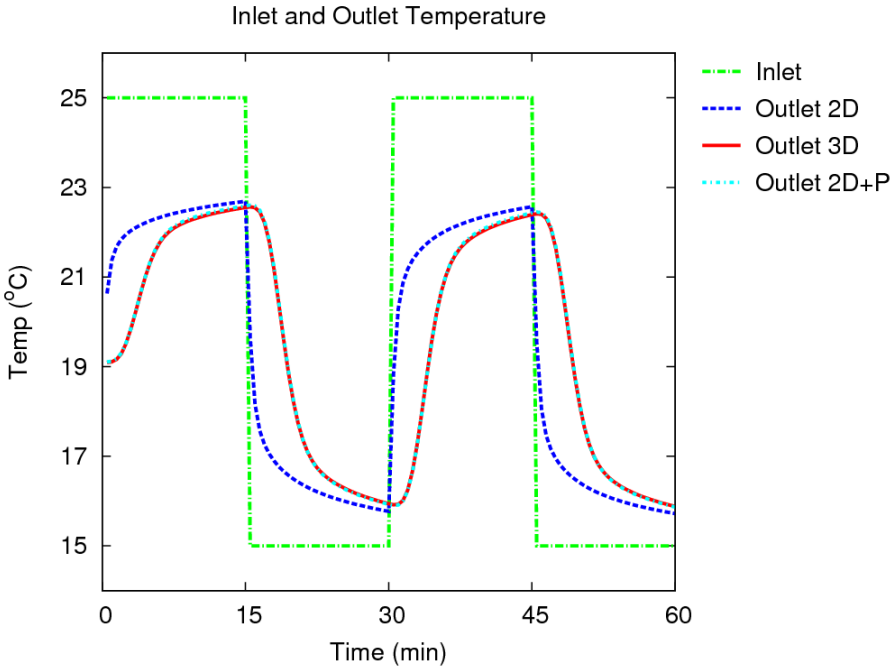

Figure 5.9 Comparison of the outlet temperatures calculated by the original 2D, 3D and 2D+Pipe models at v=1.0 m/s.

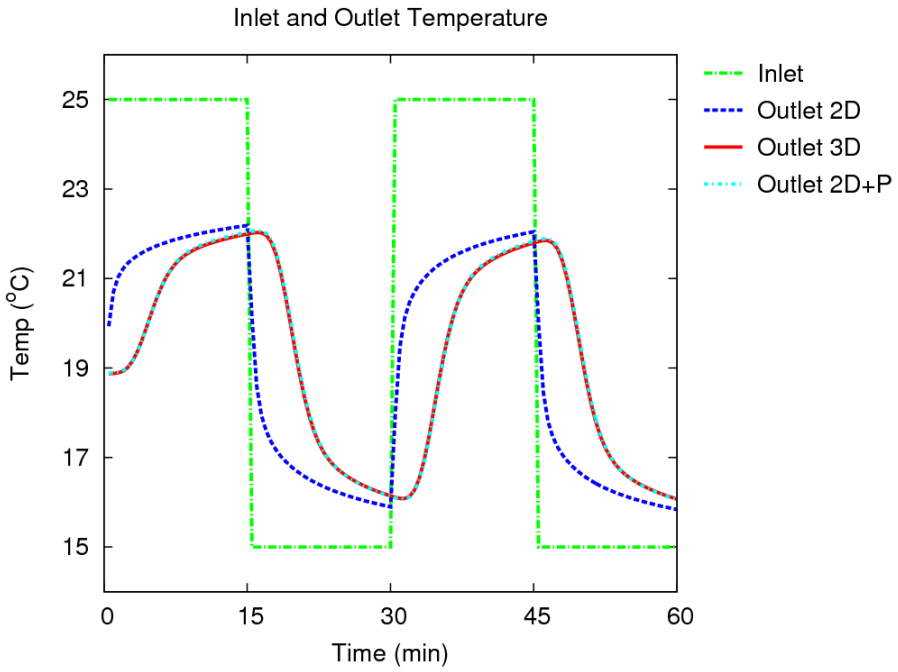

Figure 5.10 Comparison of the outlet temperatures calculated by the original 2D, 3D and 2D+Pipe models at v=0.8 m/s.

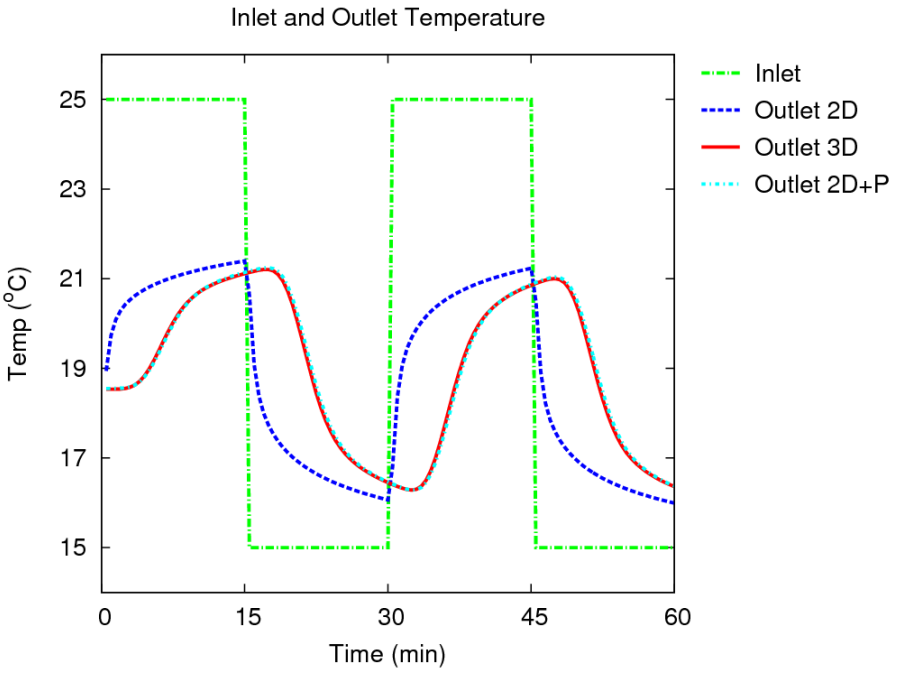

Figure 5.11 Comparison of the outlet temperatures calculated by the original 2D, 3D and 2D+Pipe models at v=0.6 m/s.

At relatively low velocity (v = 0.4m/s), some minor differences are noticeable between the outlet temperatures calculated by the 2D+Pipe model and the 3D model. In this case (Figure 5.12), the original 2D model predicts an unrealistic spike when the step change happens. This is due to the iteration process used in the original 2D model to calculate the outlet temperature. It was noted in the discussion of the results from the previous chapter (section 4.4.2) that the 2D model may not be suitable to simulate BHEs with fluid flows at low velocities at short timescales. The 2D+Pipe model, in contrast, can not only capture the delayed responses in the outlet temperature, but also can improve the stability of the original 2D model.

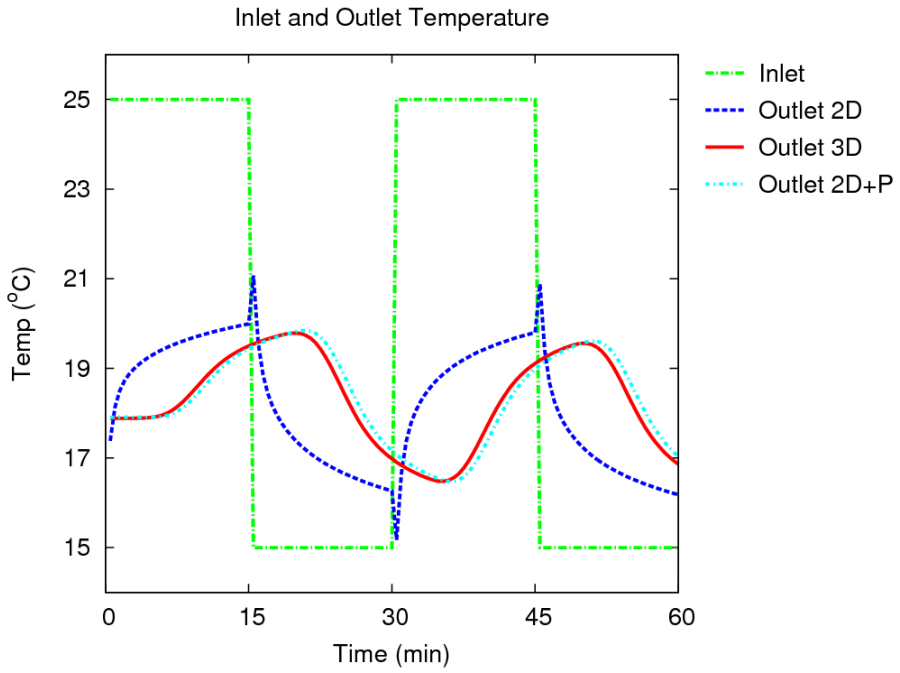

Figure 5.12 Comparison of the outlet temperatures calculated by the original 2D, 3D and 2D+Pipe models at v=0.4 m/s.

5.5 Model Frequency Response Characteristics

Frequency response tests have been carried out in order to characterise the responses of the 2D+Pipe model by imposing a periodic excitation of the inlet temperature and comparing this with that of the outlet over a range of frequencies. In a similar way to that reported in section 4.4.5, a sinusoidal variation in inlet temperature with the same amplitude (A_{in}) but different frequencies (f), or periods (P) has been applied to the 2D+Pipe model. The dynamic responses of the BHE models can then be characterised by examining the amplitude and phase (θ) of the

predicted outlet fluid temperature. The variation of the inlet and outlet temperatures can be expressed by Equation (4.2) and (4.3), respectively.

All the simulations are started from the steady-state condition (i.e. representative of operation over a long period) with a far-field temperature of 10 ^{o}C and a constant inlet temperature of 20 ^{o}C to enable a consistent and generic comparison. Figure 5.13 to Figure 5.18 shows the outlet temperatures predicted by the 2D, 3D and 2D+Pipe models while imposing the inlet temperatures across a wide range of different frequencies.

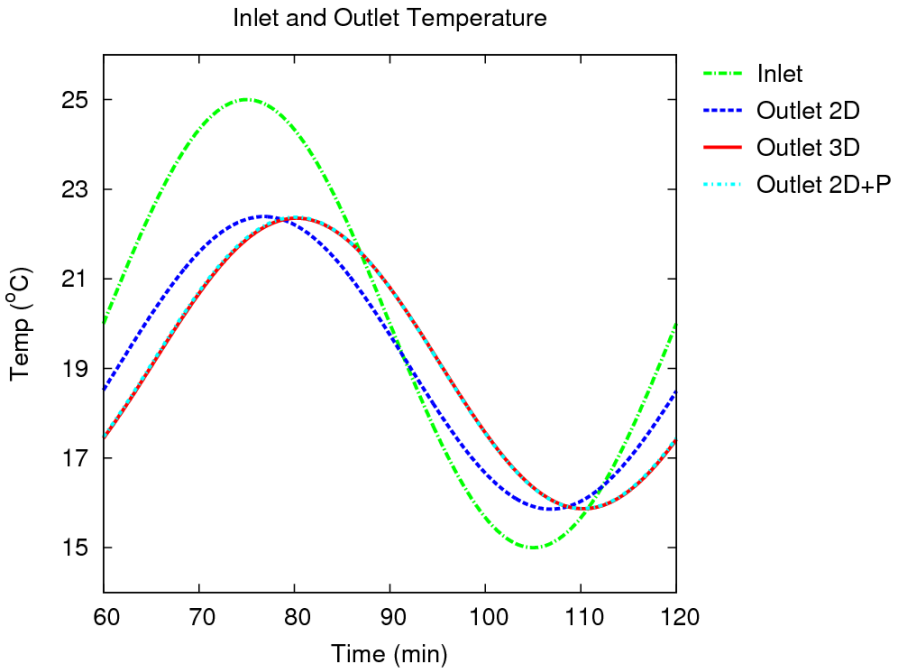

Figure 5.13 Inlet and outlet temperatures by the 2D+Pipe model at a frequency of f=1/3600 Hz, compared to the 2D and 3D models.

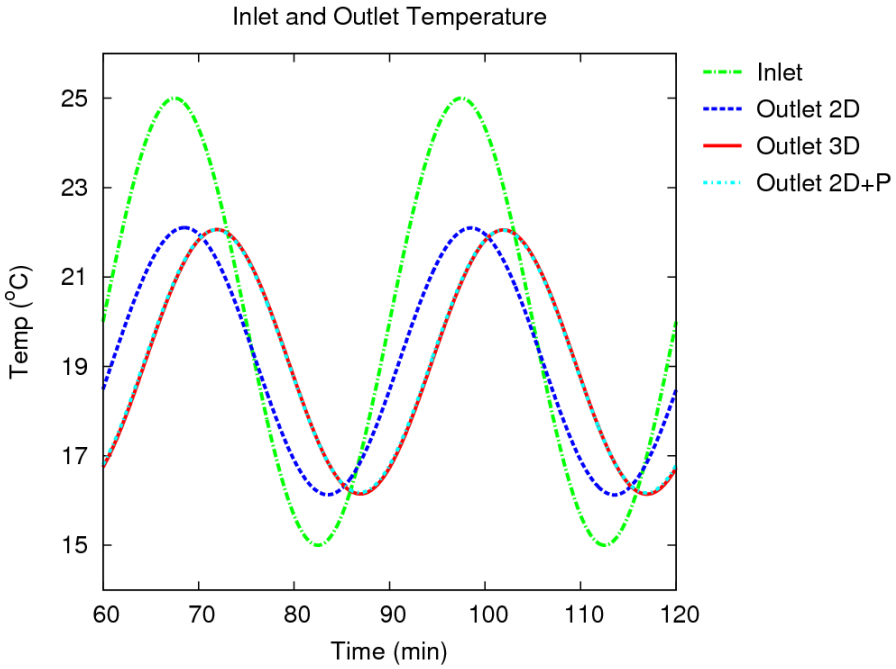

Figure 5.14 Inlet and outlet temperatures by the 2D+Pipe model at a frequency of f=1/1800 Hz, compared to the 2D and 3D models.

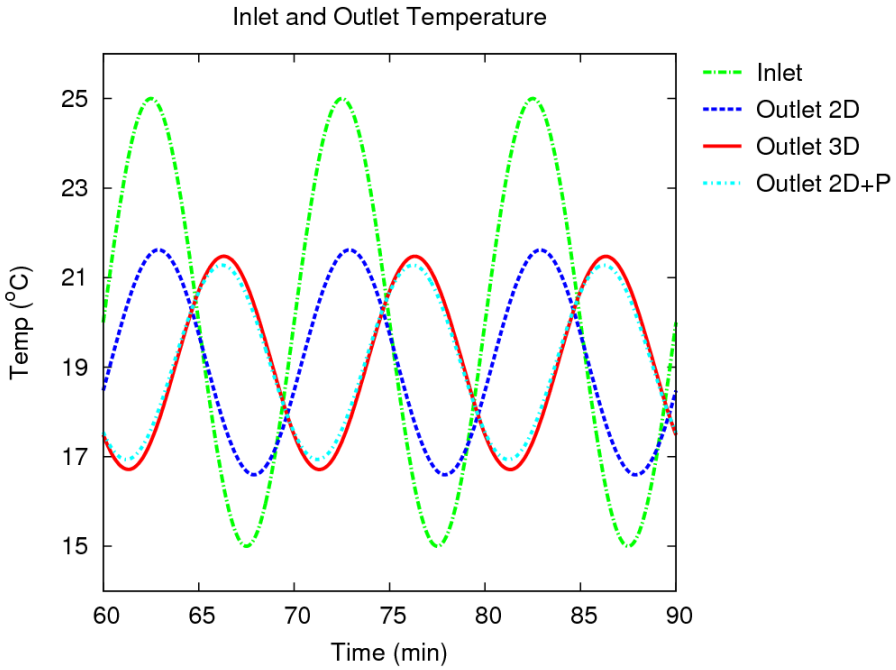

Figure 5.15 Inlet and outlet temperatures by the 2D+Pipe model at a frequency of f=1/600 Hz, compared to the 2D and 3D models.

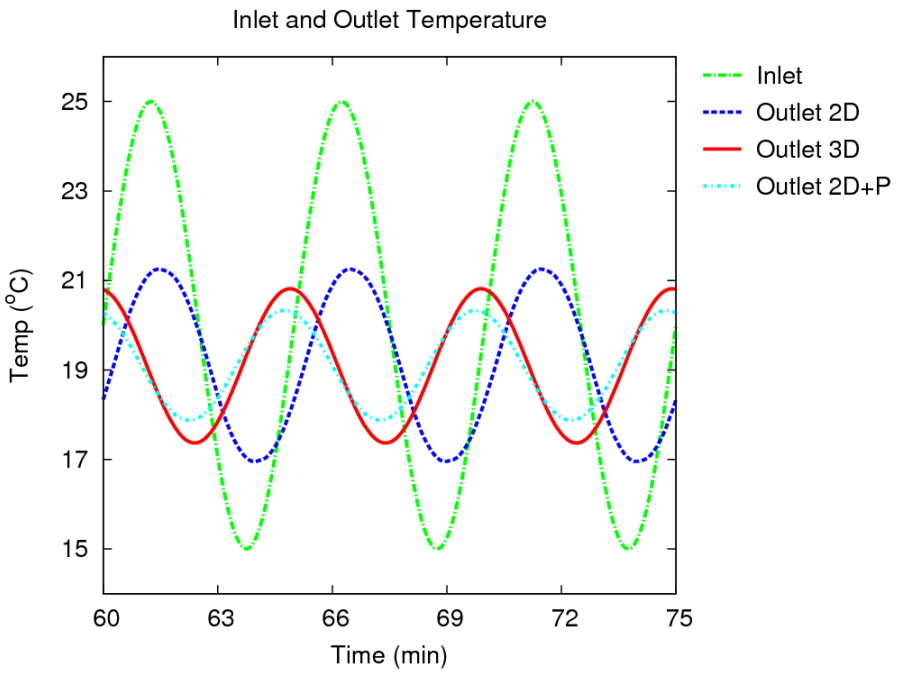

Figure 5.16 Inlet and outlet temperatures by the 2D+Pipe model at a frequency of f=1/300 Hz, compared to the 2D and 3D models.

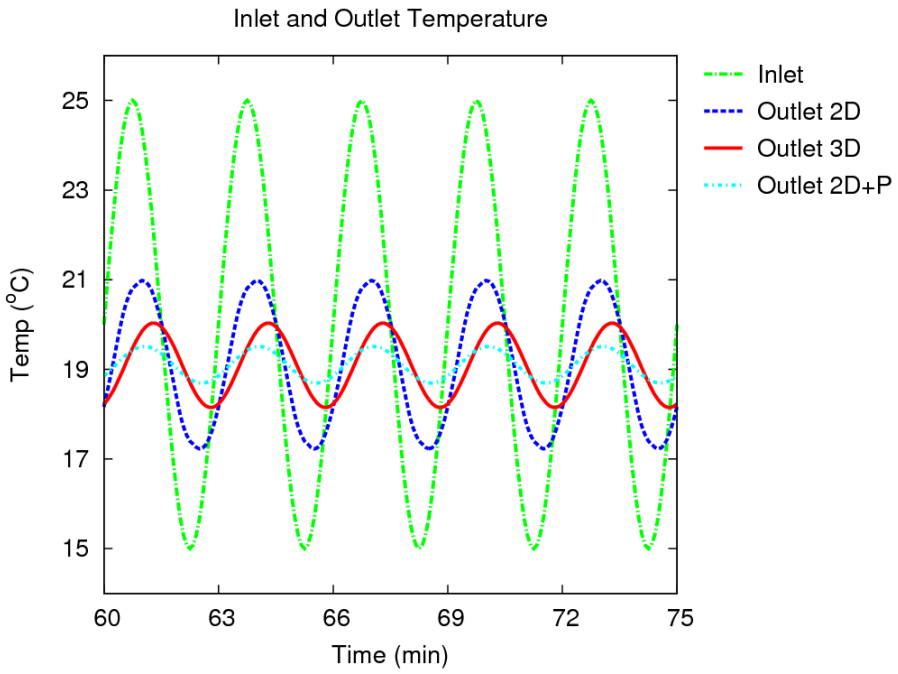

Figure 5.17 Inlet and outlet temperatures by the 2D+Pipe model at a frequency of f=1/180 Hz, compared to the 2D and 3D models.

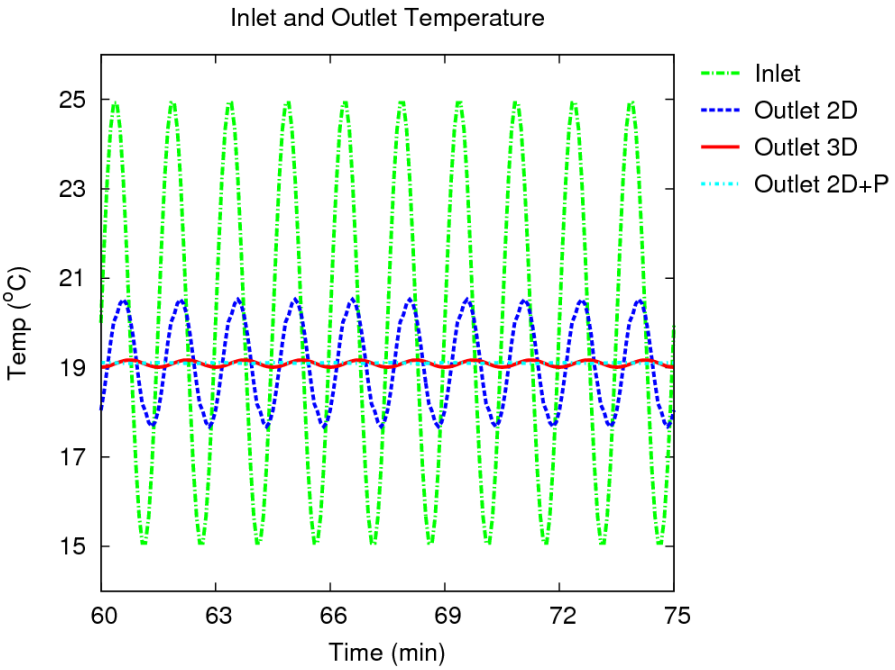

Figure 5.18 Inlet and outlet temperatures by the 2D+Pipe model at a frequency of f=1/90 Hz, compared to the 2D and 3D models.

Figure 5.19 shows the amplitude ratio between the inlet temperature and outlet temperature (A_{out}/A_{in}) calculated by the 2D+Pipe model, compared to those by the earlier 2D and 3D finite volume models. Where inlet temperature varies with low frequency (f = 1/600), the variation of the amplitude ratios predicted by these three models is very similar. At higher frequencies, the amplitude ratio predicted by the 2D+Pipe model shows a lower value that the 3D model. At the highest frequency (f = 1/90), there is no change in the outlet temperature and the amplitude ratio approaches to zero.

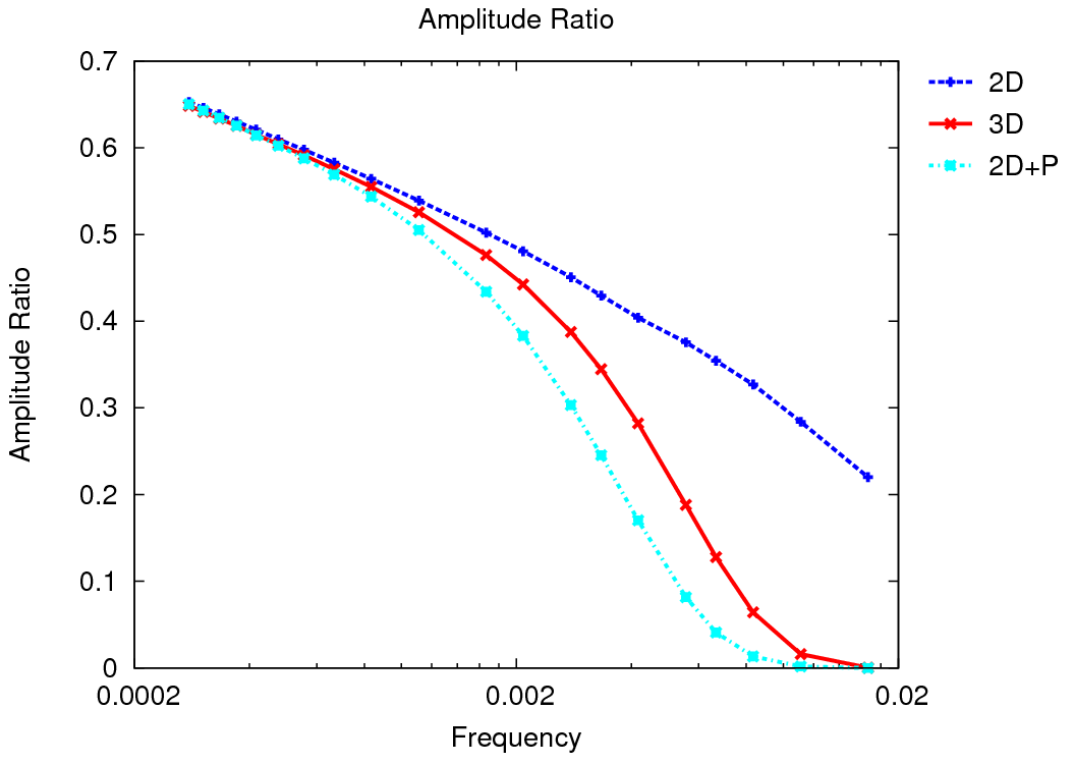

Figure 5.19 Amplitude ratio predicted by the 2D+Pipe models across a range of frequencies, compared to the 2D and 3D models.

Figure 5.20 shows the variation of phase delay in response to different frequencies of inlet temperature excitation, predicted by the 2D+Pipe model and compared to those by the earlier 2D and 3D finite volume models. The phase delays predicted by the 2D+Pipe model match the prediction of the 3D model closely, except at very high frequencies. The phase delays predicted by the 2D+Pipe model have slightly lower values than those predicted by the 3D model.

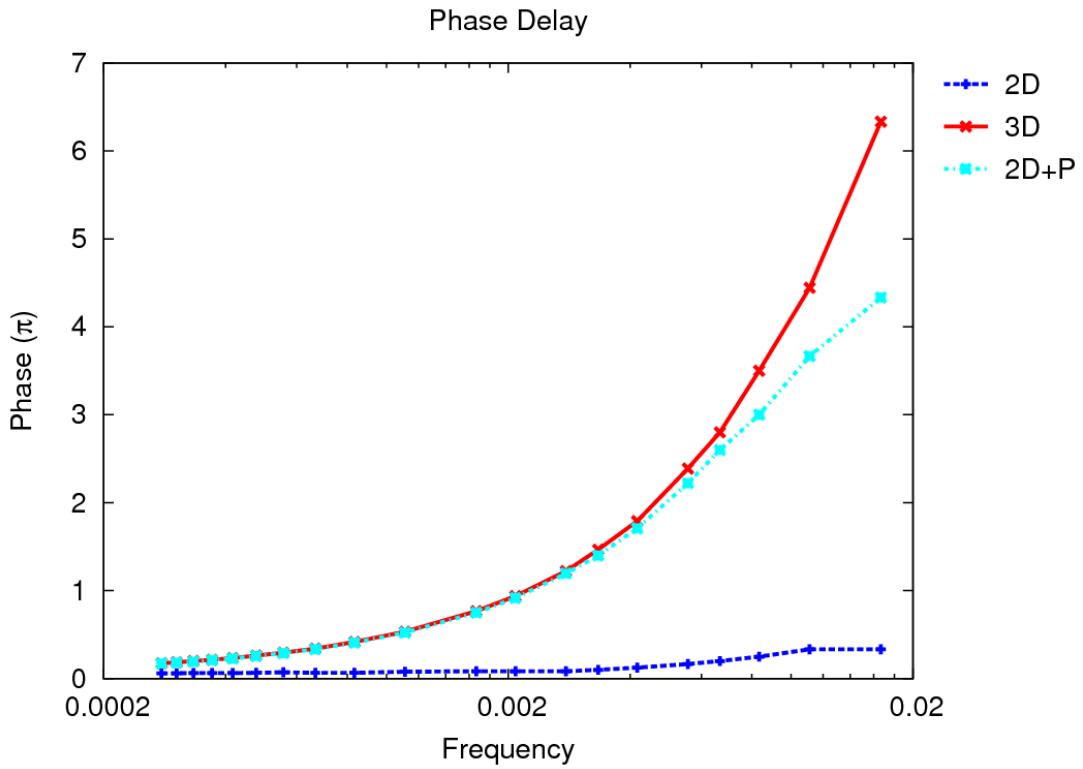

Figure 5.20 Phase delay predicted by the 2D+Pipe model, compared to the 2D and 3D models.

5.6 Comparison with Experimental Data

In a similar way that reported in Chapter 4, experimental data from the experimental facility of Oklahoma State University have been used to validate the 2D+Pipe model. The ground heat exchanger consists of three BHEs and during this one year operating period, this ground heat exchanger has relatively low borehole-to borehole interference and very little heat build-up in the ground. Thus, it is reasonable to take the average values of the three BHEs to validate the 2D+Pipe model by simulating only one BHE. The same BHE configuration as shown in Table 4.4 has been implemented in the 2D+Pipe model. The simulation has been run in two different time intervals; hourly simulation for 14 days (1-14 March) to build up the thermal history of the ground (taking the hourly average inlet temperature of the three BHEs as the input), and 1-minute intervals (taking the 1-minute average inlet temperature of the three BHEs as the input). The outlet temperature predicted by the 2D+Pipe model can be compared to the average measured outlet temperature of the three BHEs. Figure 5.21 and Figure 5.22 show the inlet fluid temperature and the comparison of the outlet fluid temperatures from the experimental data and simulations. By adding the pipe model to the earlier 2D finite volume

model, the 2D+Pipe model is able to capture the delayed response of the BHE, and this prediction matches extremely closely with that of the 3D model. In Figure 5.21, the Root Mean Square Error (RMSE) for the 2D model is 0.464 K, for the 3D Model is 0.324 K and for the 2D+Pipe model is 0.340 K. And in Figure 5.22, the RMSE for the 2D model is 0.466 K, for the 3D model is 0.320 K, and for the 2D+Pipe Model is 0.336 K.

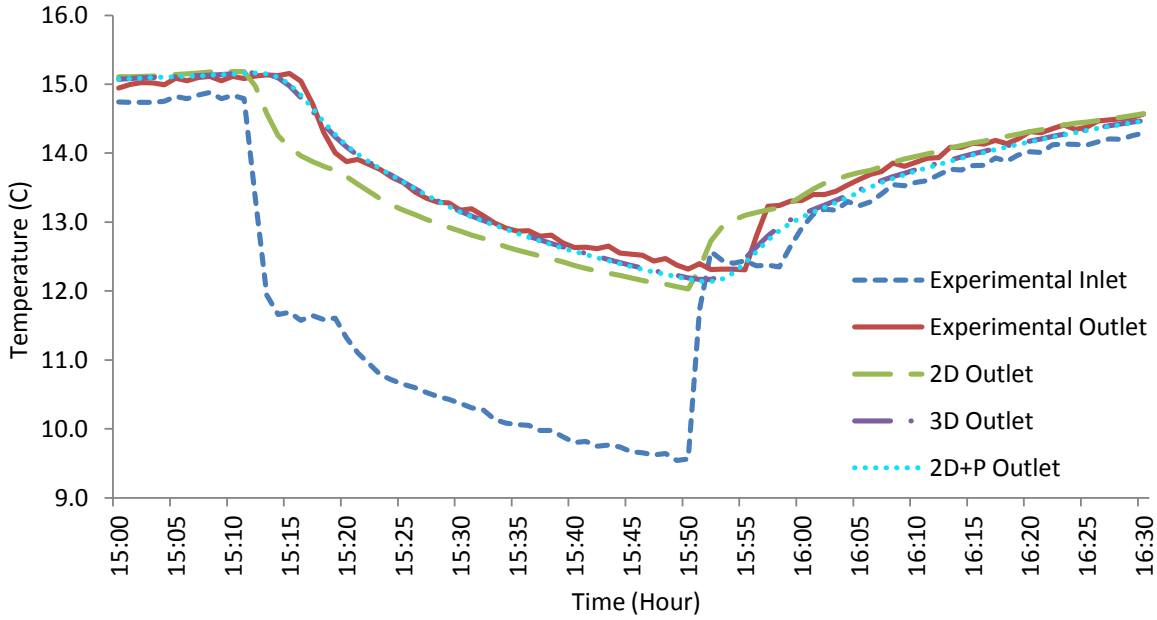

Figure 5.21 Experimental inlet and outlet temperatures, and outlet temperatures by the 2D, 3D and 2D+Pipe models (15:00 – 16:30).

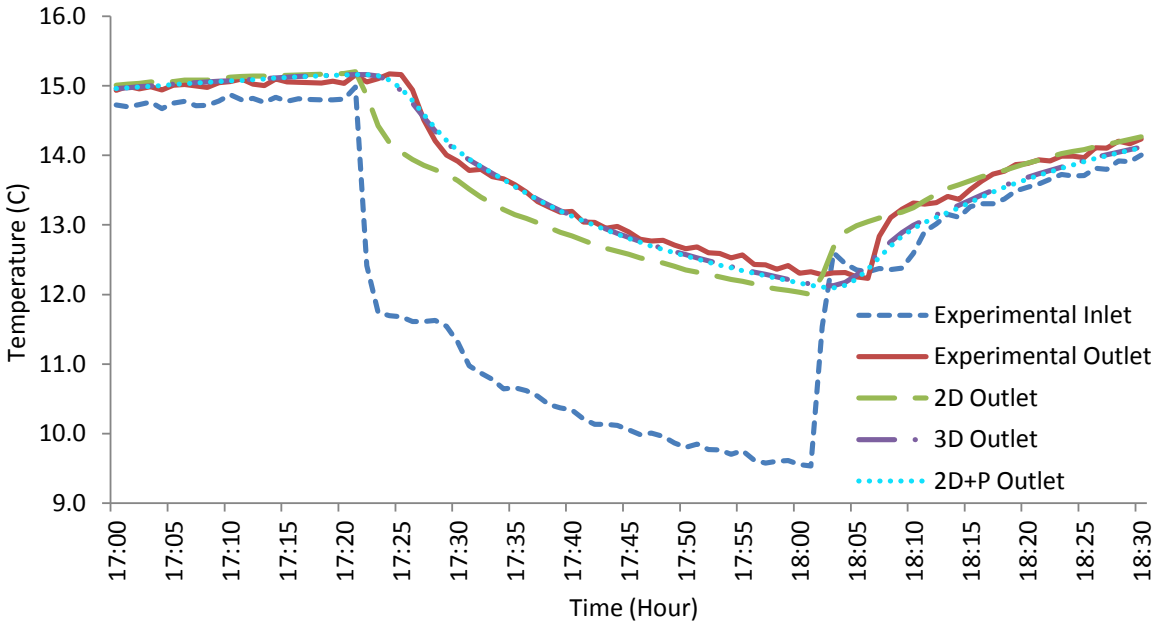

Figure 5.22 Experimental inlet and outlet temperatures, and outlet temperatures by the 2D, 3D and 2D+Pipe models (17:00 – 18:30).

5.7 Summary

This chapter has described the development of an improved 2D model for BHEs. Different methods have been proposed to simulate the thermal mass and transport of the fluid and the delayed response associated with it. These methods have been tested by implementing a single BHE using each model and comparing the results to those predicted by the original 2D and 3D finite volume models. The results indicate that by adding a tank model to simulate the thermal mass and transport of the fluid to the original 2D model, some delayed response in the outlet temperature can be reproduced but does not match the prediction of the 3D model particularly well. Using two tank models to simulate the thermal mass of the fluid, one for the downward and the other one for the upward fluid flows results in a delayed response closer to the prediction of the 3D model although the difference between them is still quite noticeable.

Coupling the original 2D finite volume model with two pipe models to simulate the thermal mass and transport of the fluid has proved to be the best method. Step change responses have been applied in the inlet fluid temperature in order to test the outlet temperature responses. The solution of the pipe model is partly dependent upon the number of cells by which the pipe has been discretised. Using 48 cells the outlet temperature response predicted by the 2D+Pipe

model matches the response predicted by the 3D model very closely. The solution is also dependent upon the fluid velocities inside the pipes. At higher velocities (v = 1.0 m/s and 0.8 m/s), the outlet temperature response predicted by the 2D+Pipe model matches closely with the prediction of the 3D model. But at lower velocities (v = 0.4 m/s), the difference between the outlet temperature responses predicted by the 2D+Pipe and 3D model is more significant.

Frequency response tests through imposing a periodic excitation of the inlet temperature at a sequent of frequencies have been carried out to further investigate frequency response predicted by the 2D+Pipe model. It has been shown that although the amplitude ratio predicted by the 2D+Pipe model is very similar to that predicted by the 3D model at low frequencies (f < 0.26 mHz), the amplitude ratio is under predicted at higher frequencies (f >0.26 mHz). The phase delay predicted by the 2D+Pipe model, on the other hand, closely matches that predicted by the 3D model except at extremely high frequencies (f > 2.4 mHz).

The experimental data from the Oklahoma State University have been used to further validate the 2D+Pipe model. This model has been proved to be able to capture the delayed response of the BHE in this case, and the prediction matches extremely closed with that of the 3D model.

To conclude, improvement of the original 2D finite volume model has been made by simulating the transport and thermal mass of the fluid using different methods. The pipe model has been demonstrated to be the best approach. The predictions of the 2D+Pipe model are able to match that of the 3D finite volume model very closely except for the cases with relatively low fluid circulating velocities. The errors of the predictions of the 2D+Pipe model can also be observed when the inlet fluid temperature changes at high frequencies.

In the next chapter, both the 3D and 2D finite volume models are integrated into system simulations in order to investigate the implication of the delayed response in temperature change on system performance.

Chapter 6 Simulations of a Ground Source Heat Pump System

In previous chapters, the heat transfer characteristics of a single BHE were investigated in great detail by applications of a dynamic three-dimensional (3D) and a two-dimensional (2D) finite volume models. The significance of the delayed response in temperature changes was highlighted in the predictions of the 3D model. The simulations of annual operation using the 3D model were demonstrated to be more accurate and realistic than that of the original 2D model when compared to experimental data.

In this chapter, the implications of the delayed response in temperature change on system performance are examined by integrating the original 2D and 3D models of the BHE into system simulations. With careful design, Ground Source Heat Pump (GSHP) systems have the potential to deliver substantial CO_2 savings of up to 60% compared with gas heating and conventional air-cooled refrigeration (Underwood and Spitler, 2007). Models for the simulation of GSHP systems have been implemented in a number of building simulation tools, for example, HVACSim+ (Clark, 1985), TRNSYS (SEL, 1997), and EnergyPlus (Crawley et al., 2001). Both HVACSim+ and EnergyPlus use the combined short time step g-function model developed by Yavuzturk and Spitler (1999) and long time step g-function model developed by Eskilson (1987)to simulate BHEs, while TRNSYS is often used with the duct storage (DST) model by Hellström (1991). Both the g-function model and the DST model neglect the dynamics of fluid transport in the pipe loops. Another dynamic BHE model has been implemented in TRNSYS by Wetter and Huber (1997), which takes into account those dynamics and is quasi-3D in nature(vertical heat transfer and the bottom of the borehole is ignored).

This study is carried out using EnergyPlus. A GSHP system with a BHE is firstly simulated using the existing combined short time step and long time step g-function model implemented in EnergyPlus. The results are compared with those of the original two-dimension (2D) and three dimension (3D) finite volume models.

6.1 Building Simulation

A typical UK domestic building with a GSHP system has been modelled in EnergyPlus. This has been done to derive fluid temperatures more typical of a building than step changes. The system simulation also allows transient heat transfer rates to be compared and differences in predicted overall efficiency to be evaluated. The building has been modelled in one zone and

the internal gains are modelled as a typical family of four. The floor area is 120 m^2 and the volume is 300 m^3. The heating period is simulated for one year. The heating set point is 22 °C and the annual heating demand is about 6.0 MWh. The annual building load profile is shown in Figure 6.1.

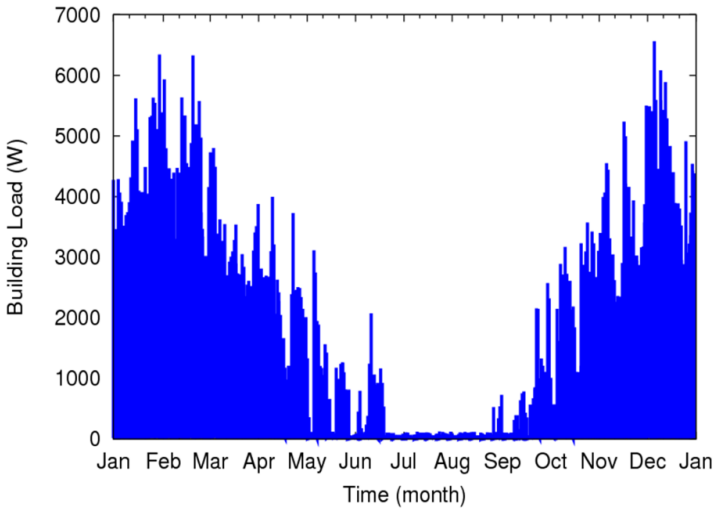

Figure 6.1 Domestic building model heating load profile.

6.2 Heat Pump Model

A ground source water-to-water heat pump is used to provide heating for the house. Hot water is delivered to the low temperature radiators installed in both zones. A simple water-water heat pump equation fit model (Tang, 2005) implemented in EnergyPlus is chosen to simulate the heat pump in this study. This model uses four non-dimensional equations or curves to predict the heat pump performance in cooling and heating mode. The methodology used to find the heat pump model parameters employed generalized least squares method to generate a set of performance coefficients from the catalogue data at indicated reference conditions. The respective coefficients and indicated reference conditions are used in the model to represent the heat pump performance. The heat pumps control system and cyclic operation is not explicitly modelled.

The only variables that influence the modelled water-to-water heat pump performance are load and source-side inlet water temperatures, providing the load and source-side water flow rates are constant. The heat pump model allows the characteristics to vary according to both temperatures and flow rates, but, as the manufacturer's data only available for single design

flow rate, the model can be defined solely in terms of load and source-side inlet temperatures. The governing equations for the heating mode are consequently simplified and can be described as follows:

$$\frac{Q_h}{Q_{h,ref}} = C1 + C2\left[\frac{T_{L,in}}{T_{ref}}\right] + C3\left[\frac{T_{S,in}}{T_{ref}}\right] \quad (6.1)$$

$$\frac{Power_h}{Power_{h,ref}} = D1 + D2\left[\frac{T_{L,in}}{T_{ref}}\right] + D3\left[\frac{T_{S,in}}{T_{ref}}\right] \quad (6.2)$$

where:

C1-D3: Equation coefficients for the heating mode

T_{ref} : Reference temperature (283K)

$T_{L,in,}$: Load side inlet water temperature, K

$T_{S,in}$: Source side inlet water temperature, K

Q_h : Load side heat transfer rate (heating), W

$Power_h$: Power consumption (heating), W.

The model coefficients have been derived from manufacturer's data for a Viessmann Vitocal 200-G Type BWP 106 water-to-water heat pump, with a rated heating capacity of 6 kW. Table 6.1 shows the derived heat pump coefficients.

Table 6.1 Heat pump coefficients.

C1	-4.04615	D1	-7.90965
C2	-1.16344	D2	6.603333
C3	6.566434	D3	1.787658

6.3 Borehole Heat Exchanger Model

The BHE design parameters have been chosen using the GLHEPro design tool (Spitler, 2000) based on the simulated heat pump monthly and peak loads. A single borehole with a diameter of 150 mm and a depth of 100 m is chosen with the configuration and thermal properties shown in Table 6.2. The short time-step g-function model, which has been implemented in EnergyPlus (Fisher et al., 2006), is applied to simulate the BHE for the annual simulation of the GSHP system. This model combines the response factors (g-functions) of the long (Eskilson, 1987) and short (Yavuzturk and Spitler, 1999) time responses. The combined response factor data has been taken directly from the output of the GLHEPro tool. The initial ground

temperature is assumed to be 13 °C. The ground loop is modelled with a mass flow rate of 0.539 kg/s and the estimated pipe convective coefficient is 3430 W/m^2K. The circulating pump operates at a fixed flow rate intermittently.

Table 6.2 BHE configuration and thermal properties.

Borehole Diameter		D	150	mm
Pipe Inner Diameter		D_{in}	26.2	mm
Pipe Outer Diameter		D_{out}	32	mm
U-tube Shank Spacing		L_s	32.2	mm
Ground Diameter		D_s	4.0	m
Fluid	Conductivity	k_f	0.6	W/mK
	Thermal Capacity	ρc_p	3.59	MJ/m^3K
Pipe	Conductivity	k_{pipe}	0.39	W/mK
	Thermal Capacity	ρc_p	1.77	MJ/m^3K
Grout	Conductivity	k_{grout}	0.75	W/mK
	Thermal Capacity	ρc_p	3.9	MJ/m^3K
Ground	Conductivity	k_{ground}	2.5	W/mK
	Thermal Capacity	ρc_p	2.5	MJ/m^3K

6.4 Results and Discussion

An annual simulation of the GSHP system has been carried out in EnergyPlus in two ways. Firstly, the borehole inlet temperatures calculated in the course of the annual simulation has been taken and used as boundary conditions at the inlet of the two and three-dimensional numerical models. The second way in which the annual simulation has been carried out is to take the calculated building loads and use these as boundary conditions in simulations integrating the numerical borehole models with the heat pump model. This allows the models to interact to determine the loop temperatures and the overall effect of the different heat transfer rates and BHE transient response to be evaluated. The EnergyPlus model uses 10-minute time steps and the 2D and 3D numerical models use 1-minute time steps.

6.4.1 Predicted Fluid Temperatures

The BHE inlet fluid temperatures (heat pump source-side outlet temperature) obtained from the short time step g-function model in EnergyPlus have been used in the first comparison of the models. Figure 6.2 shows the BHE inlet, outlet, average fluid temperatures, and BHE mass flow rate simulated EnergyPlus for a typical heating day. The outlet temperatures calculated by 3D and 2D models are also shown. When the heat pump is on the circulation pump operates

with a flow rate of 0.539 kg/s. During the period when the heat pump is off (00:00 – 05:00) the average fluid temperature of the BHE simulated in EnergyPlus shows a quick recovery to the far-field ground temperature (13 ^{o}C). The outlet temperature calculated by the 3D model shows a similar recovery pattern but to a lower temperature. The outlet temperature calculated by the 2D model, on the other hand, is not able to show such a recovery process. In the 2D model, when the flow rate is zero, the same assumption about the outlet temperature has to be made. In this case, we assume the temperature is unchanged. The meaning of the outlet temperature reported by the models when the fluid is static is somewhat a matter of convention as the outlet condition has less meaning in this state. The outlet temperatures when flow resumes is however of physical significance.

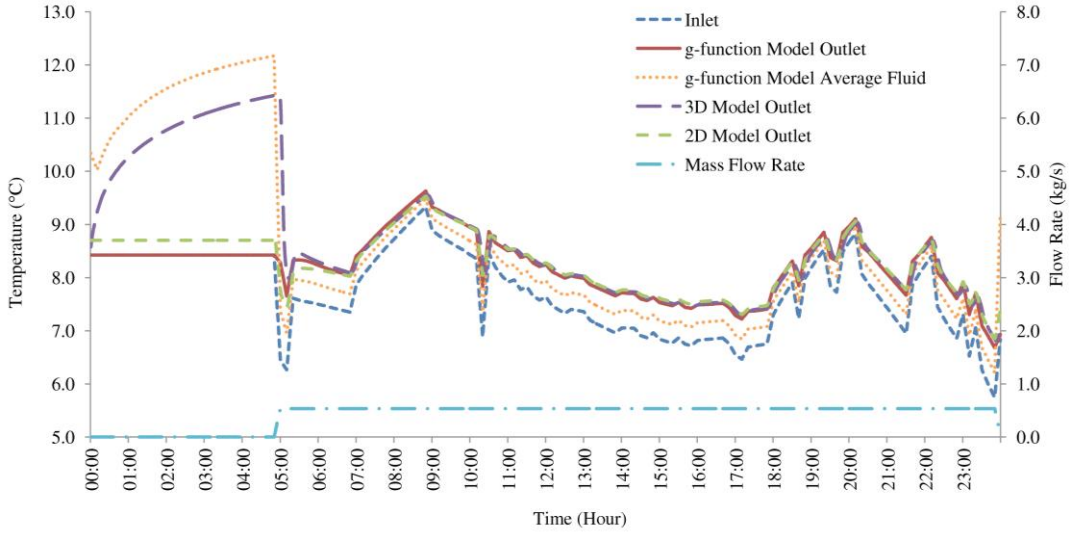

Figure 6.2 Inlet, outlet, average fluid temperatures and mass flow rate by EnergyPlus g-function model, and outlet temperatures by the 3D and 2D models for a typical heating day.

Figure 6.3 shows a comparison of outlet temperatures predicted by the short time-step g-function, 3D and original 2D models during the operating hours (05:00-24:00). Over this period of operation, the predicted outlet temperatures by these three models are quite similar. The temperatures drop very quickly when there is a sudden increase in the heating demand (10:00). The oscillatory behaviour late in the cycle (17:00-24:00) also reflects the changes in the heating demand, and subsequently the heat extraction from the ground (Figure 6.4). The most significant differences are shown during the first 10 minutes of heat pump operation (5:00 - 5:10). The 3D model predicts a much higher outlet temperature in this period as a

consequence of the delayed response as the fluid travels around the U-tube pipe as well as the inclusion of its thermal mass. The dynamics of the fluid transport can be seen to generally damp out the fluctuations in outlet temperatures, compared to that predicted by the original 2D and the short time-step g-function models.

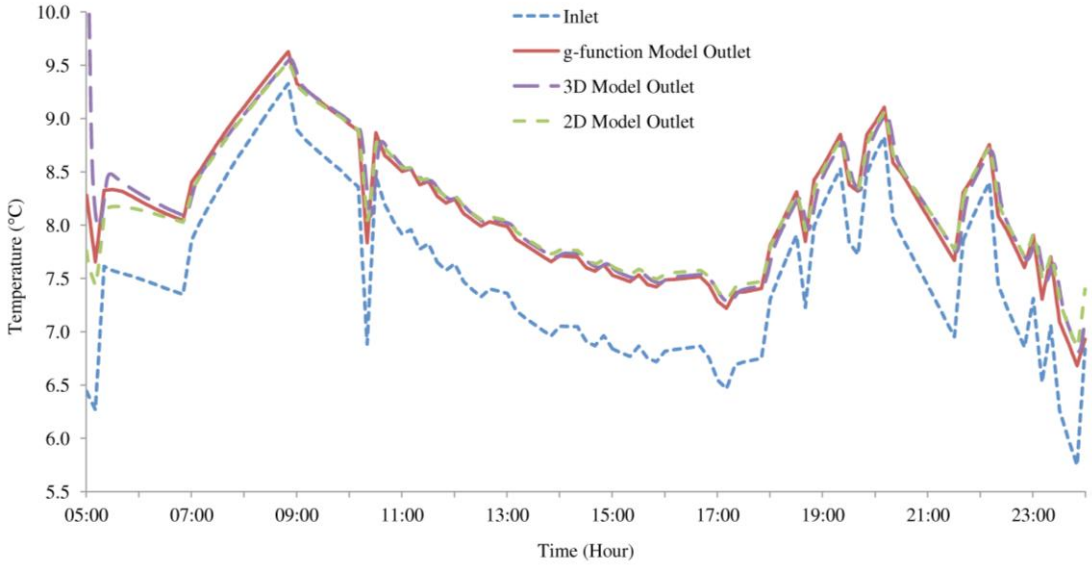

Figure 6.3 Comparison of outlet temperatures by the g-function, 3D and 2D models during the operating hours.

Heat transfer rates of the BHE calculated from the inlet and outlet temperature difference of the fluid ($Q=mc_p\Delta T$), predicted by these three models over the same operating hours are shown in Figure 6.4.

The patterns of the heat transfer rates for the short time-step g-function model and the 2D model are similar, while the heat transfer rate for the 3D model is much higher at the start of operation. In addition, the heat transfer rate for the 3D model can be either higher or lower than the 2D model, depending on whether the heat transfer rate is increasing or decreasing. The slower response in the outlet temperature is also reflected in the overall heat transfer rate being enhanced during these periods.

Over this operating period, the total heat extracted from the ground is calculated to be 25.7 kWh by g-function model, 27.1 kWh by 3D model, and 26.3 kWh by the original 2D numerical model.

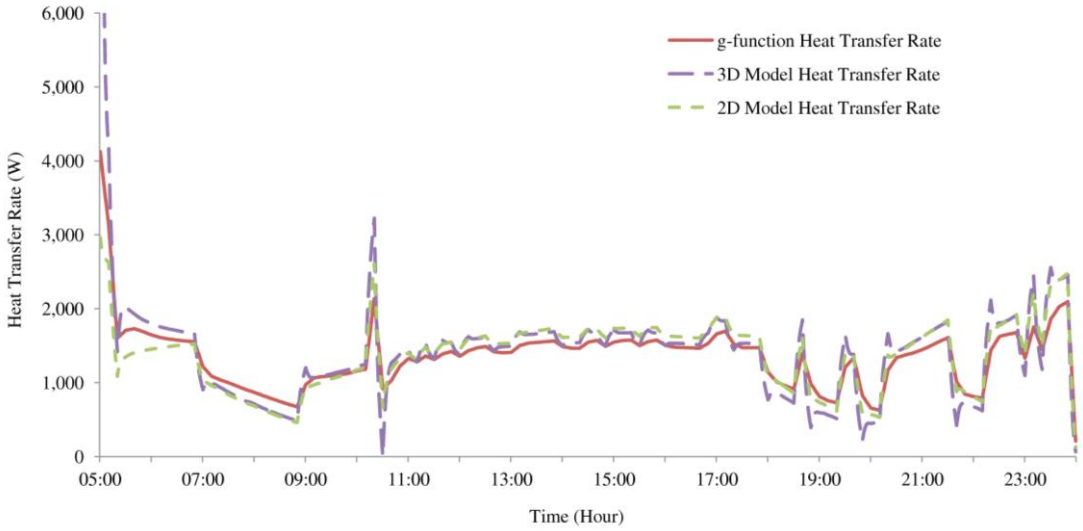

Figure 6.4 Comparison of heat transfer rates by the g-function, 3D and 2D models during the operating hours.

6.4.2 Integrated System Simulation Results

In realistic simulations of GSHP system behaviour, the appropriate boundary conditions are the building heating loads rather than inlet fluid temperatures. Ground loop conditions are dependent on heat pump characteristics as well as BHE performance in this case. In order to simulate this coupling, the BHE model needs to be coupled with a heat pump model. To this end the same heat pump model as that implemented in EnergyPlus (Equation (6.1) and (6.2)) has been implemented alongside, and directly coupled to, the numerical BHE model (without simulating any connecting pipes). The load-side heat transfer rates and load-side inlet temperatures calculated from the annual simulation in EnergyPlus have been imposed on the load-side of the heat pump model. Heat transferred to the ground loop then depends on the heat pump Coefficient of Performance (COP) that, in turn, is dependent on ground loop temperature.

The outlet temperature from the ground loop is also the entering fluid temperature to the source side of the heat pump, and this temperature together with the entering fluid temperature to the load side of the heat pump determine the COP of the heat pump. Figure 6.5 shows the outlet temperatures for the integrated system simulation by the short time-step g-function, 3D and original 2D models coupled with the heat pump model over the same operating hours as the previous section.

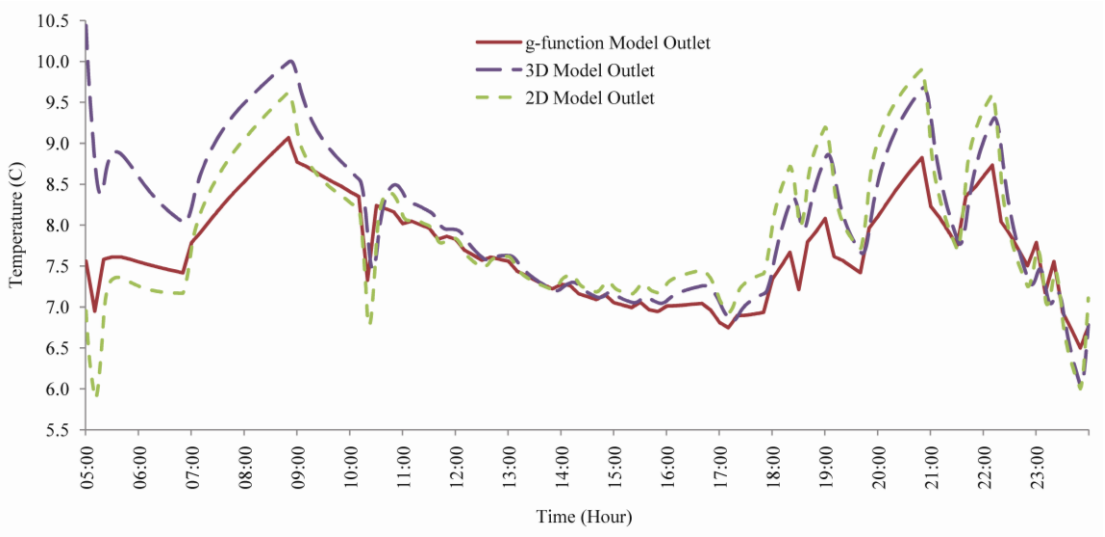

Figure 6.5 Comparison of outlet temperatures by the g-function, 3D and 2D models during the operating hours of integrated simulation.

The 3D model shows a much higher outlet temperature when the heat pump switches on, compared with the outlet temperatures predicted by the short time-step g-function model and original 2D numerical model. However, the outlet temperature difference between the 3D and original 2D models becomes smaller over time, and eventually the outlet temperature predicted by the original 2D model becomes higher than the outlet temperature predicted by the 3D model. The heat transfer rates predicted by the original 2D model and the 3D model are similar, and the difference is most noticeable when there is a rapid change in operating conditions (Figure 6.6). The total heat extracted over the operating hours are predicted to be 28.1 kWh by the EnergyPlus g-function model, 28.2 kWh by the 3D model and 28 kW by the original 2D numerical model.

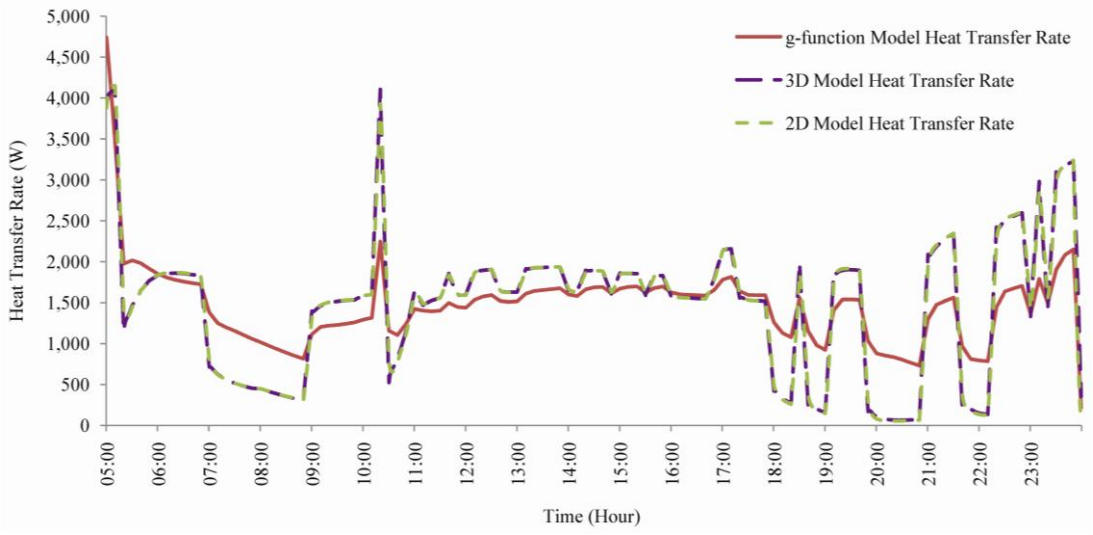

Figure 6.6 Comparison of heat transfer rates by the g-function, 3D and 2D models during the operating hours of integrated simulation.

Figure 6.7 shows the corresponding COPs of the heat pump. A much higher COP predicted by the 3D model can be seen when the heat pump starts to operate compared with the other two models. However, when considered over a longer period the values are little different. In this case, the average COP of the heat pump over the whole period of the simulation is predicted to be 4.11, 4.09, and 4.08 by g-function model, 3D model and original 2D model, respectively.

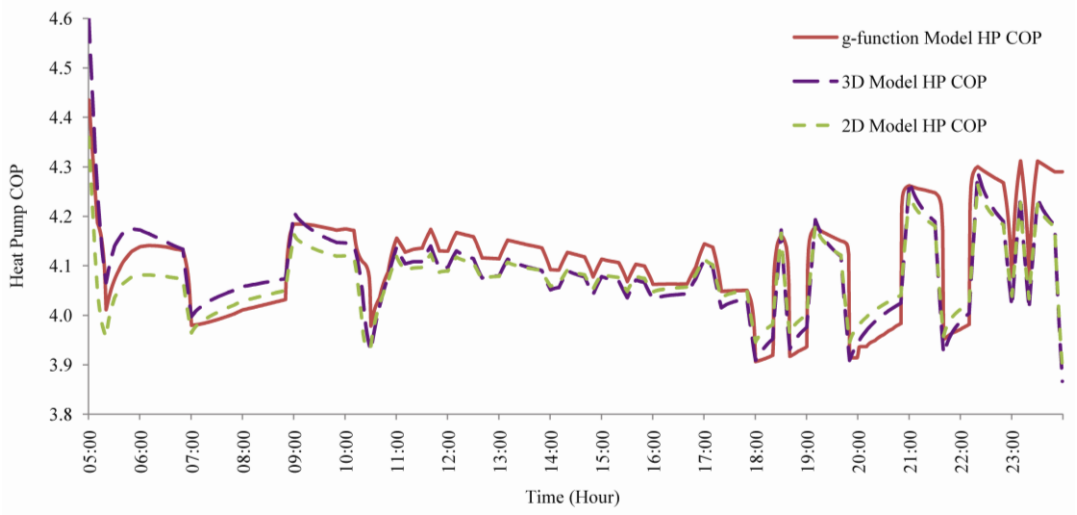

Figure 6.7 Comparison of heat pump COPs predicted in simulation with g-function model, 3D and 2D models during the operating hours.

Apparently high heat transfer rates at the start of heat pump operation are to be expected if the dynamics of the fluid in the borehole are considered. Heat transfer at a particular point down the borehole cannot be expected to be fundamentally different when three-dimensional effects are considered. However, the delay in transport of the initial cold fluid entering the loop means that, for a short period, the outlet temperature does not change and so a heat balance calculated using the inlet and outlet temperatures shows a higher overall heat transfer rate. Although the nominal transit time of the fluid is 200 seconds, the results show that the effects of the delay persist for a few hours after the start of operation at the beginning of the day.

The results shown in Figure 6.5 show that later in the day (after approximately 14:00) after the heat pump has been operating continuously, a different trend can be seen as the fluid temperature predicted by the 3D model becomes lower than that of the 2D model. The heat transfer rates and COP trends change in a corresponding manner. This indicates that the temperature difference between the borehole and the surrounding ground is larger and the predicted heat transfer rate is lower in the 3D model when it operates over longer periods.

When the steady-state is considered (or generally longer periods of continuous operation) higher heat transfer can be expected from a 2D model in that the temperature of the pipes is assumed to be the same along their whole length and are taken to be the same as the inlet and outlet temperatures. However, as demonstrated in section 4.2.1, the fluid temperature profile predicted by the 3D model varies along the borehole depth. In particular the pipe temperatures predicted by the 2D model are higher and lower than the mean pipe temperatures predicted by the 3D model when conditions approach a steady-state (He *et al*., 2009). Similarly the borehole wall temperature predicted by the 2D model does not vary with depth. It may be more accurate to say then, that the 2D model tends to over-predict the heat transfer rate when the system has been operating continuously.

In general, the conditions predicted by the 2D and 3D numerical models fluctuate more dynamically during the day than predicted by the EnergyPlus short time-step g-function model. This may be expected partly as fluid transport is not considered but also that fluid thermal mass is ignored. When the heat pump and BHE are simulated together in this way, there are some difficulties in comparing results with those from EnergyPlus due to the loop heat and mass balance procedure it uses. In the iterative solution procedure used in EnergyPlus the heat

pump inlet temperature is updated only once at the beginning of the time step. There is effectively a one time-step delay between the borehole outlet temperature and the heat pump inlet temperature. This may account for the generally smaller variations in fluid temperature and COP. At any given time-step, the loop heat balance is not guaranteed to be exact. (In our simulation using the numerical BHE models, the loop heat balance is preserved at each time step). Over a longer period, this effect becomes negligible. There is accordingly little difference in the overall heat transfer and average COP when considered over the whole period simulated.

6.5 Summary

This chapter presents simulations of a GSHP system in EnergyPlus. Three models for BHEs have been implemented in the simulations, the short time-step g-function model, the 3D model and the original 2D model, and the results are compared.

The results show that delayed response associated with the transit of fluid along the pipe loop is of some significance in moderating swings in temperature during the short period when the heat pump starts to operate. A relatively high flow rate of the fluid is chosen in this study and so it is expected that in many cases with lower flow rates, the delayed response will be far more profound. The 3D numerical model shows a lower heat transfer rate will occur over longer periods of operation when compared to the predictions by the original 2D model and the short time-step g-function model. This is due to the mean temperature differences between the fluid and the ground being lower in the 3D model – this seems more realistic.

A simple heat pump model has been used in this study and cannot simulate the on-and-off dynamic characteristics of a typical domestic heat pump in an explicit manner. Kummert and Bernier (2008) showed dynamic fluid transport could significantly change overall system behaviour when interaction with the heat pump control system (i.e. cycling) was considered. A more detailed dynamic heat pump model and an explicit representation of the control system could be applied in further work to investigate system performance and control system operation.

It is expected that when using the dynamic 3D model for BHEs in sizing GSHP systems (and generally when fluid transport and thermal mass of the fluid are considered), shorter borehole lengths will be suggested if the design is strongly influenced by peak loads rather than monthly

loads, which will result in lower initial costs and shorter payback period. In addition, the 3D numerical model would be beneficial when optimising system control and operation.

Chapter 7 Modelling Borehole Heat Exchanger Arrays

Although a single Borehole Heat Exchanger (BHE) might be sufficient for a domestic Ground Source Heat Pump (GSHP) application, for larger systems, more than one BHE will be required to extract heat from or reject heat into the ground. Thermal interaction among multiple BHEs over long timescales can limit the allowable heat extraction/rejection. It is, therefore, important that models developed for BHEs are able to estimate thermal interaction and its impacts on long term operation.

In previous chapters, studies of a single BHE using the dynamic 3D model for different applications were reported. The findings indicated that the 3D model predicts more accurate and realistic temperature responses of the BHE compared to that of the 2D model. The damping of the temperature swings during peak load operations can be captured by the 3D model. The 3D model can simulate temperature gradients along the borehole depth explicitly, and also any axial heat transfer in the surrounding ground. Although axial heat transfer is often ignored in 2D models, when long timescales are considered, heat flow is not just radial and axial effects become important.

In this chapter, the 3D model is used to simulate multiple BHEs in regular arrays. The short and long timescale responses have been characterised by examining the non-dimensional response to a single step in heat flux expressed in the form of g-function data. Results are compared to the g-functions generated by Eskilson (1987) and extended by Yavuzturk (1999).

7.1 G-function Approach

The g-function is a dimensionless step-response function which allows the calculation of the temperature response of a borehole field to a step heat extraction/rejection for a defined configuration of BHEs. This method was firstly developed by Eskilson (1987) to model BHEs for thermal storage applications over long timescales. In his approach, a two-dimensional (radial-axial) finite difference model was constructed to simulate a single BHE in order to determine its temperature response to a unit step heat pulse. The complex geometry of a borehole was simplified as a finite cylinder and a single heat flux used to apply the boundary conditions. The thermal mass of all materials inside a borehole, including fluid, pipes and grout, are neglected. For this particular reason, this solution is only valid for times to be greater than $\frac{5r_b^2}{\alpha}$. For a typical borehole, this implies time of a few hours (8 hours in our case). The superposition

technique was then applied to determine the temperature response of a borehole array to the unit step heat pulse for a pre-defined configuration of multiple BHEs. This allows the axial heat transfer and interaction between boreholes to be represented. Normalising these temperature responses to dimensionless data allows the g-function to be obtained.

Given the constant heat extraction rate Q (W/m) and constant far-field ground temperature T_g, the borehole temperature $T_b(t)$ can be written as:

$$T_b(t) = T_g - Q \cdot R_q \tag{7.1}$$

Here R_q can be regarded as a time-dependent thermal resistance for a unit heat extraction step, and is written in the following way:

$$R_q = \frac{1}{2\pi k} \cdot g\left(\frac{t}{t_s}, \frac{r_b}{H}\right) \tag{7.2}$$

Where $g(t/t_s, r_b/H)$ denotes the dimensionless step-response function, called the g-function.

Rearranging Equation (2.18) and (2.19), the g-function can be expressed as:

$$g\left(\frac{t}{t_s}, \frac{r_b}{H}\right) = \frac{2\pi k \cdot (T_b(t) - T_g)}{Q} \tag{7.3}$$

It depends on the dimensionless time t/t_s and the ratio between borehole radius and depth r_b/H. Here t_s is the steady-state time-scale:

$$\mathrm{t_s} = \frac{\mathrm{H}^2}{9\alpha} \tag{7.4}$$

The dependence on borehole radius is simply

$$\mathrm{g(t/t_s\,, r_b^*/H) = g(t/t_s\,, r_b/H) - \ln\,(r_b^*/r_b)} \tag{7.5}$$

The g-function is particularly useful as it can be determined independently of the conductivity. The function does depend on borehole configurations and the spacing/depth ratio.

Yavuzturk (1999) extended the long time-step g-function to short time steps using a two-dimensional finite volume model developed to simulate the transient heat transfer within a

borehole, which was ignored by the long time-step g-function model. In this model, the fluid in the pipes of the U-tube was not explicitly modelled; instead, the heat transfer from the fluid was treated by a heat flux boundary condition at the pipe wall. When using this model to calculate fluid temperatures it is necessary to take into account the conductive resistance of the pipe and grout and the convection resistance associated with the fluid flow inside the pipes. Instead of calculating the borehole temperature, the short time-step g-function model predicts the fluid temperature. Assuming the heat transfer between the fluid and the borehole wall can be defined by a borehole resistance, which includes the conductive resistance of the pipe and grout and the convection resistance of the fluid, the borehole temperature can be obtained through subtracting the temperature change due to the borehole resistance from the fluid temperature.

$$T_b(t) = T_f(t) - R_b \cdot Q \tag{7.6}$$

Consequently, Equation (2.21) can be recast to solve for the g-function and modified to account for the borehole thermal resistance:

$$g\left(\frac{t}{t_s}, \frac{r_b}{H}\right) = \frac{2\pi k \cdot (T_f(t) - R_{Total} \cdot Q - T_g)}{Q} \tag{7.7}$$

The independently generated short time-step g-functions can be blended with Eskilson's long time-step g-functions (i.e. the data sequence extended). For typical ratios of borehole radius to borehole depth, the short time-step g-function data correspond to time steps between 2 ½ minutes and 200 hours.

The combined short time-step and long time-step g-function model have been implemented in GLHEPro (Spitler, 2000), a design software for vertical BHEs, and EnergyPlus (Crawley et al., 2001), a whole building energy simulation program. Figure 7.1 shows some g-functions from GLHEPro for selected configurations, a single borehole, a 2x2, a 3x3, and a 4x4 array of boreholes. The short time-step g-function data produced by Yavuzturk's model is also highlighted in the graph.

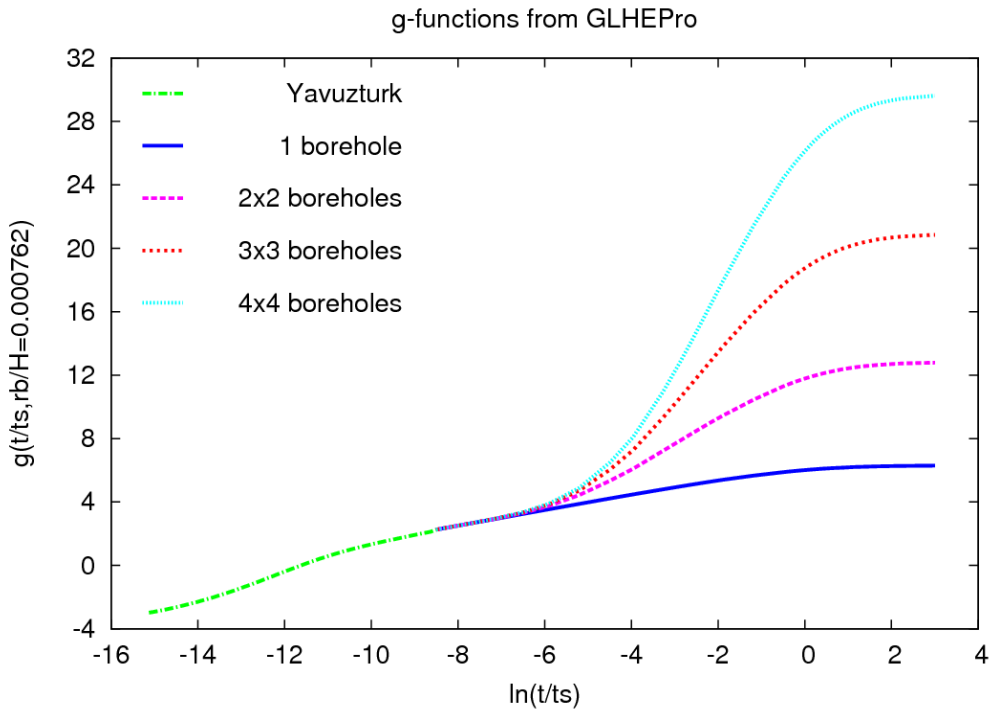

Figure 7.1 The g-functions from GLHEPro for different configurations.

7.2 Application of the 3D Model

Instead of using response factors to simulate the temperature response of a borehole field, the numerical 3D model simulates borehole fields explicitly and can take into account various configurations of multiple BHEs. There are several advantages to model a borehole field explicitly, which include:

- Fluid transport inside the pipes can be simulated;
- Flow rates of each borehole can be different;
- Analytical methods, such as superposition technique, can be avoided;
- Assumptions, such as distribution of heat flux among boreholes, can be avoided;
- Temperature distributions of the borehole field can be visualised;
- The same model can be used to calculate both the short and long timescale response.

7.2.1 Mesh Generation

Three of the most commonly used configurations of multiple BHEs are included in this study: boreholes arranged in a line, in a square and in a rectangle. Figure 7.2 shows a diagram of multiple BHEs with 3 boreholes in the x direction and 2 boreholes in the y direction, which is

denoted as a configuration of 3x2 (the notation for the configuration of multiple BHEs follows this rule in this chapter).

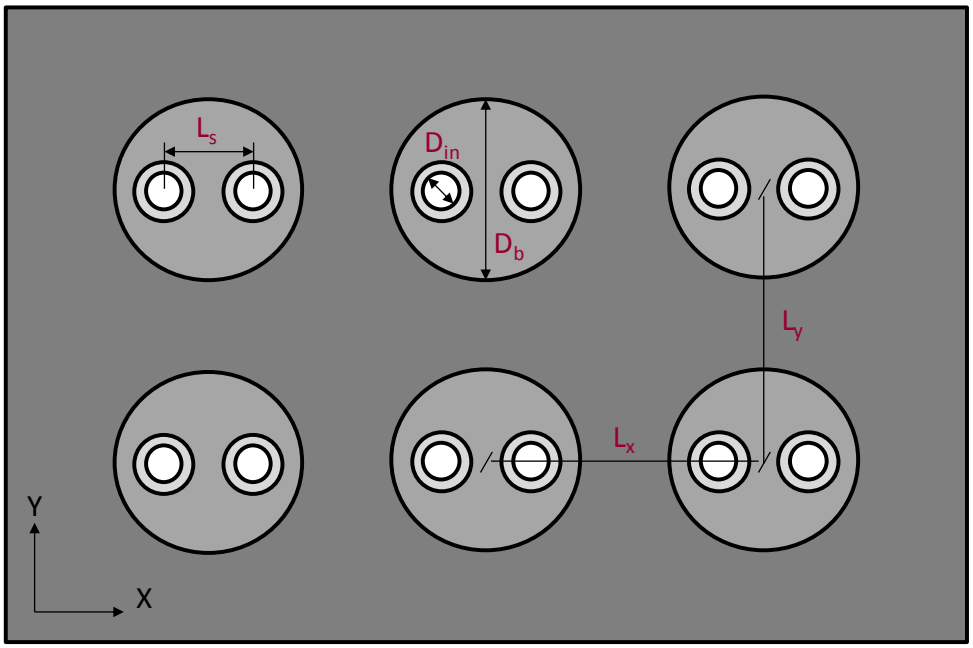

Figure 7.2 A diagram showing the geometric parameters defining multiple BHEs with a configuration of 3x2 (not to scale).

Three-dimensional multi-block boundary fitted structured meshes have been applied to discretise the geometry of each borehole field. An in-house developed program provides a simple and flexible way to generate meshes for multiple BHEs. This program only requires two sets of parameters: a set of parameters concerning the geometry inside a borehole, i.e. the diameter of the borehole (D_b), the diameter of the pipe (D_{in}), the thickness of the pipe, the spacing between the two pipes (L_s), and another set of parameters defining the geometry of the array, i.e. the distances between two boreholes at the x and y directions (L_x, L_y), the number of boreholes on the x direction and the number of boreholes on the y direction. The extent of the surrounding ground included in the simulation domain can also be specified to cater for different needs. For simulations over long timescales, larger simulation domains are required compared to that for simulations over short timescales.

The advantages of using multi-block boundary fitted structured meshes for BHEs were explained in detail in Chapter 3. Different materials, i.e. fluid, pipe, grout, and ground, can be represented by different blocks. Figure 7.3 shows the plane view of the mesh for a borehole

field with a 3x2 configuration. This mesh is essentially extruded in the third dimension (z) along the depth of the borehole.

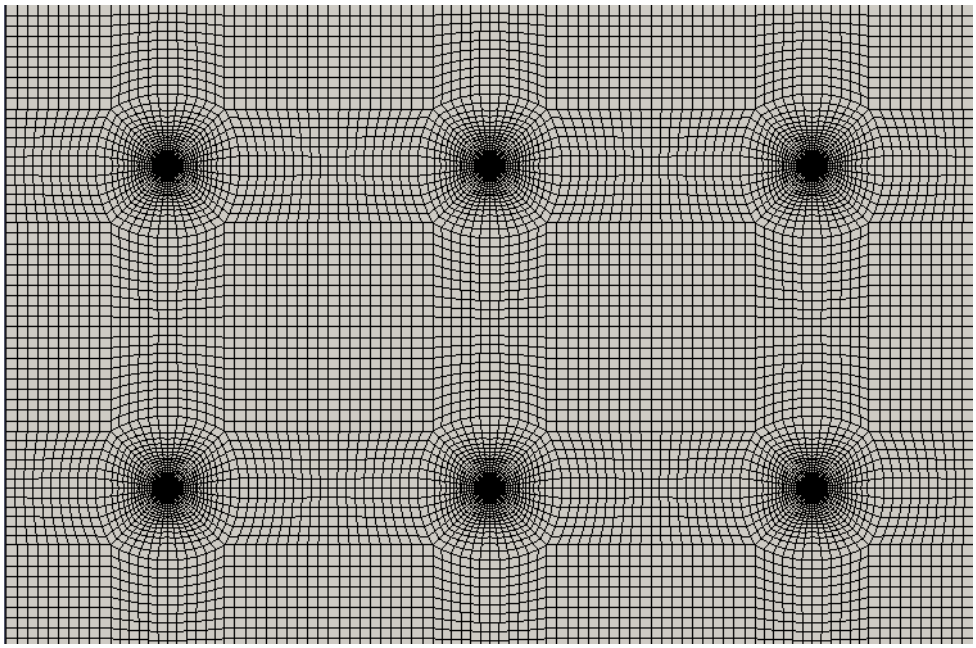

Figure 7.3 A plane view of the multi-block boundary fitted structured mesh for a borehole field with a 3x2 configuration.

Figure 7.4 shows an enlarged section of the boundary-fitted mesh of a borehole.

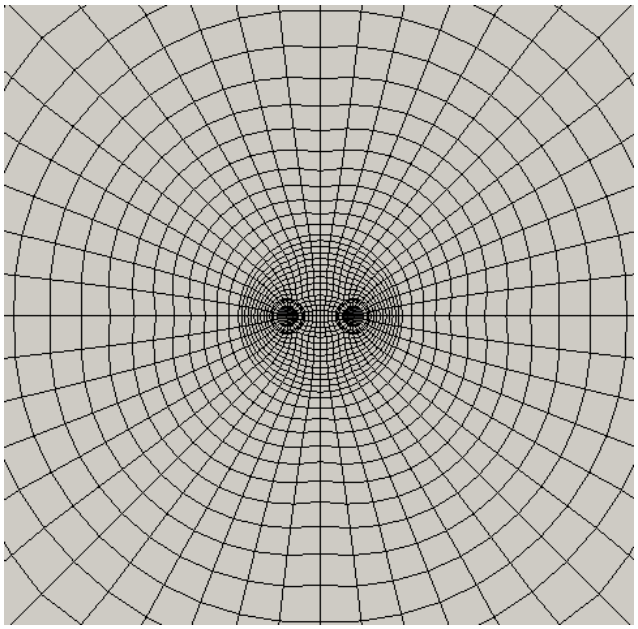

Figure 7.4 An enlarged plan view of a borehole mesh.

7.3 G-function Calculation and Verification

With appropriate boundary conditions, the 3D numerical model can be applied to calculate the g-function for a pre-defined configuration of multiple BHEs. One straight forward way to validate the 3D model is to compare the g-functions calculated with this model to those by Eskilson (1987) and Yavuzturk (1999). Four different configurations of borehole fields are chosen in this study: a single BHE and multiple BHEs with a 2x2, a 3x3, and a 4x4 configuration. Due to the symmetry of the borehole fields in the case of the 2x2 and 4x4 configurations, only a quarter of the borehole filed is simulated (Figure 7.5 and Figure 7.6). For the 3x3 configuration, a full size mesh is used (Figure 7.7).

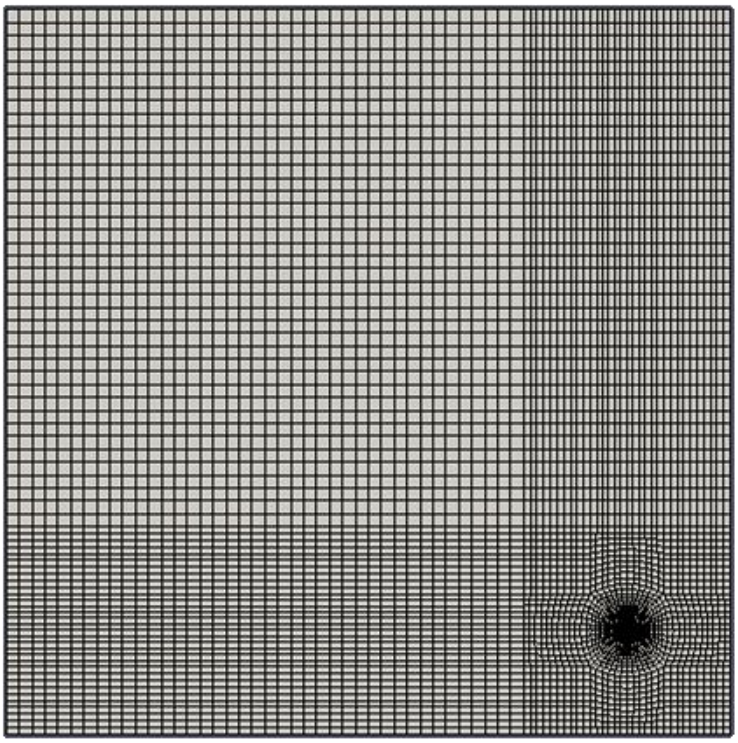

Figure 7.5 Mesh for a borehole field with a 2x2 configuration. The bottom and right edges are symmetry planes.

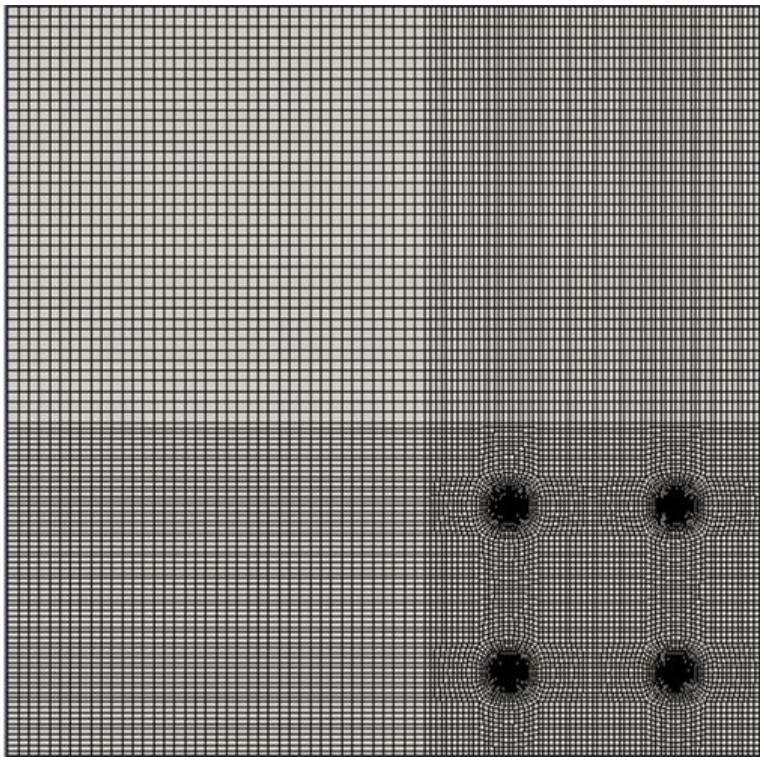

Figure 7.6 Mesh for a borehole field with a 4x4 configuration. The bottom and right edges are symmetry planes.

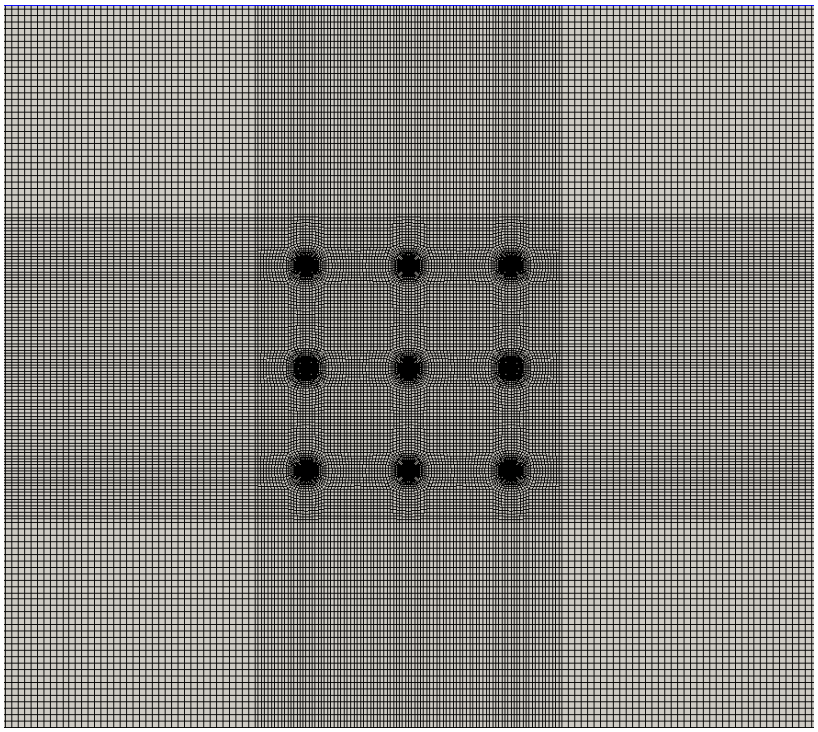

Figure 7.7 Mesh for a borehole field with a 3x3 configuration.

It is assumed that all BHEs in a borehole field are the same. The dimensions and thermal properties of the BHEs are shown in Table 7.1. The simulation domain of each borehole field is 200(L) x 200(W) x 200(H) m^3.

Table 7.1 Dimensions and thermal properties of BHEs.

Borehole Diameter		D	152.4	mm
Pipe Inner Diameter		D_{in}	27.4	mm
Pipe Outer Diameter		D_{out}	33.4	mm
U-tube Shank Spacing		L_s	28.53	mm
Pipe	Conductivity	k_{pipe}	0.39	W/mK
	Thermal Capacity	ρc_p	1.77	MJ/m^3K
Grout	Conductivity	k_{grout}	0.75	W/mK
	Thermal Capacity	ρc_p	3.9	MJ/m^3K
Ground	Conductivity	k_{ground}	2.5	W/mK
	Thermal Capacity	ρc_p	2.5	MJ/m^3K

In order to be consistent with the method that the g-function was calculated by Eskilson and Yavuzturk, the fluid inside the pipes was not modelled in the 3D model; instead, a constant heat flux of 20 W/m was applied to the inner boundary wall of the pipes as the step heat pulse. At the ground surface, and down to a few meters, the ground temperature varies strongly hourly, daily and yearly. Although the average ground surface temperature can be estimated by a sinusoidal function (Kasuda and Archenbach, 1965), the annual mean temperature (10 °C) was used as boundary condition at the ground. Average undisturbed ground temperature (10 °C) was used as the initial condition, neglecting the geothermal gradient of 0.01-0.03 K/m. The far-field ground temperature was also set to be 10 °C.

Since both the fluid and borehole temperatures can be calculated from the 3D model, both Equation (2.21) and (2.23) can be applied to calculate the g-function. The results are compared to the g-functions obtained from GLHEPro, which are essentially the combined long time-step g-function by Eskilson and short time-step g-function by Yavuzturk.

Figure 7.8 shows the g-function of a single borehole calculated by the 3D model using both the fluid temperature (T_f) and borehole temperature (T_b), compared to that obtained from GLHEPro. The g-functions calculated by the 3D model covered the simulation time from 60 seconds to over 1000 years, and the g-function from GLHEPro covered that from 5 minutes to over 600 years.

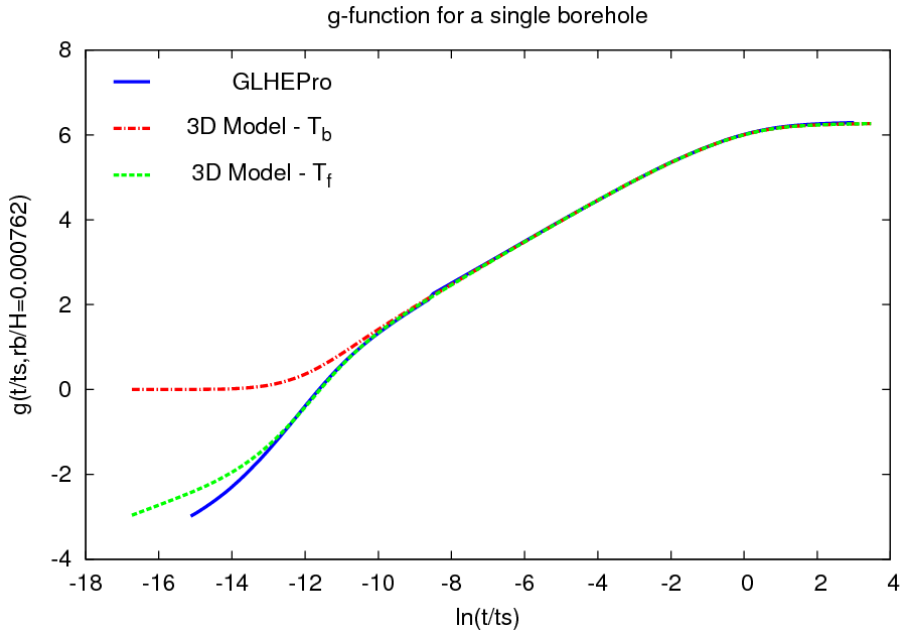

Figure 7.8 Comparison of g-function data for a single borehole.

At long timescales ln(t/ts) > -10 (in which case t > 13 hrs), the g-functions both calculated by fluid temperature and borehole temperature are the same and they match almost exactly the g-function data obtained from GLHEPro. However, at short timescales, the g-function calculated using fluid temperature is very different from that calculated using the borehole temperature. This is because, when the fluid temperature was used to calculate the g-function, the assumption was taken that the borehole temperature can be obtained through subtracting the temperature change due to the borehole resistance from the fluid temperature (Equation (7.6)). This assumption is appropriate and realistic at long timescales, but at short timescales, the thermal capacities of the fluid, pipes and grout are significant and this assumption becomes inappropriate. Consequently, the borehole temperature calculated by subtracting this temperature change from the fluid temperature can be unrealistic. This can be seen from the negative values of g-function for ln(t/ts) < -11 (in which case t < 3 hrs). Although unrealistic, when this value is used to predict the fluid temperature, the over predicted temperature

change due to the borehole resistance is added back to the equation (Equation (2.23)), so in a way, it cancels out the effect. However, if Equation (7.6) is then used to calculate the borehole temperature, the borehole temperature can then be unrealistic over short timescales, which actually happens in EnergyPlus.

The g-function calculated by the 3D model using the fluid temperature matches better to the g-function in GLHEPro over short timescales, compared to that calculated by the 3D model using the borehole temperature, since the g-function in GLHEPro was also calculated using the fluid temperature. The difference between the g-function calculated by the 3D model using the fluid temperature and the g-function in GLHEPro mainly lies in ln(t/ts) < -13 (in which case t < 40 mins). Consequently, for simulations that run at hourly time step, predictions of fluid temperatures from these two g-functions are the same. For simulations that run at shorter time steps than an hour (as EnergyPlus and TRNSYS generally do), some differences in predictions can be expected.

Figure 7.9 shows the g-function for a borehole field with a configuration of 2x2 multiple BHEs. It can be seen from the graph that the g-functions calculated by the 3D models matches exactly that from GLHEPro at long timescales, and the differences of g-functions at short timescales are the same as those of the borehole field with only a single borehole.

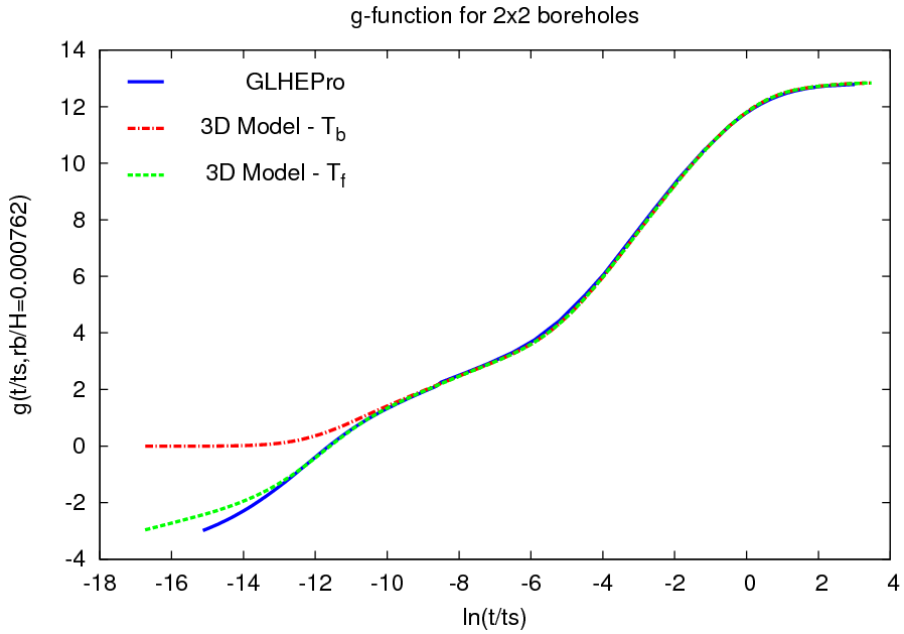

Figure 7.9 Comparison of g-function data for a 2x2 borehole array.

Figure 7.10 and Figure 7.11 show the g-function for a borehole field with a configuration of 3x3 multiple BHEs and a configuration of 4x4, respectively.

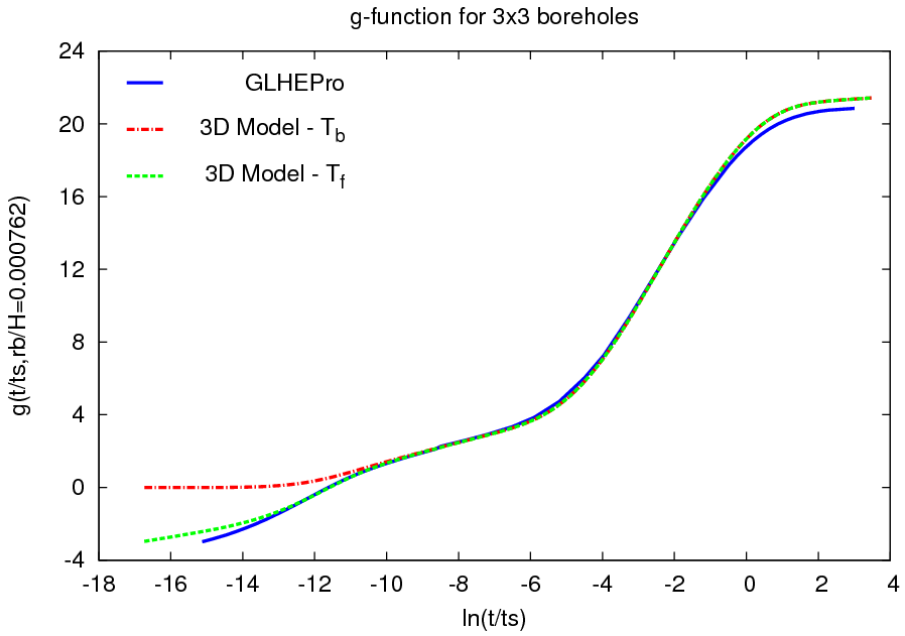

Figure 7.10 Comparison of g-function data for a 3x3 borehole array.

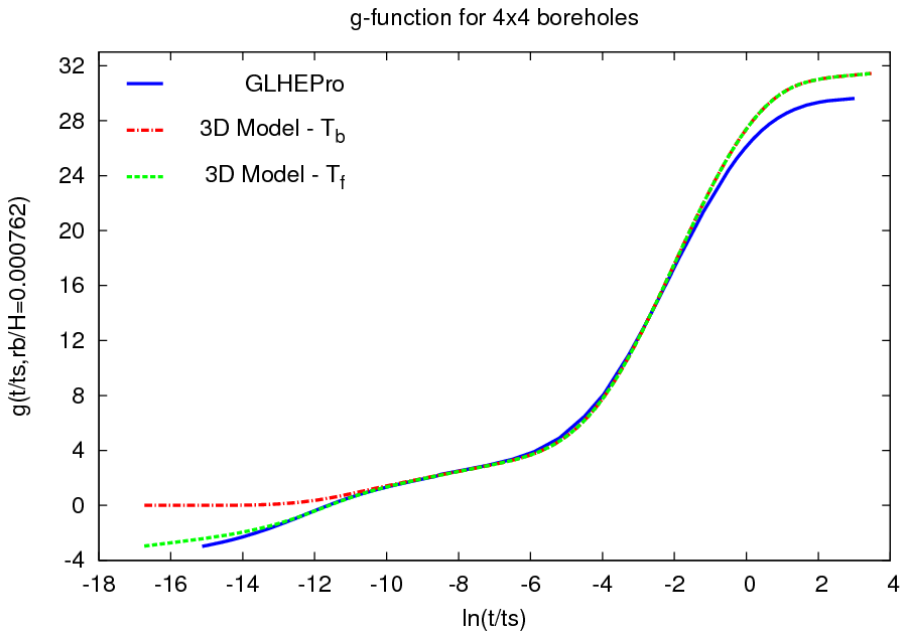

Figure 7.11 Comparison of g-function data for a 4x4 borehole array.

The g-function data calculated using the different methods are the same as that of the single borehole at short timescales, as the thermal interaction among the boreholes has not

developed. However, at long timescales, the g-functions predicted by the 3D model using both the fluid and borehole temperatures have slightly higher values than that from GLHEPro. The more boreholes the borehole field has, the bigger the difference between the g-functions predicted by the 3D model and that from GLHEPro becomes, and the earlier these difference appear.

One possible explanation is that, in the 3D models, a constant heat flux was specified in each BHE, regardless of its position among other BHEs. However, in reality, the heat flux of the BHE in the centre of the borehole field would be less than that of the BHE at the corner of the borehole field due to the interaction among the BHEs at long timescales. This effect was not considered by the 3D model but was taken into account (the method is not reported) by the superposition technique used by Eskilson. For a configuration of 2x2 multiple BHEs, there is no such effect because each borehole occupies a corner of the borehole field and the heat flux of each borehole should be the same. The more boreholes a borehole field has, and the more densely the boreholes are distributed, the more significant the effect will be. This is consistent with the difference of the g-functions shown in Figure 7.10 and Figure 7.11.

An alternative approach to this problem is to use inlet fluid temperature, instead of constant heat flux, as the boundary condition. At each time step, the average outlet temperature of the BHEs can be calculated and used to update the inlet temperature for next time step, according to the constant amount of heat rejected to the ground. In this way, the unevenly distributed heat flux of each BHE due to its position in the array can be taken into account by the 3D model itself. One main drawback of this approach is that the time step has to be small enough in order to allow the inlet temperature to be updated frequently. This implies using shorter time steps and greater computational effort.

7.4 Axial Heat Transfer

Axial heat transfer, when considering the thermal interaction of multiple BHEs over long timescales, can be very significant. Figure 7.12, Figure 7.13, and Figure 7.14 show the temperature contours on a vertical plane, for a 4x4 borehole array, after 1 year, 10 years and 100 years' simulation, respectively. All the BHEs are 100 m deep and the simulation domain is 200 (L) x 200 (W) x 200 (H) m^3. The initial ground temperature was 10 °C. A constant heat flux of 20 W/m was applied to the inner boundary wall of the pipes and a constant temperature of 10 °C was specified at both the upper surface and far-field boundary of the ground. In these

figures the contours start from 12 °C and the temperature difference between two adjacent contours is 5 °C.

As indicated by the parallel contours along the borehole depth shown in Figure 7.12 (after 1 year's simulation), the heat transfer of the BHEs can be regarded as radial heat flow i.e. normal to the borehole. The Axial heat transfer is not significant and the heat only penetrates a few meters underneath the BHEs. As the simulation progresses (e.g. after 10 years' simulation), the contours are no longer parallel (as shown in Figure 7.13), and this indicates axial heat transfer becoming more significant. The heat penetrates deeper underneath the BHEs (up to 20 meters to the 12°C contour). The contours shown in Figure 7.14 (after 100 years' simulation) demonstrate that at the outer boundary, the heat flow from the upper half of the BHEs is partly to the ground surface and the heat flow from the lower half of the BHEs is partly to the deep ground and not just radial (as indicated by the arrows). The heat penetrates much deeper below the BHEs (more than 60 meters).

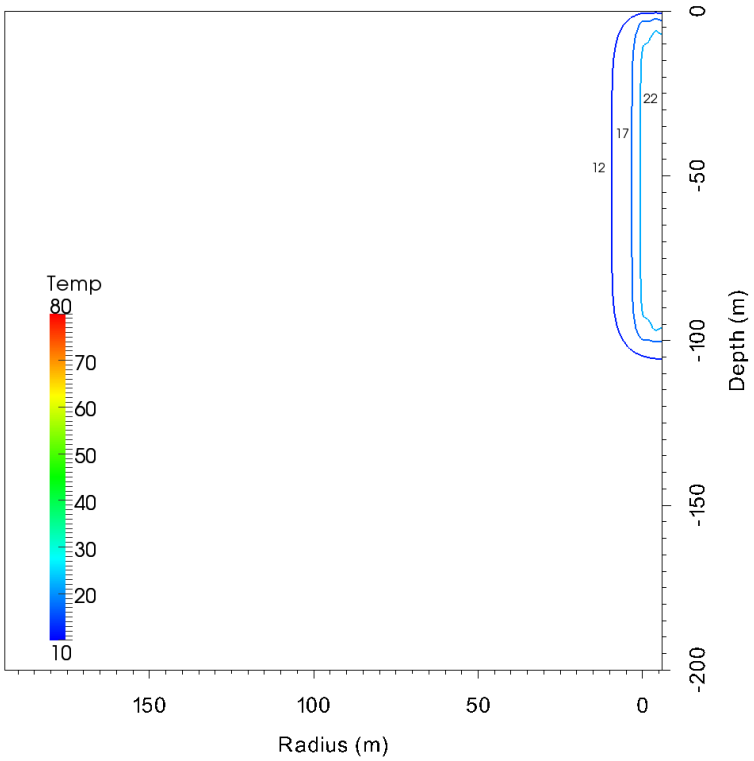

Figure 7.12 Temperature contours for a 4x4 borehole array after 1 year's simulation.

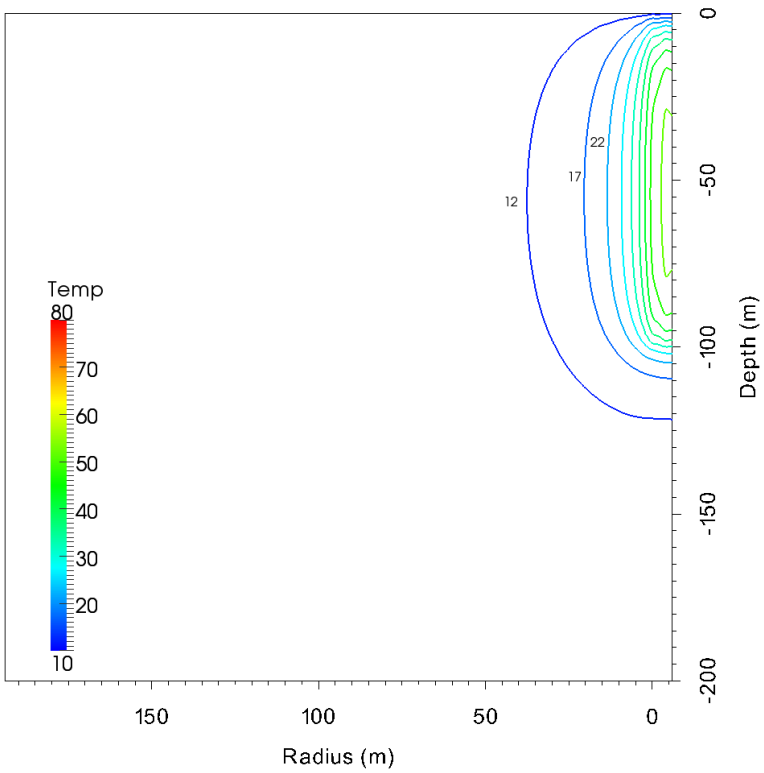

Figure 7.13 Temperature contours for a 4x4 borehole array after 10 years' simulation.

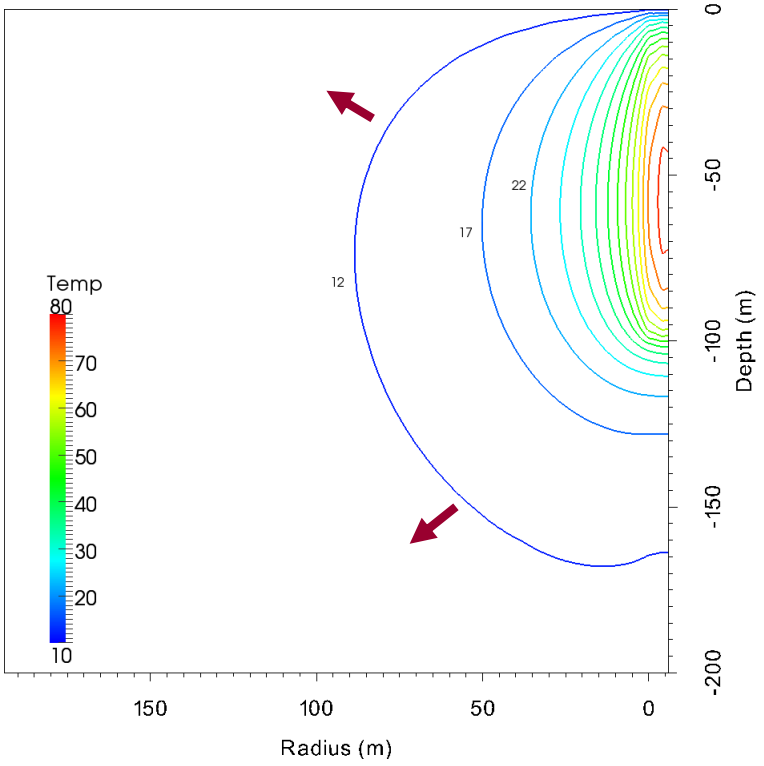

Figure 7.14 Temperature contours for a 4x4 borehole array after 100 years' simulation.

The effects of the axial heat transfer in this long timescale calculation have been simplified by setting a constant ground surface temperature (as in the g-function calculation). In reality, the ground surface temperature varies hourly, daily and yearly, and so the axial heat transfer will be more complex. Nevertheless, it is important the axial heat transfer is considered in the modelling of BHEs over long timescales.

7.5 Potential Applications

Modelling the multiple BHEs explicitly allows sophisticated control and operation of a borehole field to be simulated. Trial studies can be carried out including:

- Optimisation of the operation of a borehole field by adjusting the number of boreholes in use during part load conditions. For example, if only half of the heating demand is required, half of the boreholes can be isolated in order to reduce the pumping power but at the same time provide good heat transfer rates;
- Optimisation of the operation of a borehole field by dividing the borehole field into two sub-borehole fields (e.g. one to extract heat and the other one to reject heat) for larger systems require heating and cooling simultaneously. Switching these two sub-borehole fields periodically, theoretically, can balance the heat extract and rejection from and into the ground.

7.6 Summary

This chapter explores the potential of applying the numerical 3D model for the simulations of multiple BHEs arrays. The g-functions calculated by the 3D model have been compared to those by Eskilson and Yavuzturk for four different configurations of borehole fields, including a single borehole, a configuration with 2x2, 3x3 and 4x4 multiple BHEs. Both the fluid temperature and the borehole temperature have been used for the calculation in the 3D model.

Over short timescales, where the heat transfer process is characterised by those of a single BHE, the difference between the g-functions predicted by the 3D model using the fluid temperature and borehole temperature is significant due to the assumptions made regarding the relationship between the fluid and borehole temperatures. The g-function predicted by the 3D model using the fluid temperature better matches to the g-function obtained from

GLHEPro, which was also calculated using the fluid temperature. The differences between these two g-function, exist only at timescales less than one hour in this case.

Over long timescales, for the single borehole and the configuration with 2x2 multiple BHEs, both the g-functions predicted by the 3D model using the fluid and borehole temperatures match the g-function from GLHEPro exactly. The predicted values of the g-function for configurations with 3x3 and 4x4 multiple BHEs are slightly higher than that of the GLHEPro. This is thought to be due to the constant heat flux that was specified to each BHE in the 3D model, regardless of its position at the borehole field. This may be addressed using the inlet fluid temperature as the boundary condition and adjusting it at each step of the calculation to ensure a constant heat pulse is maintained.

Axial heat transfer over long timescales is significant and has to be considered in modelling thermal interaction of multiple BHEs.

Modelling BHEs arrays explicitly allows flexible representation of the control of the operation of the borehole field. For example, it would allow the study of optimal operating strategies that may vary the flow in different boreholes according to par load conditions.

Chapter 8 Thermal Response Test Analysis

The previous chapters reported the applications of the dynamic three-dimensional (3D) finite volume model for borehole heat exchangers (BHEs) in a number of studies, including the simulation of a single BHE (Chapter 4), integrated ground source heat pump (GSHP) system simulation (Chapter 6), and modelling of BHEs arrays (Chapter 7).

In this chapter, the 3D finite volume model is applied to evaluate the assumptions of the line source model and their implications in the analysis of Thermal Response Tests (TRT).

8.1 Estimation of Ground Conductivity

Estimating the thermal conductivity of the ground is of primary importance in any design or simulation tasks for BHEs, as the thermal conductivity describes the ability of the ground to conduct heat, and therefore it is a key factor to determine the length/numbers of boreholes required for a particular system. Underestimating the thermal conductivity will result in over estimation of the BHE array size which, in turn, will result in higher initial costs. Overestimating the thermal conductivity may result in undersizing of the whole system, which will lead to less efficient performance and might eventually cause system failure.

There are three commonly used methods to estimate the thermal conductivity of the ground. The first is to estimate the value according to the geological data of the site and use typical published value of the thermal conductivity in the literature. This method allows a quick and simple but rough estimation. The value of the thermal conductivity normally is given as a range, and this is often quite wide. For example, the thermal conductivity of sandstone according to the literature is 1.83 – 2.90 W/mK. Within this range, it is difficult to pin point the exact value of the thermal conductivity. For conservative estimation, the value of the lowest bound might be adopted, which will be 1.83 W/mK in this case. Since the actual value of the thermal conductivity might vary from 1.83 to 2.90, borehole array size and cost may be very uncertain.

Conducting laboratory experiments using samples collected from the site can also be used to estimate the thermal conductivity of the ground. The main disadvantage of this method is that only a small sample, or number of samples, can be tested and consequently this value might not be representative of the whole BHE array installation. The heterogeneity of the ground cannot be taken into account either.

Performing an in-situ Thermal Response Test (TRT) might be the most accurate method to estimate the thermal conductivity of the ground. The principle of the TRT is relatively simple. A controlled heat source – normally an electric heater – continuously rejects a constant amount of heat into a test BHE through the fluid circulating around the closed pipe loop for a period of time (at least for 50 hours). The inlet and outlet temperatures of the circulating fluid and the energy consumption of the heat source are recorded. The thermal conductivity of the ground can be estimated using different methods. Due to its simplicity, line source model has been widely used to analyze the data from the in-situ tests and estimate the thermal conductivity of the ground.

8.2 Line Source Model

The mean of the inlet and outlet temperatures of the circulating fluid is usually used in the line source model to estimate the thermal conductivity of the ground and borehole resistance. If plotting the mean temperature versus the natural logarithm of time during the TRT, according to the line source model, the thermal conductivity of the ground (k) is inversely proportional to this slope of the mean temperature. And the correlation can be expressed in Equation (8.1) (Carslaw and Jaeger, 1947).

$$k = \frac{Q}{4\pi m L} \tag{8.1}$$

where Q is the constant heat input, L is the length of borehole, and m is the slope of the mean temperature versus natural logarithm of time.

The borehole resistance can be estimated from the line source model using Equation (8.2).

$$R_b = \frac{1}{4\pi k}\left[\frac{T_m - T_g}{m} - \ln\left(\frac{4\alpha t}{\gamma r_b^2}\right)\right] \tag{8.2}$$

where T_m is the mean temperature, T_g is the undisturbed ground temperature, α is the thermal diffusivity of ground and γ is a constant and approximately equal to 1.78.

Several assumptions are made in the line source model when it is applied in this way:

- Geometry of the borehole components is ignored and the thermal mass of the circulating fluid, pipes, and grout within the borehole are assumed to be the same as the ground;
- BHE is considered to be infinitely long;

- Heat transfer in the axial direction is ignored and the heat transfer of the borehole is only modelled in the radial direction;
- Ground is assumed to be entirely homogeneous;
- Upper surface is adiabatic;
- No vertical temperature gradient.

Due to these assumptions, there are some limitations of the line source model when it is used in the analysis of TRT. The recorded inlet and outlet temperatures of the circulating fluid for the first few hours should be ignored since the heat transfer within the borehole dominates the heat transfer process at the first few hours. The changes of the fluid temperatures during this initial period only reflect the thermal properties of the material within the borehole (i.e. the circulating fluid, pipes, and grout) and not the surrounding ground.

In this chapter, a dynamic numerical three-dimensional model has been applied to evaluate the validity and limitation of the line source model used in the analysis of TRT data. The effects of the length of measurement period and the starting time of the analysis period (t_0) and the end time of the analysis period (t_E), the velocity of the circulating fluid, the thermal conductivity of the grout, and the heterogeneity of ground on the accuracy of using the line source model for the analysis of TRT are examined in detail.

8.3 Evaluation Using 3D Model Data

Various cases of TRT have been simulated using the 3D numerical model and the calculated temperatures then used with the line source model to estimate the thermal conductivity of the ground. This approach has been reported in a study carried out by Signorelli *et al.* (2007). The effects of the length of measurement period, the borehole length, heterogeneous subsurface conditions and groundwater flow on the analysis of TRT data using the line source model were presented in their study. In this study, the effects of some new factors, include the grout thermal conductivity and the velocity of the circulating fluid, have been examined. The effects of the length of measurement period and the heterogeneity of the ground have also been investigated.

The configuration and thermal properties of the BHE is shown in Table 8.1. A constant heat source of 5kW is chosen to supply the heat to the water circulating along the pipe loop inside the borehole. By running the simulation, the inlet and the outlet temperatures of the fluid can

be obtained. The thermal conductivity of the ground k_{ground} is the ground condition parameter used in the model, and this is the value that is expected when the line source model is to be used to evaluate the thermal conductivity of the ground.

Table 8.1 Configuration and thermal properties of the BHE.

Borehole Diameter		D_b	152.4	mm
Pipe Inner Diameter		D_{in}	27.4	mm
Pipe Outer Diameter		D_{out}	33.4	mm
Shank Spacing between Pipes		L_s	28.53	mm
Borehole Depth		D	100	m
Simulation Domain of BHE		$\pi x r^2 x L$	$\pi x 20^2 x 200$	m^3
Velocity of the Circulating Fluid		v	0.4	m/s
Borehole Thermal Resistance		R_b	0.2216	mK/W
Fluid	Conductivity	k_{fluid}	0.6	W/mK
	Thermal Capacity	ρc_p	4.18	MJ/m^3K
Pipe	Conductivity	k_{pipe}	0.39	W/mK
	Thermal Capacity	ρc_p	1.77	MJ/m^3K
Grout	Conductivity	k_{grout}	0.75	W/mK
	Thermal Capacity	ρc_p	3.9	MJ/m^3K
Ground	Conductivity	k_{ground}	2.5	W/mK
	Thermal Capacity	ρc_p	2.5	MJ/m^3K

For half of the circular simulation domain of $\pi x 20^2 x 200$ m^3, a total number of around 270,000 cells have been used for the discretization. The mesh is fine within and around the borehole in the horizontal direction and fine at the top and the bottom in the vertical direction, where the temperature gradients are greatest. A constant temperature of 10^oC has been specified at the circular outer wall of the simulation domain. This temperature is also assumed to be the initial temperature of the whole simulation domain. The simulation of the TRT runs continuously for 240 hours with the time step of 1 minute. The mean fluid temperature of the inlet and outlet is shown in Figure 8.1.

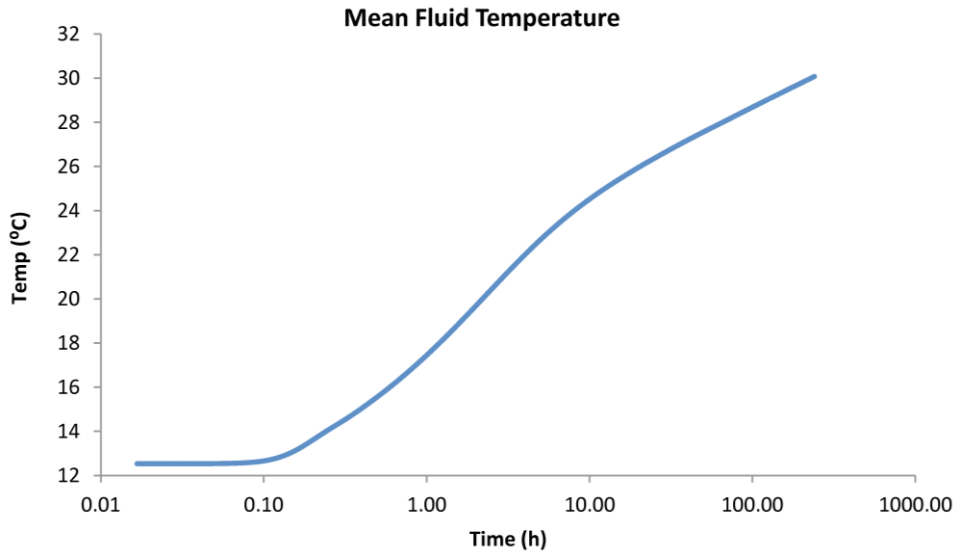

Figure 8.1 Mean circulating fluid temperature of the inlet and outlet.

The line source model can be applied to estimate the thermal conductivity of the ground based on the mean fluid temperatures obtained from the simulations. If the data from the 10th hour (t_0 = 10h) to the 240th hour (t_E = 240h) are chosen for the analysis, the mean fluid temperatures with linear trend lines plotted against the natural logarithm time are those shown in Figure 8.2.

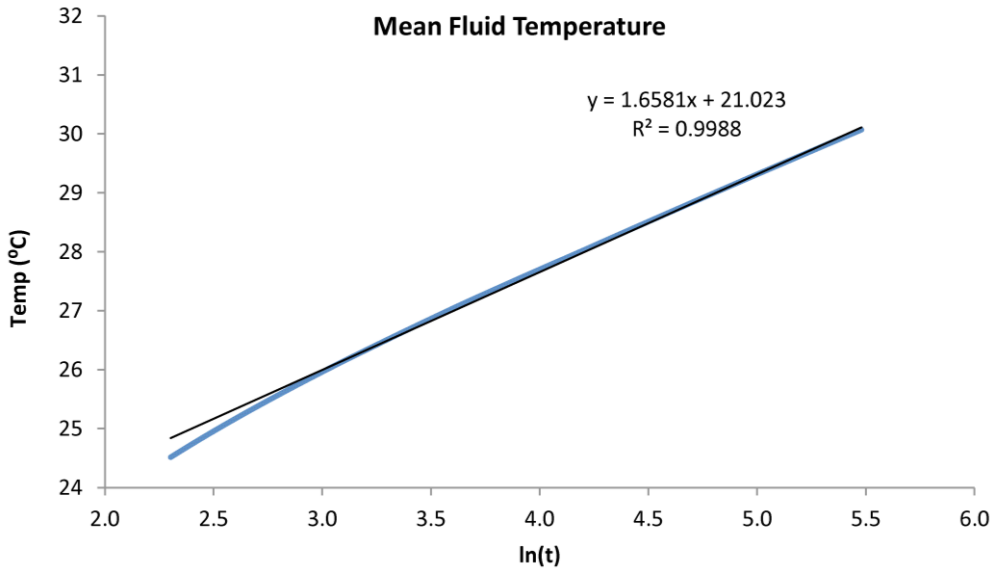

Figure 8.2 Mean fluid temperatures with linear trend lines from the 10th hour to the 240th hour plotted against ln(t) at different time steps.

Using Equation (8.1), the thermal conductivity of the ground is calculated to be 2.4 W/mK, which is 4% lower than the numerical value of 2.5 W/mK.

8.4 Sensitivity Analyses

In this section, sensitivity analyses of using the line source model to evaluate the thermal conductivity of the ground in TRT are presented. The purpose of the sensitivity analyses is to investigate the appropriate starting time t_0 from when the data should be included in the analysis, and the end time t_E upon when the testing period should be long enough to achieve acceptable accuracy. The effects of the velocity of the circulating fluid, the grout material, and the heterogeneity of the ground are examined in detail.

8.4.1 Sensitivity to the Starting Time (t_0)

To illustrate the effect of choosing different starting time t_0 on the analysis, the thermal conductivity of ground has been estimated by varying the starting time t_0 continuously but with a fixed end time t_E. The data obtained from the previous simulations of TRT for a period of 240 hours have been used. Figure 8.3 shows the estimated thermal conductivities of the ground based on the line source model when the starting time t_0 is showing on the x axis and varying continuously from 1 – 239h and the end time t_E is fixed at 240h.

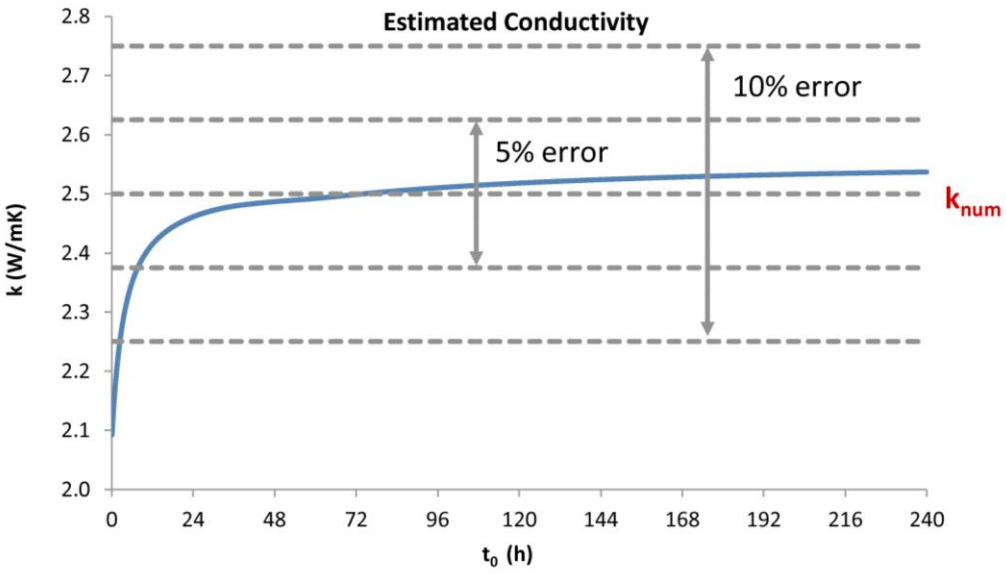

Figure 8.3 Estimated thermal conductivities based on the line source model using synthetic data, t_E is fixed at 240h, and t_0 is varying from 1 – 239h.

If neglecting the data from the first two hours, the estimation can fall within the 10% error band; if neglecting the data from the first seven hours, the estimation can be found within 5%. At higher values of t_0 the error is less than 2%.

8.4.2 Sensitivity to the End Time (t_E)

A similar technique to that in the previous section can be applied to investigate the effect of the end time t_E on the accuracy of estimated ground conductivity. Instead of a fixed end time t_E, a fixed starting time t_0 and a continuously varying end time t_E, from (t0+1) h to 240h, have been used to define the period of the data used in the estimation. The synthetic data from the 3D model have been analysed with four different starting times: t_0 = 10h, 20h, and 40h, and the results are shown in Figure 8.4.

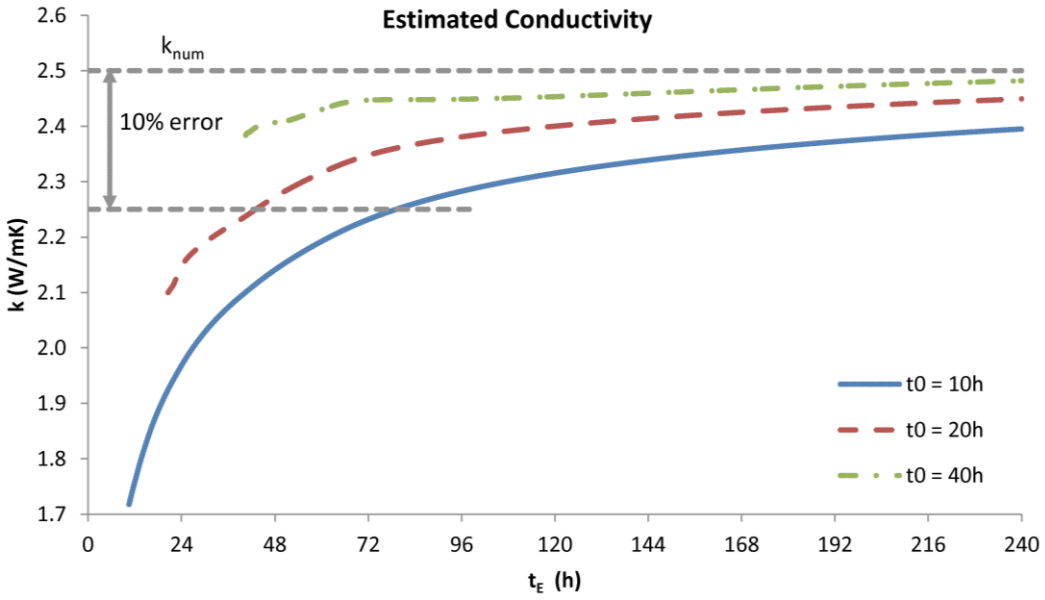

Figure 8.4 Estimated thermal conductivities based on the line source model. Four scenarios with t0 = 10h, 20h, and 40h, and tE is varying from (t0+1) – 240h.

If the duration of the test is 72 hours (t_E = 72h), for t_0 = 10h, the estimated thermal conductivity of the ground is 2.23 W/mK, which falls slightly outside of the 10% error margin (10.8%). For t_0 = 20h, the estimated conductivity is 2.35 W/mK and the error is 6%. For t_0 = 40h, the estimated conductivity is 2.45 W/mK and the error is only 2%. In order to achieve less than 10% error in the estimated value, the test should last at least 79 hours if t_0 = 10h is used in the analysis; at least 42 hours if t_0 = 20h is used. On the other hand, if only 5% of error is allowed in

the analysis, for t_0 = 10h, the test should last at least 196 hours; for t_0 = 20h, the test should last at least 89 hours. For cases with t_0 = 40h, all the estimated values are within the 5% error.

The results can also be presented differently considering different combinations of starting time t_0 and end time t_E. Figure 8.5 illustrate the results with t_0 = 10h, 20h, and 40h, shown on the x axis, t_E = 72h, 120h, and 240h, shown by different line colours/types. Taking t_0 = 10h, for example, the estimated conductivity for t_E = 72h is 2.24W/mK (around 10% error); for t_E = 120h is 2.32W/mK (around 7% error); and for t_E = 240h is 2.40W/mK (4% error). Take another example of t_0 = 20h, the estimated conductivity for t_E = 72h is 2.35W/mK (6% error); for t_E = 120h is 2.40W/mK (4% error); and for t_E = 240h is 2.45W/mK (2% error). For and t_E = 120h and 240h, the estimated conductivity is around 2.45W/mK. For t_0 = 40h, a highly accurate estimated conductivity of 2.48 W/mK can be expected.

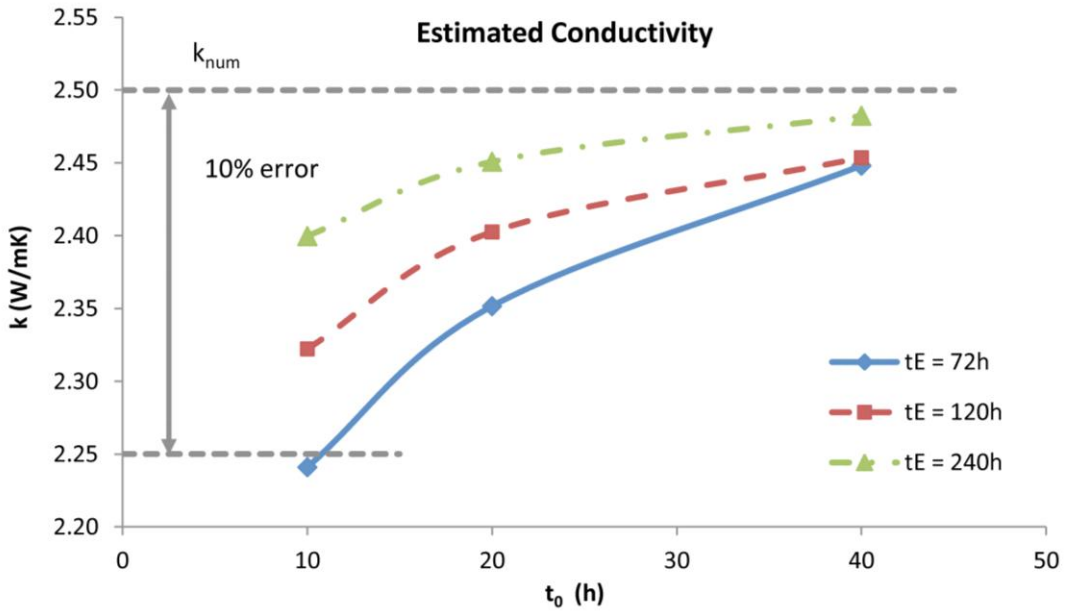

Figure 8.5 Estimated thermal conductivities based on the line source model using synthetic data with 1 minute per time step. Different combinations with t_0 = 10h, 20h, 40h and t_E = 72h, 120h, and 240h.

8.4.3 Velocity of the Circulating Fluid

Gehlin (2002) summarized the experimental apparatus for TRT around the world. It was reported that the flow rate used during the test in different countries ranged between 0.14 to 1.0 l/s. It is, therefore, useful to examine the influence of different flow rates on the accuracy of the estimated thermal conductivity of the ground when using the line source model for the analysis. The TRT on the same BHE (configuration and thermal properties shown in Table 8.1)

has been simulated in the 3D model, with the fluid circulating along the pipe loop at three different velocities, 1 m/s (0.59 l/s), 0.8 m/s (0.472 l/s), and 0.6 m/s (0.354 l/s). These results are combined with the results presented in the previous section with the velocity of the circulating fluid at 0.4 m/s (0.236 l/s).

Figure 8.6 shows the estimated thermal conductivity of the ground for fluid circulating along the pipe loop at different velocities. The conductivities are estimated by a fixed start time t_0 = 10h and a moving end time t_E from 24 – 240h. The errors in the estimations for all cases are within 2.5% at t_E = 240h. The differences of the estimations for fluid circulating at different velocities are very small.

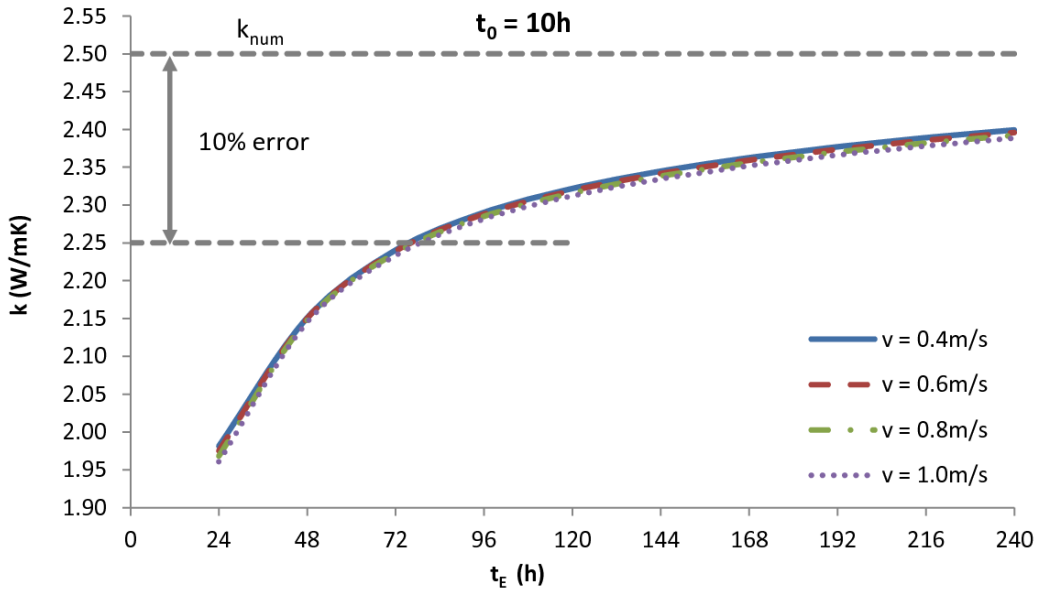

Figure 8.6 Estimated thermal conductivity of the ground for fluid circulating along the pipe loop at different velocities. With a fixed t_0 = 10h and t_E varies continuously from 24 – 240h.

8.4.4 Sensitivity to Grout Conductivity

When the line source model is used to estimate the thermal conductivity of the ground, the grout is considered to have the same thermal properties as the ground, although this is not true in most cases. In this section, the 3D numerical model is used to examine the effects of grout conductivity on the estimation of ground conductivity in TRT.

In the first testing case, the thermal properties of the grout, i.e. the thermal conductivity and specific heat capacity, are set to be the same as the ground in the 3D model. The mean

temperatures of the inlet and outlet fluid calculated from the 3D model during 240 hours are used by the line source model to estimate the ground conductivity. The numerical value set for the ground conductivity (k_{num}) is 2.5 W/mK. Figure 8.7 shows the estimated thermal conductivities of the ground with t_0 = 10, 20 and 40h. The thermal conductivity of the ground during the 240 hours testing is slightly over predicted (within 10% error margin). The predictions for different starting time t_0 are slightly different when the testing period is relatively short (t_E < 120 h), but as the test runs longer, the predictions converge. The estimated ground conductivity is 4% higher than the numerical value at the end of test (t_E = 240h).

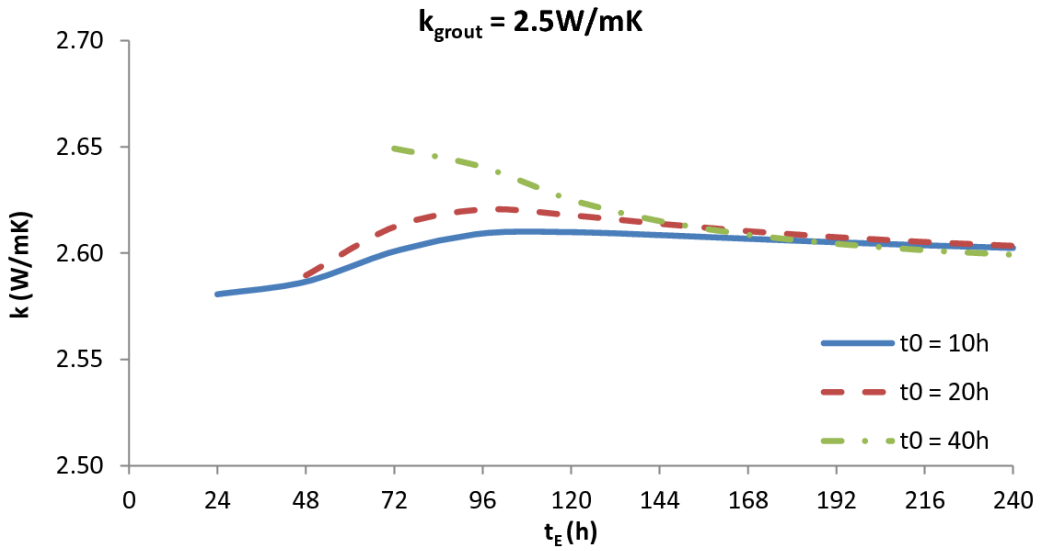

Figure 8.7 Estimated thermal conductivities of the ground for k_{grout} = 2.5 W/mK with different starting time t_0.

In the second test case, the effects of grout with relatively higher thermal conductivity than the original value (0.75 W/mK) are examined. The thermal conductivity of the grout is set to be 1.5 and 3.0 W/mK respectively, but the specific heat capacity remains the same in the 3D model.

Figure 8.8 shows the mean fluid temperatures for grout with thermal conductivity of 0.75, 1.5, and 3.0 W/mK, plotted against log time. The borehole thermal resistances in these three cases are 0.2327, 0.1461, and 0.1033 mK/W, respectively. The mean fluid temperature for grout with low thermal conductivity rises more rapidly than the mean fluid temperature for grout with high thermal conductivity. This is because, providing a constant heat input Q in all cases, the

temperature change is larger for grout with lower thermal conductivity or high borehole resistance.

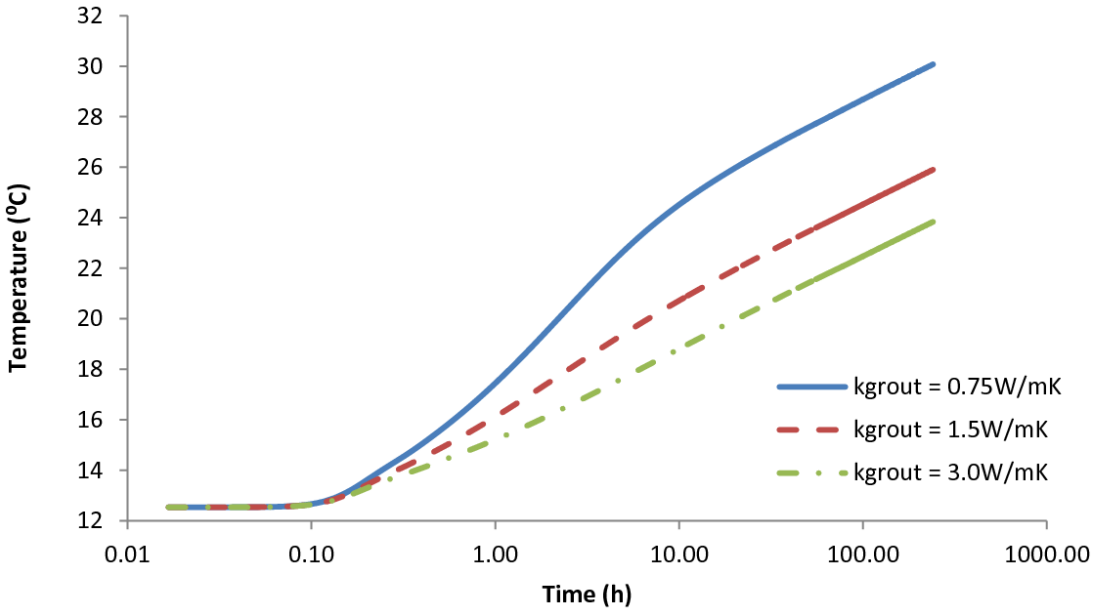

Figure 8.8 Mean fluid temperatures for grout with thermal conductivity of 0.75, 1.5 and 3.0 W/mK plotted in log scale time.

Figure 8.9 shows the heat fluxes at the borehole wall for grout with thermal conductivity of 0.75, 1.5, and 3.0 W/mK, plotted against log time. The differences in heat fluxes mainly exist within the first 10 hours, and during that period, the heat transfer from the BHE is mostly within the borehole itself and therefore, the heat transfer rate is dominated by the thermal properties of the fluid, pipe and grout. As the tests continue, eventually the heat fluxes at the borehole wall become the same.

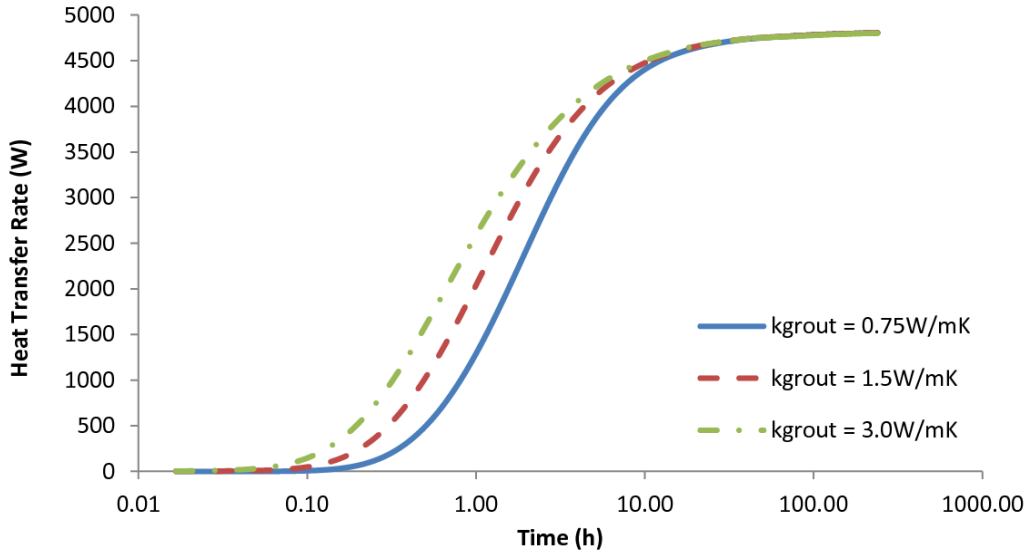

Figure 8.9 Heat flux at borehole wall for grout with thermal conductivity of 0.75, 1.5 and 3.0 W/mK plotted in log scale time.

Figure 8.10 shows the thermal conductivities of the ground estimated by a fixed start times t_0 = 10h and increasing end time t_E from 24 -240h with thermal conductivities of the grout of 0.75, 1.5, 3.0 W/mK.

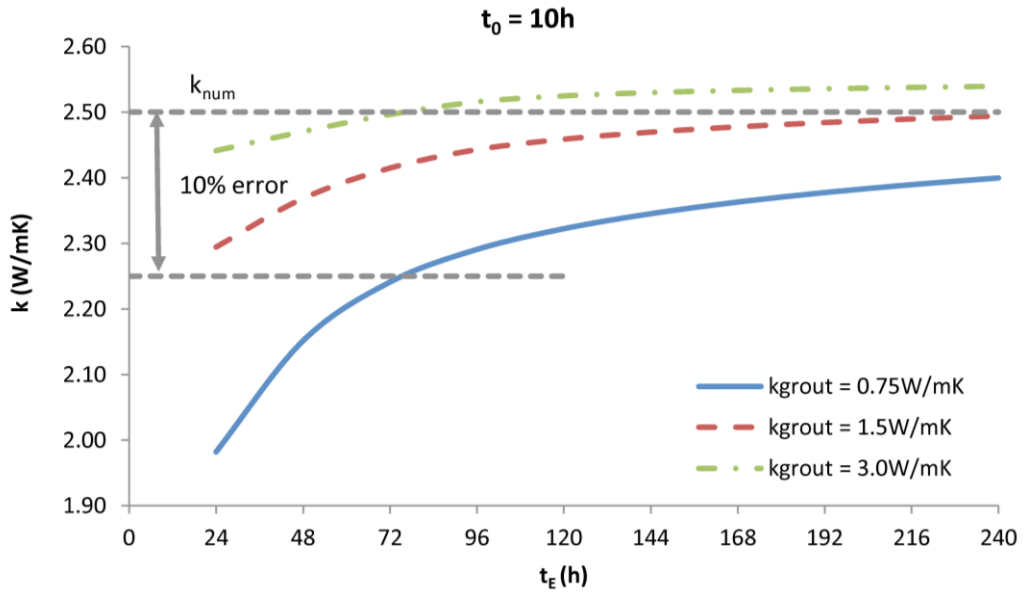

Figure 8.10 Estimated thermal conductivity of the ground at t_0 = 10h, t_E = 24 -240h, for grout conductivities of 0.75, 1.5, 3.0W/mK.

The estimated thermal conductivities of the ground with the grout of these three thermal conductivities are different at a given end time t_E. The deviation of the values for these three cases is much higher when t_E = 24h, around 11.5%, and it decreases as t_E increases from 24h to 240h. At t_E = 240h, the deviation is around 3.2%. This is because the influences of the grout with different thermal conductivities are more dominant at early hours where the heat transfer of the BHE is mostly confined to inside the borehole. With grout of low conductivity, it is likely that the thermal conductivity of the ground can be underestimated; and with grout of high conductivity, an over-estimation of the thermal conductivity of the ground can be expected.

Figure 8.11 shows the estimated thermal conductivity of the ground with grout of different thermal conductivities at t_0 = 20h.

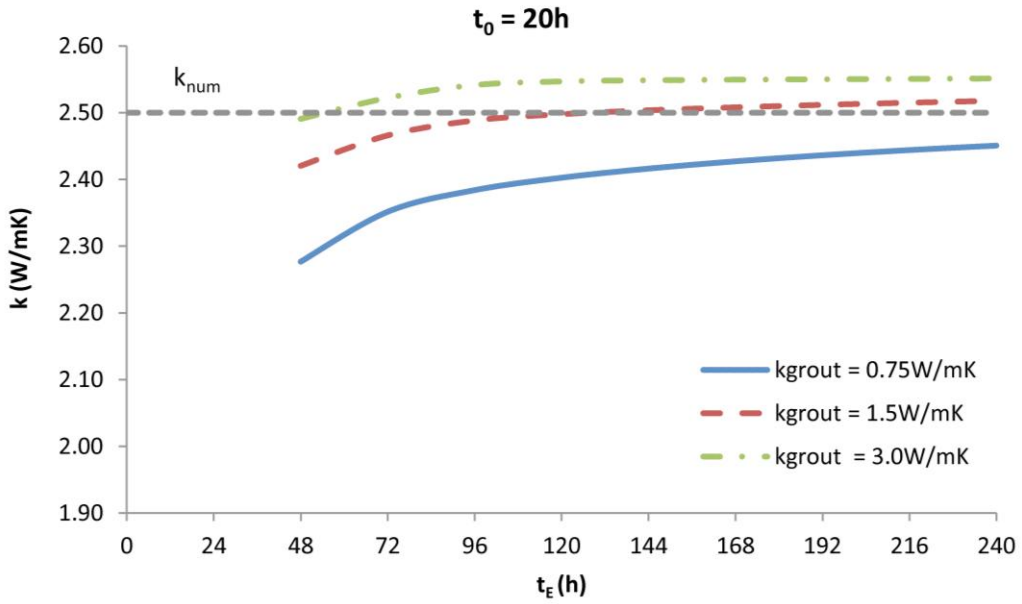

Figure 8.11 Estimated thermal conductivity of the ground at t_0 = 20h, t_E = 24 -240h, for grout conductivities of 0.75, 1.5, 3.0W/mK.

The results follow similar trend as that of t_0 = 10h. The variation of the estimated thermal conductivity of the ground is higher when shorter period is included for the analysis. The differences get more stable as t_E approaching 240h. Grout with high thermal conductivity results in over-estimation of the thermal conductivity. Conversely, grout of lower thermal conductivity results in under-estimation of thermal conductivity. The deviation of the estimated thermal conductivities of the ground at t_E = 240h is approximately 2.2% for t_0 = 20h.

The deviation decreases as t_0 increase, which can also be expected since the influences of the thermal conductivity of the grout becomes weaker as the test duration increases. The errors in the estimated values are within 10% in all cases.

8.4.5 Sensitivity to the Heterogeneity of Ground

The ground is normally considered to be homogeneous in TRT analysis. In reality, the ground is usually stratified along the BHE depth with layers of different material, e.g. sand, clay, rock and so on. It is interesting to examine the effect of the heterogeneity of the ground on the analysis of the data from TRT.

The borehole with same configuration as shown in Table 8.1 is tested. The ground of the first 100m (the whole borehole depth) is divided into two equal layers (50m) along the depth, and the other 100m below the borehole is treated as a third layer.

In all the tests where the ground is assumed to be homogeneous, the thermal conductivity of the ground was 2.5 W/mK. In order to test the heterogeneous ground, different conductivities are set for the first two layers, while the third layer has a thermal conductivity of 2.5 W/mK. The resulting mean thermal conductivity of the two layers is 2.5 W/mK in all cases.

Three combinations of the thermal conductivities for the first two layers are tested. The first combination is 2.0 and 3.0 W/mK; the second is 1.5 and 3.5 W/mK; and, the last is 1.0 and 4.0 W/mK. The mean thermal conductivity of the two layers in these three combinations is 2.5 W/mK.

Figure 8.12 shows the mean fluid temperatures for the three test cases with heterogeneous ground, along with the mean fluid temperature for the homogeneous ground. All the simulations run at 1 minute per time step and continuously for 240 hours. For the first few hours, the mean fluid temperatures for all cases are identical, and the differences start to show after 10 hours. This is because during the first few hours, the heat transfer is mostly confined to the borehole. It takes 10 hours for any noticeable heat flux to reach outside the borehole and the heterogeneity of the ground becomes apparent. The mean fluid temperature rises faster when the difference of the thermal conductivities of two layers is larger.

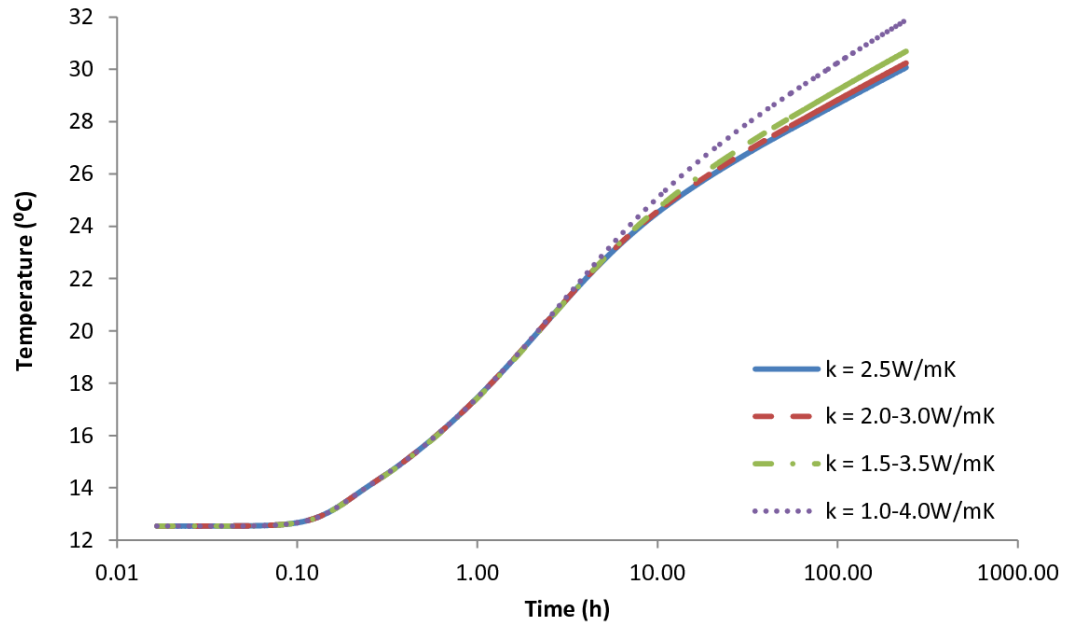

Figure 8.12 Mean fluid temperatures for heterogeneous ground with reference to the homogeneous ground.

Figure 8.13 show the borehole wall heat transfer rate for the same test cases.

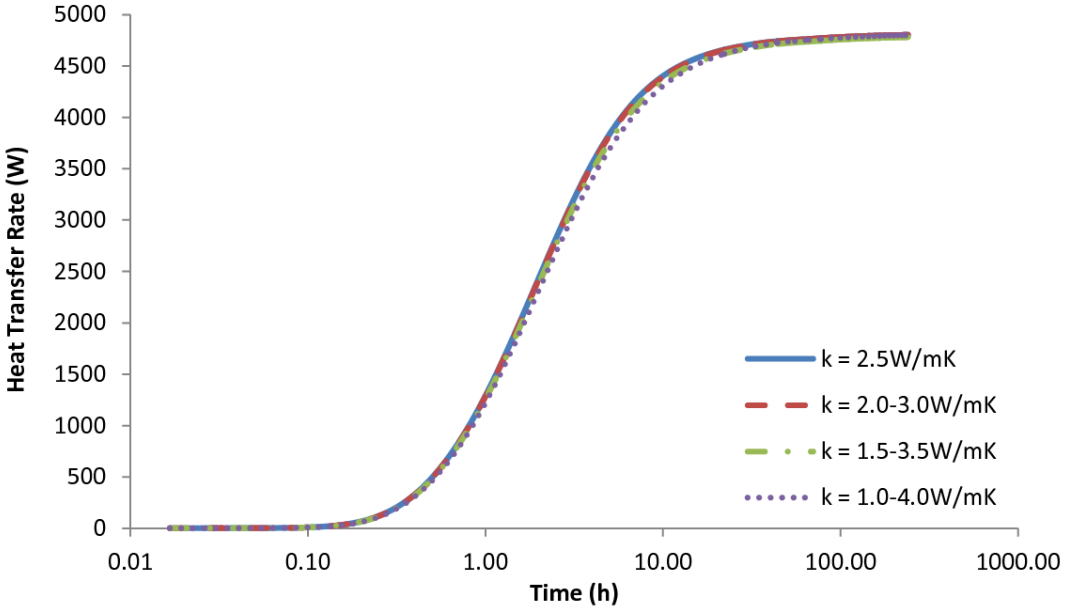

Figure 8.13 Borehole heat fluxes for heterogeneous ground with reference to the homogeneous ground.

The borehole heat transfer rates for all test cases are the same due to the same total heat input being rejected to the ground. Therefore, if a thermal resistance is applied to the whole simulating domain, the ground with larger difference of thermal conductivities between the two divided layers has higher thermal resistance than the ground with smaller difference of thermal conductivities between the two divided layers. The homogenous ground has the smallest thermal resistance.

Figure 8.14 shows the estimated thermal conductivity of the heterogeneous ground at t_0 = 10h and t_E varies from 24h to 240h. Although in these four cases, the mean conductivity of the ground is the same, as the difference between the upper two layers of ground increases, the conductivity of the ground estimated using the line source model decreases. For example, in case where t_0 = 10h and t_E = 48h, the estimated conductivity of the ground for k_{num} = 2.5 W/mK is 2.15 W/mK; for k_{num} = 2.0-3.0 W/mK is 2.10 W/mK; for k_{num} = 1.5-3.5 W/mK is 1.97 W/mK; and for k_{num} = 1.0-4.0 W/mK is 1.71 W/mK. These results indicate that simply taking the mean conductivity of the heterogeneous ground at different layers may result in over estimation of the ground thermal conductivity.

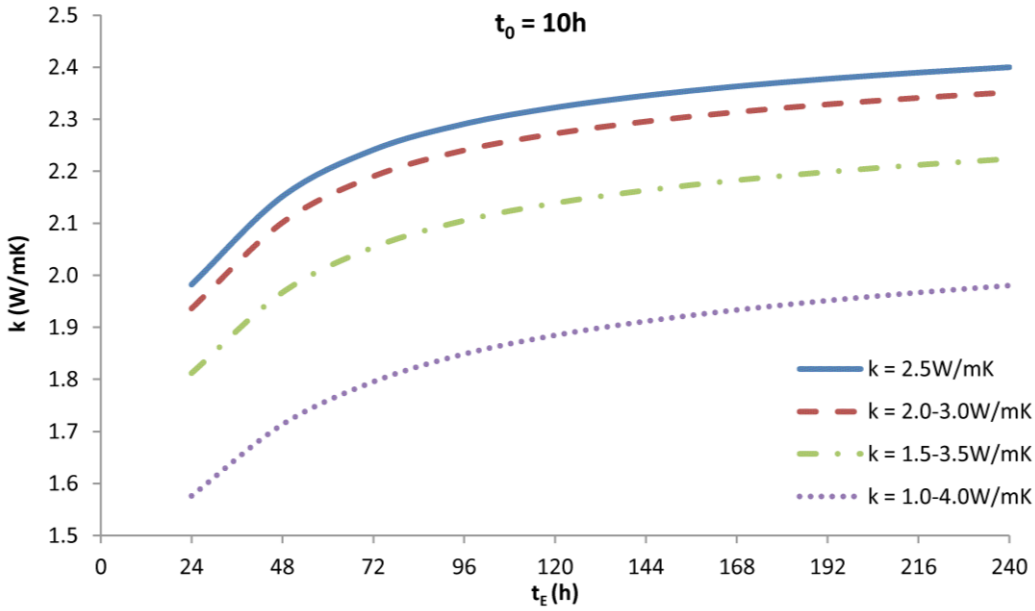

Figure 8.14 Estimated thermal conductivity of the ground at t_0 = 10h, t_E = 24 -240h, for heterogeneous ground.

A similar trend can be seen in Figure 8.15, where the estimated thermal conductivities of the heterogeneous ground at t_0 = 20h and t_E varies from 48h to 240h for four cases are shown.

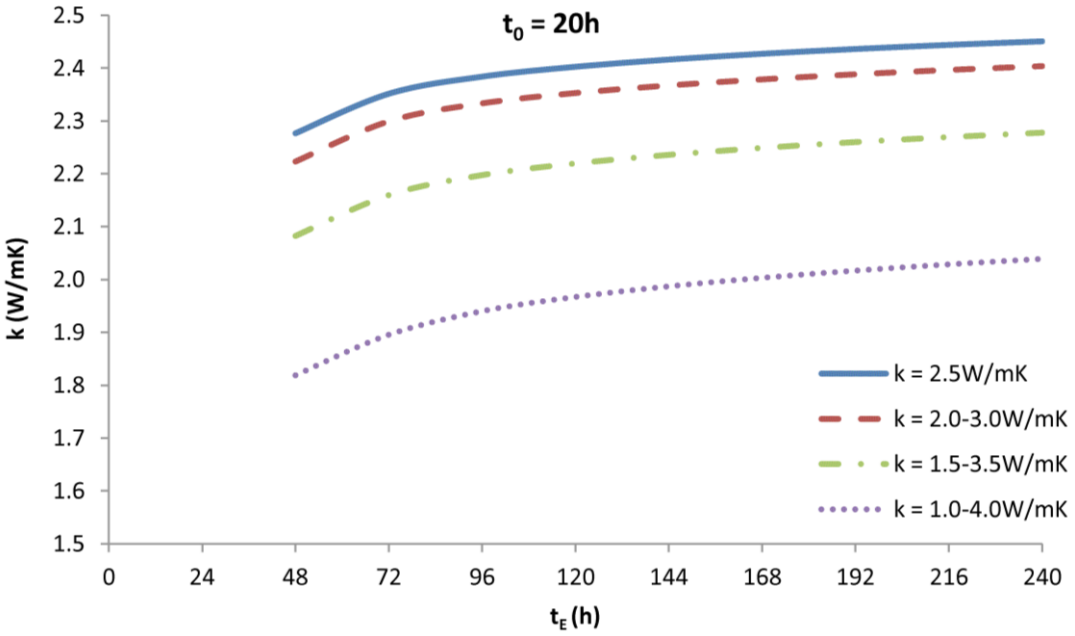

Figure 8.15 Estimated thermal conductivity of the ground at t_0 = 20h, t_E = 48 -240h, for heterogeneous ground.

One explanation of this phenomenon can be traced back to the assumptions of the line source model used to estimate the ground thermal conductivity. In the line source model, it is assumed that the ground is entirely homogeneous, and the mean temperature of the fluid is taken as the average of the inlet and outlet fluid temperature. The underlying assumption of taking the average of the inlet and outlet fluid temperature as the mean fluid temperature is that the fluid temperature varies linearly along the depth of the borehole. However, for a BHE with heterogeneous ground, the vertical fluid temperature profiles are not linear. Figure 8.16 shows the vertical fluid temperature profiles for homogeneous and heterogeneous ground at the end of 240h simulations. The bigger the difference between the two conductivities is, the more obvious the non-linearity of the fluid temperature profile becomes.

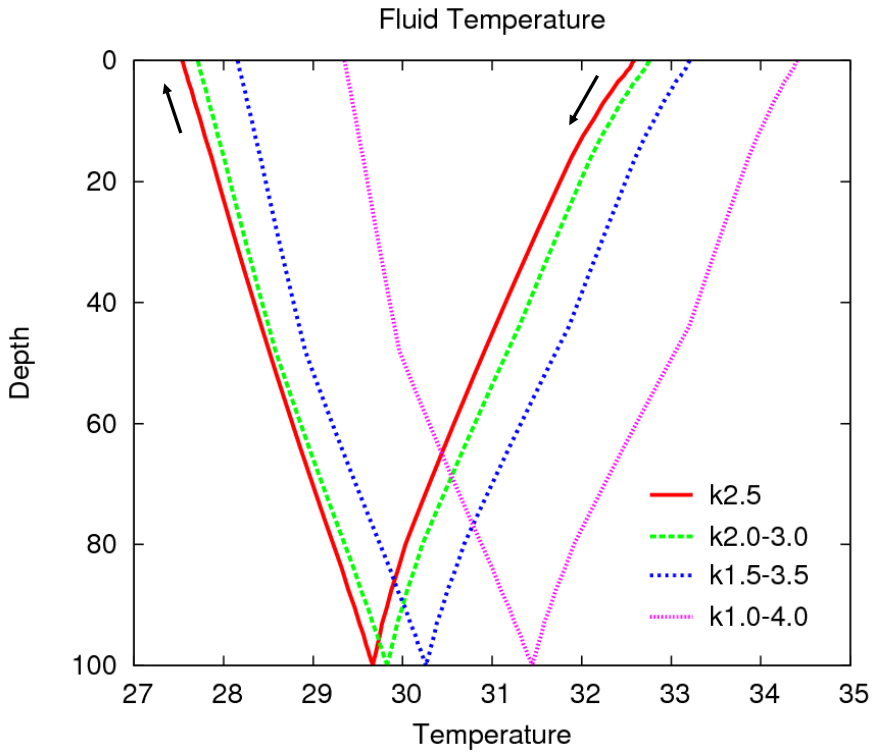

Figure 8.16 Vertical fluid temperature profiles for homogeneous and heterogeneous ground.

8.5 Summary

In this chapter, the 3D model has been used to evaluate the assumptions of the line source model and their implications for the analysis of TRT data. Five factors were investigated, including the starting time t_0, the end time t_E of the analysis period, the velocity of the circulating fluid, the conductivity of the grout, and the heterogeneity of the ground.

Various test cases of TRT have been simulated using the 3D numerical model with a pre-defined ground thermal conductivity (k_{num}). The mean temperatures of the inlet and outlet fluid data obtained from the simulation have then been used by the line source model to estimate the ground thermal conductivity (k_{est}). By comparing the estimated ground thermal conductivity to the pre-defined ground conductivity used by the model, it has been possible to quantify the uncertainty of the line source model used in the analysis of TRT. Data of different periods were used in the analyses in order to examine the effects of the starting time t_0 and the end time t_E of the analysis period on the estimation of ground conductivity. It was found that for a relatively large BHE with relatively low grout conductivity, the estimated ground conductivity was always underestimated. Neglecting more initial data during the test could

result more accurate estimation. If the data of the first 10 hours are excluded, the test should last at least 72 hours in order that the error in the estimated conductivity falls within the 10% bench mark. If data of the first 20 hours are excluded, a test that lasts 48 hours can achieve less than 10% error in estimation.

The results also show that different velocities of the circulating fluid used in TRT do not have any influence on the analysis of the data if the line source model is applied to estimate the ground conductivity. The thermal conductivity of the grout, in contrast, has a significant effect on the estimation of the thermal conductivity of the ground. For BHEs with relatively low grout conductivity, the ground conductivity is usually underestimated, and the lower the grout conductivity, the longer the test would need to last in order to achieve 10% error bench mark. For BHEs with relatively high grout conductivity, the ground conductivity can be either underestimated if the test is relatively in short period, or overestimated if the test is relatively in long period. The errors for cases with high grout conductivity were found to be within 10% of the bench mark value.

The effect of the assumption of heterogeneous ground on the analysis of TRT data using the line source model appears to be significant. Three test cases have been studied by dividing the ground of the first 100 meters into two layers of equal depth and assigning two different conductivities but keep the mean conductivities of the ground the same as the homogeneous case ($k = 2.5$ W/mK). The findings highlight that a larger difference between the conductivities of the two layers of ground results in a lower estimated ground conductivity when applying the line source model.

Further application of this 3D finite volume model in the analysis of TRT data includes its use in parameter estimation techniques to estimate both the grout and ground thermal conductivities. The whole temperature profile could be applied to the model if available. A boundary condition at the surface could also be applied to take into account the varying heat transfer rates at the surface according to climate conditions.

Chapter 9 Conclusions and Further Research

The primary aim of this work was to develop a dynamic three-dimensional numerical model for borehole heat exchangers (BHEs) in order to investigate the implications of simulating the transient heat transfer in and around BHEs in three dimensions. Seven objectives were identified in order to achieve this aim.

In this chapter, a summary of main findings with respect to its aims and objectives is presented. This is followed by a discussion concerning its contribution to knowledge. Limitations of the research are briefly discussed along with potential areas for further research.

9.1 Main Findings

The main findings of this study can be summarised in two sections. The first section concerns the model development and validation and the second section concerns applications of the model.

Through reviewing model developments on BHEs in literature, it was found a fully-discretised three-dimensional (3D) model for BHEs which can simulate the fluid transport along the pipe loop was needed in order to fully understand the three-dimensional characteristics of heat transfer in and around BHEs (Chapter 2).

9.1.1 Model Development and Validation

A dynamic 3D finite volume model was developed and validated. A general convection-diffusion partial differential equation was employed to describe the transient heat transfer in and around BHEs in three dimensions. Multi-block boundary fitted structured mesh was employed to discretise the simulation domain, allowing the complex geometries inside BHEs and the surrounding ground to be represented explicitly. The discretisation of the fluid along the depth of the borehole allows the fluid to be modelled in a similar way to a Compartments-In-Series model, in which each finite volume cell can be considered as a well-mixed node that is defined by a single temperature and is transported at an average velocity.

For comparison purposes, a two-dimensional (2D) model was implemented using the same numerical method as that of the 3D model. This 2D model was equivalent to the 3D model of one metre depth and with adiabatic upper and lower surfaces. The fluid transport was not

explicitly modelled; instead, the heat transfer from the fluid was treated by a mixed boundary condition at the pipe walls.

The validation of the 3D model was done by reference to analytical models in terms of borehole thermal resistance and fluid transport in pipes. The values of borehole thermal resistance calculated using the numerical model with various mesh densities matched the analytical results extremely well. Moreover, the characteristics of the fluid transport were validated against an analytical solution of the residence time distribution.

Both the 3D and 2D models were further validated against to the experimental data from Oklahoma State University. Using the inlet fluid temperature and the flow rates as the input for both models, the predicted outlet fluid temperatures show a close match to the measured outlet fluid temperature over the simulation period. Only the 3D model proved able to capture the delayed responses that were demonstrated in the experimental data, due to the explicit modelling of pipe fluid transport (Chapter 3).

9.1.2 Three-Dimensional Heat Transfer Characteristics

The dynamic 3D model was applied to investigate the three-dimensional characteristics of heat transfer in and around a BHE. Both steady-state and transient simulations were carried out in order to examine the long timescale and short timescale characteristics. Over short timescales (i.e. less than 5 minutes) both the fluid temperature profile and borehole heat flux profile were shown to be non-linear, regardless of the fluid velocity. Over longer timescales and for cases with relatively high fluid velocity, the fluid temperature profile and borehole heat flux profile approach linear. The non-linearity in the fluid temperature profile and borehole heat flux profile remained for cases with relatively low fluid velocity. Consequently, in models which assume linear fluid temperature or borehole heat flux profiles, some errors in overall heat transfer rate can be expected. The significance of the inter-tube heat flux compared to the total borehole heat flux at long timescales was also examined. It was found this ratio was also dependent on fluid velocity. For cases with low fluid velocities, the inter-tube heat flux could be 10% of the total borehole heat flux. This percentage is lower (around 2%) for cases with high fluid velocities.

A step change in inlet fluid temperature was applied to examine the dynamic response in the outlet temperatures predicted by the 3D and 2D models. A delayed response in the outlet

temperature predicted by the 3D model was demonstrated, in contrast to the instant change in the outlet temperature predicted by the 2D model. The delayed response, although associated with the transit of the fluid along the pipe loop, was not just delayed according to the nominal transit time but could be seen to be significant for several times this period.

Pipe fluid transport also proved to have practical implications for heat pump operation. This was demonstrated through simulating a step change in inlet temperature represent a typical on-and-off operation of a domestic heat pump. The delayed response could be of some significance in moderating swings in temperature during heat pump cyclic operation. The temperature swings damping effects were further investigated through frequency response analysis (Chapter 4).

9.1.3 Improvement of the Two-Dimensional Model

Comparison of the 2D and 3D model predictions has highlighted the limitations of the 2D model. As a result, methods have been proposed to improve the accuracy of the original 2D model by including representations of the thermal mass of the fluid and the dynamic effect of transport of fluid in the pipe loop. Coupling the original 2D model with two pipe models to simulate the downward and upward fluid flows was proved to provide the best accuracy. The solution of the pipe model is partly dependent upon the number of cells used to discretise the pipe. It was found the delayed response predicted by the 2D+Pipe model matched to the prediction by the 3D model closely using 48 cells. It was found the outlet temperature response predicted by the 2D+Pipe model matched closely with the predictions of the 3D model for cases with high fluid velocity, although differences between the two predictions was noticeable for cases with low fluid velocity.

Frequency response analysis was carried out to further characterise the response of the 2D+Pipe model. The results showed that although the amplitude ratio predicted by the 2D+Pipe model resembled to that predicted by the 3D model at low frequencies, the amplitude ratio was under predicted by the 2D+Pipe model at high frequency. The phase delay predicted by the 2D+Pipe model, on the other hand, matched closely with the predictions of the 3D model except at extremely high frequencies. Moreover, the 2D+Pipe model was validated against the experimental data from the Oklahoma State University (Chapter 5).

9.1.4 Simulation of Ground Source Heat Pump Systems

The effects of simulating a BHE using a dynamic 3D numerical model on the predictions of system performance were investigated by simulating a Ground Source Heat Pump (GSHP) system in EnergyPlus. Three models were implemented to simulate a single BHE, the g-function model, the 3D model and the original 2D model, and the results were compared.

The delayed response associated with the transit of fluid along the pipe loop was proved to be of some significance in moderating swings in temperature during the short periods when the heat pump starts to operate. A relatively high fluid flow rate was chosen for the simulation and so it was expected that in many cases with lower flow rates, the effect of the delayed response would be more profound. The 3D numerical model predicted a lower heat transfer rate over longer periods of operation when compared to the predictions by the original 2D model and the g-function model. This is due to the mean temperature differences between the fluid and the ground being lower in the 3D mode.

It is expected that when using the dynamic 3D model for sizing GSHP systems (at least when the design is sensitive to peak load), shorter borehole lengths would be suggested, which would result in lower initial costs and shorter payback period. In addition, the 3D model would be beneficial when optimising system control and operation (Chapter 6).

9.1.5 Simulation of Multiple BHEs Arrays

The dynamic 3D numerical model was applied to examine the short timescale and long timescale behaviour of multiple BHEs arrays. The g-functions calculated by the 3D model were compared to those by Eskilson (1987) and Yavuzturk (1999) for four different configurations of borehole fields.

At short timescales, the g-function calculated by the 3D model using the fluid temperature showed good agreement with the g-function calculated by Yavuzturk but with some differences during the first hour. At long timescales, for the single borehole and the configuration with 2x2 multiple BHEs, the g-function data calculated by the 3D model corresponded exactly with the g-function data calculated by Eskilson. The predicted values of the g-function for configurations with 3x3 and 4x4 multiple BHEs by the 3D model had slightly higher values than that of Eskilson at very long timescales. This was thought to be due to the constant heat flux boundary condition that was applied to each BHE in the 3D model,

regardless of its position at the borehole field. It is possible that this issue could be addressed by using the inlet fluid temperature as the boundary condition and adjusting this at each step to ensure a constant heat flux was applied (Chapter 7).

9.1.6 Evaluation of Thermal Response Test Data

The dynamic 3D model was used to evaluate the accuracy of applying the line source model in the analysis of thermal response tests (TRT) by examining the assumptions made and their implications on TRT results. Five factors were investigated, including the analysis starting time t_0, the test end time t_E, the velocity of the circulating fluid, the conductivity of the grout and the heterogeneity of the ground.

A relatively large BHE with relative low grout conductivity was studied. For this BHE, it was found that applying the line source model always under estimates the ground conductivity. Neglecting more initial data during the test could result more accurate estimation. If neglecting the data of the first 10 hours, the test should last at least 72 hours to ensure the error of the estimation could fall within the 10% bench mark. If neglecting the data of the first 20 hours, test that lasted 48 hours could achieve the same accuracy.

The results also showed that different velocities of the circulating fluid used in TRT did not have any effects on the results of the analysis when applying the line source model to estimate the ground conductivity.

The thermal conductivity of the grout was found to have a significant impact on the estimation of ground conductivity. For BHEs with relatively low grout conductivity, the ground conductivity was usually under estimated, and the lower the grout conductivity, the longer the test would need to be in order to fall within the 10% error bench mark. For BHEs with relatively high grout conductivity, the ground conductivity can be either under estimated if the test period is relatively short, or over estimated if the test period is relatively long, although the error for cases with high grout conductivity was within 10% bond.

The effects of heterogeneity of the ground on the line source model TRT analysis were studied. It was found that a larger difference between the conductivities of two layers resulted in a lower estimation of effective ground thermal conductivity when using the line source model (Chapter 8).

9.2 Contribution to Knowledge

A primary contribution to knowledge from this study is the development and validation of a dynamic 3D finite volume model for BHEs. This model is of value in that it enables detailed simulation of transient heat transfer in and around BHEs in a truly three-dimensional manner, including the modelling of fluid transport along the pipe loop. In addition, using this model to investigate the three-dimensional heat transfer characteristics of BHEs and their influence on the performance of ground source heat pump systems has resulted in a number of insights into their significance. Furthermore, this model has been applied to examine thermal interactions within borehole fields and evaluate the accuracy of applying line source model in the analysis of thermal response tests. The results from this study add to the debate that having a detailed dynamic model for BHEs is necessary, especially when heat transfer at short timescales is important and cannot be ignored.

An original contribution has also been made in developing an improved two-dimensional model that is able to reproduce some of the effects of the fluid transport at short timescales. This model should be useful for system simulation and response factor data generation at short timescales.

9.3 Limitations and Further Research

The limitations of this study concerning model development and model applications have been discussed in corresponding chapters in this thesis. A brief summary of limitations is given in this section along with opportunities for further research that have been identified.

A multi-block boundary fitted structured mesh has been employed to discretise the BHE model simulation domain. Although this mesh generation method provides an explicit representation of the borehole geometry in two dimensions, the mesh is essentially extruded in the third dimension along the depth of the borehole. As a result, the u-fitting at the bottom of the borehole cannot be represented explicitly. Instead, boundary conditions have been applied to connect the downward and upward fluid flows at the bottom of the two separated pipes.

Regarding the modelling of the fluid transport, the two-dimensional fluid flow in the pipes has effectively been simplified to be one-dimensional. Due to this simplification, the model always tends to over-predict the degree of diffusion. This might be addressed by Computational Fluid Dynamics (CFD) calculation of the pipe fluid flow but this would add unreasonable

computation burden. Some overestimation of the diffusion process is not unreasonable as additional diffusion occurs in practice by virtue of the horizontal header pipes in a typical borehole array. Development of an improved but computationally effective pipe transport model would be valuable.

In the study of the integrated simulation of the Ground Source Heat Pump (GSHP) system with the 3D model, a simple heat pump model has been used. This heat pump model cannot simulate the on-and-off dynamic characteristics of a typical heat pump. This limits the ability to study the overall dynamic system behaviour. A more detailed dynamic heat pump model and an explicit representation of the control system may be beneficial to investigate system performance and control system operation further.

The potential of modelling BHEs arrays using the 3D model have been briefly explored in this study. Modelling BHEs arrays in full scale allows flexible control over the operation of the borehole field. One application would be to design and simulate a GSHP system with a borehole field in which flow can be varied in some of the boreholes during part load operation. Consequently, pumping energy and heat exchanger performance may be optimised. Further research on optimising the performance of a borehole field would be greatly beneficial.

References

AL-KHOURY, R. & BONNIER, P. G. 2006. Efficient finite element formulation for geothermal heating systems Part II: Transient. *International Journal for Numerical Methods in Engineering,* 67**,** 725-745.

AL-KHOURY, R., BONNIER, P. G. & BRINKGREVE, R. B. J. 2005. Efficient finite element formulation for geothermal heating systems Part I: Steady state. *International Journal for Numerical Methods in Engineering,* 63**,** 988-1013.

BENNET, J., CLAESSON, J. & HELLSTROM, G. 1987. *Multipole Method to Compute the Conductive Heat Flows To and Between Pipes In a Composite Cylinder.* University of Lund, Sweden.

BOSE, J. E. (ed.) 1991. *Design and Installations Standards,* Stillwater, Oklahoma: Internation Ground Source Heat Pump Association.

BOSWORTH, R. C. L. 1949. Distribution of reaction time for turbulent flow in cylindrical reactors. *Philosophical Magazine Series,* 40**,** 314-324.

CARSLAW, H. S. & JAEGER, J. C. 1947. *Conduction of Heat in Solid,* Oxford, Claremore Press.

CLARK, D. R. 1985. HVACSim+ Building System and Equipment Simulation Program - Reference Mnual. . *NBSIR 84-2996.* Washington, DC: National Bureau of Standards.

CRAWLEY, D. B., LAWRIE, L. K., PEDERSEN, C. O., STRAND, R. K., LIESEN, R. J., WINKELMANN, F. C., BUHK, W. F., Y. HUANG, A. E. E., FISHER, D. E., WITTE, M. J. & GLAZER, J. 2001. EnergyPlus: Creating a New-Generation Building Energy Simulation Program. *Energy & Buildings,* 33**,** 319-331.

DE CARLI, M., TONON, M., ZARRELA, A. & ZECCHIN, R. 2010. A computational capacity resistance model (CaRM) for vertical ground-coupled heat exchangers. *Renewable Energy,* 35**,** 1537-1550.

DHI-WASY 2010. FEFLOW finite element subsurface flow and transport simulation system - User's manual/reference manual/white papers. *Recent release 6.0.* Berlin: Tech.rep., DHI-WASY GmbH.

DIERSCH, H.-J. G., BAUER, D., HEIDEMANN, W., RUHAAK, W. & SCHATZL, P. 2011a. Finite element modeling of borehole heat exchanger systems Part 1. Fundamentals. *Computers & Geosciences,* 37**,** 1122-1135.

DIERSCH, H.-J. G., BAUER, D., HEIDEMANN, W., RUHAAK, W. & SCHATZL, P. 2011b. Finite element modeling of borehole heat exchanger systems Part 2. Numerical simulation. *Computers & Geosciences,* 37**,** 1136-1147.

ESKILSON, P. 1987. *Thermal Analysis of Heat Extraction Boreholes.* PhD, University of Lund.

FISHER, D. E., REES, S. J., PADHMANABHAN, S. K. & MURUGAPPAN, A. 2006. Implementation and Validation of Ground-Source Heat Pump System Models in an Integrated Building and System Simulation Environment. *HVAC&R Research Special Issue,* 12**,** 693-710.

GEHLIN, S. 2002. *Thermal Response Test - Method Development and Evaluation.* Doctoral, Lulea University of Technology.

GU, Y. & O'NEAL, D. 1998. Development of an equivalent diameter expression for vertical u-tubes used in ground-coupled heat pumps. *ASHRAE Transactions,* 104**,** 347-355.

HANBY, V. I., WRIGHT, J. A., FLETCHER, D. W. & JONES, D. N. T. 2002. Modeling the dynamic response of conduits. *HVAC&R Research,* 8**,** 1-12.

HART, D. P. & COUVILLION, R. (eds.) 1986. *Earth Coupled Heat Transfer*: Publication of the National Water Well Association.

HE, M., REES, S. J. & SHAO, L. 2009. *RE: Applications of a Dynamic Three-Dimensional Numerical Model for Borehole Heat Exchangers.*

HE, M., REES, S. J. & SHAO, L. 2010. Simulation of a domestic ground source heat pump system using a three-dimensional numerical borehole heat exchanger model. *Journal of Building Performance Simulation,* 4**,** 141-155.

HELLSTROM, G. 1991. *Ground Heat Storage: Thermal Analysis of Duct Storage Systems: Part I Theory.* PhD, University of Lund.

HERN, S. A. 2004. *Design of an experimental facility for hybrid ground source heat pump systems.* MSc, Oklahoma State University.

INCROPERA, F. P., DEWITT, D. P., BERGMAN, T. L. & LAVINE, A. S. 2007. *Fundamentals of Heat and Mass Transfer*, Wiley.

INGERSOLL, L. R., ZOBEL, O. J. & INGERSOLL, A. C. 1954. *Heat Conduction with Engineering, Geological, and Other Applications,* New York, McGraw-Hill.

KASUDA, T. & ARCHENBACH, P. R. 1965. Earth temperature and thermal diffusivity at selected stations in the United States. *ASHRAE Transactions,* 71**,** Part 1.

KAVANAUGH, S. P. 1985. *Simulation and experimental verification of vertical ground-coupled heat pump systems.* PhD, Oklahoma State University.

KAVANAUGH, S. P. 1992. Field test of a vertical ground coupled heat pump in alabama. *ASHRAE Transactions*.

KELVIN, S. W. T. 1882. Mathematical and Physical Papers, II. 41, cited by Ingersoll, et al. (1954).

KUMMERT, M. & BERNIER, M. 2008. Sub-hourly Simulation of Residential Ground Coupled Heat Pump Systems. *Building Serv. Eng. Res. Technol. ,* 29**,** 27-44.

OPPELT, T., RIEHL, I. & GROSS, U. 2010. Modelling of the borehole filling of double U-tube heat exchangers. *Geothermics,* 39**,** 270-276.

PATANKAR, S. V. 1980. *Numerical Heat Transfer and Fluid Flow*, Taylor & Francis.

PAUL, N. D. 1996. *The effect of grout thermal conductivity on vertical geothermal heat exchanger design and performance.* Master of Science, South Dakota State University.

PEREZ-LOMBARD, L., ORTIZ, J. & POUT, C. 2008. A review on buildings energy consumption information. *Energy and Buildings,* 40**,** 394-398.

REES, S. J., SPITLER, J. D., DENG, Z., ORIO, C. D. & JOHNSON, C. N. 2004. A study of geothermal heat pump and standing column well performance. *ASHRAE Transactions,* 109**,** 3-13.

REES, S. J., SPITLER, J. D. & XIAO, X. 2002. Transient analysis of snow-melting system performance. *ASHRAE Transactions,* 108**,** 406-423.

SEL 1997. A Transient Systems Simulaion Program, User's Manual, Version 14.2. Solar Energy Laboratory, University of Wisconsin-Madison.

SEL 2005. TRNSYS 16 - A Transient System Simulation Program - Documentation Set (9 Volumes). Solar Energy Laboratory, University of Wisconsin-Madison, Madison, WI.

SIGNORELLI, S., BASSETTI, S., PAHUD, D. & KOHL, T. 2007. Numerical evaluation of thermal response tests. *Geothermics,* 36**,** 141.

SPITLER, J. D. 2000. GLHEPRO - A Design Tool For Commercial Building Ground Loop Heat Exchangers. *the Fourth International Heat Pumps in Cold Climates Conference.* Aylmer, Quebec.

SPITLER, J. D., CULLINE, J., BERNIER, M., KUMMERT, M., CUI, P., LIU, X., LEE, E. & FISHER, D. E. 2009. Preliminary intermodel comparison of ground heat exchanger simulation models. *11th International Conference on Thermal Energy Storage; Effstock 2009.* Stockholm, Sweden.

TANG, C. 2005. *Modeling Packadged Heat Pumps in a Quasi-Steady State Energy Simulation Program.* MSc, Oklahoma State University.

UNDERWOOD, C. P. & SPITLER, J. D. 2007. Analysis of Vertical Ground Loop Heat Exchangers Applied to Buildings in the UK. *Building Serv. Eng. Res. Technol.,* 28**,** 133-159.

WEN, C. Y. & FAN, L. T. 1975. *Models for Flow Systems and Chemical Reactors,* New York, Marcel Dekker, Inc.

WETTER, M. & HUBER, A. 1997. TRNSYS Type 451: Vertical Borehole Heat Exchanger EWS Model, Version 3.1 - Model Description and Implementing into TRNSYS. Transsolar GmbH, Stuttgart, Germany.

YAVUZTURK, C. 1999. *Modeling of Vertical Ground Loop Heat Exchangers for Ground Source Heat Pump Systems.* PhD, Oklahoma State University.

YAVUZTURK, C. & SPITLER, J. D. 1999. A Short Time Step Response Factor Model for Vertical Ground Loop Heat Exchangers. *ASHRAE Transactions,* 105**,** 475-485.

YAVUZTURK, C., SPITLER, J. D. & REES, S. J. 1999. A Transient Two-Dimensional Finite Volume Model for the Simulation of Vertical U-Tube Ground Heat Exchangers. *ASHRAE Transactions,* 105**,** 465-474.

YOUNG, T. R. 2004. *Development, Verification, and Design Analysis of the Borehole Fluid Thermal Mass Model for Approximating Short Term Borehole Thermal Responser.* Master of Science, Oklahoma State University.

ZARRELA, A., SCARPA, M. & DE CARLI, M. 2011. Short time step analysis of vertical ground-coupled heat exchangers: the approach of CaRM. *Renewable Energy,* 36**,** 2357-2367.